SCHOLARLY PUBLICATIONS

A CURRENT AWARENESS BULLETIN
OF RESEARCH OUTPUT

@DTU

(17th Edition)

MAY 2014

BY: CENTRAL LIBRARY

DELHI TECHNOLOGICAL UNIVERSITY
(FORMERLY *DELHI COLLEGE OF ENGINEERING)*
GOVT. OF N.C.T. OF DELHI
SHAHBAD DAULATPUR, MAIN BAWANA ROAD
DELHI 110042

PREFACE

This is the Seventeenth Issue of Current Awareness Bulletin started by Delhi Technological University, Central Library. The aim of the bulletin is to compile, preserve and disseminate information published by the faculty, students and alumni for mutual benefits. The bulletin also aims to propagate the intellectual contribution of Delhi Technological University (DTU) as a whole to the academia.

The bulletin contains information resources available in the internet in the form of articles, reports, presentations published in international journals, websites, etc. by the faculty and students of DTU. The publications of faculty and student which are not covered in this bulletin may be because of the reason that the full text either was not accessible or could not be searched by the search engine used by the library for this purpose.

The learned faculty and students are requested to provide their uncovered publications to the library either through email or in CD, etc to make the bulletin more comprehensive.

This issue contains the information published during May 2014. The arrangement of the contents is alphabetical. The full text of the article which is either subscribed by the university or available in the web is provided in this bulletin.

Central Library

CONTENTS

9. Investigation of variation of energy of laser beam on structural, electrical and optical properties of pulsed laser deposited CuO thin films, ***V. Dahiya, *G. Kaur, *A. Mitra**, and ***A. Kumar**, Department of Applied Physics

10. Manufacturing blood ex vivo: a futuristic approach to deal with the supply and safety concerns Running Title: Blood production using stem cells, ***Vimal Kishor Singh, *Abhishek Saini**, Kohichiro Tsuji, ***P B Sharma**, Ramesh Chandra, Department of Biotechnology

11. Method for improving thermal performance of Dual Pressure Linde system for liquefaction of gases using energy exergy analysis for reducing global warming and ozone depletion, ***Devender Kumar** and ***R.S Mishra**, Mechanical Department,

12. Optimization of UPFC Controller Parameters Using Bacterial Foraging Technique for Enhancing Power System Stability, Poonam Singhal, S. K. Agarwal and ***Narender Kumar**

13. Pharmacogenomics for Precision Medicine in the Era of Collaborative Co-creation and Crowdsourcing, Jameel Ahmad Khan, Vinod Scaria and ***Yasha Hasija**, Biotechnology

14. Production and Performance Testing of Waste Frying Oil Biodiesel, ***Amit Pal, *Shashank Mohan** and Dhananjay Trivedi, Department of Mechanical Engineering

15. Renewable Energy Advancements in India, ***M. Rizwan, *N. Kumar, *A. H. Quadri**, Department of Electrical Engineering

16. Reptiles Inspired Biomimetic Materials and Their Novel Applications, Kishor Kalauni, K. M. Gupta, and ***!Isha Bharti**, Teaching-cum-Research Fellow, Department of Applied Physics

17. Risk Management in Supply Chain using PetriNet, ***Pranay Bhardwaj,*Prateek Singh** and ***Girish Kumar**

18. Spectral characterization of Sm3þ ions doped Oxy-fluoroborate glasses for Visible Orange Luminescent Applications, Sk. Mahamuda, K. Swapna, M. Venkateswarlu, Suman Latha Shakya, G. Vijaya Prakash and ***A. Srinivasa Rao***, Department of Applied Physics

19. Supercooling transition in phase separated manganite thin films: An electrical transport study, ***Sandeep Singh***, Pawan Kumar, P. K. Siwach, ***Pawan Kumar Tyagi***, and H. K. Singh, Department of Applied Physics

20. Implementation of 5S practices: A review, Jagtar Singh, Richa Sharma, and ***Vikas Rastogi*** Department of Mechanical &Production Engineering,

***Faculty** **@Research Scholar** **$PG Scholar #Alumni**
£Undergraduate Student **~ Ex Faculty** **<Ex Research Scholar**
! Teaching-cum-Research Fellow

Scientific Online

OPEN JOURNAL OF MOBILE COMPUTING AND CLOUD COMPUTING
In Press

OPEN JOURNAL OF MOBILE COMPUTING AND CLOUD COMPUTING

Comparative Study on Load Balancing Techniques in Cloud Computing

N. S. Raghava* and Deepti Singh

Department of Information Technology, Delhi Technological University, Delhi, India.
***Corresponding author**: nsraghava@gmail.com

Abstract:
The present era has witnessed tremendous growth of the internet and various applications that are running over it. Cloud computing is the internet based technology, emphasizing its utility and follows pay-as-you-go model, hence became so popular with high demanding features. Load balancing is one of the interesting and prominent research topics in cloud computing, which has gained a large attention recently. Users are demanding more services with better results. Many algorithms and approaches are proposed by various researchers throughout the world, with the aim of balancing the overall workload among given nodes, while attaining the maximum throughput and minimum time. In this paper, various proposed algorithms addressing the issue of load balancing in Cloud Computing are analyzed and compared to provide a gist of the latest approaches in this research area.

Keywords:
Cloud Computing; Green Computing; Load Balancing; Virtualization

1. INTRODUCTION

Cloud Computing is the most recent emerging paradigm promising to turn the vision of "computing utilities" into reality, it provides a flexible and easy way to store and retrieve huge data without worrying about the hardware needed. As the number of users on cloud increases, the existing resources decreases automatically which leads to the problem of delay between the users and the cloud service providers. Thus, the load balancing comes into the picture. The traffic over the network must be dealt smartly such that the situation in which some nodes are overloaded and some other are under loaded should never arise. To overcome this situation, many load balancing algorithms are proposed by researchers, with their own pros and cons.

In this paper,an overall review of the current load balancing algorithms in the Cloud Computing environment is presented. Theideas of each algorithm are discussed and finally summarized as an overview.

The rest of the paper is organized as follows. The issues related to load balancing in cloud computing environmentare discussed in Section 2. In Section 3, the current literature and the load balancing algorithm in cloud proposed by various researchers were discussed. In section 4, the proposed approacheswere discussed and compared. Finally, in Section 5 we concluded the paper and also presented some ideas which can be implemented in the future.

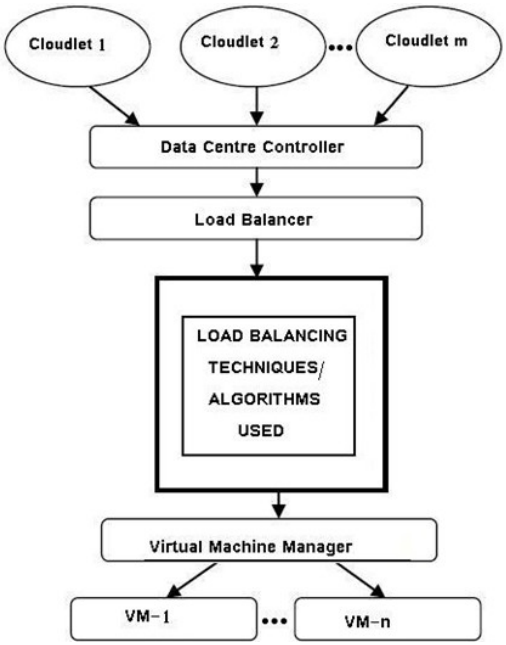

Figure 1. **Load Balancing Algorithms Execution**

2. ISSUE EFFECTING LOAD BALANCING IN CLOUD COMPUTING

There are various issues while dealing with load balancing in a cloud computing environment. Each load balancing algorithm must be such as to achieve the desired goal. Some algorithms aims at achieving higher throughput, some aims at achieving minimum response time, some other aims to achieve maximum resource utilization while some aims at achieving a trade-off between all these metrics. **Figure 1** presents a framework under which various load balancing algorithms work in a cloud computing environment.

Some major issues which must be considered while designing any load balancing algorithm are as follows:

2.1 Geographical distribution of nodes

The geographical distribution of the nodes matters a lot in the overall performance of any real time cloud computing systems, especially in case of the large scaled applications like Facebook, Twitter, etc. A well-distributed system of nodes in cloud environment is helpful in handling fault tolerance and maintaining the efficiency of the system.

2.2 Dynamic Vs Static behavior of algorithms

Any algorithm concerning load balancing is designed, based on the state or behavior of the system, which may be static or dynamic.

2.2.1 Static Algorithms

These algorithms do not depend upon the current state of the system and have prior knowledge regarding system resources and details of all tasks in an application. These kinds of algorithms face a major drawback in case of sudden failure of system resource and tasks.

2.2.2 Dynamic Algorithms

These algorithms take decisionsconcerning load balancing based upon the current state of the system and don't need any prior knowledge about the system. This approach is an improvement over the static approach. The algorithms in this category are considered complex, but have better fault tolerance and overall performance.

2.3 Algorithm Complexity

The complexity of any load balancing algorithm affects the overall performance of the system. Sometimes the algorithm is complex, but is better in terms of throughput and resource utilization. On the other hand, the algorithms which are simpler in terms of complexity may give poor performance in terms of fault tolerance, migration time and response time. Therefore, based on the system requirements, care should be taken to decide a better or suitable load balancing algorithm. A trade-off between all the parameters must be set wisely.

2.4 Traffic analyses over different geographical location.

For any load balancing algorithm, it is very important to analyze the traffic flow in real-time scenarios over different geographic regions, and then balance the overall workload accordingly. All regions over the globe have a different time zone and have certain peak hours during which the network load is supposed to be at its peak. Therefore, load balancer must be capable of handling the traffic in peak hours in every location so as to achieve maximum resource utilization and throughput.

3. EXISTING LOAD BALANCING TECHNIQUES IN CLOUD COMPUTING

In this section, some significant contributions on load balancing in cloud computing, as mentioned in the literature are discussed.A. Khiyaita *et al.* [1], in their paper gave an overview of load balancing in cloud computing, classification of load balancing algorithms based upon system load and system topology, examples of load balancing and different research challenges in load balancing. While in [2] authors discussed most of the existing techniques which are aimed at reducing the associated overhead, service response time and improving performance of the technique. The paper also provides details about various parameters, used to compare the existing techniques. D. A. Menasce *et al.* [3] discussed the concept of cloud computing, its advantages, disadvantages and described several existing cloud computing platforms. He also discussed the results of quantitative experiments carried out using PlanetLab, a cloud computing platform and capacity planning methods for cloud users and cloud service providers. To maintain the load balancing in the cloud computing system, Kuo-Qin Yan *et al.* [4] proposed a scheduling algorithm. Their algorithm combined the capabilities of both OLB (Opportunistic Load Balancing) [5] and LBMM (Load

Balance Min-Min) [6] scheduling algorithms, and is comparatively more efficient. In [7], idea is to find the best cloud resource while considering Co-operative Power aware Scheduled Load Balancing, solution to the Cloud load balancing challenge. The algorithm proposed in this paper, utilizes the benefits of both distributed and centralized approach of computing. Inherent efficiency of centralized approach as well as the energy efficiency and fault-tolerance nature of distributed approach is well used in this algorithm.

In PALB [8] approach, the utilization percentages of each compute node is estimated. This helps in deciding the number of compute nodes which must keep operating while other nodes completely shuts down. The algorithm has three sections: Balancing section, Upscale section and Downscale section. Balancing section is responsible for determining where virtual machines will be instantiated based on utilization percentages. The upscale section power-on's the additional compute nodes. And the downscale section shut-downs the idle compute nodes. This algorithm is guaranteed to decrease the overall power consumption while maintaining the availability of resources as compared to other load balancing algorithms. Raul Alonso-Calvo *et al.* [9] have discussed on managing large image collections in companies and institutions. A cloud computing service and its application for storage and analysis of very large images have been created and the data operations are adapted for working in a distributed mode by using different sub-images that can be stored and processed separately by different agents in the system, facilitating processing very-large images in a parallel manner. This work can be viewed as another way of load balancing in cloud computing. Apart from availability of resources, other factors like scaling of resources and power consumption are also important concerns in load balancing that cannot be ignored. Load balancing techniques should be such as to obtain measurable improvements in resource utilization and availability of resources in the cloud computing environment [10]. Alexandru Iosup *et al.* [11] Analyzed the performance of cloud computing services for scientific computing workloads and quantified the presence in real scientific computing workloads of Many-Task Computing (MTC) users, that is, of users who employ loosely coupled applications comprises many tasks to achieve their scientific goals. They also perform an empirical evaluation of the performance of four commercial cloud computing services.

Srinivas Sethi *et al.* [12] proposed a load balancing algorithm using fuzzy logic in a cloud computing environment. This algorithm uses two parameters processor speed and assigned a load of virtual machine, to balance the overall load through fuzzy logic,although in [13], the authors have introduced a new fuzzy logic based dynamic load balancing algorithm with additional parameters- memory usage, bandwidth usage, disk space usage and virtual machine status and named it as Fuzzy Active Monitoring Load Balancer (FAMLB). Milan E. Sokile [14], have discussed different load balancing techniques in a distributed environment, namely diffusive load, static, round robin and shortest queue in different client environments. Experimental analysis have been done showing diffusive load balancing is more efficient than static and round robin load balancing in a dynamic environment. Ankush P. Deshmukh and Prof. Kumarswamy Pamu [15], discussed on different load balancing strategies, algorithms and methods. The research also shows that the dynamic load balancing is more efficient than other static load balancing techniques. Efficient load balancing can clearly give major performance benefits [16]. A Network Processor consists of a number of on-chip processors to carry out packet level parallel processing operations, ensuring good load balancing among the processors. This process increases the throughput of the system. However, such type of multiprocessing increases out-of-order departure of processed packets. In this paper, the authors first propose an Ordered Round Robin (ORR) scheme to schedule packets in a heterogeneous network processor, assuming that the workload is perfectly divisible. The processed loads from the processors are perfectly ordered. This paper analyzes the throughput and derives expressions for the batch size, scheduling time and maximum number of schedulable processors. Jaspreet Kaur [17] has discussed active vm load balancer algorithm to find a suitable virtual machine in less time period. She has done simulation showing comparative analysis of round robin and equal spread current execution policies

of load balancing with varying service broker policies for data center in a cloud computing environment and comparedtheir response time and cost.

Zhang Bo *et al.* [18], proposed an algorithm which adds capacity to the dynamic balance mechanism for the cloud. The experiments demonstrate that the algorithm has obtained a better load balancing degree and used less time in loading all tasks. Soumya Ray and Ajanta De Sarkar [19] have discussed various algorithms of load balancing like Round robin algorithm, Central queuing algorithm and Randomized algorithm, their analysis is carried out on MIPS vs. VM and MIPS vs. HOST basis. Their results demonstrate that these algorithms can possibly improve the response time in order of magnitude, with respect to number of VMs in Datacenter. Execution analysis of the simulation shows that the change of MIPS will affect the response time. Increasing MIPS vs. VM decreases the response time. In order to handle the random selection based load distribution problem, dynamic load balancing algorithm can be implemented as the future course of work to evaluate various parameters. In [20], the authors have proposed an algorithm on load distribution of workloads among nodes of a cloud, by the use of Ant Colony Optimization (ACO). This algorithm uses the concept of the ant colony optimization method.

Shridhar G. Domanal and G. Ram Mohana Reddy [21] have proposed a local optimized load balancing approach for distributing incoming job request uniformly between the servers or virtual machines. They analyzed the performance of their algorithm using the Cloud Analyst simulator. Further, they also compared their approach with Round Robin [22] and Throttled algorithm [23]. A similar work was done by Shridhar G. Domanal and G. Ram Mohana [21] using CloudSim and Virtual Cloud simulators. In [24], the authors have analyzed various policies in combination with different load balancing algorithms using a tool called Cloud Analyst. They presented various variants of Round Robin load balancing algorithm, demonstrating the pros and cons of each. The Dynamic Round Robin algorithm is an improvement over static Round Robin algorithm [25], this paper analyzed the Dynamic Round Robin algorithm with varying parameters of host bandwidth, cloudlet length, VM image size and VM bandwidth. Results have been analyzed based upon the simulation carried in CloudSim simulator. In [26], the authors Ching-Chi Lin, Pangfeng Liu, Jan-Jan Wu, have proposed a new Dynamic Round Robin (DRR) algorithm for energy-aware virtual machine scheduling and consolidation. This algorithm is compared with other existing algorithms, namely Greedy, Round Robin and Powersave strategies used in Eucalyptus.

4. DISCUSSION AND COMPARISION

In the previous section different load balancing techniques proposed by various researchers have been discussed. **Table 1** gives a comparative analysis of different load balancing techniques with respect to different performance parameters.

In **Table 1** various metrics have been considered to compare different techniques. The metrics on which the existing load balancing techniques have been measured are discussed below:

1. *Throughput*

   This metric is used to estimate the total number of tasks, whose execution has been completed successfully. High throughput is necessary for overall system performance.

2. *Overhead*

   Overhead associated with any load balancing algorithm indicates the extra cost involved in implementing the algorithm. It should be as low as possible.

3. *Fault Tolerance*

Table 1. Comparison of existing Load Balancing Techniques

Metrics/ Techniques	Throughput	Overhead	Fault tolerance	Migration time	Response time	Resource Utilization	Scalability	Performance
Round Robin [22]	YES	YES	NO	NO	YES	YES	YES	YES
Dynamic Round Robin [26]	YES	YES	YES	YES	NO	YES	NO	NO
PALB [8]	YES	YES	YES	YES	YES	YES	NO	NO
Active Monitoring [23]	YES	YES	NO	YES	YES	YES	YES	NO
FAMLB [13]	YES	YES	YES	YES	NO	YES	YES	YES
Min-Min [6]	YES	YES	NO	NO	YES	YES	NO	YES
Max-Min [27]	YES	YES	NO	NO	YES	YES	NO	YES
OLB+LBMM [4]	NO	NO	NO	NO	NO	YES	NO	YES
Throttled [23]	NO	NO	YES	YES	YES	YES	YES	YES
Honeybee Foraging [28]	NO	NO	NO	NO	NO	YES	NO	NO
Active Clustering [28]	NO	YES	NO	YES	NO	YES	NO	NO
Biased Random Sampling [28]	NO	YES	NO	NO	NO	YES	NO	YES

It measures the capability of an algorithm to perform uniform load balancing in case of any failure. A good load balancing algorithm must be highly fault tolerable.

4. *Migration Time*

   It is defined as, the total time required in migrating the jobs or resources from one node to another. It should be minimized.

5. *Response Time*

   It can be measured as, the time interval between sending a request and receiving its response. It should be minimized to boost the overall performance.

6. *Resource Utilization*

   It is used to ensure the proper utilization of all those resources, which comprised the whole system. This factor must be optimized to have an efficient load balancing algorithm.

7. *Scalability*

   It is the ability of an algorithm to perform uniform load balancing in a system with the increase in the number of nodes, according to the requirements. Algorithm with higher scalability is preferred.

8. *Performance*

   It is used to check, how efficient the system is. This has to be improved at a reasonable cost, e.g., reducing the response time though keeping the acceptable delays.

5. CONCLUSION AND FUTURE WORK

In this paper, we have surveyed various load balancing algorithms in the Cloud Computing environment. We discussed major issues which must be taken into consideration while designing any load balancing algorithm. We have discussed the already proposed algorithms by various researchers in literature, their advantages and disadvantages. A comparison has been done on the basis of different criteria like scalability, network overhead, resource utilization, algorithm complexity, fault tolerance, response time, etc. In future we will focus on designing algorithms which will maintain a better trade-off among all performance parameters.

References

[1] A. Khiyaita, M. Zbakh, H. El Bakkali, and D. El Kettani, "Load balancing cloud computing: state of art," in *Network Security and Systems (JNS2), 2012 National Days of*, pp. 106–109, IEEE, 2012.

[2] N. J. Kansal and I. Chana, "Existing load balancing techniques in cloud computing: A systematic review.," *Journal of Information Systems & Communication*, vol. 3, no. 1, 2012.

[3] D. A. Menascé and P. Ngo, "Understanding cloud computing: Experimentation and capacity planning," in *Computer Measurement Group Conference*, 2009.

[4] S.-C. Wang, K.-Q. Yan, W.-P. Liao, and S.-S. Wang, "Towards a load balancing in a three-level cloud computing network," in *Computer Science and Information Technology (ICCSIT), 2010 3rd IEEE International Conference on*, vol. 1, pp. 108–113, IEEE, 2010.

[5] T. D. Braun, H. J. Siegel, N. Beck, L. L. Bölöni, M. Maheswaran, A. I. Reuther, J. P. Robertson, M. D. Theys, B. Yao, D. Hensgen, *et al.*, "A comparison of eleven static heuristics for mapping a class of independent tasks onto heterogeneous distributed computing systems," *Journal of Parallel and Distributed computing*, vol. 61, no. 6, pp. 810–837, 2001.

[6] T. Kokilavani and D. Amalarethinam, "Load balanced min-min algorithm for static meta-task scheduling in grid computing.," *International Journal of Computer Applications*, vol. 20, no. 2, 2011.

[7] T. Anandharajan and M. Bhagyaveni, "Co-operative scheduled energy aware load-balancing technique for an efficient computational cloud.," *International Journal of Computer Science Issues (IJCSI)*, vol. 8, no. 2, 2011.

[8] J. M. Galloway, K. L. Smith, and S. S. Vrbsky, "Power aware load balancing for cloud computing," in *Proceedings of the World Congress on Engineering and Computer Science*, vol. 1, pp. 19–21, 2011.

[9] R. Alonso-Calvo, J. Crespo, M. Garcia-Remesal, A. Anguita, and V. Maojo, "On distributing load in cloud computing: A real application for very-large image datasets," *Procedia Computer Science*, vol. 1, no. 1, pp. 2669–2677, 2010.

[10] Z. Chaczko, V. Mahadevan, S. Aslanzadeh, and C. Mcdermid, "Availability and load balancing in cloud computing," in *International Conference on Computer and Software Modeling, Singapore*, vol. 14, 2011.

[11] A. Iosup, S. Ostermann, M. N. Yigitbasi, R. Prodan, T. Fahringer, and D. H. Epema, "Performance analysis of cloud computing services for many-tasks scientific computing," *Parallel and Distributed Systems, IEEE Transactions on*, vol. 22, no. 6, pp. 931–945, 2011.

[12] S. Sethi, A. Sahu, and S. K. Jena, "Efficient load balancing in cloud computing using fuzzy logic," *IOSR Journal of Engineering*, vol. 2, no. 7, pp. 65–71, 2012.

[13] Z. Nine, M. SQ, M. Azad, A. Kalam, S. Abdullah, and R. M. Rahman, "Fuzzy logic based dynamic load balancing in virtualized data centers," in *Fuzzy Systems (FUZZ), 2013 IEEE International Conference on*, pp. 1–7, IEEE, 2013.

[14] M. E. Soklic, "Simulation of load balancing algorithms: a comparative study," *ACM SIGCSE Bulletin*, vol. 34, no. 4, pp. 138–141, 2002.

[15] A. P. Deshmukh and K. Pamu, "Applying load balancing: A dynamic approach," *International Journal*, vol. 2, no. 6, 2012.

[16] J. Yao, J. Guo, and L. N. Bhuyan, "Ordered round-robin: An efficient sequence preserving packet scheduler," *Computers, IEEE Transactions on*, vol. 57, no. 12, pp. 1690–1703, 2008.

[17] J. Kaur, "Comparison of load balancing algorithms in a cloud," *International Journal of Engineering Research and Applications*, vol. 2, no. 3, pp. 1169–173, 2012.

[18] Z. Bo, G. Ji, and A. Jieqing, "Cloud loading balance algorithm," in *Information Science and Engineering (ICISE), 2010 2nd International Conference on*, pp. 5001–5004, IEEE, 2010.

[19] S. Ray and A. De Sarkar, "Execution analysis of load balancing algorithms in cloud computing environment.," *International Journal on Cloud Computing: Services & Architecture*, vol. 2, no. 5, 2012.

[20] K. Nishant, P. Sharma, V. Krishna, C. Gupta, K. P. Singh, N. Nitin, and R. Rastogi, "Load balancing of nodes in cloud using ant colony optimization," in *Computer Modelling and Simulation (UKSim), 2012 UKSim 14th International Conference on*, pp. 3–8, IEEE, 2012.

[21] S. G. Domanal and G. R. M. Reddy, "Load balancing in cloud computing using modified throttled algorithm," 2013.

[22] S. Subramanian, G. Nitish Krishna, M. Kiran Kumar, P. Sreesh, and G. Karpagam, "An adaptive algorithm for dynamic priority based virtual machine scheduling in cloud.," *International Journal of Computer Science Issues (IJCSI)*, vol. 9, no. 6, 2012.

[23] B. Wickremasinghe, "Cloudanalyst: A cloudsim-based tool for modelling and analysis of large scale cloud computing environments," *MEDC Project Report*, vol. 22, no. 6, pp. 433–659, 2009.

[24] S. Mohapatra, S. Mohanty, and K. S. Rekha, "Analysis of different variants in round robin algorithms for load balancing in cloud computing," *International Journal of Computer Applications*, vol. 69, no. 22, 2013.

[25] A. Gulati and R. K. Chopra, "Dynamic round robin for load balancing in a cloud computing," 2013.

[26] C.-C. Lin, P. Liu, and J.-J. Wu, "Energy-aware virtual machine dynamic provision and scheduling for cloud computing," in *Cloud Computing (CLOUD), 2011 IEEE International Conference on*, pp. 736–737, IEEE, 2011.

[27] Y. Mao, X. Chen, and X. Li, "Max–min task scheduling algorithm for load balance in cloud computing," in *Proceedings of International Conference on Computer Science and Information Technology*, pp. 457–465, Springer, 2014.

[28] M. Randles, D. Lamb, and A. Taleb-Bendiab, "A comparative study into distributed load balancing algorithms for cloud computing," in *Advanced Information Networking and Applications Workshops (WAINA), 2010 IEEE 24th International Conference on*, pp. 551–556, IEEE, 2010.

2014 Fourth International Conference on Communication Systems and Network Technologies

Dynamic Growth of Hidden-Layer Neurons Using the Non-extensive Entropy

Seba Susan and Mayank Dwivedi
Department of Information Technology,
Delhi Technological University, New Delhi, India
e-mail: seba_406@yahoo.in

Abstract—**In this paper we present a dynamic neural network that dynamically grows the number of the hidden-layer neurons based on an increase in the entropy of the weights during training. The weights are normalized to probability values prior to the computation of the entropy. The entropy being referred is the non-extensive entropy proposed recently by Susan and Hanmandlu for the representation of structured data. Incrementally growing the hidden layer as per requirement leads to better tuning of network weights and high classification performance as proved by the empirical results.**

Keywords— Hidden layer neurons; Dynamic Neural Network; Dynamic growth of neurons; Multi-layer perceptron; Susan and Hanmandlu entropy; Non-extensive entropy; Weighted sum of non-extensive entropies

I. INTRODUCTION

The advent of dynamic neural networks marks a significant advancement in the field of machine learning due to the manifold benefits it offers over the conventional neural network with a fixed architecture. The word dynamic refers to either dynamically changing the neural network architecture by adding or deleting neurons [1] or incorporating dynamic units [2]. The use of statistical probability theory for improvisation in the performance of neural networks has been investigated before [3-5]. The scope of using statistics in neural networks is due to the possibility of visualizing the neural network as a statistical model of non-linear regression and discriminant analysis. In [3] for instance the error entropy is minimized instead of the conventional mean square error for adaptive systems training. The Renyi entropy of order α and the Csiszar distance measure is used for the minimization. In [4] efficient training algorithms are devised using Information theoretic learning. The minimum error entropy was used recently in [5] for kernel adaptive filtering and a new kernel minimum error criterion algorithm was developed. The dynamic growth of hidden units and the pruning strategy has been sufficiently investigated in the case of the Radial Basis Function (RBF) neural network [6-9] but relatively less in the case of the feedforward Multi-layer Perceptron (MLP) due to the similarity in the hidden units in the MLP, though related research has picked up recently [10-12]. The growth or pruning of the number of hidden units is mostly decided by the weights emanating from the training process. In [10] the neurons are added and the weights are updated incrementally till the error is minimized. In [11] the neural network is likened to a linear regression model and the selection of optimal number of hidden units is based on the minimization of a risk estimation criterion. Dynamic fuzzy neural networks have also been proposed that perform the addition and deletion of RBF units as the learning progresses [13]. Our paper focuses on the dynamic growth of hidden units in the MLP neural network on a one by one basis as the training progresses, using the non-extensive entropy of weights as the yardstick for effecting a change. The paper is organized as follows: The significance of the hidden layer unit of a MLP neural network is described in brief in Section II. The Susan and Hanmandlu non-extensive entropy is described in Section III. The proposed dynamic growth of hidden layer neurons using the weighted sum of non-extensive entropies is described in Section IV. The empirical results are described in Section V and the overall conclusions are drawn in Section VI.

II. DETERMINING THE HIDDEN LAYER PARAMETERS OF A DYNAMIC NEURAL NETWORK

The feedforward neural network differs from the recurrent neural network in that there is no connection between the hidden units in a single layer. The first layer in a feedforward neural network is the input layer for feeding the inputs into the network, and the last layer is the output layer in which the overall output pertaining to the category or class is available. In between these two layers we have a number of internal or hidden layers each containing a number of hidden units or neurons. The main computing takes place in these layers. Associated with each hidden neuron is a set of weights that are the scales of the connections between the hidden layer neuron and the neurons in the input and output layers. These weights are significant since they are responsible for the fraction of the input that is fed into the activation function of the hidden neuron and thereby influences its output. The hidden layer units are significant due to their ability to interpret the data in a meaningful way. The internal or hidden layers remap the inputs to achieve a more linearly separable representation of the data and hence behave as "feature detectors" [14]. The choice of the number of hidden layers and the number of hidden neurons per layer is a topic of debate, with more the number the more accurate the result, at

978-1-4799-3070-8/14 $31.00 © 2014 IEEE
DOI 10.1109/CSNT.2014.104

a cost of increasing the training time and the network size. Usually the number of hidden neurons is kept lesser than the size of the training data for efficient results [10]. The single-hidden-layer-feedforward network (SLFN) that has several practical applications [15,16] and uses a random number of hidden nodes [17] was improvised by Huang *et al* in [18] to devise a three step learning method called the Extreme Learning Machine (ELM) that does not use back-propagation (BP) or other iterative techniques. Instead of tuning the hidden layer parameters as in traditional neural networks, the ELM generates the hidden layer parameters by calculating the output weights. In [10] the error minimized extreme learning machine (EM-ELM) is used for dynamically growing the hidden layer units in an ELM and updating the output weights simultaneously. In our paper we focus on the conventional SLFN architecture with random number of hidden neurons wherein the weights are first tuned iteratively by back-propagation and then evaluated for ambiguity or a state of chaos which implies an equal status for all connections. Since the entropy function is a measure of the chaos or uncertainty regarding an event, we use it to measure the state of chaos among the weights associated with the hidden layer in the neural network. We grow the hidden layer dynamically by incrementing the hidden neurons by one if the chaos among the weights increases after a training session. Since we desire a state of order or declining entropy as training progresses, we use the Susan and Hanmandlu non-extensive entropy to measure the chaos among the tuned weights, since it is proved successful for the representation of structured information in regular textures [19].

III. THE SUSAN AND HANMANDLU NON-EXTENSIVE ENTROPY

The Susan and Hanmandlu non-extensive entropy was proposed as a feature for texture identification and classification [19]. Its specialty lies in identifying regular textures containing repetitive patterns that translate to high co-occurrence probabilities. The non-extensive entropy function as defined by Susan and Hanmandlu is given below.

Consider a random variable $X=\{x_1,x_2,\ldots,x_n\}$ with the associated probabilities $P=\{p_1,p_2,\ldots p_n\}$. Assume that the probability distribution is complete i.e. $p_i \in [0,1]$ and $\sum_{i=1}^{n} p_i = 1$ for i=1,2,…n where, n is the number of probabilistic experiments.

Let the information gain on the ith event of X with an associated probability p_i be defined by the Gaussian function

$$I(p_i) = e^{-p_i^2} \tag{1}$$

The non-extensive entropy of X is then defined as

$$H(P) = E(I(p_i)) = \sum_{i=1}^{n} p_i I(p_i) = \sum_{i=1}^{n} p_i e^{-p_i^2} \tag{2}$$

The entropy in (2) is non-extensive due to its non-additive property which holds true under all conditions unlike Tsallis entropy [20] which is pseudo-additive and behaves like the extensive or additive Shannon entropy [21] under certain conditions. The normalized entropy H_N is of the form

$$H_N = \frac{H - H_{\min}}{H_{\max} - H_{\min}} \tag{3}$$

i.e.

$$H_N = \frac{H - e^{-1}}{e^{-\frac{1}{n^2}} - e^{-1}} \tag{4}$$

It is especially at an advantage when computing the entropy in a structured environment as opposed to Shannon entropy which serves best for finding the entropy in a chaotic environment, as proved in the fuzzy domain [22].

IV. DYNAMICAL GROWTH OF HIDDEN UNITS USING THE NON-EXTENSIVE ENTROPY OF NORMALIZED WEIGHTS

The weighted sum of non-extensive entropies over two consecutive frame pairs was used in [23] for the detection of video anomalies. The significance of this weighted sum is that any significant departure from the normal will result in a positive spike indicating an anomaly. In our work we compute over time the weighted sum of non-extensive entropies associated with the trained weights of a feedforward network, tuned by back-propagation. A positive spike or an increase in the weighted sum indicates an anomaly in training inputs and increments the number of hidden neurons by one. The weighted sum of non-extensive entropies, also called the entropy of the source $H(S)$ is defined as

$$H(S) = \sum_{x \in X} p(x) H(p(y|x)) \tag{5}$$

Solving for the entropy $H(p(y|x))$ using (2), we have

$$H(p(y|x)) = \sum_{y \in Y} p(y|x) e^{-p(y|x)^2} \tag{6}$$

Here $p(x)$ denotes the probability associated with the weight between the output neuron and the x^{th} hidden unit. The set $\{p(y|x)\}$ indicates the probabilities associated with the input connection weights of the x^{th} hidden unit, and $H(p(y|x))$ is the non-extensive entropy associated with $\{p(y|x)\}$ computed using (6).

The multi-layer perceptron architecture 4-3-1 with the actual weights associated with each layer is shown in Fig. 1. Let $w_{ki}^{\ t}$ denote the weight associated with the connection between the kth input dimension and the ith hidden layer neuron after the training of the tth training data sample. The computation of the entropy in (5) from the network weights $\{w_{ki}^{\ t}\}$ and $\{w_{ij}^{\ t}\}$ is explained below. The normalized weights $\{w_{kiN}^{\ t}\}$ are obtained from $\{w_{ki}^{\ t}\}$ by transforming the value of the weights $\{w_{ki}^{\ t}\}$ in the range of 0 to 1, and dividing by the total sum of weights as shown in (7) and (8).

$$w_{kip}^{\ t} = \frac{w_{ki}^{\ t} - \min_{\forall k}(w_{ki}^{\ t})}{\max_{\forall k}(w_{ki}^{\ t}) - \min_{\forall k}(w_{ki}^{\ t})}, \text{k=1,2,3,…,M} \tag{7}$$

$$w_{kiN}^{\ t} = \frac{w_{kip}^{\ t}}{\sum_{i=1}^{M} w_{kip}^{\ t}}, \text{k=1,2,3,…,M} \tag{8}$$

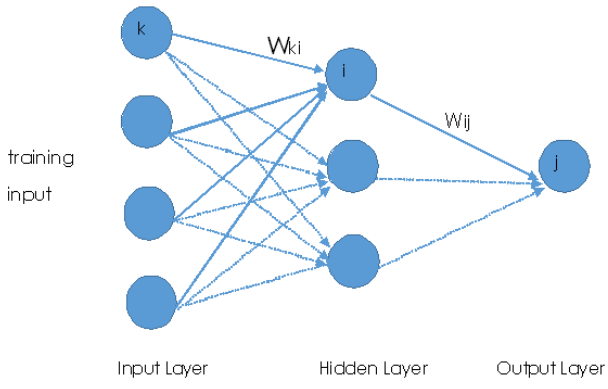

Fig. 1 The multi-layer perceptron (MLP) neural network and the connection weights during training

Here M is the number of connection weights between the input layer and the hidden neuron i. The normalized weights $\{w_{1iN}{}^t, w_{2iN}{}^t, ..., w_{MiN}{}^t\}$ are equal to probability values $\{p(y|x)\}$ for a given x, with values in the range of 0 to 1 and $\sum_{k=1}^{M} w_{kiN}{}^t = 1$. This probability distribution can be used for the computation of the entropy $H(p(y|x))$ using (6). The probabilities $\{p(x)\}$ associated with the H hidden neurons and the single output neuron $(j=1)$ are the normalized weights $\{w_{ijN}{}^t\}$ which are computed from $\{w_{ij}{}^t\}$ in a similar manner. The weighted sum of non-extensive entropies given by (5) is generalized for O equally significant outputs as

$$H(S) = \sum_{j=1}^{O} \frac{1}{O} \sum_{i=1}^{H} w_{ijN}{}^t \sum_{k=1}^{M} w_{kiN}{}^t e^{-w^2_{kiN}{}^t} \qquad (9)$$

In our example $O=1$. The entropy value computed using (9) for the t^{th} training sample is compared with the entropy value for the previous training data sample $t-1$. If a positive spike in entropy $H(S)$ is encountered, the number of hidden neurons is increased by one and the training proceeds for sample $t+1$. A single memory storage for the previous entropy value is only required for comparison purpose. The steps of the proposed method are summarized below.

1. Initialize the neural network architecture with 3 hidden neurons with all network weights initialized to 0.1.
2. Tune the weights for a training input using BP.
3. Calculate the probabilities of the tuned weights of each layer using (7) and (8).
4. Compute the weighted sum of non-extensive entropies of the tuned network using (9).
5. If this entropy value is greater than that for previous training sample then increment the number of hidden neurons by one, its weights being initialized to 0.1.
6. Repeat the training process for the next sample using the tuned weights of the existing neurons and the newly added neuron.
7. Repeat above steps 2-6 until the training is complete.

The highlight of our method is thus that a new computational unit is added whenever an unusual pattern occurs in the training. This trend was also observed before in the case of the Resource-allocating network in [24] which however requires memorizing of specific input patterns that perform poorly, in order to achieve desired accuracy.

V. EXPERIMENTAL RESULTS

The single hidden layer Multi-layer Perceptron 4-3-1 shown in Fig. 1 is used as the initial configuration for our experiments, with a learning rate η of 0.2 and an error threshold ε of 0.01. The number of hidden layer units is initialized to 3 at the beginning of the training procedure and is grown dynamically as explained in Section IV. The coding is done in the C++ platform on a 2.2 GHz Pentium processor. The experiments are conducted on a linearly separable synthetic dataset containing 100 data samples distributed into two classes shown in Fig. 2. The result of the dynamic growth of hidden neurons as training progresses is shown in Table 1 for both non-extensive and extensive entropy. As observed from the slow growth of hidden nodes in Table 1, when consecutive training patterns follow a similar pattern irrespective of the actual range of values, the non-extensive entropy of the weights decreases (or remains stable) indicating a decline in the chaos in the weights as some weights are assigned higher values than the others due to the higher significance of their connections. An unnatural training pattern is said to be encountered when it is different from its predecessors in its relationship between the features, training samples 9 and 34 in Table 1 being examples where feature 2 and 3 are closer than usual. The distinct training inputs are detected correctly by the non-extensive entropy (samples 4,9,34,36) while the Shannon entropy is highly sensitive and includes lots of false alarms (samples 2,5,7,18,33,35,39), for instance sample 2 is a normally occurring pattern in the dataset. This fact was also observed for the video anomaly example in [23] where Shannon entropy gives rise to false alarms due to random crowd movement. The results are summarized in Table 2 for the proposed dynamic neural network and the static neural network with fixed number of hidden neurons. We observe a slow and steady rise of the number of hidden neurons for the non-extensive entropy (hidden nodes=7), while Shannon entropy results in growth of 11 hidden neurons taking more training time than the non-extensive entropy. Apart from a reduced MLP architecture with only 7 hidden nodes, the overall training time required by the proposed method is much less than the equivalent fixed neuron architecture, while its classification performance (98.33%) is higher than any possible static neural network configuration. This suggests that the dynamic growth of hidden layer as proposed in our work not only gives the optimal number of hidden neurons for a dataset, at the same time it provides a better tuning of weights and faster training than any static neural network configuration.

VI. CONCLUSIONS

In this paper, the dynamical growth of hidden units is proposed that is based on the non-extensive entropy of the network weights that are normalized to probability values. A decrease in entropy of weights is observed as the training progresses and if this criterion is not met the number of hidden units is incrementally increased. The performance is improved as compared to the fixed architecture feedforward neural network in terms of convergence and testing accuracy. The highlight of our approach is that it can grow the hidden-layer dynamically while training and the weights are tuned better than any configuration of the static neural network leading to high classification performance.

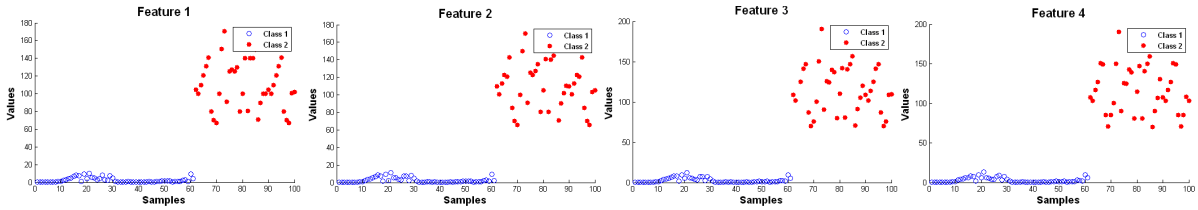

Fig. 2 The linearly separable four dimensional artificial dataset used for the experimentation

Table 1: Growth of hidden neurons dynamically using the proposed method for training set of 40 samples

Training input Sample number	Training Feature 1	Training Feature 2	Training Feature 3	Training Feature 4	Class	Growth of hidden neurons using the non-extensive Susan and Hanmandlu entropy	Growth of hidden neurons using the extensive Shannon entropy
1	0.01	0.02	0.03	0.04	1	3	3
2	0.4	0.5	0.6	0.7	1	3	**4**
3	0.10	0.11	0.12	0.13	1	3	4
4	**0.12**	**0.1**	**0.16**	**0.18**	1	**4**	4
5	0.35	0.25	0.45	0.55	1	4	**5**
6	0.55	0.40	0.56	0.65	1	4	5
7	0.05	0.06	0.07	0.08	1	4	**6**
8	0.61	0.63	0.67	0.69	1	4	6
9	**0.71**	**0.73**	**0.74**	**0.77**	1	**5**	6
10	0.94	0.91	0.93	0.95	1	5	**7**
11	2.3	2.5	2.57	2.9	1	5	7
12	3.1	3.25	3.7	3.9	1	5	7
13	4.3	4.5	4.7	4.9	1	5	7
14	5.1	5.4	5.6	5.9	1	5	7
15	6.7	6.9	6.4	6.45	1	5	7
16	8.0	8.5	8.3	8.4	1	5	7
17	7.5	7.7	7.9	7.2	1	5	7
18	1.2	1.3	1.5	1.7	1	5	**8**
19	9.2	9.3	9.5	9.7	1	5	8
20	3.9	2.4	5.4	5.9	1	5	8
21	10.0	11.1	12.2	13.3	1	5	8
22	5.2	5.5	5.7	5.9	1	5	8
23	5.1	5.3	5.4	5.7	1	5	8
24	3.2	3.4	3.6	3.8	1	5	8
25	3.9	3.1	3.5	3.7	1	5	8
26	7.9	7.4	7.2	7.5	1	5	8
27	3.2	7.7	7.5	9.2	1	5	8
28	2.3	2.5	2.7	2.9	1	5	8
29	7.3	7.9	7.7	7.5	1	5	8
30	4.7	4.55	4.3	4.1	1	5	8
31	1.2	1.9	1.59	1.7	1	5	8
32	104.5	109.6	108.7	107.8	2	5	8
33	100	101	102	103	2	5	**9**
34	**110**	**113**	**114**	**117**	2	**6**	9
35	121	123	125	127	2	6	**10**
36	**131**	**121**	**141**	**151**	2	**7**	10
37	141	143	147	149	2	7	10
38	80.1	85.11	87.2	84.9	2	7	10
39	70.0	70.2	70.3	70.7	2	7	**11**
40	67.2	65.5	75.5	85.0	2	7	11

Table 2: Performance analysis of the proposed dynamic neural network and various static neural network configurations, in terms of training time in secs (s), number of hidden nodes and the testing accuracy in (%). (Proposed method is shown in gray)

Methods	Dynamic growth of hidden neurons using Susan and Hanmandlu entropy	Dynamic growth of hidden neurons using Shannon entropy	Static 3 hidden neuron	Static 7 hidden neuron	Static 11 hidden neuron	Static 22 hidden neuron	Static 34 hidden neuron	Static 40 hidden neuron
Total training time (for 40 samples)	0.39s	0.78s	0.25s	0.51s	0.58s	0.6s	0.62s	0.62s
Number of hidden nodes	7	11	3	7	11	22	34	40
Testing Accuracy (for 60 samples)	98.33%	98.33%	83.4%	83.4%	93.4%	93.4%	83.4%	83.4%

REFERENCES

[1] Yang, Hong, and Jun Ni. "Dynamic neural network modeling for nonlinear, nonstationary machine tool thermally induced error." *International Journal of Machine Tools and Manufacture* 45.4 (2005): 455-465.

[2] Gupta, Madan M., Liang Jin, and Noriyasu Homma. *Static and dynamic neural networks: from fundamentals to advanced theory*. Wiley-IEEE Press, 2004.

[3] Erdogmus, Deniz, and Jose C. Principe. "An error-entropy minimization algorithm for supervised training of nonlinear adaptive systems." *Signal Processing, IEEE Transactions on* 50.7 (2002): 1780-1786.

[4] Ben-David, Arie. "Monotonicity maintenance in information-theoretic machine learning algorithms." *Machine Learning* 19.1 (1995): 29-43.

[5] Morejon, Rodney A., and Jose C. Principe. "Advanced search algorithms for information-theoretic learning with kernel-based estimators." *Neural Networks, IEEE Transactions on* 15.4 (2004): 874-884.

[6] Ciabattoni, Lucio, et al. "Supervisory control of PV-battery systems by online tuned neural networks." *Mechatronics (ICM), 2013 IEEE International Conference on*. IEEE, 2013.

[7] Yingwei, Lu, Narashiman Sundararajan, and Paramasivan Saratchandran. "Performance evaluation of a sequential minimal radial basis function (RBF) neural network learning algorithm." *Neural Networks, IEEE Transactions on* 9.2 (1998): 308-318.

[8] Huang, Guang-Bin, Paramasivan Saratchandran, and Narasimhan Sundararajan. "An efficient sequential learning algorithm for growing and pruning RBF (GAP-RBF) networks." *Systems, Man, and Cybernetics, Part B: Cybernetics, IEEE Transactions on* 34.6 (2004): 2284-2292.

[9] Wu, Shiqian, and Meng Joo Er. "Dynamic fuzzy neural networks-a novel approach to function approximation." *Systems, Man, and Cybernetics, Part B: Cybernetics, IEEE Transactions on* 30.2 (2000): 358-364.

[10] Feng, Guorui, et al. "Error minimized extreme learning machine with growth of hidden nodes and incremental learning." *Neural Networks, IEEE Transactions on* 20.8 (2009): 1352-1357.

[11] Lan, Yuan, Yeng Chai Soh, and Guang-Bin Huang. "Constructive hidden nodes selection of extreme learning machine for regression." *Neurocomputing* 73.16 (2010): 3191-3199.

[12] Kurino, Ryusuke, Masanori Sugisaka, and Katsunari Shibata. "Growing neural network with hidden neurons." *Proc. 9th Int. Symp. on Artificial Lifeand Robotics (AROB'04)*. Vol. 1. 2004.

[13] Wu, Shiqian, and Meng Joo Er. "Dynamic fuzzy neural networks-a novel approach to function approximation." *Systems, Man, and Cybernetics, Part B: Cybernetics, IEEE Transactions on* 30.2 (2000): 358-364.

[14] Robert J.Schalkoff, **Artificial Neural Networks**, McGraw-Hill, 2011.

[15] Singh, Rampal, and S. Balasundaram. "Application of extreme learning machine method for time series analysis." *International Journal of Intelligent Technology* 2.4 (2007): 256-262.

[16] Huynh, Hieu Trung, Jung-Ja Kim, and Yonggwan Won. "Performance comparison of SLFN training algorithms for DNA microarray classification." *Software Tools and Algorithms for Biological Systems*. Springer New York, 2011. 135-143.

[17] Huang, Guang-Bin, Lei Chen, and Chee-Kheong Siew. "Universal approximation using incremental constructive feedforward networks with random hidden nodes." *Neural Networks, IEEE Transactions on* 17.4 (2006): 879-892.

[18] Huang, Guang-Bin, Lei Chen, and Chee-Kheong Siew. "Universal approximation using incremental constructive feedforward networks with random hidden nodes." *Neural Networks, IEEE Transactions on* 17.4 (2006): 879-892.

[19] Seba Susan, Madasu Hanmandlu, "A Non-Extensive entropy feature and its application to texture classification", *Neurocomputing,* Volume 120, November 2013, pp. 214–225.

[20] Tsallis, Constantino. "Possible generalization of Boltzmann-Gibbs statistics." *Journal of statistical physics* 52.1-2 (1988): 479-487.

[21] C.E.Shannon, "A Mathematical theory of communication", *The Bell system Technical Journal*, Vol.27, pp.379-423 July,1948.

[22] Seba Susan, Madasu Hanmandlu," A novel Fuzzy Entropy based on the Non-Extensive Entropy and its application for feature selection"*, FUZZ-IEEE 2013*

[23] Susan, Seba, and Madasu Hanmandlu. "Unsupervised detection of nonlinearity in motion using weighted average of non-extensive entropies." *Signal, Image and Video Processing* (2013): 1-15.

[24] Platt, John. "A resource-allocating network for function interpolation." *Neural computation* 3.2 (1991): 213-225.

IOSR Journal of Mechanical and Civil Engineering (IOSR-JMCE)
e-ISSN: 2278-1684,p-ISSN: 2320-334X, Volume 11, Issue 3 Ver. IV (May- Jun. 2014), PP 07-11
www.iosrjournals.org

Effect of tool pin profile on mechanical properties of Al6082 and Al6082-Cu composite by friction stir processing

Vikrant Yadav[1], Vinay Kumar[2], Vatsalya Tiwari[3]
[1,2,3]*(Delhi Technological University, India)*

Abstract : *With the surge of applications incorporating MMCs which provide enhanced mechanical properties, the need of better technologies for fabrication of these materials has attracted lot of work. One of the latest techniques to produce these specialised defect-free materials is Friction Stir Processing (FSP) which is derived from the principles of Friction Stir Welding. In the present study, a metal matrix composite was fabricated by using Al-6082 T651 alloy as the substrate. Copper particles with 37µm particle size were the added reinforcement. Two tool pin profiles; a square profile and a threaded cylindrical profile, were employed to carry out the processing. With each tool pin profile, two specimens; one with reinforcement and one without reinforcement, were processed. The five specimens including the base metal were then critically examined for changes in mechanical properties. Rockwell test for hardness was conducted and tensile properties evaluated using digital UTM.*

Keywords - *MMC, Aluminium 6082, Tool Pin Profile, Tensile Properties, Hardness, Elongation.*

I. Introduction

The modern high service applications in aerospace, automotive and other manufacturing sectors call for high duty materials that can provide long life under extreme conditions of service. Employment of metal-matrix composites (MMCs) serves the purpose. The reinforcing material can be another metal (Cu, Mn, etc.) or ceramic phases (SiC, WC, TiC, etc.). These materials exhibit high strength, high elastic modulus and improved resistance to wear, creep and fatigue. However these also suffer from loss in ductility and toughness due to incorporation of reinforcement in the main core [1]. It is hence desirable that only the surface layer is fabricated by the foreign material so that the main bulk retains the toughness and surface layer develops the requisite hardness and hence wear resistance. MMCs are obviously costlier than the parent material and hence lot of work has gone in past few decades to develop and optimise new technologies to have low cost but effective composite materials.

Aluminium alloy 6082 is a medium strength alloy and has the highest strength of the 6000 series alloys. It is known as a structural alloy and used in applications involving high stresses, in trusses, bridges, cranes, milk churns and transport applications. As a relatively new alloy, the higher strength of 6082 has led to replacement of alloy 6061 in many applications. It also characterizes excellent corrosion resistance, good weldability and machinability. Recent works have revealed that addition of Mn, Mg and/or Cu phases in aluminium matrix have significantly improved the mechanical properties of the materials. Out of various surface fabrication techniques, a latest and cost effective technique namely Friction Stir Processing (FSP) has witnessed a lot of work since its inception in the past decade. FSP was developed by Mishra et al. [2,3] based on basic principles of friction stir welding (FSW). FSW was developed at The Welding Institute (TWI) of UK in 1991 as a solid state joining process [4]. A non consumable rotating tool consisting of a pin and shoulder is inserted into given material and traversed along a desired line for microstructural modification in that region [1]. The intense frictional heating and plastic deformation leads to formation of defect free, recrystallised and fine grained equiaxed microstructure. FSP performed on 5083Al using nano-sized Cu particles showed higher tensile strength, ultimate tensile strength, elongation and hardness than the base metal [5]. On a work with hybrid MMC using Al5083 plate with SiC and MoS_2 particles, the hardness and wear resistance properties were improved by FSP [6]. Even dispersion of fullerene into A5083 matrix using FSP resulted in increased microhardness by promotion of grain refinement due to pinning effect and high hardness of fullerene particles [7].

In the present investigation, Aluminium 6082 and Copper reinforcement have been used as very little work has gone into study of this particular alloy with any reinforcement. FSP is employed to generate MMCs using Aluminium 6082-T651 plate with copper particle reinforcement with two different tool pin profiles and to study the effect on mechanical properties due to both inclusion of Cu in the matrix and the variation of tool profile. Square and threaded cylindrical pin profiles were employed and copper powder with 400 mesh size added in the aluminium substrate.

II. Experimental Procedure

Commercial 6082-T651 Aluminium plates – 6mm thick, 70mm wide and 230mm, 4 plates in total were cut out from a parent sheet using an automatic wire cut machine. The composition of Aluminium 6082-T651 by weight is Mn 1%, Mg 1.2%, Si 1.3%, Fe 0.5% and Zn Ti Cr in small amounts and balance Aluminium. The tools were made of AISI H-13 Tool Steel with two pin profiles ; square and threaded cylindrical profiles, both concentric with flat circular shoulders. One tool was made with no pin i.e. a flat tool for the purpose of covering up the composite copper metal powder. The dimensions of the tool are shown in Table 1.

Table 1: Tool Dimensions

Dimension	Values
Shoulder Diameter	16mm
Pin Depth	2.5mm
Diameter of pin of circular cross section	5.5mm
Side of pin of square cross section	3.89mm
Pitch of threads	1.5 Threads per mm

The copper metal powder used was of 300 mesh size. Friction stir process was carried out on a vertical milling machine. Four cases were considered; 1) FSP with cylindrical tool pin, 2) FSP with square profile tool pin, 3) FSP with cylindrical tool pin with copper metal powder reinforcement and 4) FSP with square profile tool pin with copper metal powder reinforcement.

The tool rotation rate used was 1000 rpm and the transverse speed of the tool was 16mm per second in all the cases. Single pass processing was simply done on the plates using the simple cylindrical and the square profile tool.

For FSP using the copper powder, a groove of depth 2mm and width 2mm was cut along the length of two of the plates. Copper metal powder was filled in the groove and the groove containing the powder was covered by processing the plate once by the flat shoulder tool. Two such plates were prepared and further processing was done using the threaded cylindrical tool and a square profile tool. After all the plates were processed, test specimen for tensile strength, microstructure and hardness were cut from the FSPed region of the processed plates. The specimen cut for hardness test was of circular profile of diameter 10mm. The specimens went under Rockwell Hardness Testing Machine, with class B, Shell Ball type indenter (Dia=1/16th Inches) with major load-100kgf and minor load 10Kgf. For tensile Strength, four dogbone specimens were prepared from the processed plates and one from the base plate as per ASTM standards. Tests were conducted on the specimens using Digital UTM.

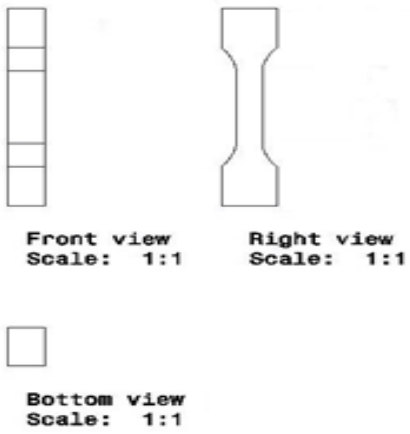

Fig.1: Tension Test Specimen

III. Results And Discussions

3.1 Tensile Strength and Hardness

Table 2: UTS values

Specimen	Ultimate Tensile Strength (MPa)
Base metal without composites	316
Threaded Cylindrical profile without composite	152
Square Profile without composites	133
Threaded Cylindrical Profile with composites	161
Square Profile with Composite	156

Table 3: Hardness Rockwell B (HRB) values

Specimen	Hardness B Rockwell
Base metal without composites	33
Threaded Cylindrical profile without composite	70
Square Profile without composites	64
Threaded Cylindrical Profile with composites	84
Square Profile with Composite	77

The base metal exhibited highest ultimate tensile strength (UTS) of 316MPa but lowest hardness of 33B Rockwell. The specimen processed without copper reinforcement had UTS of 152MPa and Hardness of 74B Rockwell for processing done with threaded cylindrical profile tool whereas a UTS of 133MPa and Hardness of 64B Rockwell for processing done with square profile tool. For sample processed with copper powder using the threaded cylindrical tool pin profile, UTS of 161 MPa and hardness of 84B Rockwell was obtained whereas for the processing using square profile tool with reinforcement, UTS of 156MPa and Hardness of 77B Rockwell was measured.

The samples processed without the Cu powder were defect free and the stir zone was characterised by equiaxed and finer grains due to severe plastic deformation and frictional heating leading to recrystallisation [5,8,9]. On the contrary, the specimens processed with the copper composite possessed groove defects and great particle agglomeration leading to non homogeneous properties inferior to that of the base metal. The probable reason for the defects is wider gap of powder filled slot as well as too high a rotational speed and traverse speed.

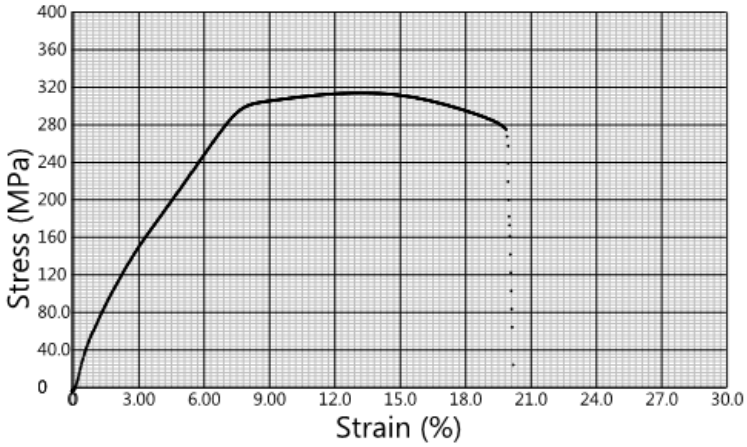

Fig.1: Stress-Strain Curve For Pure Al-6082 profile

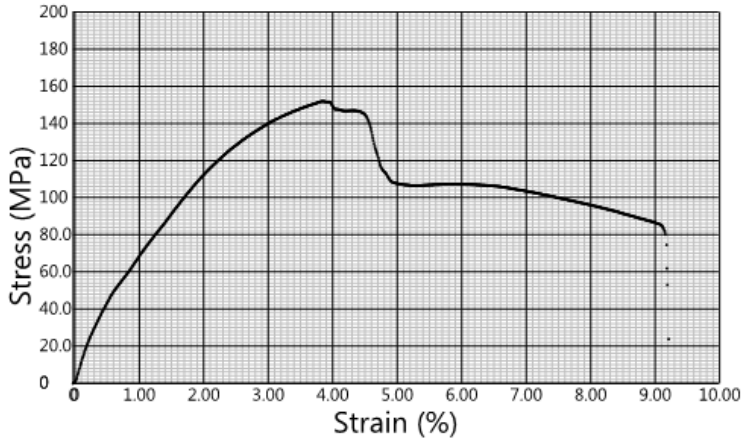

Fig.2: Stress-Strain Curve for Plate processed with threaded cylindrical pin profile

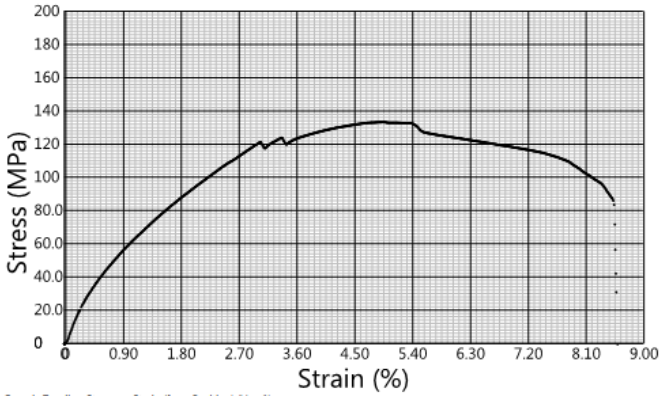

Fig.3: Stress-Strain Curve for Plate processed with square pin profile

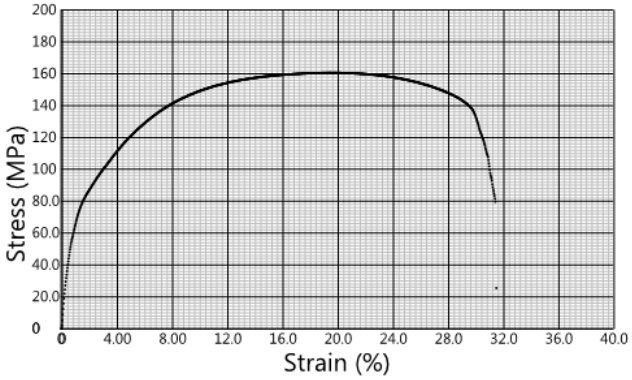

Fig.4: Stress-Strain Curve for Plate processed with metal composite and threaded Cylindrical pin profile

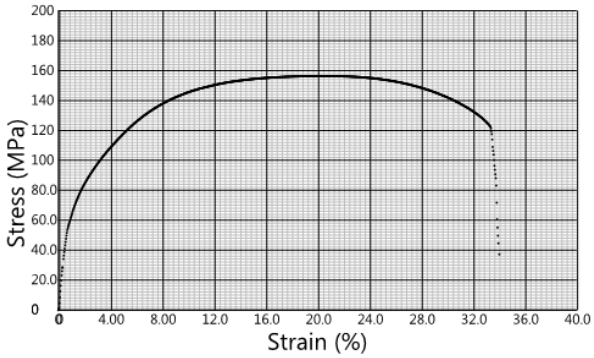

Fig 5: Stress-Strain Curve for Plate processed with metal composite and Square pin profile

In specimen processed without reinforcement, a fall in the UTS values is observed as compared to the base metal (314MPa). For specimen processed with threaded cylindrical profile tool, the UTS of 152MPa is higher than that of 133MPa for the square profile tool. The reason to this can be attributed to the whirling effect of the threads on the threaded cylindrical tool. But the overall decrease compared to the base metal can be attributed to the high rotational speed of 1000rpm, which on one hand did cause severe plastic deformation by breaking grains to smaller size but at the same time also led to greater heat input to the stirred zone leading to grain growth and hence deterioration of properties concerning both UTS and hardness.

The specimens processed with copper powder too showed a decline in tensile properties when compared to base metal but an increment to properties was seen when compared with the specimens processed without copper. The UTS of 161 MPa for plate processed with Cu using threaded cylindrical profile was higher to that of 156MPa of the plate processed using square profile with Cu. The greater strength obtained using threaded cylindrical profile is again attributed to the whirling action of revolving threads of threaded cylindrical profile which was absent in case of square profile. Also at the given combination of rotational speed (1000rpm) and traverse speed (16mm/s), the eccentric stirring of square profile [10] became less effective compared to the whirling action of threaded cylindrical profile. The higher strengths of the composite specimens compared to the specimens processed without reinforcement is explained with the help of Orowan Theory [5,11]. According to

Orowan theory, when the rotational speed increases, more intermetallic phases are formed. Homogeneous distribution of particles in stirred zone pins the dislocations and enhances the strength and hardness values. With respect to given study, the intermetallic phase formed was $CuAl_2$ which caused effective precipitation hardening. But the overall decrease in tensile properties to base metal was attributed to high rotational speed which led to high heat input and consecutive grain growth.

3.2 Percentage Elongation

Table 4: Percentage Elongation Values

Specimen	Percentage Elongation (%)
Base metal without composites	19.9
Threaded Cylindrical profile without composite	30.9
Square Profile without composites	33.4
Threaded Cylindrical Profile with composites	9.18
Square Profile with Composite	8.14

With regards to percentage elongation, the specimens processed without Cu possessed the highest elongation values as evident from a value of 30.9% for the processing done with threaded cylindrical profile tool and 33.4% for square tool profile processing. The values obtained in case of composite processed with threaded cylindrical tool and square tool of 9.18% and 8.14% respectively are the lowest compared to the base metal with 19.9% and the non-composite specimens. This is due to the fact that the copper particles as well as the intermetallic phases formed provide pinning effect to movement of dislocations in case of composite specimens and hence lower elongation or ductility[12]. But these are absent in the specimens without composite and base metal and hence greater elongation values.

IV. Conclusion

The UTS of the base metal (314MPa) decreases after processing without composite (133-152MPa). It was observed that the UTS of samples processed using cylindrical threaded tool profile (152MPa) is more than that of square profile (133MPa). For sample processed with copper composite using the threaded cylindrical tool pin profile, UTS of 161 MPa whereas for the processing using square profile tool with composite, UTS of 156MPa was measured. Better hardness values were obtained for plates processed with composite (77HRB – 84HRB) compared to those measured for non composite processed plates (64HRB- 70HRB). It was also observed that the percentage elongation in the specimen without composite (30.9%-33.4%) were higher than those with composite.

The Al-6082–Cu MMC can have possible applications in fields requiring high surface hardness values, especially for localized treatment of machine components that suffer extensive wear during service. Also the non composite Friction Stir Processed Al- 6082 can have varied applications in fields like automotive, aerospace and other metal forming sectors that desire high plasticity as achieved through application of FSP. But the optimum values of the process parameters needs to be selected so as to avoid degradation in tensile properties.

References

[1] R.S Mishra, Z.Y Ma, I Charit, Friction stir processing: a novel technique for fabrication of surface composite, Material Science and Engineering, A 341(2003) 307-310.
[2] R.S. Mishra, M.W. Mahoney, S.X. McFadden, N.A. Mara, A.K. Mukherjee, Scripta Mater 42 (2000) 163.
[3] R.S. Mishra, M.W. Mahoney, Mater. Sci. Forum 357-359 (2001) 507.
[4] Thomas WM et al., Patent Application No. 9125978.8, December 1991.
[5] M.Zohoor, M.K. Besharti Givi, P.Salam, Effect of processing parameters on fabrication of Al-Mg/Cu composites via Firction Stir Processing, Materials and Design 39(2012) 358-365.
[6] S.Soleymani, A.Abdollah-zadeh, S.A.Alidokht, Microstructural and tribological properties of Al5083 based surface hybrid composite produced by FSP, WEAR, 278-279(2012) 41-47.
[7] Y.Morisada, H.Fujii, T.Nagaoka, K.Nogi, M.Fukusumi, Fullerene/A5083 composites fabricated by material flow during FSP, Composites Part A. 38(2007)2097-2101.
[8] Zahmatkesh B, Enayati MH, Karimzadeh F, Tribological and microstructural evaluation of friction stir processed AL2024 alloy. Mater Des 2010;31(10):4891-6
[9] Kumbhar NT, Sahoo SK, Samajdar I, Dey GK, Bhanumurthy K, Microstructural and microtextural studies of friction stir welded aluminium alloy5082. Mater Des 2011;32(3):1657-66
[10] Elangovan K, V. Balasubramanian V,Influences of tool pin profile and welding speed on the formation of friction stir processing zone in AA2219 aluminium alloy. Journal of material processing technology 200(2008) 163-175.
[11] Azizieh M.,Kokabi AH, Abachi P, Effect of rotational speed and probe profile on microstructure and hardness of AZ31/Al2O3 nanocompposites fabricated by friction stir processing, Mater Des 2011;32(4):2034-41.
[12] Zhang Z, Chen DL., Consideration of Orowan strengthening effect in particulate reinforced metal matrix nanocomposites: a model for predicting their yield strength. Scripta Mater 2006;54(7):1321-6.

Energy-efficient Wireless Network-on-Chip Architecture with Log-Periodic On-Chip Antennas

Md Shahriar Shamim,
Naseef Mansoor,
Amlan Ganguly
Rochester Institute of Technology
(ms5614,nxm4026,amlan.ganguly)@rit.edu

Aman Samaiyar
Delhi Technological University
aman.samaiyar@dce.edu

Sujay Deb,
Shobha Sunndar Ram
Indraprastha Institute of Technology
(sdeb,shobha)@iiitd.ac.in

ABSTRACT
On-chip wireless interconnects have emerged as a promising alternative to conventional wireline interconnects in Network-on-Chip (NoC) fabrics for multicore systems. However, it is not practical in the immediate future to arbitrarily scale up the number of wireless links without innovations in the physical layer. Here, we explore the design of a directional on-chip antenna based on a log-periodic structure. In this paper we propose the design of a wireless NoC (WiNoC) architecture with concurrent wireless links using these directional on-chip antennas. Through cycle accurate simulations we demonstrate that this novel WiNoC architecture attains better performance and energy efficiency compared to the state-of-the-art token based WiNoC of similar topology.

Categories and Subject Descriptors
C.2.1 **[Computer-Communication Networks]**: Network Architecture and Design

General Terms
Performance, Design.

Keywords
Network-on-Chip; wireless interconnect; directional antenna.

1. INTRODUCTION
In the era of multicore chips the number of cores per chip is predicted to increase up to several hundreds in the near future. Networks-on-Chips (NoCs) have emerged as a communication backbone for such systems. Conventional NoCs with metal/dielectric based interconnects are not scalable in terms of performance and energy consumption due to long multi-hop wireline paths. On-chip wireless interconnects are shown to alleviate this problem by introducing direct long-range links [1]. Many on-chip wireless architectures are explored with different physical layer design technologies. However, the CMOS process-compatible zig-zag antennas [1] widely studied in on-chip environments so far do not have good directional characteristics. Moreover, creating multiple millimeter-wave transceivers tuned to non-overlapping channels to enable concurrent links is an extremely challenging problem. Therefore some wireless NoC (WiNoC) architectures adopt a token passing based wireless medium access mechanism to transmit data over the shared wireless channel. Although this is a simple distributed mechanism without the need for any centralized synchronization, only a single transmitter can access the wireless channel at any given instant of time. This limits the performance benefits of the wireless interconnection although multiple transceivers are deployed over the entire NoC. In this paper, we propose to use log periodic on-chip directional antennas to enable multiple concurrent links, which will eventually improve performance and energy efficiency of the WiNoC.

GLSVLSI'14, May 21–23, 2014, Houston, Texas, USA.
ACM 978-1-4503-2816-6/14/05
http://dx.doi.org/10.1145/2591513.2591566

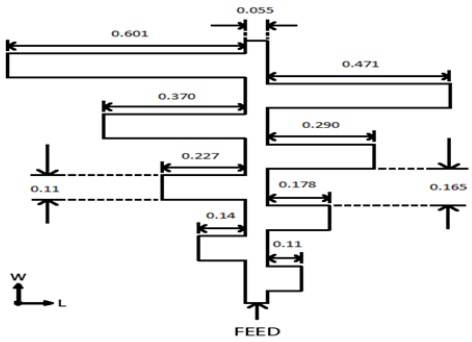

Figure 1. On-chip planar log periodic antenna with dimensions in mm

2. WIRELESS NOC ARCHITECTURE
The architecture and consequently the performance of the WiNoC with directional antennas (DWiNoC) strongly depend on the physical layer design strategy, which are discussed in this section.

2.1 Physical Layer
In this section we discuss the directional log-periodic antenna we propose to use in the DWiNoC. Planar log periodic antennas (PLPA) are very popular and widely studied for their ease of manufacturing and for their wide-band properties [2]. In this paper, we propose the design for an on-chip planar log-periodic antenna with wide bandwidth and high end-fire directivity in the millimeter wave frequency range. The generalized design parameters allow the flexibility towards designing the antennas for specified frequencies. The design of the log-periodic antenna adopted in this paper with eight teeth is shown in Figure. 1. The sizes of the teeth increase in a logarithmic manner. The dimensions mentioned in the figure are specifically for 60 GHz and can be scaled appropriately for any desired frequency of operation within micro and millimeter wave range. The longest dimension of the antenna is 1.1825 mm that is comparable to the wavelength of the signal in the dielectric medium.
A wireless interconnect can be implemented by establishing a communication link between antennas on the same substrate with

one antenna in the end-fire region of another. We adopt the transceiver design from [1] where a simple non-coherent On-Off Keying (OOK) based transceiver is demonstrated for power-efficiency.

2.2 Topology and routing of the DWiNoC

The topology of the proposed DWiNoC is a small-world network where the wireline links between switches are established following an inverse power-law distribution discussed in [3]. This strategy of developing a small-world network has been shown to be most efficient in terms of wiring costs.

The location of the WIs is optimized for minimum average distance or hop-count between source-destination pairs while ensuring that no WI is in the path of communication between other pairs of WIs. This optimization is performed following a Simulated Annealing based heuristics while observing the following constraints:

1) Linearity constraints: There will be no such node in any pairs that will be in the end-fire region of other antennas.
2) Angularity constrains: There will be no such element in any pairs that will be in the same line passing through the side lobes of any other antenna as seen in Figure 2.

Following these constraints in the SA optimization we are able to establish concurrent links, which do not interfere with each other and design the DWiNoC with the minimum average hop-count. In the DWiNoC data is transferred via wormhole routing using virtual channel (VC) based NoC switches. Deadlock is avoided by using a forwarding-table based routing over precomputed shortest paths determined by Dijkstra's algorithm.

3. EXPERIMENTAL RESULTS

In this section, we demonstrate the characteristics of the PLPA antennas and evaluate the performance and energy efficiency of the proposed DWiNoC architecture. In this work, the NoC architecture is characterized using a cycle accurate simulator accounting for those flits that reach the destination as well as those that are dropped. The width of all wired links is considered to be same as the flit size, which is considered to be 32 bits. We consider a moderate packet size of 64 flits for all our experiments. Similar to the wired links, we have adopted wormhole routing in the wireless links too.

3.1 Antenna characteristics and link budget analysis

The 60 GHz on-chip PLPA is simulated using FEM based HFSS software. Here, a 10-20 Ω-cm silicon substrate is considered. The radiation patterns of the antenna in the azimuth and elevation plane are shown in Figure 2. It demonstrates the end-fire beamwidth of the on-chip PLPA is 33°. Similarly, the half-power beamwidth along the elevation, is 30°.

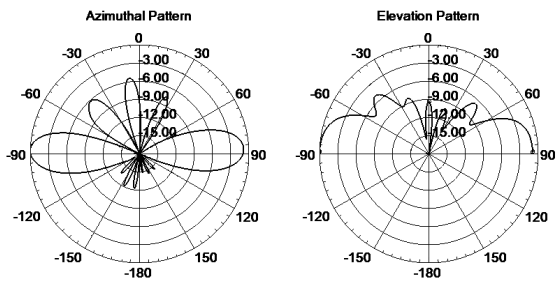

Figure 2. Radiation pattern along the azimuthal and elevation plane

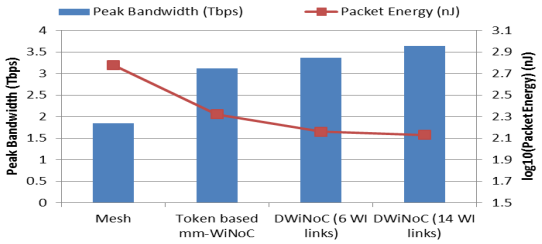

Figure 3. Peak bandwidth and packet energy dissipation of various NoC architectures for 64-core system

3.2 Performance Evaluation of the DWiNoC

In this section, we evaluate the peak bandwidth and energy efficiency of the proposed directional antenna based DWiNoC architecture for a 64-core system with uniform random traffic distribution and the results are shown in Figure 3. We also compare it with a conventional wireline mesh and the token-based WiNoC with similar topology. We found that our proposed architecture achieves higher bandwidth and lower packet energy compared to both mesh and token based WiNoC. The token based WiNoC has higher bandwidth and about three times less packet energy compared to mesh of the same system size due to the efficient small-world network topology and energy-efficient wireless links. However, in the token-based WiNoC only a single wireless link is active at any given point of time. We have evaluated the directional antenna based DWiNoC with similar number of WIs (6 links or 12 WIs for the 64 core system) as the token based WiNoC optimized for best performance. Even for the same overheads in wireless transceivers we see that the proposed architecture achieves higher bandwidth and lower packet energy compared to the token-based system due to multiple concurrent wireless links. On increasing the number of concurrent links to 14 with 28 WIs, we observe that the packet energy and bandwidth are further improved compared to the DWiNoC with 6 links.

4. CONCLUSIONS

In this paper we present the design of a wireless NoC architecture with directional log-periodic antennas. Through system level simulations we demonstrate that such a WiNoC is capable of improving the performance and reduce packet energy dissipation compared to the state-of-the-art token passing based WiNoC as well as a conventional electronic mesh based NoC.

5. ACKNOWLEDGEMENTS

This work is supported in part by the US National Science Foundation, under grant CCF1162123.

6. REFERENCES

[1] S. Deb, A. Ganguly, P. P. Pande, B. Belzer, and D. Heo, "Wireless NoC as Interconnection Backbone for Multicore Chips: Promises and Challenges," *IEEE J. on Emerging and Selected Topics in Circuits and Systems*, vol. 2, no. 2, pp. 228–239, 2012.

[2] Z. N. Chen, M. J. Ammann, X. Qing, X. H. We, T. S. P. See and A. Cai, "Planar antennas", *IEEE Microw. Mag.*, vol. 7, no. 6, pp. 63-73, Dec. 2006.

[3] A. Ganguly, P. Wettin, K. Chang, and P. Pande, "Complex network inspired fault-tolerant NoC architectures with wireless links," in *IEEE/ACM International Symposium on Networks on Chip (NoCS)*, pp. 169–176, 2011.

Estimation of Radiation Characteristics of Different Slotted Microstrip Antennas Using a Knowledge-Based Neural Networks Model

Taimoor Khan, Asok De

Department of Electronics and Communication Engineering, National Institute of Technology, Patna 800 005, India

Received 12 December 2013; accepted 4 May 2013

ABSTRACT: In this article, a common neural model incorporated with prior knowledge is suggested for estimating radiation characteristics (i.e., resonance frequencies, gains, directivities, antenna efficiencies, and radiation efficiencies) of four-slotted microstrip antennas with inserted air-gap for dual-frequency operation. By incorporating prior knowledge in the existing neural networks, the required numbers of training patterns are drastically reduced. Further, the proposed approach is capable for accurately estimating the radiation characteristics in extrapolation region too. The proposed neural approach is also validated with measured results. A very good agreement is achieved in simulated, estimated, and measured results. © 2014 Wiley Periodicals, Inc. Int J RF and Microwave CAE 00:000–000, 2014.

Keywords: different slots; radiation characteristics; microstrip antenna; rectangular patch; neural networks; prior knowledge

I. INTRODUCTION

Modern wireless communication systems like satellite communication, radar systems, global positioning system, and so forth require dual-frequency operation. Microstrip antennas (MSAs) have eliminated two single frequency operated antennas in these applications [1]. Dual-resonance in MSAs can be achieved using multilayered stacked patch [2, 3], slotted rectangular patch [4], square patch with notches [5], patch loaded with shorting posts [6] or varactor diodes [7], and rectangular patch fed by an inclined slot [8]. These methods [2–8] can roughly be sorted as analytical methods and numerical methods. The analytical methods provide a good spontaneous explanation for operation of MSAs but these techniques are based on physical assumptions for simplifying the radiation mechanism of the MSAs and are suitable for thin substrates only. The numerical methods, conversely, provide accurate results but only at the cost of using complex mathematical expressions in the form of integral equations. In these methods, the solutions appear to be more critical without initial assumptions in the final stage of numerical results. Also, these techniques require a new solution even for an infinitesimal alteration in the geometry. Thus, the requirement for having a new solution for every small alteration in the geometry and the problems associated with the thickness of substrates in analytical methods lead to complexities and processing cost.

In last decade, artificial neural networks (ANN) models have attained remarkable achievements in wireless communication due to their ability and adaptability to learn and generalization features [9]. The reliability of a neural model depends on numbers of training patterns. In addition, even with sufficient training patterns, the consistency of most of the neural models is not guaranteed when used for extrapolation purpose. The learning patterns for these models are generally created through simulation and/or measurement [9]. Generating sufficient numbers of training patterns for a complex geometry becomes time consuming and sometimes very expensive. It is so because the simulation and measurement approaches are to be performed for several combinations of each input parameter associated to that geometry. Towell and Shavlik [10] have proposed a novel concept of incorporating prior knowledge in neural networks for reducing the required training patterns. Wang and Zhang [11, 12] have then embedded the prior knowledge in the form of empirical functions to resolve three different microwave design problems. Watson et al. [13, 14] have proposed

Correspondence to: T. Khan; e-mail: ktaimoor@gmail.com

DOI: 10.1002/mmce.20811

Published online 00 Month 2014 in Wiley Online Library (wileyonlinelibrary.com).

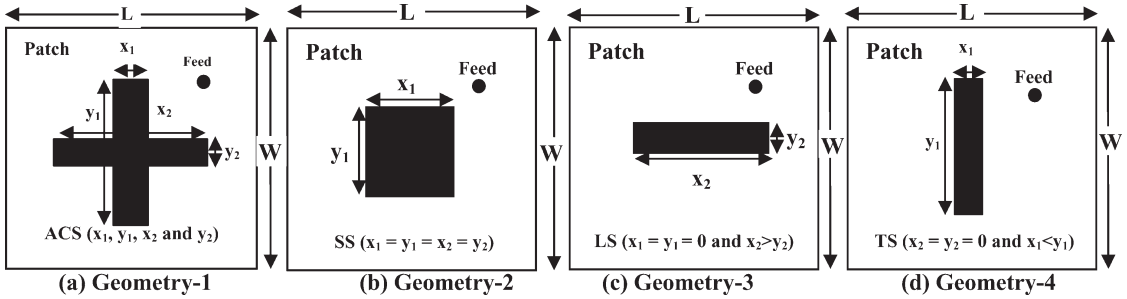

Figure 1 Proposed antenna geometries (top-views). The terms (a) Geometry-1, (b) Geometry-2, (c) Geometry-3 and (d) Geometry-4 must be just below of their respective geometries.

knowledge-based neural networks (KBNN) models for microwave components modeling. Dandurand and Lowther [15] have used KBNN model for identifying the performance of electromagnetic devices. Watson et al. [16] have designed wideband coplanar waveguide patch/slot antennas using KBNN model. Wang et al. [17] have modeled stripline discontinuities by neural networks with knowledge-based neurons. Zingg and Gupta [18] have designed microwave reflection and loaded types phase shifters using knowledge-aided design neural networks. Hong and Wing [19] have used neural networks with knowledge-based neurons in hidden layer for modeling microstrip T-junction. Devabhaktuni et al. [20] have recently, proposed an efficient knowledge-based automatic model generation technique for microwave modeling. Some innovative strategies including knowledge-based microwave design and optimization have been proposed by Sanchez [21]. Sanchez and Zhang [22] have proposed KBNN-based advanced electromagnetic data sampling algorithms for modeling several microwave structures. Recently, Devabhaktuni et al. [23] have introduced a novel ANN-based reverse-modeling approach for efficient electromagnetic compatibility analysis of printed circuit boards and shielding enclosures. Thus, in referenced literature [10–23], different cases have been resolved using KBNN approach. But the radiation characteristics of different slotted MSAs with inserted air-gap have been rarely estimated as it is essentially required for the antenna designers. Hence, the proposed work is based on method optimization in which a generalized neural analysis of four-slotted MSAs with inserted air-gap is suggested as to create a generalized analytical or numerical approach for such a complicated case is still a challenge before the electromagnetic community. This article is organized as follows: Section II describes different geometries for pattern generations. Neural networks modeling and KBNN modeling is then discussed in Sections III and IV, respectively. Section V illustrates experimental validation. A conclusion followed by references is discussed in Section VI.

II. PROPOSED GEOMETRIES FOR PATTERN GENERATIONS

Four-slotted MSA geometries are used for pattern generation and the top-views of these geometries are shown in Figure 1.

A rectangular patch of dimensions 61 × 56 mm^2 is designed on RT-Duroid substrate RO3003 ($\varepsilon_r = 3$, $h = 0.762$ mm, and $\tan\delta = 0.0045$) using method of moment-based IE3D simulator [24]. Two resonating modes TM_{10} and TM_{01} are excited by a single probe for getting dual-resonance. The performance of patch antenna is further improved by inserting an air-gap (i.e., t mm) between substrate sheet and ground plane [25].

Different slotted antennas are revealed in Figure 1 in which an asymmetric cross-slot (ACS) of dimensions, x_1, y_1, x_2, and y_2 is inserted on radiating surface of a rectangular patch. In a specific case, if all slot-dimensions becomes equal, that is, $x_1 = y_1 = x_2 = y_2$, a square-slotted (SS) geometry is acquired. This is shown in Figure 1(b). Two more specific cases are also obtained by making two slot-dimensions zero, that is, either $x_1 = y_1 = 0$ or $x_2 = y_2 = 0$. These two specific cases are obtained as longitudinal-slot (LS) and transverse-slot (TS), respectively. These two slotted geometries are shown in Figures 1(c) and 1(d), respectively.

For excited TM_{10} and TM_{01} modes, the radiation characteristics like gains, directivities, antenna efficiencies, and radiation efficiencies are observed by varying slot-dimensions between 1 mm ≤ slot-dimensions ≤ 50 mm and inserted air-gap (t) between 1 mm ≤ air-gap ≤ 10 mm for each slotted geometry. Total 1960 sets of patterns (@ 490 patterns for each slot) are created in IE3D software. These patterns are used for training and testing of the neural modeling schemes to be discussed in Sections III and IV, respectively. Table I shows the sampling strategy used in these patterns generation.

III. NEURAL NETWORKS AND MODELING

Neural networks modeling scheme promises to become a powerful means for obtaining solutions quickly and accurately to the problems that are cross-disciplinary in nature [9]. ANN are massively distributed parallel processors that have natural propensity for storing experiential knowledge during training and making it available for use during testing. ANN models resemble the brain since knowledge is acquired through a learning process, and interneuron connection strengths are used to store this acquired knowledge. Neural networks learn by known

TABLE I Sampling Strategy for Patterns Generations

Dimension	Specified Range	Step-Size	Generated Patterns
x_1	1 mm $\leq x_1 \leq$ 50 mm	0.1 mm	1960 sets
y_1	1 mm $\leq y_1 \leq$ 50 mm	0.1 mm	
x_2	1 mm $\leq x_2 \leq$ 50 mm	0.1 mm	
y_2	1 mm $\leq y_2 \leq$ 50 mm	0.1 mm	
t	1 mm $\leq t \leq$ 10 mm	5.0 μm	

examples of a problem to acquire knowledge about it. Once successfully trained, the neural networks can be put to effective use in solving "unknown" or "untrained" instances of the problem.

Antenna designers generally prefer a generalized approach for computing different performance parameters instead of having individual one for individual parameters. Creating a flexible mathematical model for such cases is still a challenging job. It has recently been overcome by introducing the concept of generalized neural networks [26–36]. In this article, authors have extended their earlier works on generalized neural networks [30–36] for computing 10 different target parameters for the given six source parameters. For this purpose, the existing literature on modeling of slotted MSAs [37–40], is also considered carefully.

A multilayered perceptron (MLP) neural network consists of one input layer, a number of hidden layers, and one output layer in which each layer is having entirely different roles [26–40]. There are three common steps used to train the MLP neural networks. First, the training patterns are generated, then the structural configuration of hidden layer neurons is selected in second step and finally, in third step the weights are optimized using training algorithm [41]. To build an effective application, training of neural networks is one of the more critical phases. Methods created from field of optimization theory have played an important role in developing training algorithms for neural networks [9]. Training a neural model basically consists of adjusting weights with the help of a training algorithm. The training performance is observed by varying number of hidden layers as well as neurons in each hidden layer. After many trials, it is optimized with 87 neurons for first hidden layer and 36 neurons for second hidden layer to get the best performance. Before doing training, the generated 1960 patterns are normalized between +0.1 to +0.9 to avoid the convergence problem during training of the neural models using MATLAB software [42]. The concept of normalization has been very much popular in the neural networks modeling of MSAs [26–36]. Further, the training performance of the model is also observed with seven different training algorithms [41, 42]. These are mentioned as: BFGS quasi-Newton backpropagation (BFG), Bayesian regularization (BR), Scaled conjugate gradient backpropagation (SCG), Powell-Beale conjugate gradient backpropagation (CGB), Fletcher-Powell conjugate gradient backpropagation (CGF), One step secant backpropagation (OSS), and Levenberg–Marquardt (LM).

In Section II, 1960 performance parameters are generated by varying slot-dimensions (x_1, y_1, x_2, and y_2) and inserted air-gap (t) in IE3D software. These patterns are used by considering four different slotted geometries; ACS, SS, LS, and TS, respectively. Here an arbitrary parameter, M is included in the input layer to distinguish these four different slots; $M = 1$, 2, 3, and 4 corresponds to ACS, SS, LS, and TS, respectively. Further, the proposed MLP neural networks model is being used for estimating different radiation characteristics; resonance frequencies, gains, directivities, antenna efficiencies, and radiation efficiencies for dual-frequency operations, hence it becomes necessary to distinguish these characteristics at two-dimensional output (denoted by variables r_1 and r_2) of the neural networks model. For this purpose, an arbitrary parameter, N is also included in the output layer for distinguishing these characteristics where $N = 1$, 2, 3, 4, and 5 corresponds to dual-resonance (f_1 and f_2), dual-frequency gains (G_1 and G_2), dual-frequency directivities (D_1 and D_2), dual-frequencies antenna efficiencies (A_1 and A_2), and dual-frequencies radiation efficiency (R_1 and R_2), respectively. Thus a three-dimensional response $[R] \rightarrow [r_1\ r_2\ N]$ is achieved for six-dimensional excitation $[E] \rightarrow [x_1\ y_1\ x_2\ y_2\ t\ M]$. A MLP neural networks model for computing the response for the given excitation is illustrated in Figure 2.

In Figure 2, the variables M and N are included to create a generalized concept. Details of this concept can be found in the earlier works of the authors [30–36]. The structural configuration for the MLP neural model shown in Figure 2 is mentioned as: 6*87*36*3. It means that there are 87 neurons in first hidden layer and 36 neurons in second hidden layer. Six neurons in input layer corresponds to six-dimensional excitation matrix $[x_1\ y_1\ x_2\ y_2\ t\ M]$ and 3 neurons in the output layer to three-dimensional response matrix $[r_1\ r_2\ N]$.

The structural configuration, 6*87*36*3, mentioned in Figure 2 is optimized using trial-and-error method, which is very much popular in the neural networks [26–36]. For an applied input pattern, some random values between 0 and 1 are assigned to weights and bias values of the network and the response is computed corresponding to that input pattern. The mean square error (MSE) between estimated and simulated results is also computed. All the weights and bias values are then updated accordingly. This updating process is carried out after presenting each set of excitation matrix until the calculated accuracy is deemed satisfactory. This is done by considering the

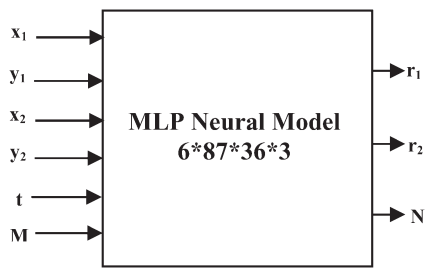

Figure 2 MLP neural networks method.

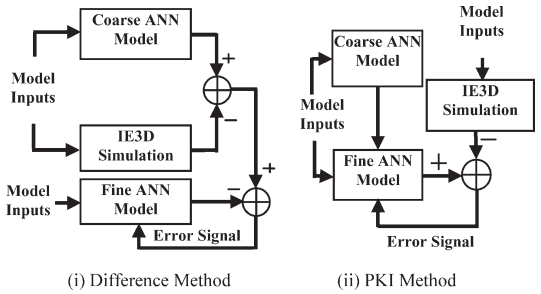

Figure 3 Knowledge-based neural methods [13, 14].

parameters: MSE = 3.58 × 10^{-5}, learning rate (η) = 0.201, momentum coefficient (μ) = 0.016, spread value (σ) = 0.469, dimensionality of input pattern (I) = 6, dimensionality of output pattern (O) = 3. After optimizing the weights and bias values, the testing algorithm is then implemented for another set of samples, which were not included during training of the model. For this implementation, the initial weights and bias values are replaced by their optimized counterparts. The trained neural model now returns the response within a fraction of a second for any selected slot-shape (ACS, SS, LS or TS) with arbitrary values of slot-dimensions (1 mm $\leq$ slot-dimensions $\leq$ 50 mm), and inserted air-gap (1 mm $\leq$ air-gap $\leq$ 10 mm).

IV. KNOWLEDGE-BASED NEURAL MODELING

The MLP neural model discussed in Section III is trained with 1372 patterns (~70% of total generated patterns) and tested for rest 588 patterns for achieving the desired level of accuracy. But generating such large number of training patterns is a time consuming process. It is so because the simulation process needs to be performed for several combinations of each input parameter associated to that geometry. To reduce this number, prior knowledge is incorporated via two different approaches; difference method and prior knowledge input (PKI) method as shown in Figure 3. This prior knowledge is attained by an already trained neural model known as coarse ANN model. However, it can also be attained by a set of analytical equations or empirical models [13, 14].

In difference method, fine ANN model is trained on difference between simulated outputs and the outputs of coarse ANN model. This method is more effective if the difference has a simpler input/output mapping as the function of the inputs than the target pattern. In PKI method, conversely, the outputs of coarse model are used as input for fine model in addition to simulation inputs. Thus, the input/output mapping of the ANN model is in between the output response of the existing model and that of the target model. The optimization strategy of both the coarse and fine ANNs models is similar to the MLP neural model discussed in Section III. In difference method, the structural configuration of coarse model and fine model is optimized as: 6*11*3 and 9*17*3 whereas for PKI method, it is optimized as: 6*9*3 and 12*15*3, respectively. The coarse model discussed here is very less accurate in itself but when it is incorporated in the two methods, then the overall accuracy increases drastically and also the required training patterns reduce significantly.

V. EXPERIMENTAL VALIDATION AND DISCUSSION

Section II has described MLP neural modeling scheme for estimating the radiation characteristics of slotted MSAs with inserted air-gap. The training performance of the model is observed with seven different algorithms; BFG, BR, SCG, CGB, CGF, OSS, and LM algorithm. But only LM back propagation is proved to be the fastest converging training algorithm as it requires only 2733 s to train the neural model and 55906 epochs that are very less as compared to other training algorithms.

Two knowledge-based neural methods (i.e., difference method and PKI method) are also used for estimating the same radiation characteristics. Table II depicts a comparison of MLP, difference, and PKI methods. The numbers of weights and bias values for MLP method are computed as: 3762 [=(6 × 87) + (87 × 36) + (36 × 3)] and 126 [=87 + 36 + 3], respectively. Similarly, the weights and bias values for difference and PKI methods can also be computed and these values are also mentioned in Table II. It is clear from this table that the weights are reduced by 91.95 and 91.87% and bias values by 73.02 and 76.19% in difference method and PKI method, respectively.

The deviations in average testing error by increasing the testing patterns (or by reducing the training patterns) for these three methods are plotted in Figure 4. This Figure shows that in MLP method, the error increases from 5.79 to 19.05% by reducing the training patterns from 60 to 30%. In difference method, it increases from 1.18 to 2.41% and in case of PKI method it increases only 1.01 to 2.05%, respectively. Thus, the PKI method is observed slightly more accurate than the difference method. Further, it is also concluded here that the MLP method produces accurate results only for adequate number of training patterns whereas the other two methods produce more accurate results even for lesser training patterns.

The weights and bias values in three neural methods are selected randomly for initialization and then optimized using training algorithm [43]. The computed errors in these three neural models are also analyzed by considering the stochastic behavior of means and standard deviations of the computed errors [43]. A relationship between mean and standard deviation is developed by considering the coefficient of variation (CoV). It is defined as the ratio of standard deviation to mean value. CoV closer to

TABLE II Comparison of Structures in Three Methods

Type of Method	Model-Size	Weights	Biases
MLP neural method	6*87*36*3	3762	126
Difference method	6*11*3 and 9*17*3	303	34
PKI method	6*9*3 and 12*15*3	306	30

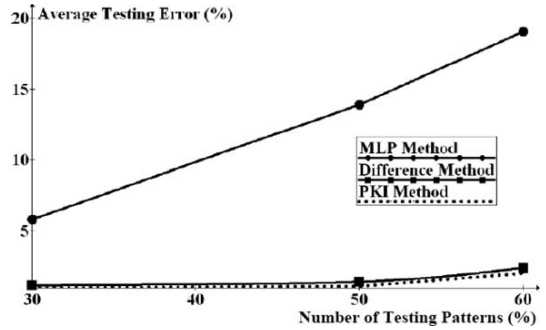

Figure 4 Average testing error versus number of testing patterns.

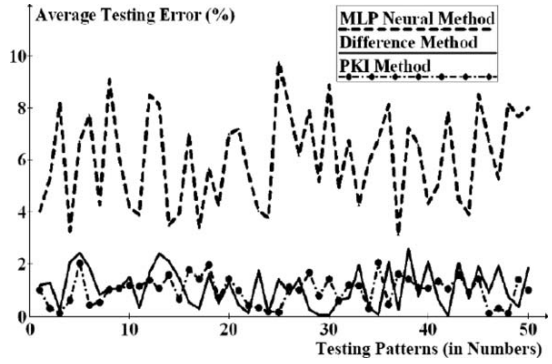

Figure 5 Extrapolation performance for dual-resonance only.

0, represents better uniformity whereas closer to 1, represents greater variability. For the PKI method, the means for three-dimensional error are computed as: 1.5127, 1.432, and 1.354, respectively, whereas their corresponding standard deviations as: 0.2030, 0.1549, and 0.1546, respectively. Hence, the coefficients of variations for these three values are coming out to be 0.1342, 0.1082, and 0.1142, respectively. Thus, it is concluded here that all the error points are uniformly distributed over a full validation set of 1960 simulated patterns [44].

During simulation, 1.5 to 3.0 GHz frequency range with 100 sampling points is used. The simulation time depends on complexity inserted in the geometry. For the geometries shown in Figure 1, it is computed as ~1 h 53 min per structure and ~36 MB memory space (RAM) is required for each simulation. The time elapsed in training and testing of the neural methods and the required memory space is mentioned in Table III.

Table III shows that both computational time and required memory storage are fairly reduced using neural networks. Table III also shows that the PKI method after training is much faster than that of the electromagnetic simulation. Further, the training of the PKI method requires only ~17 KB RAM of a system and for testing the performance, only ~1.21 KB RAM is required. Hence, the required memory space in both training and testing of the PKI method is also lesser as compared to 36MB required for simulation.

To observe the extrapolation capability of these three methods, 50 arbitrary patterns are generated for each cited performance parameters (i.e., dual-resonance, dual-frequency gains, dual-frequency directivities, dual-frequency antenna efficiencies, and dual-frequency radiation efficiencies). These patterns are generated in extrapolation region (outside region of the generated training patterns) by extending the original region of the input space by 25%. The average absolute errors are computed corresponding to each performance parameters. It is concluded that the accuracy of KBNN methods has been slightly depreciating for all cases of generated patterns as compared to MLP method. It may be due to built-in prior knowledge in the knowledge-based models to give more information to the patterns not seen during the training. Figure 5 summarizes the extrapolation capability of three neural methods in computing the dual-resonance. Same level of accuracy is observed in other performance parameters like gains, directivities, antenna efficiencies, and radiation efficiencies, respectively.

For validating the proposed work, a prototype is fabricated using RT-Duroid substrate RO3003 ($\varepsilon_r = 3$ and $h = 0.762$ mm). A rectangular patch is etched on upper side of the substrate. An air-gap of 5.1 mm is stacked using Teflon rods between substrate and ground plane. The performance parameters of the fabricated prototype are measured using Agilent N5230A network analyzer. A comparison between measured and simulated *S*-parameters is shown in Figure 6.

The prototype is excited by probe feed, which guides the electromagnetic waves to the feed point. The energy of electromagnetic waves then spreads out into the region under the slotted patch, some of which crosses the boundary of the slotted patch and radiates into the half-space above the patch. An SMA connector with 6.8 mm long pin (1 mm for ground plane + 5.1 mm for air-gap + 0.762 mm for substrate) is used for RF connection between ground plane and slotted patch. Thus, by inserting a cross-slot, the excited surface current path lengthens, increasing the

TABLE III Performance Comparison of Three Methods

			Required Memory Space	
Types of Neural Method	Training Time	Testing Time	Training	Testing
MLP method	2733 s	~46 ms	~44 KB RAM	2.96 KB RAM
Difference method	3349 s	~35 ms	~28 KB RAM	1.42 KB RAM
PKI method	1134 s	~27 ms	~17 KB RAM	1.21 KB RAM

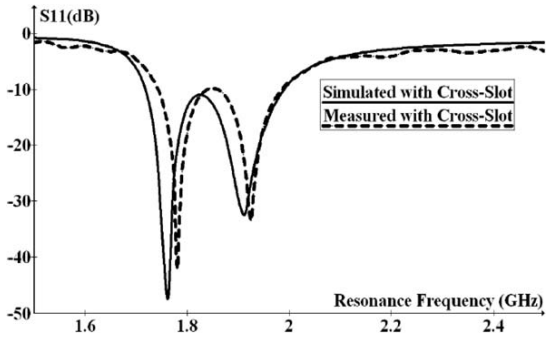

Figure 6 Comparison of measured and simulated *S*-parameters.

antenna length, and hence decreasing the resonance frequency. For slotted patch antenna, both the resonance frequencies (1.763 and 1.914 GHz) are lowered by ~13% as compared to those (2.0256 and 2.1970 GHz) of the simple rectangular patch without a slot. This reduction in the frequencies can result in a patch size reduction of ~35% for a given dual-frequency design. Hence, a good rank of compactness is achieved in the fabricated prototype. Also, the ratio (f_2/f_1) of two frequencies (1.914/1.763 = 1.0857 and 2.1970/2.0256 = 1.0846) is slightly affected by inserting the cross-slot, and mainly determined by the aspect ratio (1.89 = 61/56) of the patch; which makes the design simpler and easier to implement.

Further, it is clear from Figure 6 that during simulation, 55.5 MHz bandwidth is attained whereas in the fabricated prototype, it is measured as 250 MHz (1.99–1.74 GHz) for $S_{11} \leq -10$ dB. It may be probably due to irregularity in fabricating the prototype and/or inserting the air-gap. Further, the size and losses of the solder joints are not considered during simulation, which may cause this difference. A very good impedance matching is also achieved by inserting an air-gap of 5.1 mm. The efficiencies (both antenna and radiation efficiencies) are improved because of negligible amount of dielectric loss in the air-layer. As gain of an antenna is defined as the product of directivity and radiation efficiency, hence the gain is also improved.

Table IV shows a comparison between simulated, estimated, and measured dual-resonance. A good rank of convergence in them confirms that the Taflon rods do not affect the antenna performance. The simulated and estimated performance characteristics of the fabricated prototype are also compared and a very good agreement is achieved between them as mentioned in Table V.

The measured and simulated *E*- and *H*-plane patterns for both the frequencies (f_1 and f_2) are plotted in Figures 7 and 8, respectively, which also show a good convergence for the entire range of *E*- and *H*-planes. Here it is clear that the ratio of co- to cross-polarizations is higher than 30 and 20 dB in *E*- and *H*-planes, respectively.

TABLE IV Comparison of Results

Slot-Dimensions (mm)	Dual-Resonance (GHz)		
	Simulated	Estimated	Measured [43]
$x_1 = 38.0$, $y_1 = 1.5$, $x_2 = 1.0$, and $y_2 = 41.0$	1.7630 and 1.9140	1.7574 and 1.9136	1.7800 and 1.9250

TABLE V Comparison of Simulated and Estimated Results

Name of Parameters	Simulated Results	Estimated Results (PKI Method)
Dual-resonance (GHz)	1.7630 and 1.9140	1.7596 and 1.9068
Dual-frequency gains (dBi)	8.9365 and 8.9387	8.9285 and 8.9303
Dual-frequency directivities (dBi)	9.1122 and 9.2079	9.1055 and 9.2109
Dual-frequency antenna efficiency (%)	95.8065 and 93.9897	94.1105 and 94.0288
Dual-frequency radiation efficiencies (%)	96.3604 and 96.6599	95.4193 and 95.5837

VI. CONCLUSION

In this article, a fast and accurate generalized MLP neural method has been proposed for estimating different radiation characteristics for arbitrary slot-shape, slot-dimensions, and inserted air-gap within their specified ranges. Such a generalized neural approach is rarely proposed to the best of our knowledge. Because of simplicity, one can estimate the desired characteristics using a personal computer without having the fundamental knowledge of MSAs.

Two different approaches of incorporating prior knowledge in generalized MLP neural method have also been

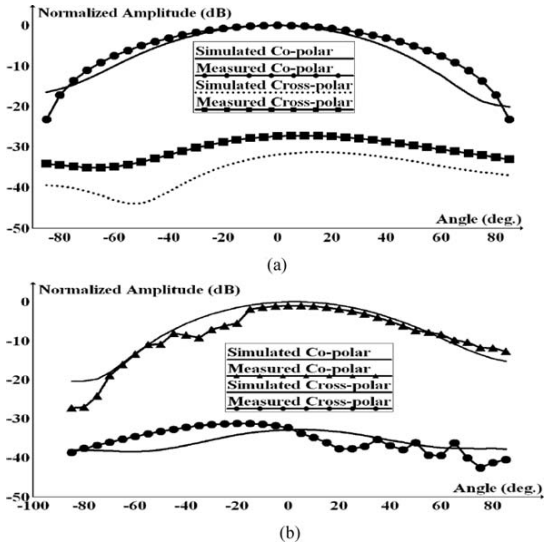

Figure 7 (a) Measured and simulated *E*-plane patterns for f_1 and (b) measured and simulated *E*-plane patterns for f_2.

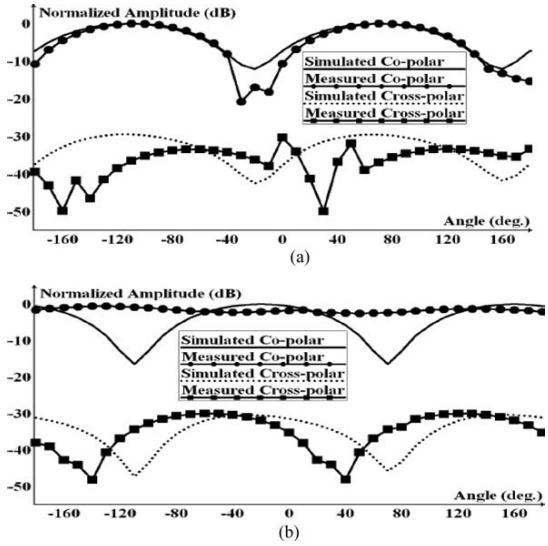

Figure 8 (a) Measured and simulated *H*-plane patterns for f_1 and (b) measured and simulated *H*-plane patterns for f_2.

used. By incorporation of this prior knowledge, the number of training patterns have been reduced drastically, which is very much advantageous when generation of training patterns is expensive and time-consuming as in case of antenna problems. Thus the knowledge-based neural methods have shown better accuracy even with least training patterns over the conventional MLP neural networks method. As the neural networks-based methods have produced more accurate results in computing 10 different parameters, hence these can be recommended to include in antenna computer-aided design algorithms. Thus the proposed neural methods have also been validated by fabricating and characterizing a prototype.

REFERENCES

1. I.J. Bahl and P. Bhartia, Microstrip antennas, Artech House, Dedham, MA, 1980.
2. J.S. Dahele, K.F. Lee, and D.P. Wong, Dual-frequency stacked annular-ring microstrip antennas, IEEE Trans Antenna Propag 35 (1987), 1281–1285.
3. S.A. Long and M.D. Walton, A dual-frequency stacked circular-disk antenna, IEEE Trans Antennas Propag 27 (1979), 270–273.
4. S. Maci, G.B. Gentili, and G. Avitabile, Single-layer dual-frequency patch antenna, Electron Lett 29 (1993), 1441–1443.
5. H. Nakano and K. Vichien, Dual-frequency square patch antenna with rectangular notch, Electron Lett 25 (1989), 1067–1068.
6. D.H. Schaubert, F.G. Farrar, A. Sindoris, and S.T. Hayes, Microstrip antennas with frequency agility and polarization diversity, IEEE Trans Antennas Propag 29 (1981), 118–123.
7. R.B. Waterhouse and N.V. Shuley, Dual-frequency microstrip rectangular patches, Electron Lett 28, 1992, 606–607.
8. Y.M.M. Antar, A.I. Ittipiboon, and A.K. Bhattacharyya, A dual-frequency antenna using a single patch and an inclined slot, Microwave Opt Technol Lett 8 (1995), 309–311.
9. Q.J. Zhang and K.C. Gupta, Neural networks for RF and microwave design, Artech House Publishers, London, 2000.
10. G.G. Towell and J.W. Shavlik, Knowledge-based artificial neural networks, Artif Intell 70 (1994), 119–165.
11. F. Wang and Q.J. Zhang, Knowledge based neural models for microwave design, IEEE Int Microwave Symp Dig, Denver, CO 2, 1997, pp. 627–630.
12. F. Wang, and Q.J. Zhang, Knowledge-based neural models for microwave design, IEEE Trans Microwave Theory Tech 45 (1997), 2333–2343.
13. P.M. Watson, K.C. Gupta, and R.L. Mahajan, Development of knowledge based artificial neural network models for microwave components, IEEE MTT-S Int Microwave Symp Dig 1, 1998, pp. 9–12.
14. P.M. Watson, K.C. Gupta and R.L. Mahajan, Applications of knowledge-based artificial neural network modeling to microwave components, Int J RF Microwave Comput-Aided Eng 9 (1999), 254–260.
15. F. Dandurand and D.A. Lowther, Electromagnetic device performance identification using knowledge based neural networks, IEEE Trans Magn 35 (1999), 1817–1820.
16. P.M. Watson, G.L. Creech and K.C. Gupta, Knowledge based EM-ANN models for the design of wide bandwidth CPW patch/slot antennas, IEEE Int Symp Antennas Propag Soc 4(1999), 2588–2591.
17. B.-Z. Wang, D. Zhao, and J. Hong, Modeling stripline discontinuities by neural network with knowledge-based neurons, IEEE Trans Adv Packaging 23 (2000), 692–698.
18. R. Zingg and K.C. Gupta, An approach for knowledge-aided-design (KAD) of microwave circuits using artificial neural networks, Microwave Symposium Digest, 2001 IEEE MTT-S International, Phoenix, AZ, USA, pp. 1011–1014.
19. J. Hong and B.-Z. Wing, NNKBN model for the microstrip T-junction structure, Antennas and Propagation Society 2003 IEEE International Symposium, 22–27 June, Columbus, OH, USA, Volume 2, 2003, pp. 92–95.
20. V.K. Devabhaktuni, B. Chattaraj, M.C.E. Yagoub, and Q.-J. Zhang, Advanced microwave modeling framework exploiting automatic model generation using knowledge neural networks and space mapping, IEEE Trans Microwave Theory Tech 51(2003), 1822–1833.
21. J.E. Rayas-Sanchez, EM-based optimization of microwave circuits using artificial neural networks: The state-of-the-art, IEEE Trans Microwave Theory Tech 52(2004), 420–435.
22. J.E. Rayas-Sanchez and Q.J. Zhang, On knowledge-based neural networks and neuro-space mapping, Microwave Symp Dig (MTT), 2012 IEEE MTT-S Int, Montreal, QC, Canada, 1–3, 17–22 June, 2012.
23. V. Devabhaktuni, C.F. Bunting, D. Green, D. Kvale, L. Mareddy and V. Rajamani, A new ANN-based modeling approach for rapid EMI/EMC analysis of PCB and shielding enclosures, IEEE Trans Electromagn Compatibility 55(2013), 385–394.
24. IE3D Version 14.0, Fremont, CA, Zeland Software, October 2007.
25. J.S. Dahele and K.F. Lee, Theory and experiment on microstrip antennas with air-gaps, IEE Proc 132 (1985), 455–460.
26. K. Guney, S. Sagiroglu, and M. Erler, Generalized neural method to determine resonant frequencies of various microstrip antennas, Int J RF Microwave Comput-Aided Eng 12 (2002), 131–139.
27. K. Guney and N. Sarikaya, A hybrid method based on combining artificial neural network and fuzzy interference system for simultaneous computation of resonance frequencies of rectangular, circular, and triangular microstrip antennas, IEEE Trans Antenna Propag 55 (2007), 659–668.
28. K. Guney and N. Sarikaya, Concurrent neuro-fuzzy systems for resonant frequency computation of rectangular, circular,

and triangular microstrip antennas, Prog Electromagn Res 84 (2008), 253–277.
29. N. Turker, F. Gunes, and T. Yildirim, Artificial neural design of microstrip antennas, Turk J Electr Eng 14 (2006), 445–453.
30. T. Khan and A. De, Computation of different parameters of triangular patch microstrip antennas using a common neural model, Int J Microwave Opt Technol 5 (2010), 219–224.
31. T. Khan and A. De, A common neural approach for computing different parameters of circular patch microstrip antennas, Int J Microwave Opt Technol 6 (2011), 259–262.
32. T. Khan and A. De, Design of circular/triangular patch microstrip antennas using a single neural model, IEEE Appl Electromagn Conf (AEMC-2011), Hyatt Regency, Kolkata, India, December 18–22, 2011.
33. T. Khan and A. De, A generalized neural simulator for computing different parameters of circular/triangular microstrip antennas simultaneously, 2012 IEEE Asia-Pac Conf Appl Electromagn (APACE-2012) Melaka, Malaysia, pp. 350–354, December 11–13, 2012.
34. T. Khan and A. De, A generalized neural method for simultaneous computation of resonant frequencies of rectangular, circular and triangular microstrip antennas, Int Conf Global Innovation Technol Sci (ICGITS-2013), Saintgits College of Engineering, Kottayam, Kerala, India, April 4–6, 2013.
35. T. Khan and A. De, Prediction of resonant frequencies of rectangular, circular and triangular microstrip antennas using a generalized RBF neural model, Int J Sci Eng Res 4 (2013), 182–187.
36. T. Khan and A. De, A generalized ANN model for analyzing and synthesizing rectangular, circular and triangular microstrip antennas, Chin J Eng, 2013, Article ID 647191.
37. D.K. Neog, S.S. Pattnaik, D.C. Panda, S. Devi, B. Khuntia, and M. Dutta, Design of a wideband microstrip antenna and the use of artificial neural networks in parameter calculation, IEEE Antenna Propag Mag 47 (2005), 60–61.
38. V.V. Thakare and P.K. Singhal, Bandwidth analysis by introducing slots in microstrip antenna design using ANN, Prog Electromagn Res M 9 (2009), 107–122.
39. V.V. Thakare and P. Singhal, Microstrip antenna design using artificial neural networks, Int J RF Microwave Comput-Aided Eng 20 (2010), 76–86.
40. Z. Wang, S. Fang, Q. Wang, and H. Liu, An ANN-based synthesis model for the single-feed circularly-polarized square microstrip antenna with truncated corners, IEEE Trans Antennas Propag 60 (2012), 5989–5992.
41. M.T. Hagan and M. Menhaj, Training feed forward networks with the Marquardt algorithms, IEEE Trans Neural Networks 5 (1994), 989–993.
42. D.J. Higham and Higham N.J., MATLAB Guide, SIAM, Philadelphia, PA, 2005.
43. T. Khan, A. De and M. Uddin, Prediction of slot-size and inserted air-gap for improving the performance of rectangular microstrip antennas using artificial neural networks, IEEE Antennas Wireless Propag Lett 12 (2013), 1367–1371.
44. A. Freni, M. Mussetta, and P. Pirinoli, Neural network characterization of reflectarray antennas, Int J Antennas Propag 2012 (2012), Article ID 541354.

BIOGRAPHIES

Taimoor Khan submitted his Ph.D. Thesis with specialization in microstrip antennas at National Institute of Technology Patna, India in February, 2014. Prior to this, he got his Master degree in Communication Engineering, Bachelor degree in Electronics and Communication Engineering, and polytechnic diploma in Electronics Engineering in 2009, 2007, 2005, and 2001, respectively. Presently, he is working as associate professor at Netaji Subhas Institute of Technology Patna, India. Prior to joining this institute, he served Delhi Technological University, Delhi, India as Assistant Professor more than 2 years. Also prior to this university, he served Shobhit University, Meerut, India in different capacities like lab instructor, lecturer, and assistant professor more than 9 years. His research interest includes microstrip antennas, artificial intelligence paradigms in electromagnetics, microwave engineering and electromagnetics. He has published over 20 research papers in international journals and international/national conference proceedings. He is an active member of IEEE (USA), life member of IEI (India), and life member of IAE (USA).

Asok De obtained his Bachelor and Master of Engineering with specialization of Electronics and Communication from Jadavpur University Kolkata in 1978 and 1980, respectively. He was awarded Ph.D. degree from Indian Institute of Technology Kharagpur in the year 1986. He joined Delhi University, Delhi, India as Lecturer in the year 1984 and promoted as Reader in the year 1987. In 1991, he joined Kolkata University, Kolkata, India, as Reader and subsequently joined Delhi College of Engineering, Delhi, India, as Professor in the year 1997 and worked as Professor in ECE Dept., Head of Computer Engineering and Head of Information Technology. In 2005, he joined Ambedkar Institute of Advanced Communication Technology and Research Delhi as Principal. At present, he is working as Director of National Institute of Technology Patna. His area of interest includes antennas, transmission lines, microwave circuits, and computational electromagnetics. He has published over 100 research papers in international journals and more than 120 research papers in international/national conference proceedings. He has supervised 12 Ph.D. Thesis and four are going on. He is a senior member IEEE (USA), fellow IEI (India), fellow IETE (India), and life member CSI (India).

EXERGY ANALYSIS OF PRE-COOLED LINDE SYSTEM FOR LIQUEFACTION OF GASES FOR IMPROVING PERFORMANCE OF LINDE BASED CRYOGENICS SYSTEMS

Devender Kumar[1], R.S Mishra[2]

[1]*Research Scholar, Mechanical Department, Delhi Technological University, Shahabad, Delhi*
[2]*Professor, Mechanical Department, Delhi Technological University, Shahabad, Delhi*

Abstract

Cryogenic temperature generally temperature below the -150^{o}C .Various number of gases are liquefy by using very first Linde Hampson cycle but due to inefficiency of system output of liquefaction mass is very low as compared to expanses. Linde Pre-cooled system is designed to meet the gap in the basic Linde system. The output as well as the second law efficiency of Linde pre-cooled system is more than the basic Linde system. A complete thermo –analysis of pre-cooled Linde system is carried out and various results are predicted. The effect of some various parameters like refrigerant mass flow ratio and compressor pressure on system with six different gases is studied by applying computational numerical technique. Effect of these parameters on system conclude that the system work good near 200 bar pressure and refrigerant mass flow ratio of 0.03 is suitable for system showing high second law efficiency and Liquefaction mass ratio and low work done per liquefaction mass ratio.

Keywords: *Thermodynamics analysis, pre-cooled Linde system, refrigerant mass flow ratio, second law efficiency*

----------***----------

1. INTRODUCTION

Cryogenic industry is a very vast business industry touching almost every field of science like space, Medical science, Bio-Technology etc. Various methods are present to achieve cryogenic temperature, but economical still a challenge. Exergy analysis of system provides a tool to find out the losses in system and give a chance to achieve economical challenge. In past history various method are invented to get high exergy efficiency. Liquefaction is currently done in more complex cycles, which require about 1080 kJ of energy for each liquefied kg [1].Linde cycle is simplest form of air liquefaction system but less second law efficiency make it economical inefficient system. Liquefaction plants are rather complicated with numerous components interacting with each other and consume a large amount of process energy, it is vital to develop efficient liquefaction processes for improving the overall system performance and economic competitiveness [2]. Various research and different method are employed to increase efficiency of cryo system. Second law efficiency are very low in all system, it value ranging from 3% to 23 % for most of systems. Advance technology like different cryo fluid includes nano one (nano fluid and nano lubricants) is also tried to reduces the losses. Ceramic technology is also used in separator to increase the high output with less losses. It is noticed that the evaporating and condensing temperatures put a strong effects on the exergy losses in the evaporator, condenser, second law of efficiency and COP of the cycle but little effects on the exergy losses in the compressor and the expansion valve. The second law efficiency and the COP increases, and the total exergy loss decreases with decreasing temperature difference between the evaporator and refrigerated space and between the condenser and outside air [3] and if advance technology like nano fluid include it noticed that Nano fluid and Nano lubricant cause to reduce the exergy losses in the compressor indirectly [4].

2. THERMO ANALYSIS OF PRE-COOLED LINDE SYSTEM FOR LIQUEFICATION OF GASES:

First and second law computational numerical analysis of Pre-cooled Linde system is done for detail studies for optimized used of system .Various parameters like refrigerant mass flow ratio and compressor pressure is varies for detailed study of system .Pre-cooled Linde Hampson system is advanced stage old simple Linde Hampson system .In this system vapour compression evaporator having R134 a refrigerant is taken as additional equipment to fill the gap of simple Linde system. In Fig.1.1 the detail block diagram of Pre-cooled Linde system is shown and Fig 1.2 show T-S diagram of Pre-cooled Linde system. Vapour compression system lower down the temperature of gases coming through the compressor which is desirable for better performance of system.

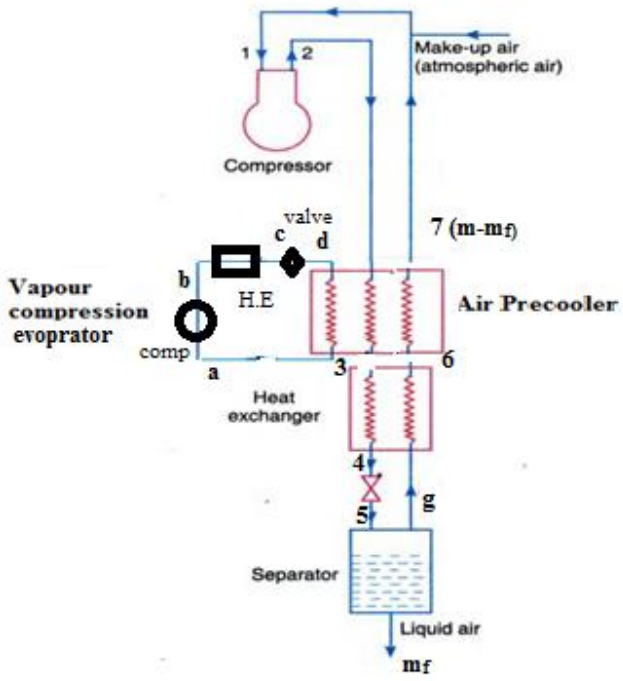

Fig 1.1:Pre-Cooled Linde sytem

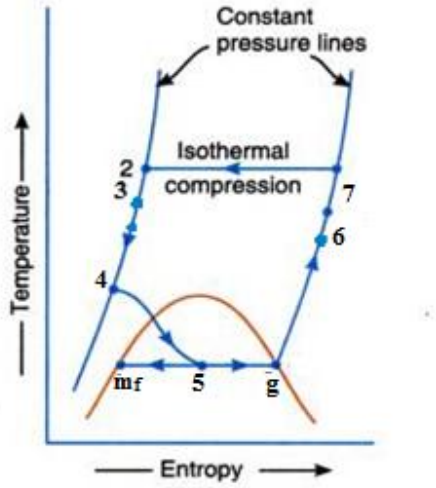

Fig 1.2 T-S diagram of pre-cooled Linde system

"Energy Balance by First Law"

$$m_r * h_d + m * h_2 = m_r * h_a + m - m_f * h_1 + m_f * h_f \quad (1)$$

$$\frac{m_f}{m} = \frac{h_1 - h_2}{h_1 - h_f} + r * \frac{h_a - h_d}{h_1 - h_f} \quad (2)$$

$$y = \frac{m_f}{m} \quad (3)$$

"Control Volume having Heat exchanger, Joule-Thomson valve, Separator"

$$m * h_3 = m_f * h_f + (m - m_f) * h_6 \quad (4)$$

$$y_{max} = \frac{h_6 - h_3}{h_6 - h_f} \quad (5)$$

"Work"

$$W_{total} = W_{c1} + W_{c2} \quad (6)$$

"Compressor work of liquefaction system"

$$E_{in} = E_{out} \quad (7)$$

$$E_{in} = m * h_1 - W_{c1} \quad (8)$$

$$E_{out} = m * h_2 - Q_R \quad (9)$$

$$Q_R = m * T_1 * (S_2 - S_1) \quad (10)$$

"Compressor work of ref system"

$$m_r * h_a - W_{c2} = m_r * h_b \quad (11)$$

$$-\frac{W_{total}}{m_f} = Z \quad (12)$$

$$-\frac{W_{total}}{m} = T_1 * (s_1 - s_2) - (h_1 - h_2) + r * (h_b - h_a) \quad (13)$$

$$-\frac{W_i}{m} = T_1 * (s_1 - s_f) - (h_1 - h_f) \quad (14)$$

$$-\frac{W_i}{m} = K \quad (15)$$

$$COP = \frac{(h_1 - h_f)}{W_{total}} \quad (16)$$

$$\eta_{2nd}\ (\%) = \frac{(h_f - h_1) - T_0 * (s_f - s_1)}{W_{total} * m_f} * 100 \quad \textbf{(17)}$$

Refrigerant Properties:

Table 1

P_a	1.013
P_b	10.013
P_c	10.013
T_a	300
T_b	373
T_c	300
h_a	278
h_c	89.07
T_d	247.1

3. RESULTS AND DISCUSSION:

On the basis of above equations and applying computational numerical technique following result about pre-cooled Linde system considering six different gases is studied. Fig 2 show variation in work done per liquefaction mass of with compressor pressure, there is sharp decrease in work done up to 200 bar but after that the decrease in work done is slow become nearly constant up to 400 bar but after that ,increment in work start with further increase in pressure. In all six gases fluorine show very high decrement in work done as compare to other gases with increasing compressor pressure. Fig 3 show the yield mass rate variation with compressor pressure, up to 200 bar the yield mass is directly proportional to compressor pressure but beyond 200 bar pressure the increment in yield mass rate of liquefaction is very small. Oxygen gas other than other gases show very different behavior because high yield rate as compared to other gases.Fig.4 show variation in work done per liquefaction mass with refrigerant mass flow ratio, the work done is very less affected by the increasing refrigerant flow rate but there is increment in work done with increment in refrigerant mass flow ratio. Fig 5 show there is decrease in second law efficiency with increase in refrigerant mass flow ratio. Whereas Fig 6 show increase in second law efficiency with compressor pressure up to 200 bar for all six gases but if there is increase in compressor pressure beyond 200,the second law efficiency start decreasing for gases except argon ,oxygen ,fluorine, they show continuous but slow increment in second law efficiency .Fig 7 show change in COP with increasing refrigerant mass flow ratio is almost constant whereas Fig 8 show decrease in COP with increasing compressor pressure.

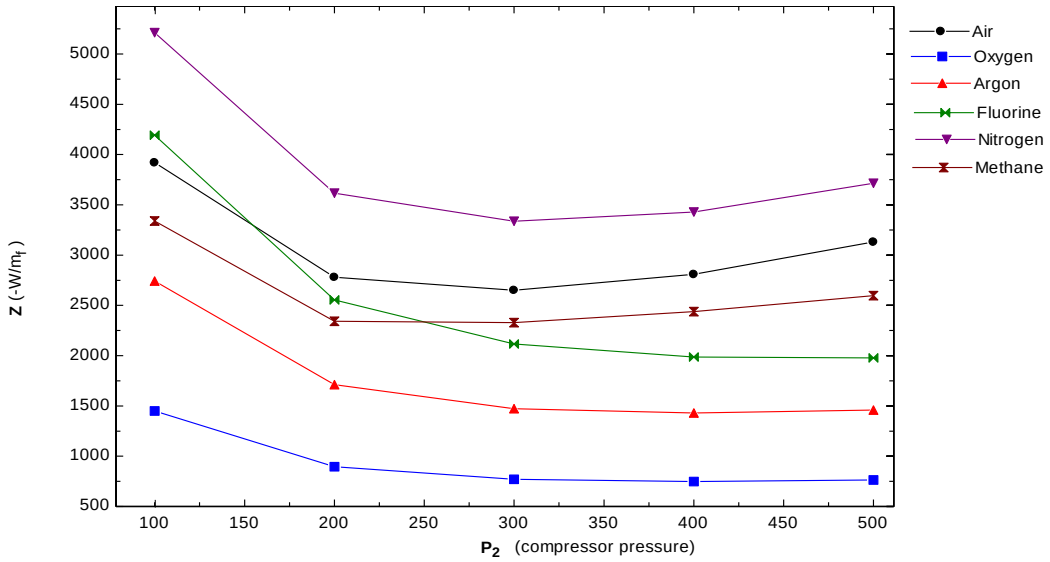

Fig: 2 Variation of work done per liquefaction with the compressor pressure

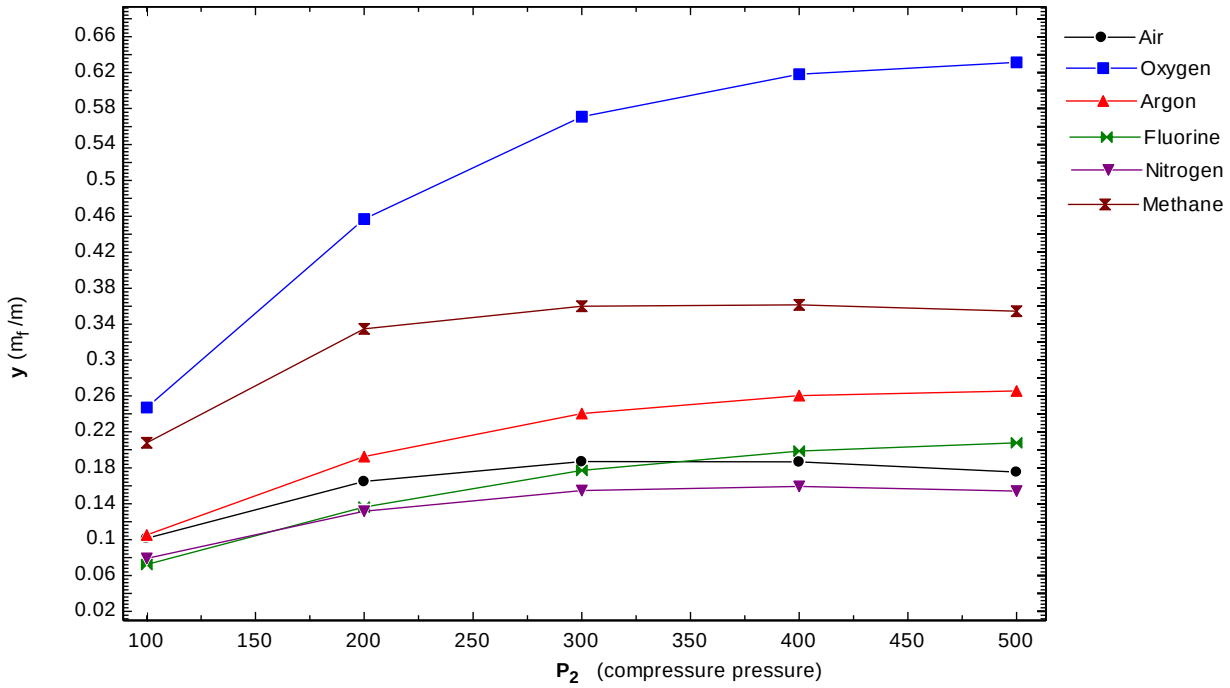

Fig: 3 Variation of liquefaction mass ratio with the compressor pressure

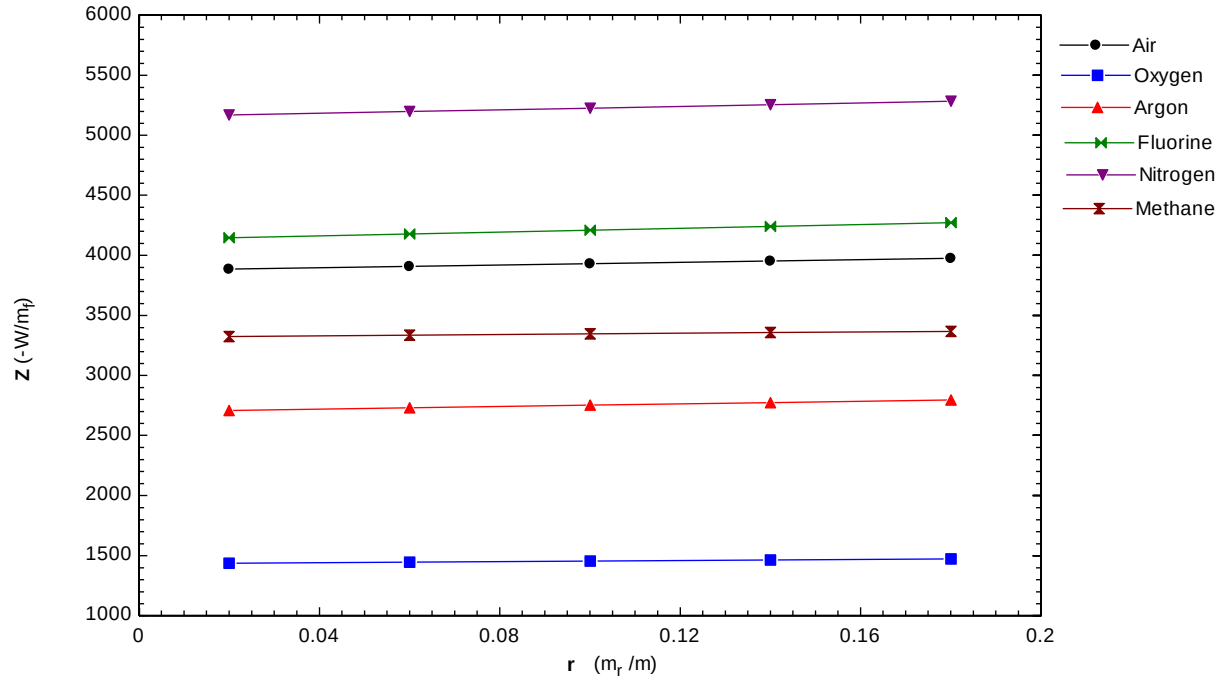

Fig: 4 Variation of work done per liquefaction mass with the refrigerant mass flow rate

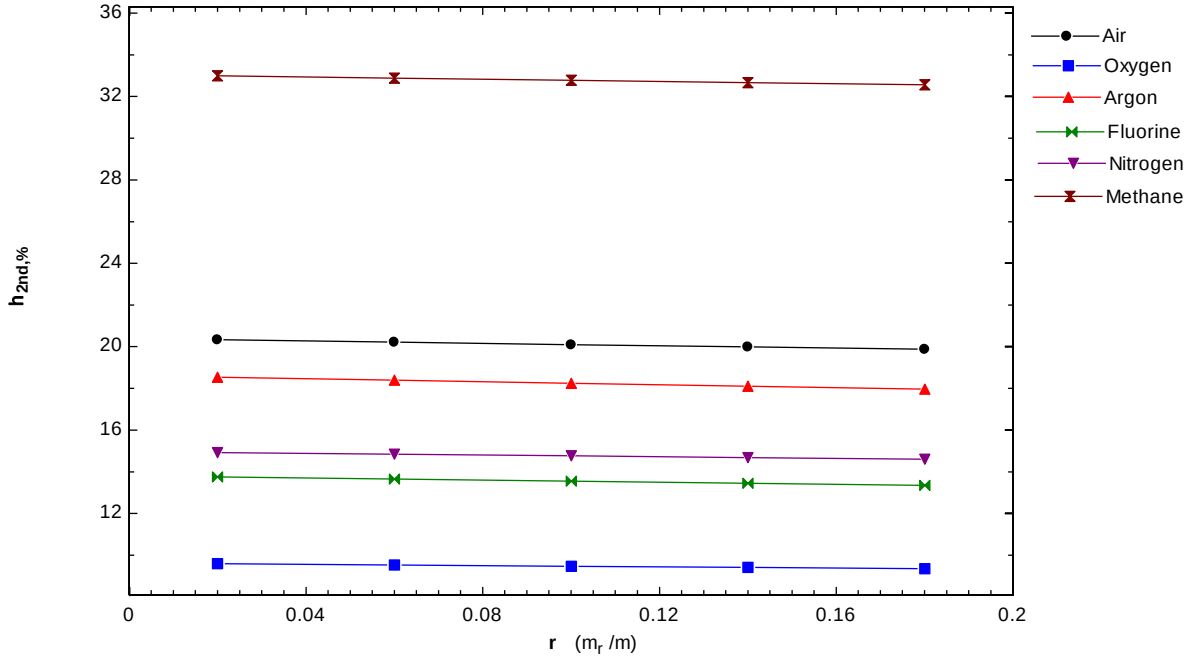

Fig: 5 Variation in second law efficiency with refrigerant mass flow rate

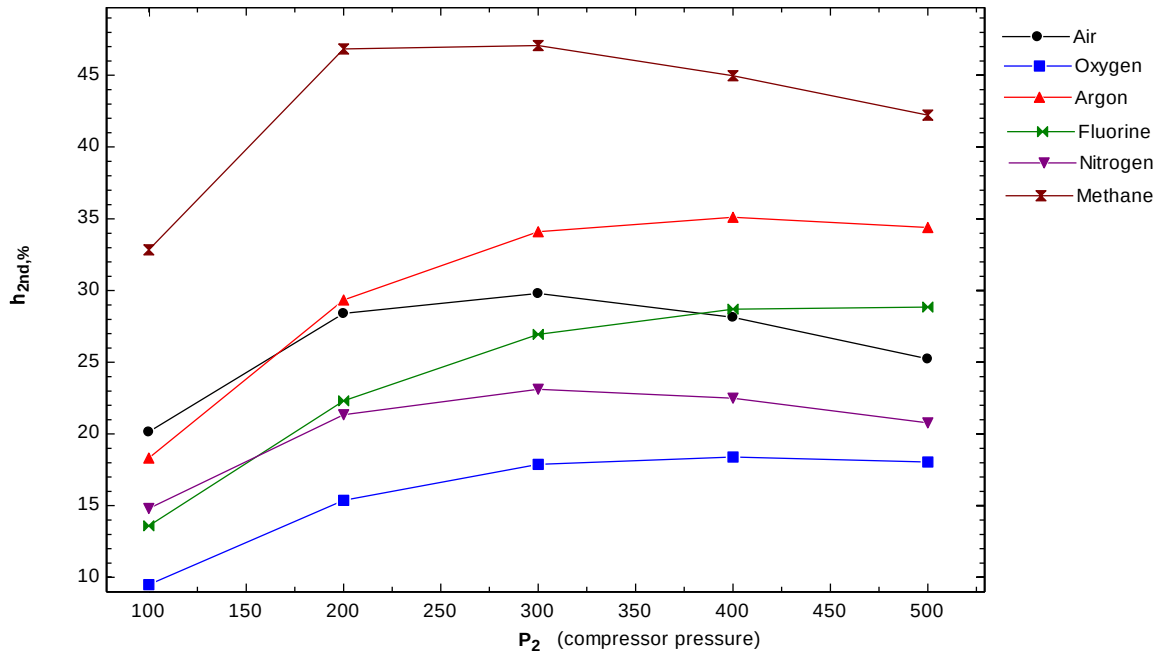

Fig: 6 Variation in second law efficiency with the compressor pressure

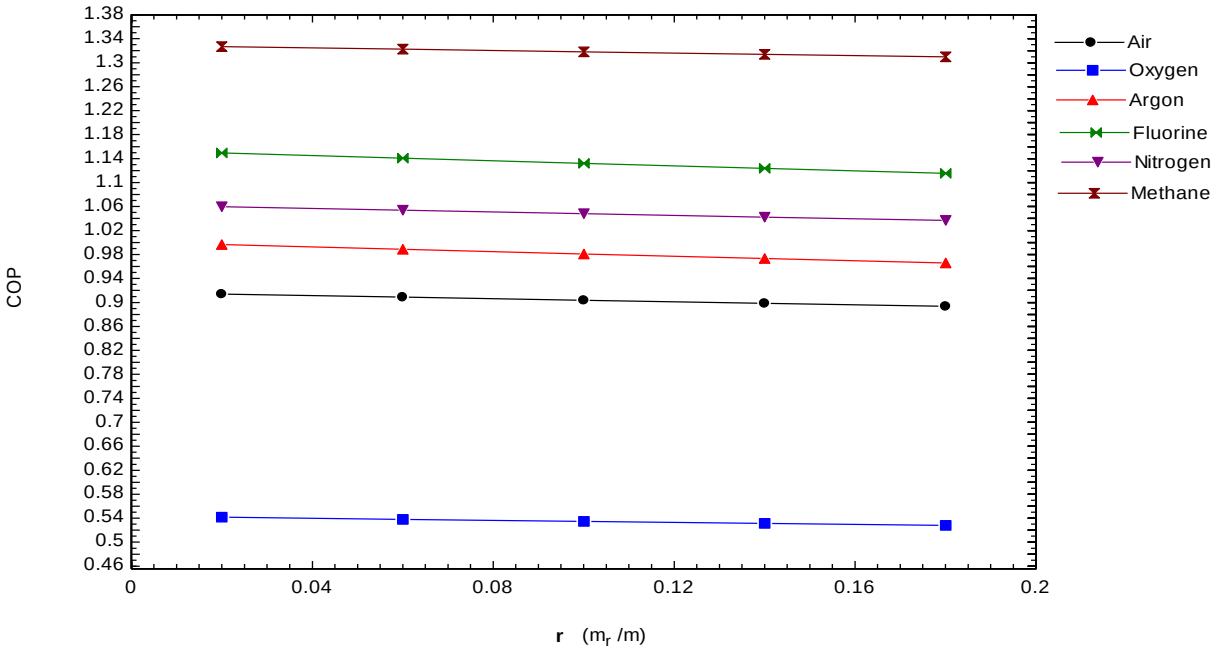

Fig: 7 Variation in COP with the refrigerant mass flow rate

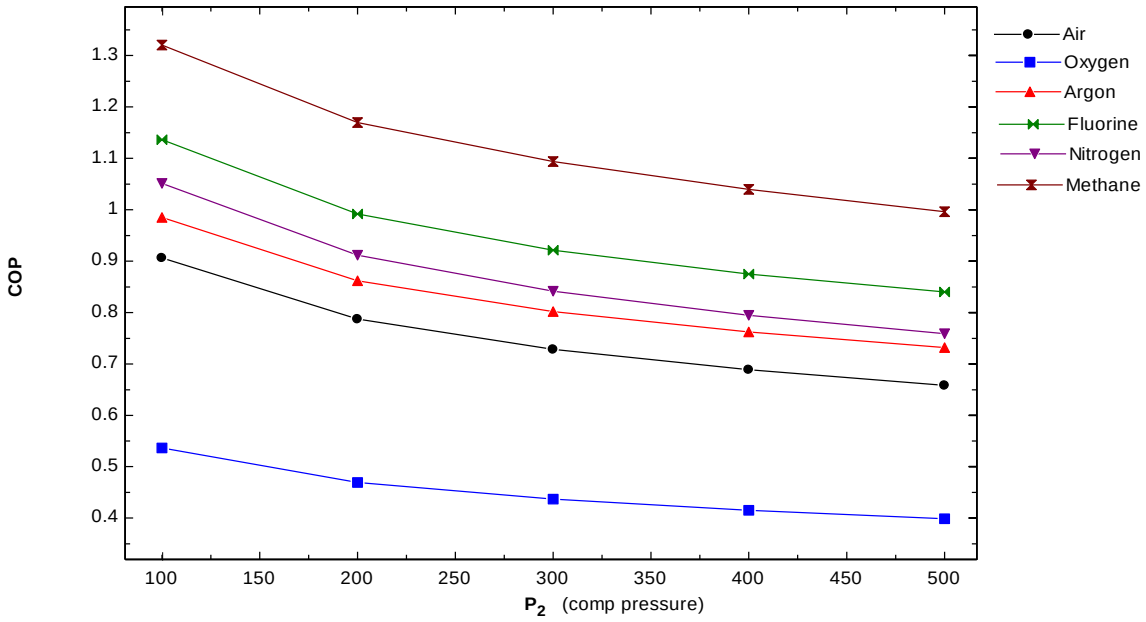

Fig: 8 Variation in COP with the compressor pressure

4. CONCLUSIONS

1) Compressor pressure up to 200 bar pressure show positive result ,up to this pressure second law efficiency and liquefaction mass ratio is show increment but after crossing this pressure rate of increasing the second law efficiency is deteriorate, and a significant dip in efficiency notice after 300 bar pressure whereas liquefaction mass ratio except oxygen show a constant extraction with negligible increment.
2) Refrigerant mass ratio also effect the second efficiency , COP show decreasing in nature while Work done per liquefaction mass of system show increasing in nature with increase in refrigerant mass flow ratio.

REFRENCES

[1]. W.F. Castle, Air separation and liquefaction: recent developments and prospects for the beginning of the new millennium, International Journal of Refrigeration-Revue Internationale Du Froid 25 (Jan. 2002) 158-172.
[2]. Kanoglu M. Cryogenic turbine efficiencies. Exergy, Int J 2001;1:202–8.
[3]. Recep Yumrutaş, Mehmet Kunduz, Mehmet Kanoğlu, Exergy analysis of vapor compression refrigeration systems, Exergy, An International Journal, Volume 2, Issue 4, 2002, Pages 266-272, ISSN 1164-0235
[4]. J.U. Ahamed, R. Saidur, H.H. Masjuki, A review on exergy analysis of vapor compression refrigeration system, Renewable and Sustainable Energy Reviews, Volume 15, Issue 3, April 2011, Pages 1593-1600, ISSN 1364-0321.

NOMENCLATURE

m_r = mass flow rate of refrigerant
m=mass flow rate of gas
m_f =Liquefaction mass
h=Enthalpy
s=Entropy
X=Dryness fraction
T=temperature
P=Pressure
$\eta_{2nd\ law}$=Second law efficiency
C=Specific heat capacity fluid or gas
W_{total} =Total Work of compression
W_{c1}=Compressor work of system
W_{c1}=Compressor work of vapour compression system
Y=liquefaction mass flow ratio
E=Energy
R=Refrigerant

IOSR Journal of Business and Management (IOSR-JBM)
e-ISSN: 2278-487X, p-ISSN: 2319-7668. Volume 16, Issue 5. Ver. III (May. 2014), PP 73-78
www.iosrjournals.org

Impact of Brand on Rural and Urban Consumer Behavior- A Study on Mobile Phone Buyers

Shaktiman Singh[1], Saurabh Kumar[2], Tanmay Goel[3], Sahib Chawla[4]
[1, 2, 3, 4]*Department of Mechanical Engineering, Delhi Technological University, India*

Abstract: *Consumers are the backbone of all business organizations & coherently all business activities concern with consumer and consumer satisfaction.Brand acts as a signal allowing customer to quickly recognize a product as they are familiar with or one they like.The powerful brand is which resides in the mind of the consumer.This paper examines how the rural and urban population conceive the notion of "BRAND". The research aims at comparing the buying behavior of rural & urban consumer & find out their priorities while making a purchase decision regarding mobile phones .This study has been conducted through literature study as well as a questionnaire administered survey of 200 respondents of different age groups, income & occupation and has been analyzed through AHP (Analytical Hierarchy Process) to comply with the objectives & also to draw conclusions.The study reveals that the urban consumer is more brand and style 'conscious' compared to its rural counterpart which prioritizes functionality and price more. It also shows that urban population relies majorly on internet as source of information whereas rural population relies on T.V. ads& Mobile phone retailers.This paper serves as a valuable guideline for management to review their advertising campaigns & modify their mobiles according to the need of the customer.*

Keywords: *AHP, Advertising, Brand management, Consumer Behavior, Mobile Phones*.

I. Introduction

Although mobile phones have become a fundamental part of personal communication across the globe during the past ten years, consumer research has devoted little specific attention to motives and choice underlying the mobile phone buying decision process. There are numerous complex factors that need to be taken into account when exploring mobile phone buying decision process, including both macro and microeconomic conditions[1] that affect the evolution of mobile phone market in general and individual consumer's motives and decision making in particular. The individual and environmental factors influences the consumer behavior. Often, consumer in India purchases the goods and services, which they want, others to accept. Behavior is therefore determined by the individual's psychological makeup and the influence of other. Thus behavior is the result of interaction of the consumer & personal influence and pressure exerted upon them by outside forces in the environment [2]. An understanding of buying behavior is essential in marketing and planning programs. Acomprehensive research of consumer behaviorgives the advertiser a deeper insight of his target section of market, which in turn proves to be very significant in strategic advertising decisions, especially in defining the target markets and creating the advertising appeal and message. Modern Urban buyers along with the product features also want to know how and why the product will benefit them. They look not only for what a product can do but also what it means to them. Thus, buying behavior involves a complicated series of stimulus and response. The mobile phone itself has also become a totemic and fashion object, with users decorating, customizing, and accessorizing their mobile phones to reflect their personality. In the rationale of modern marketing, the firm's existence is dependent on customer's satisfaction. Therefore, the knowledge of "what the customer thinks" and "what consequently would contribute to his satisfaction" is at the requirement of the marketer [3].

Usage of cell phones is not restricted to urban talk and educated youth. Brands evolve to keep up with changing demographics, changing spending habits, consumer lifestyles, and various ethnicities becoming more prevalent. Indian Marketers on rural marketing have two understanding- (i) The urban metro products and marketing products can be implemented in rural markets with some or no change. (ii) The rural marketing required the separate skills and techniques from its urban counterpart.

The Marketers have following facilities to make them believe in accepting the truth that rural markets are different in so many terms.

(i) The rural market has the opportunity for many brands.
(ii) Low priced products can be more successful in rural markets because the low purchasing, purchasing powers in rural markets.
(iii) Rural consumers have mostly homogeneous group with similar needs, economic conditions and problems.

(iv) The rural markets can be worked with the different media environment as opposed to press, film, radio and other urban centric media exposure.

How reality does affect the planning of marketers? Do villagers have same attitude like urban consumers? The question arises for the management of rural marketing effects in a significant manner so than companies can enter in the rural market with the definite goals and targets but not for a short term period but for longer duration. In this research paper, we will discuss the role of regard. The strategy, which will be presented in the paper, can be either specific or universally applicable.

II. Purpose Of The Research

This research is designed to investigate the influence of Brand name & Advertisements on two different sections of society-the urban & the rural consumer base respectively.Essentially the research aspires to study the topic through reviewing related articles & also by getting the perceptions of knowledgeable individuals regarding the topic through surveys. Moreover, this study will focus on the following goals:

- To study the significant difference, if any, in the purchasing motive, preferences, taste of the urban & rural consumer.
- To know about the awareness level of consumer regarding 'Brands'.
- To identify and analyze the difference in the factors which impinge on to the satisfaction level of both types of consumers.
- To make suggestions on the basis of findings.

III. Research Methodology

This survey was conducted at two places. For the study of rural and urban areas, we surveyed Saket (South Delhi) and Ballabgarh (Faridabad). Total 200 people were surveyed, out of which 100 people belonged to each region. The sample space included both men and women of different age groups. Depending upon the age the sample is divided into 3 groups: 12-18,19-21 and 21 above. By studying different age groups, the study aims to find the consumer behavior about brand recognition for different age groups. The study is simplified by the use of pie charts wherever necessary and the results are expressed in the form of percentages. It is assumed that all the respondents are not related to each other in any manner and the opinions of one respondent cannot affect the opinions of any other respondent.

IV. Hypotheses

1. The level of awareness of 'Branded 'products among the customers is average.
2. Brand image & Advertisement has significant relationship with consumer buying behavior.

V. Objectives Of The Study

This study was carried out with the following objectives:

1. The study aims at comparing the preference for brand recognition among urban and rural mobile users.
2. The study aims to compare the role of advertisement in the purchase of mobile phone among rural and urban mobile users.
3. The study aims to compare the preference of brand recognition among different income groups among the respondents.
4. The study aims to compare preference of functionality, quality and price over brand recognition among rural and urban mobile users.
5. The study aims at finding the most preferable mobile brands among rural and urban mobile users.

VI. Problem Statement

In present times, "Brand name" is emerging out to be one of the strongest marketing tool in all fields.Narrowing down our view to mobile phones, we can see that Brand Image plays a significant role in customer decision making process.But due to lack of technological advancements, 60% of total population residing is rural areas is still deprived of this "Notion" as compared to their urban counterparts. The present study made an attempt to investigate the influence of Brand image and advertisement on both urban and rural sections of the Indian society.

VII. Division Of Sample Space

Division On The Basis Of	Division Characteristic Of The Respondent	Area To Which The Respondent Belongs	
		URBAN	RURAL
AGE	12-18	11	24
	19-21	66	59
	Above 21	23	17
SEX	Male	67	84
	Female	33	16
FAMILY INCOME	Below 15000	15	21
	15000-35000	43	41
	Above 35000	42	38

VIII. Observations And Results

- The ownership of different mobile brands among rural and urban users.

BRAND	URBAN	RURAL
SAMSUNG	29	30
NOKIA	11	28
SONY	25	9
APPLE Iphone	13	3
BLACKBERRY	2	2
HTC	6	3
MICROMAX	10	20
KARBONN	1	3
OTHERS	3	2

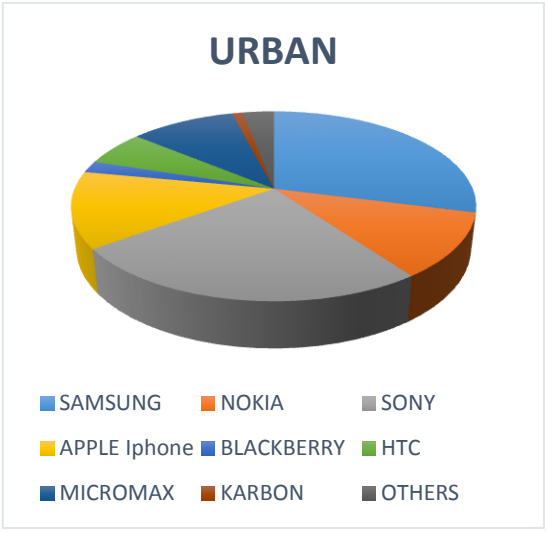

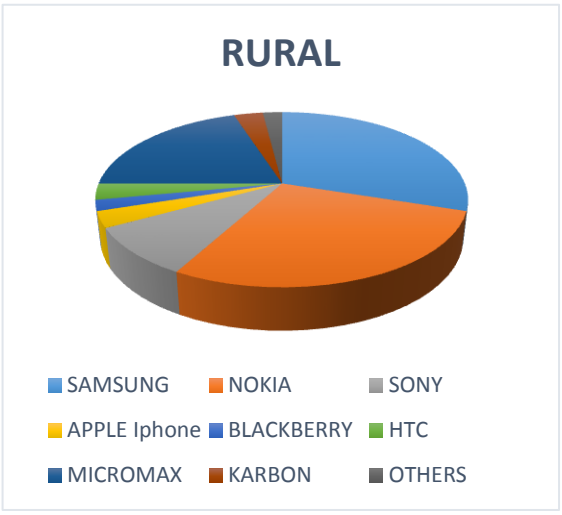

- Source of information about the product.

VARIABLE	URBAN	RURAL
T.V.	35	54
NEWSPAPER	11	23
FRIENDS	26	9
INTERNET	23	11
OTHER	5	3

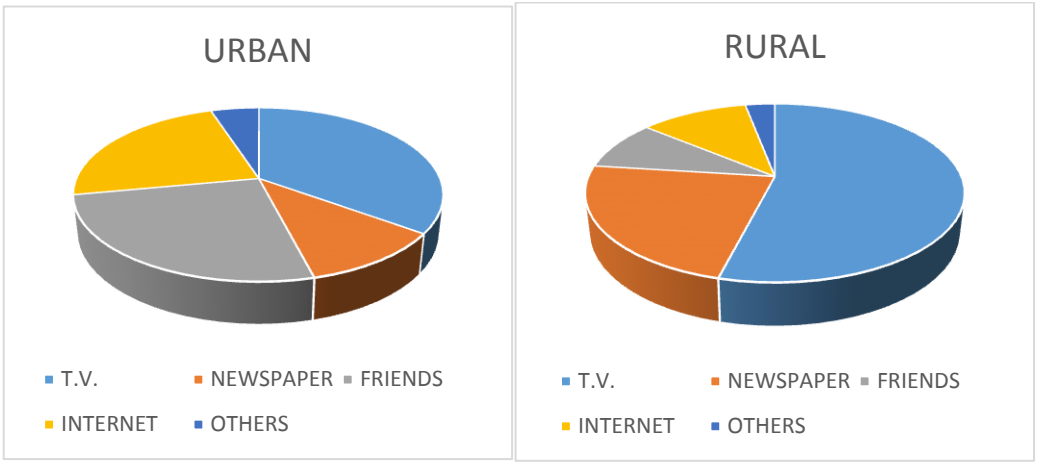

- The selection of mobile phone after considering its brand (on basis of demographic factor)

Response	Respondent	
	Urban	Rural
YES	76	51
NO	13	37
MAYBE	11	12

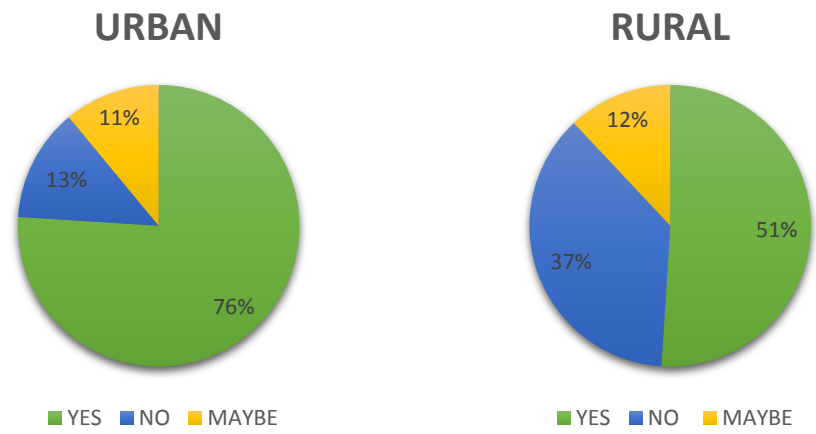

- The selection of mobile phone after considering its brand(on basis of income factor)

INCOME	RESPONSE	RESPONDENT	
(per month)		URBAN	RURAL
BELOW 15000	YES	9	4
	NO	4	17
	MAYBE	2	0
15000-35000	YES	31	21
	NO	7	12
	MAYBE	5	8
ABOVE 35000	YES	36	26
	NO	2	8
	MAYBE	4	4

- The most important factor to be considered while selecting a mobile phone.

VARIABLE	RESPONDENT	
	URBAN	RURAL
Functionality	51	44
Brand	21	12
Pricing	15	24
Quality	13	20

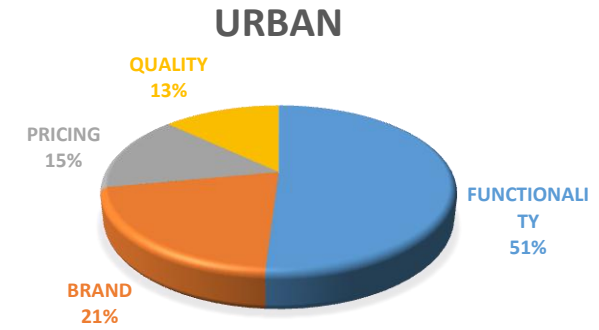

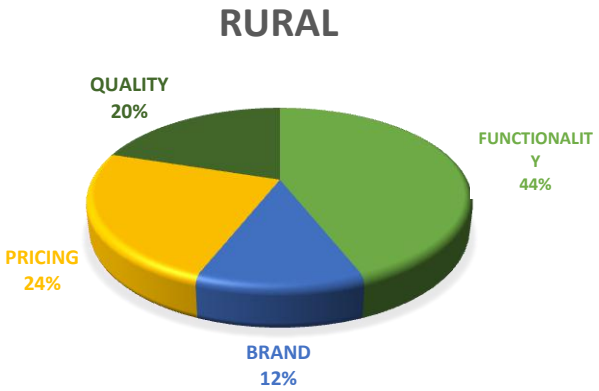

- Ownership of a new mobile phone.

VARIABLE	RESPONDENT	
	URBAN	RURAL
NEW PHONE	91	79
SECOND HANDPHONE	9	21

IX. Major Findings

- As high as 76% of the total urban respondents say that they would consider a key brand in the market for purchase of a mobile phone. Surprisingly, a healthy 51% of the rural respondents feel the same way.
- Most of the respondents from urban as well as rural areas admit that the source of information about the product they bought was T.V. advertisement.
- As expected, as the purchasing power of the buyer increases, the preference for branded products increase for both rural and urban users increases. This is mainly due to the increase in the quality of lifestyle.
- For both urban and rural users, functionality is a key trait in a mobile phone that they consider before buying a mobile phone followed by its price. It can be concluded that people a willing to spend more money to buy a mobile phone with better specifications.
- For both urban and rural users, Samsung and Nokia are preferred over other brands. This may be due to the fact that these companies offer mobile phones for every price range so that each section of society can be targeted, unlike Apple Iphone, which is owned by only a bunch of people in urban areas only. Also the brands like Micromax and Karbonn which offer high specifications for low prices are also catching up in the market.

X. Significance Of The Study

This study helps firms and organizations to improve their market strategies by understanding issues like:

1. How the psychology of an urban differs from rural consumers i.e. how they think, feel, reason & select among different alternatives (e.g. brand, product etc.)

2. How both consumers are influenced by his/her environment (e.g. culture, family, signs, media etc.)
3. How limitation in consumer knowledge & information processing abilities influence decision making & marketing
4. How companies can adapt & improve their marketing campaigning by adjusting to the difference in needs of rural & urban consumers.

XI. Conclusion

The purpose of this paper was to study the influence of brand name on the consumer decision making process and to investigate the effect of external factors on consumer behavior by comparing the choices of two different consumer bases- rural and urban. Consumer behavior is a conditioned response to external events, therefore the region and surrounding environment also have some impact on choice of consumer.To conduct the research, a questionnaire administered survey has been conducted among 200 respondents of urban and rural regions and the data revealed that brand name has strong influence on purchase decision. In rural areas, pricing is given more consideration than brand name, while in urban areas, brand name overtakes pricing factor. From the study it is also clear that well known mobile phone brands are equally popular among the people of both regions and the consumers trust the brand name. The company which offers a wide range of options to choose from is more likely to successfully gain popularity and capture market share equally well in urban as well as rural areas. The study highlights the key elements which influence the consumer behavior and can prove to be valuable to mobile phone companies as well as market analysts.

References

[1] HeikkiKarjaluoto, Factors Affecting Consumer Choice of Mobile Phones: Two Studies from Finland, Journal of Euro marketing, Vol. 14(3) 2005

[2] Dr. PratyushTripathi& Prof. Satish Kr. Singh, An Empirical Study of Consumer Behavior towards The Preference and Usage of Mobile Phone Services in Bhopal, Current Trends in Technology and Sciences Volume : 1, Issue : 2 ,Sept. 2012

[3] Jegan, A. And Dr. S. Sudalaiyandi, Consumer Behavior Towards Mobile Phone Services In Kovilpatti, Thoothukud District (India) - A Case Study by, International Journal of Current Research, Vol. 4, Issue, 04, pp.261-265, April, 2012

[4] Karjaluoto, H., J. Karvonen, et al. (2005). Factors affecting consumer choice of mobile phones: two studies from Finland. Journal ofEuro marketing 14(3): 59-82.

[5] Bettman, J.R. and Zins, M.A. (1977),"Constructive Processes in Consume Choice", Journal of Consumer Research, 4, September, pp. 75-85.

[6] Sun, T. and G. Wu (2004). Consumption patterns of Chinese urban and rural consumers.Journal of Consumer Marketing21(4):245-253.

[7] Keller, K. L., (2008) Strategic Brand Management, Second Edition, Prentice Hall of India, New Delhi.

[8] Gosh, Aparisim, 'The New Rules of Rural Marketing', Business World, April, 1994

[9] Alba, J.W. and Hutchinson, J.W. (1988), "Dimensions of Consumer Expertise", Journal of Consumer Research, 13, March, pp. 411-454.

[10] Rogers M.J 1988. "Expenditures of rural and urban consumers", Monthly Labour Review, Vo.41

[11] Blythe, J. 2006 Essentials of Marketing Communications. 3rd Edition Pearson Education Limited. Essex (UK)

[12] Stayman, D.M. and Deshpande, R. (1989), "Situational Ethnicity and Consumer Behavior", Journal of Consumer Research, 16, December, pp. 361-371.

[13] Nithila Vincent, A Study on Brand Consciousness Among Children and its Effect on Family Buying Behavior in Bangalore City, Indian Journal of Marketing, Volume XXXVI • Number 1 • January 2006

[14] Schmitt, B. H. & Pan, Y. (1994). Managing corporate and brand identities in the Asia-Pacific region. California Management Review, 36 (4), 32-48.

[15] Nedungadi, P. (1990). Recall and consumer consideration sets: Influencingchoice without altering brand evaluations. Journal of Consumer Research, 17(3), 263-276.

[16] Dr. L. Shashikumar SharmaAn Empirical Study of Consumer Behavior in Mobile Phone Market in Bhutan Management Convergence, Vol 1, No 1 (2010)

[17] V. AlaguPandian et al. An Empirical Study of Consumer Behavior towards the Preference and Usage of Mobile Phone Services in Bhopal IJRFM Volume 2, Issue 3 (March 2012)

[18] Dr. HeenaUpadhyay et al. Consumer Expenditure Behavior in India: A Case of Rural and Urban Consumer International Journal of Business and Management InventionVolume 2 Issue 2 (February. 2013)

[19] Schiffman and Kannuk, Consumer Behavior, Pearson 4th edition, (1991)

[20] Home N (2002). "Rural consumers' patronage behavior in Finland", International Review of Retail, Distribution and Consumer Research, pp.149–164.

[21] Sampath Kumar Ravikanthi. Indian urban and rural market: a comparative study on place of purchase in selected consumer products, International Trade & Academic Research Conference (ITARC), 7 – 8th November, 2012, London.UK.

Investigation of variation of energy of laser beam on structural, electrical and optical properties of pulsed laser deposited CuO thin films

V. Dahiya, G. Kaur, A. Mitra, and A. Kumar

Citation: AIP Conference Proceedings **1591**, 941 (2014); doi: 10.1063/1.4872810
View online: http://dx.doi.org/10.1063/1.4872810
View Table of Contents: http://scitation.aip.org/content/aip/proceeding/aipcp/1591?ver=pdfcov
Published by the AIP Publishing

Investigation of Variation of Energy of Laser Beam on Structural, Electrical and Optical Properties of Pulsed Laser Deposited CuO Thin Films

V. Dahiya [1,*], G. Kaur [2], A. Mitra [2] and A. Kumar [1]

[1] *Department of Applied Physics, Delhi Technological University, Delhi, India*
[2] *Department of Physics, Indian Institute of Technology Roorkee, Roorkee, India*
**E-mail:vinitadce@gmail.com*

Abstract. In this paper, copper oxide (CuO) thin films have been deposited successfully by pulsed laser deposition technique using copper metal as target material. Thin films have been prepared under different energy of laser pulses ranging from 100mJ/pulse to 250 mJ/pulse. These films have been characterized for their structural, electrical and optical properties by using X-Ray Diffractometer (XRD), Four probe method and UV spectroscopy. Morphological and structural studies show that there is increase in crystallite size with the increase in energy of laser beam. Thus resulting in improved crystallinity and degree of orientation of the CuO thin films. Optoelectrical properties show direct relation between conductivity and energy of laser beam. Optical analysis of CuO thin films prepared under different energy of laser beam shows good agreement with structural analysis. The prepared CuO thin films show high absorbance in the UV and visible range and thus are suitable candidate for thin films solar cell application.

Keywords: Thin films, Cupric oxide films, Pulsed laser deposition, electrical properties, optical properties.
PACS: **85.40. Xx, 73.61. Ph, 78.66. Qn**

INTRODUCTION

Copper oxides are semiconductors that have been studied for several reasons such as the natural abundance of starting material copper (Cu); the easiness of production by Cu oxidation; their non-toxic nature and the reasonably good electrical and optical properties by CuO [1]. Copper forms two well-known oxides: tenorite (CuO) and cuprite (Cu_2O). Both the tenorite and cuprite were p-type semiconductors having band gap energy of 1.21 to 1.51 eV and 2.10 to 2.60 eV repectively [2,3]. As a p-type semiconductor, conduction arises from the presence of holes in the valence band due to doping/annealing [4]. Copper (II) Oxide or Cupric Oxide is the higher oxide of copper.

Semiconductor oxides are promising alternative to silicon-based solar cells because they possess high optical absorption and are composed of low cost materials [5]. CuO is attractive as a selective solar absorber since it has high solar absorbency and a low thermal emittance [6]. It has been used as a hole transfer layer and barrier layer for dye-sensitized solar cells [7], active layer in various types of solar cells [8], passive layer in solar-selective surfaces and in photo-electrochemical cells [9]. The film of cupric oxide can be obtained by various deposition techniques like reactive sputtering deposition, pulsed laser deposition (PLD), chemical bath deposition (CBD), sol-gel, thermal deposition or electrospun. To obtain the exact monoclinic CuO crystal structure, the aforementioned deposition techniques involves real-time substrate heating [10-14], post-annealing [15-17]. Although, the sol-gel method is the most preferred technique due to the simple equipment involved and low costs compared to other techniques. This method needs a large quantity of solution, longer processing time and heat treatment for crystallization [13,17]. Alternatively, high power delivery to the source material during thin film deposition can effectively reduce the dependence of substrate heating to obtain high quality crystal film, such as PLD [18] along with high equipment cost. The XRD, SEM, electrical and optical techniques have been used to characterize crystal structure, surface morphology, electrical conductivity and optical properties.

EXPERIMENTAL DETAILS

CuO thin films have been deposited using Pulse Laser Deposition technique using copper as basic target material. Physical conditions like substrate temperature, pressure have been maintained to 600˚C and 50 mTorr respectively. Four samples of CuO thin films have been deposited by varying energy of laser beam from 100 mJ/pulse to 250 mJ/pulse in steps of 50 mJ/pulse at 355 nm. To improve the grain size and crystallinity of thin

Solid State Physics
AIP Conf. Proc. 1591, 941-943 (2014); doi: 10.1063/1.4872810

films post deposition annealing has been done for around 20 minutes inside the vacuum chamber. Structural characterization of prepared CuO thin films sample has been done using X-ray diffractometer (Bruker AXS D8 Advanced). The optical properties transmittance, absorbance and reflectance for these thin films have been examined using UV-1800, SHIMADZU-UV spectrophotometer and JASCO Model V-650 spectrophotometer while the current - voltage (I–V) characteristics ranging from 0-50V, have been observed at room temperature using Keithley 2636A dual channel source major unit sealed in Black Box and provided with a probe station.

RESULTS AND DISCUSSIONS

Structural Analysis

Figure 1 shows the XRD pattern observed for CuO thin films deposited at different energies of laser beam. Two different reflections along directions (002) and (111) are prominently seen when thin films were deposited at different energies from 100 mJ/pulse to 250 mJ/pulse which corresponds to characteristics of CuO monoclinic phase. The reflection peaks are indexed by comparing the data with JCPDS card file no.80-1917. As the laser energy increases from 100mJ/pulse to 200 mJ/pulse peak corresponding to direction (002) increases and for (111) decreases. While at 250 mJ/pulse of energy peak corresponding to (111) direction is more prominent than (002) direction. Only small reflection corresponding to (002) direction has been observed. It has been concluded that all the thin films prepared are polycrystalline with monoclinic phase. The crystallite size of CuO thin films has been calculated using Debye Scherer's formula given by

$$L=0.9\lambda/\beta\cos\theta \qquad (1)$$

where λ is the wavelength of X-rays used for obtaining diffraction pattern, β is the full width at half maximum (FWHM) of peak i.e. half width of the diffraction peak measured in radians.
The FWHM corresponding to direction (111) decreases as energy increases from 100 mJ/pulse to 200 mJ/pulse which implies the improved crystallinity at higher energy. The crystallite size varying from 127 to 168 Aº has been observed with increase in energy of laser beam. This can be attributed to the coalescences of grains at higher energy of laser beam . As a result; it implies that the crystallinity of the CuO thin films is improved at higher energies. These may be due to providing energy to crystallites gaining enough energy to orient in proper equilibrium sites, resulting in the improvement of crystallinity and degree of orientation of the CuO films.

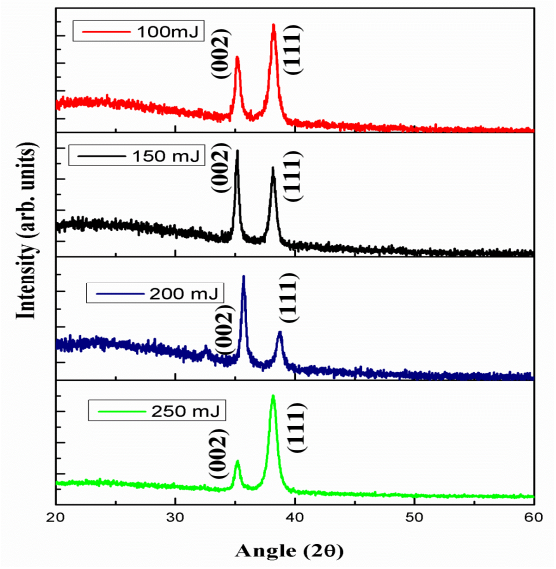

FIGURE 1. X- Ray diffraction pattern of CuO thin films deposited at different energies of Laser beam

Electrical Analysis

The four-point probe method of dark electrical conductivity measurement was used to study the variation of electrical conductivity of the film with laser beam energy. The room temperature Current versus Voltage (I-V) behaviour of the CuO thin films has been depicted in Fig. 2. The conductivity ranging from 0. 095 $(\Omega\text{-cm})^{-1}$ to 0.212 $(\Omega\text{-cm})^{-1}$ has been observed. With increase in energy of laser beam conductivity of CuO thin films also increases. Room temperature electrical conductivity has been increased with increasing the energy which indicates the semiconducting electrical behavior of CuO thin films. Increase in the electrical conductivity can be attributed towards improved crystallite structure at higher energy and reduction in amorphous phase of CuO thin films.

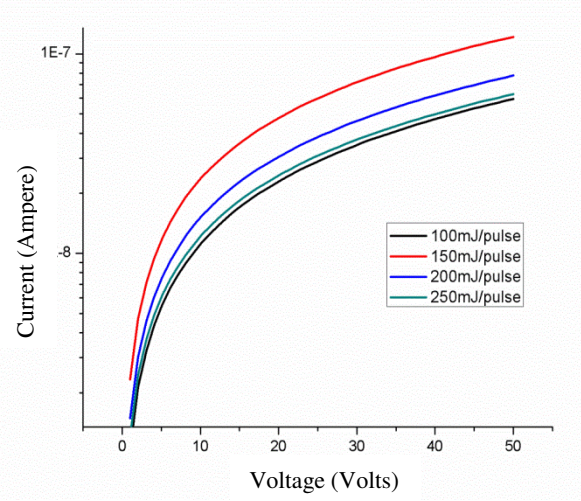

FIGURE 2. I-V characteristics of CuO thin films deposited at different energies of laser beam

Optical Analysis

Figure 3 shows the absorption spectra of CuO thin films obtained from PLD at different energies of laser beam.

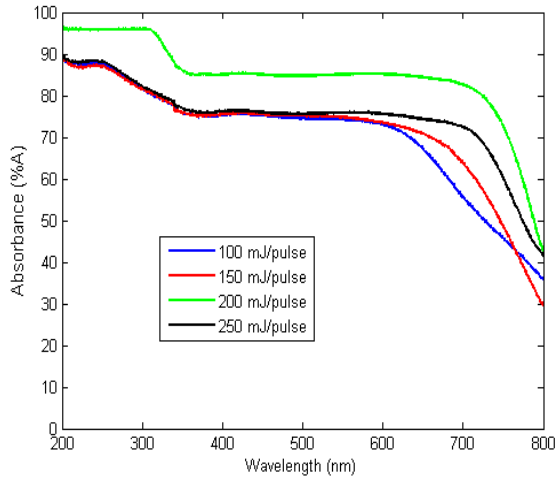

FIGURE 3. Absorbance spectra of CuO thin films

CuO thin films have higher absorption in the UV and visible region while low absorption in the infrared region. The absorption is almost uniform in the visible range and absorption edge shifts upwards as the energy of laser pulse increases. The theory of optical absorption gives the Tauc relationship between the absorption coefficient α and the photon energy $h\nu$ as

$$\alpha = \frac{(h\nu - E_g)^{1/2}}{h\nu} \qquad (2)$$

where E_g is the bandgap energy in eV. The E_g value is found to decrease from 1.93 - 1.67 eV with increasing laser beam energy from 100 mJ/pulse to 200 mJ/pulse. The decrease in E_g indicates an improvement of the quality of the film due to the annealing out of the structural defects. This is in agreement with the experimental results of XRD analysis. According to XRD results, the crystallite size increased with increased laser beam energy. Uniform deposition of CuO thin films may be attributed to the improvement in the crystalline quality of the films along with reduction in porosity.

CONCLUSIONS

CuO thin films deposited using PLD technique at different incoming laser beam energies show increase in crystallite size as there is increase in energy of laser pulse. This implies improved crystallinity of CuO thin films at higher energies which might be due to the supply of enough energy to crystallites to orient in proper direction. Also, there is increase in electrical conductivity at higher laser beam energy which attributes towards improvement in crystallite structure and reduction of amorphous phase of CuO thin films. Optical absorption studies show higher absorption in the visible and UV region with bandgap 1.93 eV which has been reduced to 1.67 eV with increase in laser beam energy. This has been attributed towards reduction in porosity. Higher absorption of these films render them suitable for application of thin film solar cells.

ACKNOWLEDGEMENTS

V. Dahiya acknowledges support from Indian Institute of Technology Roorkee, India for carrying out this work as a part of her summer project.

REFERENCES

1. G. Papadimitropoulos, N. Vourdas, V. Vamvakas Em and D. Davazoglou, *Thin Solid Films* **515**, 2428–2432 (2006).
2. K. H. Yoon, W. J. Choi and D.H. Kang, *Thin Solid Films* **372**, 250 (2000).
3. A.Y. Oral, E. Mensur, M. H. Aslan and E. Basaran, *Mater. Chem. Phys*. **83**, 140 (2004).
4. C. R. Sekhar, *Solar Energy Mater*.**68,** 307 (2001).
5. A.N. Banerjee and K. Chattopadhyay, *Progress in Crystal Growth and Characterization of Material*. 2005; **50**, 52-105 (2005).
6. T. Maruyama, *Sol. Energy Mater. Solar Cells* **56**, 85-92 (1998).
7. P. Raksa, S. Nilphai, A. Gardchareon, S. Choopun, *Thin Solid Films*, 517 (2009)
8. E. P. S. Tan, Y. Zhu, T. Yu, L. Dai, C. H. Sow, V. B. C. Tan, and C. T. Lim, *Applied Physics Letters* **90**, 163112 (2007).
9. Y. Lim, J. J. Choi, T. Hanrath, *Journal of Nanomaterials*, (2012).
10. J.K. Feng, H. Xia, M.O. Lai, and L. Lu, *Mater. Res. Bull.*, (2010).
11. P. Samarasekara, N. T. R. N. Kumara and N. U. S. Yapa, *Physica B* **404**, 4831-4834 (2009).
12. A. A. Ogwu, E. Bouquerel, O. Ademosu, S. Moh, E. Crossan and F. Placido, *J. Phys. D-Appl. Phys.* **38**, 266-271 (2005).
13. K. P. Muthe, J. C. Vyas, S. N. Narang, D. K. Aswal, S. K. Gupta, D. Bhattacharya, R. Pinto, G. P. Kothiyal and S. C. Sabharwal, *Thin Solid Films* **324**, 37-43 (1998).
14. D. Barreca, E. Comini, A. Gasparotto, C. Maccato, C. Sada, G. Sberveglieri and E. Tondello, *Sens. Actuator B-Chem.* **141**, 270-275 (2009).
15. A. Aslani and V. Oroojpour, *Physica B*, **406**, 144-149 (2011).
16. R. P. Wijesundera, *Semicond. Sci. Technol.* **25**, 0450 (2011).
17. G. Papadimitropoulos, N. Vourdas, V. Em. Vamvakas and D. Davazoglou, *Thin Solid Films* **515**, 2428-2432 (2006).
18. W. Seiler, E. Millon, J. Perriere, R. Benzerga and C. Boulmer-Leborgne, *J. Cryst. Growth* **311**, 3352-3358 (2009).

frontiers in
CELL AND DEVELOPMENTAL BIOLOGY

Stem Cell Treatments

Manufacturing blood ex vivo: a futuristic approach to deal with the supply and safety concerns

Vimal kishor Singh

Journal Name:	Frontiers in Cell and Developmental Biology
ISSN:	2296-634X
Article type:	Review Article
Received on:	25 Jan 2014
Accepted on:	26 May 2014
Provisional PDF published on:	26 May 2014
www.frontiersin.org:	www.frontiersin.org
Citation:	Singh VK(2014) Manufacturing blood ex vivo: a futuristic approach to deal with the supply and safety concerns. *Front. Cell Dev. Biol.* 2:26. doi:10.3389/fcell.2014.00026
/Journal/Abstract.aspx?s=1471&name=stem%20cell%20treatments&ART_DOI=10.3389/fcell.2014.00026:	/Journal/Abstract.aspx?s=1471&name=stem%20cell%20treatments&ART_DOI=10.3389/fcell.2014.00026
	(If clicking on the link doesn't work, try copying and pasting it into your browser.)

Title:

Manufacturing blood ex vivo: a futuristic approach to deal with the supply and safety concerns

Running Title:

Blood production using stem cells

Authors:

Vimal Kishor Singh[1*], Abhishek Saini[1,] Kohichiro Tsuji[2], PB Sharma[1], Ramesh Chandra[3]

Authors' affiliations:

1. Stem cell research laboratory, Department of Biotechnology, Delhi Technological University, Shahbad Daulatpur, Bawana road, Delhi-110042, India;
2. The University of Tokyo Hospital The Institute of Medical Science Research Hospital Department of Pediatric Hematology/Oncology;
3. Dr B. R. Ambedkar Center for Biomedical Research, University of Delhi Delhi-110 007, India

***Correspondence:**

Dr. Vimal Kishor Singh: Stem cell research laboratory, Department of Biotechnology, Delhi Technological University, Shahbad Daulatpur, Bawana road, Delhi-110042 vim_kissor@yahoo.co.in; vimalkishorsingh@gmail.com.

Key words:

RBCs, ex-vivo erythrocytes, manufacturing blood, hematopoietic stem cells, induced pluripotent stem cells

Abstract

Blood transfusions are routinely done in every medical regimen and a worldwide established collection, processing/storage centers provide their services for the same. There have been extreme global demands for both raising the current collections and supply of safe/adequate blood due to increasingly demanding population. With, various risks remain associated with the donor derived blood, and a number of post collection blood screening and processing methods put extreme constraints on supply system especially in the underdeveloped countries. A logistic approach to manufacture erythrocytes ex-vivo by using modern tissue culture techniques have surfaced in the past few years. There are several reports showing the possibilities of RBCs (and even platelets/ neutrophils) expansion under tightly regulated conditions. In fact, ex vivo synthesis of the few units of clinical grade RBCs from a single dose of starting material such as umbilical cord blood has been well established. Similarly, many different sources are also being explored for the same purpose, such as embryonic stem cells, induced pluripotent stem cells. However, the major concerns remain elusive before the manufacture and clinical use of different blood components may be used to successfully replace the present system of donor derived blood transfusion. The most important factor shall include the large scale of RBCs production from each donated unit within a limited time period and cost of their production, both of these issues need to be handled carefully since many of the recipients among developing countries are unable to pay even for the freely available donor derived blood. Anyways, keeping these issues in mind, present article shall be focused on the possibilities of blood production and their use in the near future.

Introduction

Initially, started by Harvey's studies of blood circulation system, blood transfusion began in the 17th century with animal blood transfusion experiments. The first fully documented report on blood transfusion in humans was from *Dr. Jean-Baptiste Denys,* who in 1665 successfully transfused blood from a sheep in a 15 year old boy. Though, he could not succeed in later transfusions as recipients died after transfusions were made. In similar studies, *Dr. Richard Lower* demonstrated the effects of changes in blood volume in circulatory function and developed methods for cross-circulatory study of animals. The first successful human blood transfusion was reported by *Dr. James Blundel* (1818) between a married couple for a postpartum hemorrhage. However, in 1901, the breakthrough was achieved in human transfusion with the discovery of blood group antigen by Austrian researcher *Karl Landsteiner,* who discovered that red blood cells got clumped when incompatible blood types were mixed and immunological reaction occurred if the recipient of a blood transfusion had antibodies against the donor blood cells. This 'Nobel Prize' (1930) winning discovery made it possible to determine blood type and paved the way for safe blood transfusions. Since then many other blood groups have been discovered. Following to these discoveries a number of blood banks were established during 1940-1950s and it is an inevitable part of all the modern clinical modalities [1].

The global blood collection was reported to be about 103 million units **(www.who.int/worldblooddonorday/en/**) [2-4]. The quality and quantity of donor derived blood collection remain unevenly scattered in economically developed and developing countries. Almost 50% of these blood collections is made in developed countries, which accommodate only a mere 15% fraction of the world's population. Presently, the blood collection seems to be

sufficient in economically developed countries. It is supported by reports showing 30000 annual blood donations on an average per blood center through ~8000 blood centers scattered in 159 high-income countries [3,4]. For example, in U.S. the total no. of blood unit collected were 5% more than the actual transfusion made during year 2011 [4]. On the contrary, this number of collections/ per center is very less (3700) in developing countries. As per WHO report 82 low income and middle income countries have only 10 donations per 1000 people in the population that would remain highly insufficient to supply a comparable large population residing in these countries [2]. Further, the screening facilities are very much inefficient in most of the developing countries. As per WHO record, 39 countries are not able to screen all blood donations for one or more of the following transfusion-transmissible infections (TTIs): HIV, hepatitis B, hepatitis C and syphilis [**4**]. Again, there are only 106 countries which have national guidelines on the appropriate clinical use of blood. It would be worth noticing that only 13% of low-income countries have a national haemovigilance system to monitor and improve the safety of the transfusion process. Moreover, the blood supply may look sufficient for the time being in developed countries, it likely becomes inefficient to keep supporting a rapidly growing proportion of elderly population (>60 years age) and burgeoning demand for blood transfusions for surgical treatments by the year of 2050 [**5, 6,**].

One of the major challenges in clinical settings is to find blood group compatibility for more than 30 blood group system (308 recognized antigens) including ABO & Rh antigens (7).

There are a number of situations such as rare phenotypes, hemoglobinopathies, polytransfusion patients and polyimmunization that may result in significant complications (2) adding more

complexity to the supply constraints. Recent technologies such as antigen masking and enzymatic cleavage to generate universal donor blood groups (O and RhD antigens) have been proposed. But these methods are yet to be developed (8). While keeping these issues in mind, it is worth noticing that the donated blood is tested for various kinds of infections before any transfusion could be made [e.g. HIV-1, HIV-2, HTLV-1, HTLV-2, Hepatitis B, Hepatitis C, Syphilis (*T pallidum*), Chagas disease (*T cruzi*), and West Nile Virus, Cytomegalovirus (CMV)], and a number of precautionary measures are followed during transfusion procedures. Even then blood transfusions are often associated with several complications [1, 2]. These complications not only compromise the quality of treatment, but may add to the overall cost of the regime also which remain associated with it in any clinical setting (3). This is true even in the developed countries where 0.24 % transfusion has been reported to be associated with adverse reactions [4]). For example, adverse events from transfusions in the US only may account for approximately $17Billion every year. These complications depend upon the patient status or specific transfusion quantity involved. These situations have evoked researchers to develop alternate methods to get blood from various non-donor derived sources. In the search of blood alternates researchers have developed various artificial molecules mimicking functionalities of blood RBCs. The majority of these molecules is either hemoglobin based oxygen carriers or perfluorocarbon solutions. Hemoglobin based carriers are reported to be inefficient as compared to the oxygen carrying capacity of native RBCs. Whereas, perflorocarbons could not become popular due to their limited functional applications [9-13]. .

Ex vivo expansion of erythrocytes or manufacturing blood from stem cell is the most attracting approach among the global research community for the last few years. The basis for the principle that ex vivo cultivated RBCs (or other blood cells) may be of clinical use was provided by

Nakamura and his colleagues who have demonstrated that RBCs derived from the immobilized ESCs cell line can protect mice from lethal anemia [14]. Recently, the proof-of-concept was described by first in-human blood transfusion using ex-vivo generated RBCs [15]. In a major landmark study, **Giarratana et al**, shown **the** survival capacity of ex vivo cultivated RBCs in humans. As described by them, the $CD34^+$ cells obtained from volunteer donors as an aphaeresis product were cultured in a serum free media (with the addition of Stem cell factor (SCF), Interleukin-3 (IL-3) and Erythropoietin (EPO) resulting into 2 ml of blood RBCs equivalent (10^{10} cells) under GMP conditions. The ex vivo expanded RBCs were labeled with ^{51}Cs to trace their fate in patients as approved by FDA U.S. [15] and demonstrated to be comparable with any native RBCs transfusion. These findings established the proof-of-concept for clinical utilization of ex vivo generated RBCs globally. As discussed in the next section, a number of methods have been demonstrated so far (**Fig.2**), which ensure the feasibilities of ex vivo RBCs expansion from various source materials (e.g. $CD34^+$ HSCs, Embryonic stem cells and IPSCs) (**Fig.3**). There are various factors which essentially regulate the yield and the level of RBCs maturation through these protocols. Reports are there, showing numerical expansion of erythrocyte precursors up to ~0.5 transfusion unit/ donation from UCB $CD34^+$ cells, and approximately 2 million fold expansions of enucleated erythrocytes functionally comparable to native RBCs through slight modification of culturing techniques [16]. Further, large scale production (up to 10 transfusion unit) from two units of UCB have been demonstrated by technically complex protocols (described in later sections) which presently may appear ill suited from the commercial scale production point of view but strengthen the concept that with the advancement of techniques sufficient transfusable units may be produced [17]. Besides that, RBCs precursors, cellular intermediates/ nucleated erythroid precursors are generated through these protocols, which may

also be of use if transfused. It is expected that these cells are likely to become functionally matured in vivo while interacting with internal factors governing their maturation. The same has been reported both in human and animal models [**16, 18**]. Conceptually, the maturing cells along with functionally matured cells may aid to maintain the cellular content at the time of transfusion. These maturing cells may proliferate and each cell may give rise to 4-64 cells before they get enucleated and functionally matured in vivo. This hypothesis is supported by the data available from clinical observations in developing countries where 40-80 ml of compatible CB blood (containing 4-7x 10^{10} RBCs and 2-8x10^{9} erythroblast cells) is occasionally used for transfusion in emergent conditions [**18**]. Together, these reports strengthen the concept that ex vivo RBCs expansion likely support the different clinical short-comes to exist due to limited supply and various rare blood based disorder.

However, a number of factors such as technological barriers associated with large scale production and per unit production cost remain to be considered in order to support a large population. The present scale of RBCs production would require to be enhanced several times in a more cost-effective and timely manner. Commercial production of blood may lack essential background financial support in developing countries which are suffering from even more sensitive issues. Moreover, in the absence of more realistic, achievable goals it may become hard even in the capitalistic developed countries. Present article focuses on various issues related to current methods and their feasibilities to realize limited 'blood pharming' in near future.

Erythropoiesis in vivo

Hematopoiesis, a dynamic process, is regulated both temporally and spatially. It may be classified as '*primitive hematopoiesis'* in featus where specified cells termed as 'blood islands'

are generated by yolk sac (YS). In yolk sac, nucleated RBCs exclusively expresses embryonic Hbs (Gower-1, Gower-2, and Hb Portland) are generated for a small period of time. Following to that, a second wave of hematopoiesis or *definitive hematopoiesis'* produce hematopoietic stem cells, which have the potential of transfusion and includes enucleated RBCs along with various other hematopoietic cells. This event takes place largely in the fetal liver and up to a little extent in YS. In later stages of featus development Definitive hematopoiesis occurs in bone marrow and that serves as the only site of hematopoiesis in adults through their life. The hematopoietic cells from fetal and adult definitive hematopoietic stages may be differentiated on the basis of their HB contents. In the fetus hematopoiesis α and γ globins, (the components of fetal Hb) (Hb F), are expressed, and in the later β globins (the components of adult-type) (HbA), are expressed **[19, 20**].

Erythropoiesis or generation of RBCs includes hematopoietic progenitor cells, which are first differentiated into committed erythroid progenitors and thereafter proliferate/converted to functional red blood cells in a highly regulated hierarchal manner. This dynamic process is tightly regulated through a number of growth factors which ensure the maintenance of regular homeostasis of the RBCs mass.

The entire process of erythropoiesis may be defined to occur in three stages: (1) Erythropoietic commitment of HSCs: this includes development of erythroid committed blast cells from multipotent hematopoietic progenitors; (2) Division and differentiation of these morphologically identifiable erythroid progenitor cells; and (3) Terminal differentiation including cellular morphological changes such as enucleation, to produce reticulocytes and ultimately maturation: of RBCs (**Fig.1**)

The Hematopoietic stem cells are generated in Yolk sack and may be differentiated into a common myeloid progenitor that, in turn, gives rise to bipotent progenitors restricted to either the granulocyte/ macrophage or the erythroid/megakaryocytic pathways [**21-24**]. A comparable stage of development defined *in vitro* using cytokine containing semisolid medium (**Fig.1**) is the colony-forming unit granulocyte, erythroid, macrophage, megakaryocytic (CFU-GEMM) precursor that gives rise to bipotent progenitors restricted to either granulocyte/macrophage or erythroid/megakaryocytic pathways [**22-24**]. Those progenitors which express erythropoietin receptor (EPOR) remain responsive to erythropoietin (EPO) and are committed to the erythroid/megakaryocytic pathway,

On the other hand, EPOR deficient progenitor cells are committed to the myeloid pathway. The burst-forming unit–erythroid (BFU–E), which gives rise to colony-forming unit–erythroid (CFU–E) is termed as the most immature erythroid-restricted progenitor. Among them, early BFU–E (blast-like cells) are highly proliferative, and give rise to clustered burst colonies of up to 20,000 cells in semisolid culture assays.

However, BFU–E bear comparatively small number of EPOR but later progenies (daughter cells) derived from them acquire a high expression level of EPOR and become EPO responsive, transferrin receptor positive, and begin to express hemoglobin [**25, 26**]. Later on, CFU–E are derived from these cells, which are highly responsive to EPO, but generate smaller colonies, and express many of the gene products required for definitive erythroid development (Fig. 1). There are reports describing a cell division stimulating anti-apoptotic role of EPO in late-stage erythroid cells derived from CFU–E. At this stage of development cells may start the synthesis of

hemoglobin and acquire cytoskeletal proteins in tissue culture systems. Moreover, cellular adhesion molecules are expressed in these cells that help define them as nucleated erythroblasts. Thereafter morphologically identifiable nucleated erythroid precursor become visible, which progress from the pro-erythroblast to basophilic, polychromatophilic, and orthochromatic cell forms leading to the reticulocyte (Fig. 1) [**26-28**]**.**

Erythroid differentiation encompasses four distinct major cellular processes such as, (1) the accumulation of hemoglobin that participates in driving the basophilic to acidophilic cytoplasmic changes seen during maturation, (2) limited erythroblast expansion, (3) a continued decrease in cell size, (4) and nuclear condensation leading to their final enucleation. These highly regulated developmental changes take place in the microenvironment of BM niche where 'erythroblast islands' are closely associated with macrophages that serve as stromal or nurse cells [29-**31**]. These erythroid development stages end up with the exit of reticulocytes from the marrow, which now enter the circulation and get matured into erythrocytes. The characteristic features of this stage include disassembly of ribosomes, Golgi bodies, and other cellular machinery, removal of organelles, enucleation, changes in the cytoskeleton leading to the classic biconcave discoid shape, and then release into the circulation [4]. Terminal maturation takes place in the erythroblast islands, which involves participation macrophages of with maturing erythrocytes [29-31].

The mature erythrocyte have a life span of 120 days in blood circulation, and afterwards 'senescence' occurs reflected through changes in surface antigen expression or physical characteristics of the cell triggering their removal from the blood by macrophages/

reticuloendothelial system [**32**]. Thus hematopoiesis is regulated through changes in body compartments during mammalian development, from embryo to adult, and depending on the age of development, specialized microenvirnmental niches precisely regulate hematopoietic development [**33-37**].

Ex vivo erythropoiesis: an overview

There has been considerable progress in the field of developing biological control over the expansion of erythrocytes to generate terminally differentiated, fully functional RBCs [38]. The in vivo hematopoietic development process have been studied (**Fig.1**) and an in depth knowledge of the generation of erythroblast regulated through various growth factors have paved the way to mimic the process in vitro [39]. Altogether, these reports demonstrated the enormous potential inherited by three major cell types including (i) $CD34^+$ HSPCs, (II) Embryonic stem cells/induced pluripotent stem cells, and (III) immortalized erythroid precursors which can be differentiated into erythroid lineages by using almost similar/overlapping protocols (**Fig.2**) (**Table 1**). Regardless of their types, stem cells are promoted to become erythroid progenitor in three basic steps viz. commitment, expansion, and maturation. There are a number of reports showing use of various cytokines/growth factors (stem cell factor and EPO are most common) to generate variable yields of immature progenitors or mature RBCs with or without using animal/human derived feeder coculture system (**Fig.2**). Recently, a new concept of transdifferentiation (directly differentiating human fibroblast cells into erythroblasts) has been shown to bypass the HSPC state (**Fig.3**) (40). Although promising, but the technique remains to

be evaluated for their potential to generate large scale RBCs. Most of these protocols suffer from similar problems such as degree of enucleation or erythrocyte formation, predominate form of Hb expressed by them, use of animal derived products such as serum and feeder cell coculture, and clinical transfusion related problems such as blood type matching and unavailability of sufficient number of RBCs for transfusion. All these issues can be summarized in the following sections:

CD34$^+$ hematopoietic cells from various sources and their use for ex vivo RBCs culture

CD34$^+$ cells from peripheral blood (PB), cord blood (CB) and Bone marrow (BM) have been in use for clinical transplantations for more than two decades (**41**). Initialed by **Fibach et al,** the methods to generate RBCs from CD34$^+$ HSPCs have been existing for a long time (**42-44**). **Douay et al** were quick to demonstrate functional characteristics of the erythrocytes generated by CB derived CD34$^+$ HSPCs [**16,45**]**.** Their studies confirmed a higher erythrocyte generating potential in comparison to myeloid precursors with low (4%) enucleation efficiency [**16**]. **Giarratana et al** further modified the protocol and demonstrated 90% enucleation efficiency in a similar 3 step method for adult blood/BM derived CD34$^+$ cells [**46**] by co-culturing them with murine stromal cell line (MS5) or Human mesenchymal stem cells (HuMSC). The procedure resulted in, 20,000 fold, 30000 fold and 2x 10^5 fold increment in the erythrocytic cell generation when BM, GM-CSF mobilized PB and CB derived CD34$^+$ cells were used respectively [**47-49**]. This group further reported 5-10 units of blood cells on prolonged culture with feeder cell coculture system [47-**49**]. The cells were reported to have native RBCs like functional characteristics as described by normal glucose-6-phosphate dehydrogenase (G6PD) and Pyruvate

Kinase (PK) enzyme levels, membrane deformability and oxygen dissociation characteristics. This was also evident by their similar survival rate in non-obese diabetic/severe combined immunodeficient (NOD/SCID) mice following to intraperitoneal infusion of carboxyfluorescein diacetate succinidyl acetate (CFSE) labeled cells.

These methods suffer from two major drawbacks such as (i) use of animal serum and co-culture system and (ii) low yield of functionally matured RBCs per unit of blood cells, which tempted researchers to identify more defined cocktail of growth factors to achieve a better control over erythrocytes proliferation and differentiation. **Malik et al.,** demonstrated generation of ~10-40% enucleated erythrocytes by enriched $CD34^+$ cells from cord blood, PB, and BM [**50**] in a serum free liquid culture system (with Flt-3, GM-CSF, EPO). This report indicated the possibilities of generating erythrocytic progenitors in the absence of animal derived serum that is strongly recommended by most clinicians. Following to these reports 10^5 - 1.5 x 10^8 folds erythroid cell expansion have been reported in similar serum free environment. [**51-52**].

Fujimi et al, demonstrated massive production of terminally matured erythrocytes from $CD34^+$ CB cells in the serum free environment while avoiding xenogenic feeder by using hTERT transduced human stromal cell line [**17**]. These methods could result in massive growth of $6x10^{12}$ RBCs from one unit of cord blood and also the highest RBC number per starting cell ($3.52\ x10^6$) in any static culture. However, use of the AB blood group, serum to derive macrophages in a 14 days culture and an additional step of magnetic separation leaves this method ill suited for the scaling up purposes**.** **Beak et al**, showed up to 64% enucleation efficiency by using CB or BM derived mesenchymal stem cells as feeder layer which would

require an additional MSCs donor for the feeder cells and thus may not be suitable for large scale production procedures (**53**). **Xi et al**, has demonstrated an *in vitro* model of human erythropoiesis to study the erythroid differentiation in normal and pathological conditions (5**4**). $CD34^{+}$ cells were shown to undergo up to 35 doublings in a prolonged 50 days culture in serum free media supplemented with EPO, synthetic glucocorticoid Dex, IGF-1, SCF, and iron saturated human transferrin. In a subsequent step, matured RBCs could be generated by coculturing erythroid progenitors with human fetal liver stromal cells. The procedure resulted in 10^{9} fold expansion of erythrocytes. [5**4**].

Recent findings have indicated a significant erythropoietic potential in the CD34neg cell fraction which should also be exploited to enhance the production (**55-57)**. **Leberbauer et al,** described a culture method which exploited the signal transduction cascades of stress erythropoiesis, achieving a 10^{9}-fold expansion of erythroblasts of cord blood cells without prior CD34+ isolation (55). **Akker et al.,** describe a culture method modified from Leberbauer et al, and obtained a homogenous population of erythroblasts from peripheral blood mononuclear cells (PBMC) without prior purification of CD34+ cells. This pure population of immature erythroblasts can be expanded to obtain $4x10^{8}$ erythroblasts from $1x10^{8}$ PBMC after 13-14 days in culture. Upon synchronizing differentiation, high levels of enucleation (80-90%) and low levels of cell death (<10%) are achieved. These studies indicated $CD34^{Neg}$ cells as most significant early erythroid progenitor population (56). **Tirelli et al.**, also demonstrated significant enhancement (log scale) in the erythroid cell generation by using total MNC in Human Erythroid Massive Culture (HEMA) [**57**]. The careful phenotypes examination showed a significantly more erythropoietic potential of $CD34^{neg}$ population as compared to $CD34^{+}$ cells [**57**]. .

One of the major criteria for calculating efficiency of various ex vivo expansion protocols remains to describe the degree of enucleation of these maturing erythrocytic cells. The interactions with macrophages/ stromal cells play a crucial role in developing high degree of enucleated erythrocytes as described through various researchers [**58]**. However, most of the stromal cells support used by various researchers are of animal origin and may conflict with the interests of the few clinicians to describe these cells as clinical grade blood products. These issues raised the interest of the research community to define methods without a need for animal based products. **Miharada et a**l, who showed generation of 4.5x 10^{12} erythroid cells from 5 x 10^6 $CD34^+$ cells in the absence of any feeder cell layer or macrophage cells by using VEGF-1, TGF-1 and a glucocorticoid antagonist Mifepriostone to avoid dependence of these methods on feeder cells [**59**]. **Maggakis-Kelemen et al** also reported similar results to improve the yield by using DMSO, Ferrous Citrate and Transferrin in the culture medium [**60**]. Though these factors significantly increased the yield, but precursor cells shown higher degree of deformability and reticulocytes/ erythrocytes were demonstrated to have reduced shear modulus. **Beak et al** demonstrated the use of a polymer Poloxamer 188 to yield >95% enucleated RBCs in similar protocols without using any feeder cell support [61]. Poloxamer 188 enhances the production by protecting cellular lysis during nucleation due to hydrodynamic stress. It provides support to the membranes and protects fragile cells from lysis at the time of enucleation. Thus, it seems that a large number of terminally matured clinical grade RBCs may be obtained regularly with the advent of similar protocol, while introducing newer alternatives at different levels of their expansion. Earlier, similar results were reported by **Timmins et al**., who demonstrated feeder

free culture system by using a bioreactor and resulted in a massive 500 units (10^8 fold) per UCB donations [**62**].

While considering these findings, it seems that both CB and PB derived $CD34^+$ cells possess enormous expansion potential with some marginal differences such as the predominant form of Hb expressed and % yield of enucleated RBCs. For example, RBCs from CB derived cells are predominantly rich in fetal Hb [**15, 16, 46**], whereas, RBCs from PB derived cells majorly express adult Hb [**15,46**]. Apart from that, there have been a significant difference in the expansion potential of CB/ PB derived HSPCs. With the current technologies available for their expansion PB derived cells have shown comparatively low (120,000 fold) yields [**46**]. In contrast, CB derived cells are reported to expand up to 2 million folds. Even more, a single unit of CB derived cells can result into 500 units of transfusable RBCs [**62**]. However, the later method has not been applied for the PB derived cells so far. Thus, it seems that cord blood shall provide a better option for initial source to be selected under present circumstances, and, if presence of fetal Hb is acceptable [**65-66**], it shall remain the most attractive alternate for RBCs expansion protocols. The infrastructure for cord blood collection is well developed. According to a report in 2010, about 4,50,000 CB units were collected through 131 CB Banks worldwide [65]. There is enough information available through these blood bank registries regarding the blood types and combinations of the antigen present on these blood groups for each CB donation. Though, the exact percentage for each rare blood type may not be available and even if the specialized donor could be found for each rare antigen combination, it may be difficult to fulfill a regular demand of transfusion in every 3-4 weeks due to the limited life span of these cells.

However, even then a large fraction of the population may be benefitted from the existing technologies without any risk for rare antigen combinations.

Embryonic stem cells and induced pluripotent stem cells

Embryonic stem cells [**66**] and induced pluripotent stem cells [**67-68**] are defined as immortal cells with the self-renewing capacity and if the requisite growth environment is made available have potential to differentiate into all kinds of cells of the organism. Embryonic stem cells were first isolated from 3-4 day old Blastocysts [68], and subsequent studies by various research groups described their capabilities to be maintained indefinitely in cultures due to high telomerase activities. Takahashi and Yamanaka's group firstly demonstrated iPSCs or ESC-like cells that may be generated by reprogramming somatic cells. They showed the transformation of murine fibroblast cells in to ESC by transfection of transcription factors such as POUSF-1, KLF-4, SOX-2,and Myc [67-68]. These cells were further demonstrated to form teratoma on infusion in NOD-SCID mice and differentiation into cells from all the three germ cell lines respectively [69-**70**]. Generation of Human IPSCs (hips) was also defined by transformation of human neonatal or adult fibroblast by the same set of genes [**68**]. **Yu et al** also generated of hIPSCs from fibroblast cell by using lentivirus mediated transfection of Nanog and LIN28 to reduce the undesired effects of c-Myc [**71**]. Subsequently, other methods of generating IPSCs have been reported such as ectopic expression of the same set of transcription factors [72] and use of excisable transposons [73]. Alternatively, these factors could also be provided from outside attached to a cell penetrating peptide sequence [74]. Together these cells provide an alternate to

generate HSPC. The mononuclear cells (CB/PB) may be reprogrammed in IPSCs and in subsequent procedure human IPSCs could be differentiated into $CD34^{+}CD45^{+}$ HSPC by using similar protocols used for ESCs [**75-76]**.

There are a number of groups who have demonstrated hematopoietic differentiation of hESCs/IPSCs (**77-79**) (**Table 1**). These methods can largely be grouped into two categories of (1) Embryoid body formation through suspension culture of hESCs without feeder cells, and (2) co culture of hESCs with murine stromal cell lines such as S17 or OP9 [**80-83**]. In the first approach, cells grow in suspension culture resulting in 3-dimensional structured aggregates of differentiating cells called Erythroid Bodies (EBs) [**80**]. **Chang et al** described a method of generating erythroid cells from embryoid bodies [**81**]. Nakamura's group described a method for the generation of enucleated erythrocytes from mouse ESCs (14) which was followed by several researchers who demonstrated procedures for the generation of enucleated erythrocytes by using human ESCs [79, 84-86]

During last 10-11 year significant development has occurred in the procedure to develop hESCs/iPSCs and high yields of approximately up to 10^{11}-10^{12} erythrocytic cells have been achieved from a single plate of hESCs [**79**]. While comparing these reports, most procedures have indicated an important role of erythropoietin (along with other growth factors BMP-4, VEGF, bFGF etc.) and coculturing them with a feeder cell to derive sufficient yield of enucleated RBCs [87-91]. His can be a Co cultured with a number of feeder cells available, including mesenchymal cell Murine stromal cell line S17, OP9 [**80-81**]. Yolk sac endothelial

cell lines [**90**], cell lines derived from murine AGM stroma, liver or other developmental niche [**91**] (Murine AGM derived AM20-1B4 cells) are described as best supporting cells providing higher yields.

In order to achieve animal cell free clinical grade blood products efforts have been made by various researchers. It hass been described that the use of feeder cell layer derived from human tissue itself e.g. human foreskin derived fibroblast cells support to generate similar results [**92-94**]. Genbacey and his colleagues, has reported expansion of hESCs in serum free conditions by growing them on cells derived from human early gestation placental fibroblast cells or human placental laminin substrates [95]. hESCs can also be grown in serum free and feeder free conditions by using fibronectin, TGF beta 1, bFGF and leukemia inhibitory factor [**92**]. Bouhasara's group demonstrated hESCs culture on hTERT cell line and their subsequent differentiation into erythrocytic cells in suspension culture method [**96, 97**].

However, there have been ambiguities about the role of EPO/feeder layer played in erythrocytic enucleation; their presence in the final step of most protocols seems to remain inevitable. This is evident from the results obtained by growing these cells in the absence of both the above mentioned factors that result to meager 10% enucleating efficiency [**85, 86**]. Whereas, inclusion of both EPO/ feeder cells has been shown to yield remarkable up to 65% enucleation efficiency of these methods [**79,84**]. Similarly, IPSCS derived erythrocytes have been shown to depend on a feeder layer for their enucleation in final steps of maturation [77, 78, 84, and 85]. Recently, heparin and insulin have been reported to enhance enucleation efficiency of IPSCs derived erythrocytes in a feeder free system, but that also remains only 26% [**78**]

Another important factor is the expression of fetal Hb as a predominant form of protein by the erythrocytes generated in almost all these protocols [77-**79, 84, and 85**]. This is quite obvious because of the embryonic state of development of both ESCs/IPSc and a more primary route of hematopoietic development (indefinitive) likely to yield predominant expression of fetal/embryonic Hb through these protocols. However, researchers have demonstrated the possibilities of selective expression of adult Hb in erythrocytes by either increasing the time length for coculture [86], or enforced transgene expression of RUNX1a to enhance hematopoiesis from human ESCs and iPSCs [57] reporting a higher level of β- globin expression in differentiated erythrocytes [**98**].

So far, there has been no significant difference in the erythroid expansion potential of ESCs and IPSC lines [**85**]. The findings reported by Douay's group about 7-8 fold higher erythrocytic expansion potential of human H1 ESC line in comparison to the human IPSCs line (IMR90-16) may be attributed to the viral vectors used for deriving IPSC that has been reported to decrease hematopoietic and erythrocytic expansion potential [**99**]. Further, epigenetic variation (integration of viral genomes at different loci) associated with IPSCs generating methods could also contribute to these variations. Similarly, altered hematopoietic potential have been reported for various hESCs lines [**100**].

IPSCs may be advantageous in the conditions where no other alternate in present of generating rare blood group such as $O^{-}Rh^{-}$ type of blood group. It has been postulated that only three selected human IPSC lines may be sufficient to generate required blood groups for almost 95.5% of patients in France [**101**]. While, no such ESC line lines with universal blood donor group has

been identified so far in the current list of NIH-approved-for-research [**79**]. In addition, IPSCs can be helpful to support autologous transfusion which is highly recommended for alloimmune patients. On the other hand, it has promising reports to generate functional RBCs to cure rare hemoglobinopathies such as sickle cell anemia and β-Thalassemia [**102, 103**].

Erythroid precursor from stress erythropoiesis

In addition to the above mentioned stem cells, researchers have shown a significant RBCs generation potential in the extensively proliferating erythroid precursors which are developed due to stress conditions such as erythrolysis or hypoxia (**Fig.3**). The process, generally termed as 'stress erythropoiesis', relies upon glucocorticoids and their counter receptor interactions. There are reports showing up to 10^{10}-fold expansion of CB-derived erythroid precursors using Dexamethasone as a glucocorticoid agonist along with other growth factors, e.g. SCF, EPO and IGF-1 [**55, 104-105**]. Similar results could be obtained for the PB derived erythroid precursors with the use of IL-3 along with above mentioned cytokines [**106**]. However, these approaches were reported to be of limited use due to their minimal fold expansion (<20 fold) which remain insufficient as per clinical transfusion is concerned [**107**].

In contrast, there have been advancements in generating immortalized or extensively expanding erythroblast cell lines from embryonic stem cells with the ability to produce enucleated erythrocytes in mouse [**14, 108**]. Similar extensive expansion potential has been demonstrated by mouse embryos [**109**], which indicated a higher proliferation potential of embryonic erythroid progenitors than postnatal cells. It is hypothesized that if postnatal erythroid cells

could be reprogrammed by using existing techniques to the state of embryonic erythroid progenitor cells they could also proliferate up to a similar extent. In fact, it has been demonstrated by Cheng's group [**110**], who has demonstrated immortalization of human CB-derived erythroblast by using similar reprogramming factors defined by Yamasaki's group [**67**]. The Author has demonstrated a significant 10^{68}-fold expansion of CB-derived erythroblasts (in~12 months) in a serum-free culture. The ectopic expression of three genetic factors Sox2, c-Myc, and a shRNA against TP53 gene enabled these cells to undergo an expanded expansion in similar culture condition. These cells showed normal erythroblast phenotypes and morphology, a normal diploid karyotype and dependence on a specific combination of growth factors for proliferation throughout the expansion period. The coculture of these cells with irradiated mouse OP9 cell line in the presence of serum yield to 30% enucleation efficiency with increased fetal Hb expression level. Similarly, Kurita et al, demonstrated immortalization of human IPSC or CB derived cells by inducible expression of TAL-1 and HPV-16-E6/E7 viral gene [**111**]. Thus, it is expected that with more advancements in the reprogramming technology such as the use of nonviral episomal plasmids, synthetic RNA and small molecules, development of more donor cell line would facilitate generation of all blood types [**112-114**].

Ex-vivo culturing of other blood components

Platelets

Platelets are small anuleated, discoid shaped, 1-2 μm cell fragments that play essential role in the maintenance of homeostasis, stopping bleeding or wound healing (thrombosis), inflammation,

and innate immunity. There is a burgeoning use of plasma transfusions to control massive bleeding in clinics. The combination of red blood cells, platelet concentrates and plasma is used for the same Platelets are present in much higher densities in vertebrate blood (5.5 platelets x 10^{10}/ unit) that are generated from megakaryocytes and their precursor cells in Bone marrow (**115**).

Platelets are generated from megakaryocytic cells in the BM niche under the regulation of various growth factors. Unlike RBCs, committed HPCs can be easily recruited into megakaryocytic lineage differentiation pathways by their induction through a single growth factor TPO. This straight forward mechanism has tempted many researchers to mimic similar differentiation under research settings. Like RBCs, there have been efforts to generate platelets from all different sources, including CD34+ HSPC., ESCs/iPSCs and immature megakaryotic precursor cells. **Christian et al**, have demonstrated the generation of platelet precursor cells from human $CD34^+$ cells by using SCF, TPO, IL-3/IL-11, and Fetal Liver Tyrosine kinase-3 ligand (Flt-3L) in the liquid culture system [**116**]**.** However, these precursors were shown to undergo recirculation in hematopoietic tissues on transfusion in mice. **Proulx et al,** demonstrated ~300 fold expansion of MK/$CD34^+$ by growing UCB derived $CD34^+$ cells with SCF, Flt-3L, TPO and IL-6 at high concentrations **[117,118**],. Growth of MK/$CD34^+$ may further be improved by optimizing culture conditions such as temp (39^oC), O_2 tension and addition of additional factors such as SDF-1α and Nicotinamide [**119-122**]. **Matsunaga et al**, (2006), demonstrated generation of 3.4 unit platelets from UCB-$CD34^+$ cells by using hTERT mesenchymal cell coculture method in 33 days [**123**]. **Sullenberger,** also reported a 3D cartridge based perfusion bioreactor with the capacity of continuously producing platelets over a period of

30 days [**124**]. Moreover, the efforts described so far for producing platelets from UCB derived cells remain largely insufficient to fulfill even a fraction of global demand.

Recent advancements have demonstrated enormous *in vitro* platelets generation potential in pluripotent stem cells (including iPSCs/ ESCs), and a comparatively new type of cells called induced MKs (iMKs) (**125**). **Matsubara et al** showed a direct conversion of fibroblasts (mouse/human) into megakaryocytes (MKs) by using three factors p45NF-E2, Maf G, and Maf K, which subsequently can release platelets (**126**). The authors identified significance of these factors in generating abundant MKs and platelets from human subcutaneous adipose tissues (**126**, **127,128)**.

In another approach, ESCs/ IPSC mediated generation of platelets in humans has been reported (**129, 130**). **Eto et al** showed that c-Myc expression (essential for reprogramming of IPSCs) must be reactivated transiently and then shut-off [**130**] and to ensure efficient platelet production from human IPSCs. This transient expression might be essential because continuous excessive c-Myc expression in IPSCs derived MKs was shown to increase p14 (ARF) and p16 (INK4A) expression, and decreased GATA1 and NF-E2 expression, which eventually resulted MK senescence and apoptosis, as well as impaired production of functional platelets [**130**].

More recently**, Eto and colleagues** have established an immortalized MK cell line (MKCL) derived from human IPSCs (**125**). The immortalized MKCL could potentially provide a stable supply of high quality platelets for transfusion medicine. However, this method remains elusive and a detailed protocol suitable for commercial production is yet to come.

Thus, recent findings indicate strong possibilities of a regular non donor derived platelet supply in near future. However, there are several factors that shall be discussed to compare existing approaches. While comparing with IPSCs/ESCs based methods, the iMK cells (derived in these studies) are rapidly converted (2 weeks) into MKs cells, but yield remain poor as fewer platelets (5-10 platelets per iMK cell was generated. In contrast, single MKs may give rise to up to 2 000 platelets under *in vivo* conditions. Hence, one of the important factors shall remain to be discussed is the total number of cells that can be obtained from each cultural setting. For example, Matsubara et al reported generation of 8-10x 10^5 iMKs from 20 x 10^6 Human Derived Fibroblasts(HDFs) (**126**). HDFs are easily expanded following to their initiation of direct conversion with limited number of transfected cells, whereas, 200-300 IPS clones from 10^5 HDFs were reported by Eto and colleagues in their studies. Further, 1x 10^5 cultured IPSCs gave rise to 17x10^5 MKs (**130**). Thus, these results indicated low platelet production efficiency per MK in both strategies,

Another important issue is the time taken for the production of MKs and platelets through these protocols. iMKs and iPSC-mediated MKs are induced in approximately 2 weeks and 2 months, respectively. However, it is yet to be established, but MKCLs may be a much faster approach to generate platelet sources for platelet production due to their direct expandability into MKs. .

Further IPSC-mediated MKs are not completely free from the possible risk of some residual undifferentiated cells However, a possible approach may be to avoid transfusion of MKs while preferring fully matured platelets derived from these methods. Platelets (anucleated cells) may

be irradiated before transfusion and thus may become free of any contamination of residual undifferentiated cells.

IPSCs and MKCLs are immortal cell lines and thus are comparatively easy to freeze down. Similarly, HDFs are also suitable for cryopreservationm from where they can be taken out and used as starting materials for iMK induction. HDFs in comparison to platelets show better suitability for cryopreservation. The functionality of iMKs has been assessed through their infusion into irradiated immunodeficient NOD/Shi-scid/IL-2Rγ^{null} (NOG) mice showing normal release of human platelets *in vivo (*5-10 platelets per infused IMK) cells and equal capabilities of forming a thrombus in *ex vivo* conditions formation under flow condition. (**126**).

The iMKs are reported very recently and the early outcomes indicate them as a valuable option for transfusion medicine. However, there are some important issue which shall be considered in much detail such as the molecular mechanism by which iMKs are induced through the p45NF-E2 transcriptional complex, and identification of most suitable cells for direct conversion into iMKs (or for establishment of MKCLs).

One of the important issues to be discussed here is to explore the necessity of generating autologous iMKs through direct conversion for clinical transfusion. Under most clinical settings, platelet transfusion is done without any prior matching of human leukocyte antigen (HLA) between the donor and recipient. However, in rare conditions repeated platelet transfusions can elicit undesired production of anti-HLA antibodies against transfused platelets leading to an inevitable demand to identify HLA-matched platelet donor (**131**). A possible alternate may be provided by using autologous iMKs based strategies. In addition, establishment of iPSC banks

shall be an alternative approach to deal with this problem. These banks shall store homozygous HLA-typed iPSCs which would be deposited for HLA-matched tissue transplantation [**132**]. It has been demonstrated that a tissue bank from 150 selected homozygous HLA-typed volunteers could match 93% of the UK population (**132**). Yamanaka et al has also postulated that 140 unique HLA homozygous donors shall remain sufficient for 90% of the Japanese population (**133**).

Neutrophils

Neutrophils play important role in cellular immunity, but unlike RBCs and Platelets they are not routinely collected in clinics. Neutrophils are need to be transfused in relatively large amount, i.e. $>10^{10}$ calls every day in neutropenic patients. Ex vivo expansion of neutrophils has been reported by some groups showing ~ 400 fold expansion from single units of UCB-$CD34^+$ cells (5 x 10^6 $CD34^+$ cells), which equivalents to a mere 20% of the required daily dose. Although, sufficient cells may be produced by using peripheral blood mobilized by cytokines as demonstrated by Dick et al. **[134]**, who showed ~534x fold (equivalent to 10 neutrophil units) expansion on ex vivo culture of these cells. But this would mean one donor per recipient and supply constraints largely remain unsolved. Similar efforts to generate neutrophils from hESCs have also resulted in very low yields [**135**]. These reports indicated the need for developing more efficient and simple procedures to be developed first for the generation of neutrophils from either UCB-$CD34^+$, BM derived cells and/ or houses before their commercial manufacturing could be planned.

Factors regulating the fate of commercial blood manufacture & future prospects

- ***Source material suitability and availability***

Scientists have been trying to develop a consensus on the different variables controlling the fate of ex vivo RBCs expansion and clinical use. The most important of them is the source materials for various methods being explored to expand RBCs in large scale. Ideally, a source material should be a discarded material so that no extra cost would be aided in the commercial production process. At the same time, if a regular supply chain of ex vivo manufactured blood has to be maintained the source material would also be required on a regular basis i.e. unlimited availability of the source material should be ensured. The most important factor is the capability of the source cells to get developed into the finally matured RBCs cells with absolute efficiency without raising any immune response in the host i.e. it should be non-immunogenic. The criterion fits well with umbilical cord blood, which is available abundantly and is a waste product in all the maternity hospitals. In fact, a significant number of transfusion can be made for the patients who are suffering from rare hemoglobinopathies (~ 1%) by using ex vivo cultivated RBCs units that might be obtained from these sub threshold units of cord blood (>90 ml) discarded regularly. Each discarded unit of cord blood may generate 10-75 RBCs products which might be useful in transfusions for rare hemoglobinopathies [**101**]. Similarly, Leukopheresis is routinely done in clinical centers where transfusions are made to treat various leukemia patients. In these protocols the leuko-reduction buffy coat is produced as a byproduct and this contains significant amounts of RBCs producing cells (equivalent to umbilical cord blood) [74].The proof-of-the concept that these ex-vivo cultivated cells may be of clinical use was provided by demonstrating successful transfusion of $CD34^+$ cells which were obtained from a G-CSF

mobilized donor [**107**]. Apart from UCB derived $CD34^+$ cells, ESCs and hiPSCs as described in previous sections might serve as a potential source for regular manufacturing processes with the advancement in technologies.

- ***Quantitative Issues***

The most frequently transfused blood component, RBCs, are present in $2x10^{12}$ cells/ unit (200 ml of blood) with an expected cell density of $3x\ 10^6$ cells/ml. According to the WHO data >100 million units of blood is collected every year worldwide. In order to replace this huge volume with synthetic blood/ blood components, an extremely large amount of ingredients along with skilled manpower would be an inevitable requirement. It is hypothesized that a cell density of $5x10^7$ cells/ml would be essential to produce regularly to support this much demand. Further, according to an assumption, manufacturing of a single unit of blood by using present static culture methods, would require 660 liters of culturing medium and 9500 lab scale 175 cm^2 culturing flasks (70 ml medium/ flask) [**136, 137**].

Ensuring such a high concentration of RBCs would attract development of more automated methods like bioreactors that might be helpful in reducing the culturing assets and associated labor. Fortunately a wealth of information regarding the use of various types of bioreactors for HSCs expansion has been accumulating during the last two decades. This could help researchers achieve required cell density. It was reported by Timmins et al that similar density of RBCs as in static culture can be produced in a wave bioreactor [**62**]. A maximum cell density of 10^7 cells/ml was also reported in a stirred small scale bioreactor [**138]**. Housler et al, reported a massive yield of $2x\ 10^8$ cells/ ml in a hollow fiber bioreactor [**139**]. These 3D bioreactors can be scaled up with current design to produce 1-2 units of RBCs in 3-4 weeks of time. These reports indicate possibilities of ensuring a regular production of large amounts of RBCs , however, a

number of factors such as degree of cell maturation and various cultural parameters are yet to be defined in a more elaborated manner.

Further, an important achievement could be the development of methods to commit the source material directly into the erythropoietic lineages reducing both the time and cost of production. There are few preliminary reports about various efforts to define alternate sources such as (i) generation of erythropoietic cell lines from ESCs/ IPSCc (i) reprogramming any somatic cells directly into erythroblasts by passing the pluripotent state through over expression of suitable genes.

This has been reported for megakaryocytic differentiation also where human fibroblast cells are directed to differentiate directly into megakaryocytic cells through over expression of p45NF and E2/MaF transcription factors [**140,141**]. Cheng's group reported in humans the differentiated erythroid cells obtained from human embryo might be used as a potential initial source for RBCs production [**110,111**]. Thus, it is conceivable that with more advancements in the culture methods and initial source material a significant amount of RBCs could be produced for limited clinical uses.

- ***Growth factors***

Growth factors used in various phases of ex vivo culturing should also be explored to regulate the fate of commercial manufacturing. Both the '*concentration*' and '*time*' of their administration would play an important role in the optimization of the expansion process. It is also to be noticed that there are various growth factors which express gene polymorphism, for example,. >260 isoforms of human glucocorticoids receptors are expressed which are likely to differ in their potency and effects. In order to secure a large scale production of RBCs, it is

conceivable to determine an in depth knowledge about the functioning and efficiency of various isoforms through high throughput screening methods regularly. A good example might be the use of reverse phase proteomic analysis of $CD34^+$ cells to define molecular mechanism of signaling pathways activated during erythroid differentiation. Recently, similar studies have been reported by various groups showing activation of different set of gene(s) in $CD34^+$ cells and erythroblasts. Genes that are involved in the inhibition of apoptosis, transcription, and proliferation are more active in $CD34^+$ cells, whereas erythroblasts predominantly express those genes which play important roles in regulation of cell cycle, transcription and translation [**138**]. This information may be of use if specific pharmacological agents enhancing erythrocytic pathways and blocking apoptotic pathways may be introduced at various phases of ex vivo expansion.

- ***Biophysical and biochemical parameters***

Generation of clinical grade RBCs would require development of stringent quality checks for ex vivo expanded RBCs. The major parameters would include determination of antigenic profiles, hemoglobin contents and physical progenies derived from these culture processes. As described by various laboratories ex vivo generated RBCs are slightly macrocytic but normal in size. These RBCs also expresses a great level of α-hemoglobin stabilizing proteins (AHSP), BCL11A and globin gene with great donor to donor heterogeneity [**142**]. It is also reported that ex vivo generated erythroblasts contain γ-globin in a slightly greater amount in comparison to RBCS which are generated in vivo (0.12-0.20 pg/ cell with respect to total protein content of 18.723.7 per cell) (79).

- ***Antigenic profile***

Surface antigens are vital for the function of RBCs and a large number of surface antigen have been identified on the surface of mature RBCs. Ex vivo generated RBCs are reported to express normal level of antigens present on both the Ankyrin A (GPA, M/N, Ena FS, RhAO, and band 3/ 4.1 R) and Glycophorin B complex, the urea transporter, the complement receptor, and receptors that protect RBCs from complement mediated lysis Recent reports about the surface antigenic analysis of the ex vivo generated RBCs ensured that appropriate level of surface antigen such as band 3 and Rh antigen is assured at the beginning of the maturation process [**143**].

- ***Ethnicity***

Recently, there have been some reports demonstrating effects of ethnicity on the source material used for ex vivo expansion. African-American donor derived MNC were found to be found to be more useful as per as fold expansion is concerned since they could be expanded up to 14-40 fold in comparison to the Caucasian population derived MNCs which give rise to 1.7-30 fold expansion [**144, 145**]

- ***Enucleation of RBCs***

Since, Ex vivo expanded RBCs shall essentially be evaluated for their degree of terminal maturation in all the production units. Hence, high level of enucleation of maturing erythroblast is an inevitable requirement. Erythroblasts derived from ESCs are demonstrated to yield >60% enucleated RBCs [**79**] while the nucleation efficiency of maturing erythroblast from ups could be demonstrated to a mere 4-10% of RBCs produced [**146**]. Recently, there have been efforts to define the factors regulating enucleation efficiency of RBCs indicating the significance of proteins such as Huston deacetylase (specifically HDAC-2 isoform) which are required for chromatin condensation and enucleation in mice fetal erythroblast [**77**]. Since, glucocorticoids

play important negative regulators for these proteins as mentioned above, application of molecular agents which specifically activates HDACs could be employed in phase-3 cultures to enhance the enucleation yields. As mentioned in a number of reports, co -culturing of maturating erythroblast along with stromal cells may enhance their terminal maturation, but on the other hand it might impose an additional risk of poorly defined potentially immunogenic and/or infectious agent which may compromise the production of GMP for RBCs in the developmental process. These issues indicate the need for the development of biochemical alternatives to avoid the use of stromal co-cultures in these protocols. There are preliminary reports on the use of drugs like Mifepristone and plasmanate which are defined to have similar effects on promoting enucleation efficiency during ex vivo expansion of RBCs [**59**]. In addition, factors promoting the functioning of proteins involved in vesicle trafficking such as 'vaccuoline' may also be used to improve the enucleation efficiency if phase-3 cultures [**147**].

- ***Production cost***

The regular commercial production of RBCs would be heavily affected by their cost of production. According to a hypothetical estimation, producing RBCs in desired range would cost approximately $8000-15000 per unit [**136, 137**]. Whereas, the hospital cost for leuco-reduced RBCs is only $225 that is significantly lower in comparison to synthetic product. There are situations such as matching of rare phenotypes of RBCs and the present cost of a phenotypically matched unit of RBCs is ~$700-1200**.** Producing blood on a commercial scale would require a huge monetary investment and it will be difficult to keep the momentum in the direction of R&D for developing more and more efficient protocols due to lack of money especially in low income grade countries. It would be important to find out immediate goals which can be achieved from the outcomes of the existing research findings to generate alternate sources of money. For

example, immediate use of these small scale products may be useful in developing various immediately achievable goals. There are few promising examples, such as the use of ex vivo cultured cells for Reagent RBCs diagnostics in specifically alloimmunized patients and they can be used as drug delivery vehicles for personalized therapies. The requirement of relatively small no. of RBCs in these methods makes them most suitable for these kinds of assays, for example, ~ 2x 10^8 RBCs will be sufficient to perform 100xs of these assays in clinical settings and with the present methodologies 10^9-10^{10} RBCs can be expanded regularly.

Summary

In brief, it seems feasible that commercial production of RBCs may take place in near future. There are enough technological evidences available supporting the concept and with the advent of newer source materials, optimal methods for ex vivo cultivation of RBCs and highly stringent, comprehensive quality control, analytical measures, the regular production of blood may take place to support a smaller fraction of the population at least. All the three major sources of like $CD34^{+-}$ HSCs (UCB, PB and BM derived cells), hESCs and, iPSCs have enough potential of generating huge amounts of RBCs and if more sophisticated methods are generated such as development of erythropoietic hESC cell lines, it would be possible to generate an unlimited source of initial source material for the production measures.

Moreover, with the development of more in depth knowledge about the molecular mechanisms involved in various stages of ex vivo erythropoiesis. It would become more efficient to support even larger population's blood demands. The fundamental information shall also be helpful in developing pharmacological alternates for the various stages of erythropoietic development

which presently depend upon their interactions with feeder cell support systems in most of the protocols. Development of pharmacological alternates is essential to simplify the production processes for clinical grade blood. Avoiding the need of feeder cells may also help in reducing the unexpected risks associated with their use due to undefined immunogenic and infectious exposures which are likely imposed to the recipients by animal derived feeder cell support methods. The omission of feeder cells from ex vivo RBCs expansion protocols would also simplify the commercial scale production methods and may also be helpful in reducing the cost of production. As per as cost is concerned, a small fraction of the population may be capable of bearing the cost of commercially produced blood in economically developed countries. However, more liberal government policies such as lowering both the sale and services taxes, provisions for subsidized input materials (like electricity, water, etc.), direct subsidy offered for the products may be helpful in supporting the low cost production of blood. Besides that, a small amount of remuneration may also be generated from the various smaller/ specific products such as reagent RBCs, RBCs for the specific drug delivery targets to cure rare hemoglobinopathies and that might support the ongoing research and development in the same direction.

Acknowledgement

We thank the Honorable Chairman and the Honorable Vice-Chancellor of the Delhi Technological University, Shahbad Daulatput, Bawana road, Delhi-42, for support. Dr. Vimal Kishor Singh particularly thanks the Dept. of Science and Technology and Indian National Science Academy (INSA), INDIA, for the research grant. .

References

1 Alter, H.J., and Klein, H.G. (2008). The hazards of blood transfusion in historical perspective. *Blood.* 112, 2617-2626.

2 World Health Organization. "Global Database on Blood Safety: Summary report 2011." Accessed May-04-2014.

. http://www.who.int/bloodsafety/global_database/GDBS_Summary_Report_2011.pdf.

3 Department of Health and Human Services. "The 2009 national blood collection and utilization survey report. Washington, DC: DHHS, 2010." Accessed May-04-2014.

http://www.aabb.org/programs/biovigilance/nbcus/Documents/09-nbcus-report.pdf.

4 Department of Health and Human Services. "The 2011 national blood collection and utilization survey report. Washington, DC: DHHS, 2013." Accessed May-04-2014.

http://www.aabb.org/programs/biovigilance/nbcus/Documents/11-nbcus-report.pdf.

5 Ali, A., Auvinen, M.K., and Rautonen, J. (2010). The aging population poses a global challenge for blood services. *Transfusion.* 50, 584-588.

6 U.S. Census Bureau. "Global population composition." Accessed September 14, 2012. http://www.census.gov/population/international/files/wp02/wp-02004.pdf.

7 Daniels, G., Castilho, L., Flegel, W.A., Fletcher, A., Garratty, G., Levene, C., Lomas-Francis, C., Moulds, J.M., Moulds, J.J., Olsson, M.L., Overbeeke, M., Poole, J., Reid, M.E., Rouger, P., van der Schoot, E., Scott, M., Sistonen, P., Smart, E., Storry, J.R., Tani, Y., Yu, L.C., Wendel, S., Westhoff, C., Yahalom, V., and Zelinski, T. (2009). International Society of Blood Transfusion Committee on terminology for red blood cell surface antigens: Macao report. *Vox. Sang.* **96**:2. doi: 10.1111/j.1423-0410.2008.01133.x.

8 Bagnis, C., Chiaroni, J., and Bailly, P. (2011). Elimination of blood group antigens: Hope and reality. Br. J. *Haematol.* 15s2, 392-400.

9 Winslow, R. M. (2006). Current status of oxygen carriers (’blood substitutes’):2006. *Vox. Sang*. 91, 102–110.

10 Henkel-Honke, T., and Oleck, M. (2007). Artificial oxygen carriers: a current review. *AANA. J.* 75**,** 205–211.

11 Castro, C.I., and Briceno, J.C. (2010). Perfluorocarbonbased oxygen carriers: Review of products and trials. *Artif. Organs.* 34, 622–634.

12 Silverman, T.A., and Weiskopf, R.B. (2009). Hemoglobinbased oxygen carriers: Current status and future directions. *Transfusion.* 49, 2495–2515.

13 Natanson, C., Kern, S. J., Lurie, P., Banks, S. M. and Wolfe, S.M. (2008).Cell-free hemoglobin-based blood substitutes and risk of myocardial infarction and death: a meta-analysis. *J. Am. Med. Assoc.* 299, 2304-2312.

14 Hiroyama, T., Miharada, K., Sudo, K., Danjo, I., Aoki, N., and Nakamura, Y. (2008). Establishment of mouse embryonic stem cell-derived erythroid progenitor cell lines able to produce functional red blood cells. *PLoS. One.* **6:**3. doi: 10.1371/journal.pone.0001544.

15 Giarratana, M.C., Rouard, H., Dumont, A., Kiger, L., Safeukui, I., Le Pennec, P.Y., Francois, S., Truqnan, G., Peyrard, T., Marie, T., Jolly, S., Hebert, N., Mazurier, C., Mario, N., Harmand, L., Lapillonne, H., Devaux, J.Y., and Douay, L. (2011). Proof of principle for transfusion of in vitro-generated red blood cells. *Blood.* 118, 5071-5079.

16 Neildez-Nguyen, T.M., Wajcman, H., Marden, M.C., Bensidhoum, M., Moncollin, V., Giarratana, M.C., Kobari, L., Thierry, D., and Douay, L. (2002). Human erythroid cells produced cx vivo at large scale differentiate into red blood cells in vivo. *Nat. Biotechnol.* 20, 467-472.

17 Fujimi, A., Matsunaga, T., Kobune, M., Kawano, Y., Nagaya, T., Tanaka, I., Iyama, S., Hayashi, T., Sato, T., Miyanishi, K., Sagawa, T., Sato, Y., Takimoto, R., Takayama, T., Kato, J., Gasa, S., Sakai, H., Tsuchida, E., Ikebuchi, K., Hamada, H., and Niitsu, Y. (2008). Ex vivo large-scale generation of human red blood cells from cord blood $CD34^+$ cells by co-culturing with macrophages. *International Journal of Hematology*. 87, 339-350.

18 Ende, M., and Ende, N. (1972). Hematopoietic transplantation by means of fetal (cord) blood. A new method. *Va. Med. Mon.* 99, 276-280.

19 Baron, M.H., Isern, J., and Fraser, S.T. (2012). The embryonic origins of erythropoiesis in mammals. *Blood*.119, 4828-4837.

20 Palis, J. (2008). Ontogeny of erythropoiesis. *CurrOpin. Hematol.* 15, 155-161

21 Akashi, K., Traver, D., Miyamoto, T., and Weissman, I.L. (2000). A clonogenic common myeloid progenitor that gives rise to all myeloid lineages. *Nature.* 404, 193-197.

22 Debili, N., Coulombel, L., Croisille, L., Katz, A., Guichardv, Breton-Gorius, J., and Vainchenker, W. (1996). Characterization of a bipotent erythro megakaryocyticprogenitor in human bone marrow. *Blood.* 88, 1284-1296.

23 McLeod, D.L., Shreve, M.M., and Axelrad, A.A. (1996). Induction of megakaryocyte colonies with platelet formation *in vitro*. *Nature.* 88, 492-494.

24 Suda, T., Suda, J., and Ogawa, M. (1983). Single-cell origin of mouse hemopoietic colonies expressing multiplelineages in variable combinations. *Proc. Natl. Acad. Sci. USA.* 80, 6689-6693.

25 Heath, D.S., Axelrad, A.A., McLeod, D.L., and Shreeve, M.M. (1976). Separation of the erythropoietin-responsive progenitors BFU–E and CFU–E in mouse bone marrow by unit gravity sedimentation. *Blood.* 47, 777-792.

26 Lichtman, M.A., Beutler, E., Kipps, T.J., Kaushansky, K., Seligsohn, U. and Prchal, J., (2007). *Williams hematology*. New York:McGraw-Hill.

27 Jing, L., Jianhua, Z., Yelena, G., Huihui, L., Fumin, X., Lucia, D.F., Joel, A.C., Narla, M., and An, X. (2013). An: Quantitative analysis of murine terminal erythroid differentiation in vivo: novel method to study normal and disordered erythropoiesis *Blood.* **121**:8. doi: 10.1182/blood-2012-09-456079.

28 Stephenson, J.R., Axelrad, A.A., McLeod, D.L., and Shreevel, M.M. (1971). Induction of colonies of hemoglobin-synthesizing cells by erythropoietin *in vitro*. *Proc. Natl. Acad. Sci. USA* 68, 1542-1546.

29 Bessis, M., Mize, C., and Prenant, M. (1978). Erythropoiesis: comparison of *in vivo* and *in vitro* amplification. *Blood. Cells.* 4, 155-174.

30 Manwani, D., and Bieker, J.J. (2008). The erythroblastic island. *Curr. Top. Dev. Biol.* 82, 23-53.

31 Rhodes, M.M., Kopsombut, P., Bondurant, M.C., Price, J.O., and Koury, M.J. (2008). Adherence to macrophages in erythroblastic islands enhances erythroblast proliferation and increases erythrocyte production by a different mechanism than erythropoietin. *Blood.* 111, 1700-1708.

32 Gifford, S.C., Derganc, J., Shevkoplyas, S.S., Yoshida, T., and Bitensky, M.W. (2006). A detailed study of time-dependent changes in human red blood cells: from reticulocyte maturation to erythrocyte senescence. *Br. J. Haematol.* 135, 395-404.

33 Baron, M.H., and Fraser, S.T. (2005). The specification of early hematopoiesis in the mammal. *Curr. Opin. Hematol.* 12, 217-221.

34 McGrath, K., and Palis, J. (2008). Ontogeny of erythropoiesis in the mammalian embryo. *Curr. Top. Dev. Biol.* 82, 1-22.

35 Migliaccio, G., Migliaccio, A.R., Petti, S., Mavilio, F., Russo, G., Lazzaro, D., Testa, U., Marinucci, M., and Peschle, C. (1986). Human embryonic hemopoiesis. Kinetics of

progenitors and precursors underlying the yolk sac – liver transition. *J Clin Invest* 78, 51-60.

36 Mikkola, H.K., Gekas, C., Orkin, S.H., and Dieterlen-Lievre, F. (2005). Placenta as a site for hematopoietic stem cell development. *Exp. Hematol.* 33, 1048-1054.

37 Palis, J., and Yoder, M.C. (2001). Yolk-sac hematopoiesis: the first blood cells of mouse and man. *Exp. Hematol.* 29, 927-936.

38 Migliaccio, A. R., Masselli, E., Varricchio, L., and Whitsett, C. (2012). Ex-vivo expansion of red blood cells: how real for transfusion in humans? *Blood. Rev.* 26, 81-95.

39 Lodish, H., Flygare, J., and Chou, S. (2010). From stem cell to erythroblast: regulation of red cell production at multiple levels by multiple hormones. *IUBMB. Life.* 62, 492-496.

40 Szabo, E., Rampalli, S., Risueno, R.M., Schnerch, A., Mitchell, R., Fiebig-Comyn, A., Levadoux-Martin, M., and Bhatia, M. (2010). Direct conversion of human fibroblasts to multilineage blood progenitors. *Nature.* **468**:7323 doi: 10.1038/nature09591.

41 Carmelo, C. S., Mario, C., Paolo, D. F., Armando, D. V., Lessandro, M.G., Francesco, L., Francesco, L., Roberto, M. L., Corrado, T., Paola Z., and Sante, T. (1995). CD34-positive cells: biology and clinical relevance *Haematologica.* 80, 367-387.

42 Fibach, E., Manor, D., Oppenheim, A., and Rachmilewitz, E.A. (1989). Proliferation and maturation of human erythroid progenitors in liquid culture. *Blood.* 73, 100-103.

43 Fibach, E., Manor, D., Oppenheim, A., and Rachmilewitz, E.A. (1991). Growth of human normal erythroid progenitors in liquid culture: a comparison with colony growth in semisolid culture. *Int. J. Cell. Cloning*. 9, 57-64

44 Wada, H., Suda, T., Miura, Y., Kajii, E., Ikemoto, S., and Yawata, Y. (1990). Expression of major blood group antigens on human erythroid cells in a two phase liquid culture system. *Blood.* 75, 505-511

45 Douay, L. (2001). Experimental culture conditions are critical for ex vivo expansion of hematopoietic cells. *J. Hematother. Stem. Cell. Res*. 10, 341-346.

46 Giarratana, M.C., Kobari, L., Lapillonne, H., Chalmers, D., Kiger, L., Cynober, T., Marden, M.C., Wajcman, H., and Douay, L., (2005). Ex vivo generation of fully mature human red blood cells from hematopoietic stem cells. *Nat. Biotechnol*. 23, 69-74.

47 Douay, L., and Andreu, G., (2007). Ex vivo production of human red blood cells from hematopoietic stem cells: what is the future in transfusion? *Transfus. Med. Rev*. 21, 91-100.

48 Douay, L., and Giarratana, M.C. (2009). Ex vivo production of human red blood cells: a newadvance in stem cell engineering. *Methods. Mol. Biol.* **482:**127. doi: 10.1007/978-1-59745-060-7_8.

49 Douay, L., Lapillonne, H., and Turhan, A.G. (2009). Stem cells-A source of adult red blood cells for transfusion purposes: Present and future. *Critical. Care. Clinics.* 25, 383-398.

50 Malik, P., Fisher, T.C., Barsky, L.L.W., Zeng, L., Izadi, P., Hiti, A.L., Weinberg, K.I., Coates, T.D., Meiselman, H.J., and Kohn, D.B. (1998). An In Vitro Model of Human Red Blood Cell Production from Hematopoietic Progenitor Cells. *Blood*. 91, 2664-2671.

51 Panzenböck, B., Bartunek, P., Mapara, M.Y., and Zenke, M. (1998). Growth and differentiation of human stem cell factor/erythropoietin-dependent erythroid progenitor cells in vitro. *Blood.* 15, 3658-3668.

52 Freyssinier, J.M., Lecoq-Lafon, C., Amsellem, S., Picard, F., Ducrocq, R., Mayeux, P., Lacombe, C., and Fichelson, S. (1999). Purification, amplification and characterization of a population of human erythroid progenitors. *J. Haematol*. 106, 912-922.

53 Baek, E.J., Kim, H.S., Kim, S., Jin, H., Choi, T.Y. and Kim, H.O. (2008). In vitro clinical grade generation of red blood cells from human umbilical cord blood $CD34^+$ cells. *Transfusion*. 48, 2235-2245.

54 Xi, J., Li, Y., Wang, R., Wang, Y., Nan, X., He, L., Zhang, P., Chen, L., Yue, W., and Pei, X. (2013). In vitro large scale production of human mature red blood cells from hematopoietic stem cells by coculturing with human fetal liver stromal cells. *BioMed. Res. Int.* **2013**:807863. doi: 10.1155/2013/807863.

55 Leberbauer, C., Boulme, F., Unfried, G., Huber, J., Beug, H., Mullner, E.W. (2005). Different steroids coregulate long-term expansion versus terminal differentiation in primary human erythroid progenitors. *Blood*. 105, 85-94.

56 Van den Akker, E., Satchwell, T. J., Pellegrin, S., Daniels, G., and Toye, A. M. (2010). The majority of the in vitro erythroid expansion potential resides in CD34 (-) cells, outweighing the contribution of CD34 (+) cells and significantly increasing the erythroblast yield from peripheral blood samples. *Haematologica*. 95, 1594-1598.

57 Tirelli, V., Ghinassi, B., Migliaccio, A. R., Whitsett, C., Masiello, F., Sanchez, M., and Migliaccio, G. (2011). Phenotypic definition of the progenitor cells with erythroid differentiation potential present in human adult blood. *Stem. Cells. Int.* **2011**:602483. doi: 10.4061/2011/602483.

58 Kawano, Y., Kobune, M., Yamaguchi, M., Nakamura, K., Ito, Y., Sasaki, K., Takahashi, S., Nakamura, T., Chiba, H., Sato, T., Matsunaga, T., Azuma, H., Ikebuchi, K., Ikeda, H., Kato, J., Niitsu, Y., and Hamada, H. (2003). Ex vivo expansion of human umbilical cord hematopoietic progenitor cells using a coculture system with human telomerase catalytic subunit (hTERT)-transfected human stromal cells. *Blood*. 15:101, 532-40.

59 Miharada, K., Hiroyama, T., Sudo, K., Nagasawa, T., and Nakamura, Y. (2006). Efficient enucleation of eryth' roblasts differentiated in vitro from hematopoietic stem and progenitor cells. *Nat. Biotechnol.* 24, 1255-1256.

60 Maggakis-Kelemen, C., Bork, M., Kayser, P., Biselli, M., and Artmann, G.M. (2003). Biological and mechanical quality of red blood cells cultured from human umbilical cord blood stem cells. *Med. Biol. Eng. Compuz*. 41, 350-356

61 Baek, E.J., Kim, H.S., Kim, J.H., Kim, N.J., Kim, and H.O. (2009). Stroma-free mass production of clinical-grade red blood cells (RBCs) by using poloxamer 188 as an RBC survival enhancer. *Transfusion.* **49**:11 doi: 10.1111/j.1537-2995.2009.02303.x.

62 Timmins, N. E., Athanasas, S., Günther, M., Buntine, P., and Nielsen, L.K. (2011). Ultrahigh-yield manufacture of red blood cells from hematopoietic stem cells. *Tissue Eng. Part. C Methods*. 17, 1131-1137.

63 Conley, C.L., Weatherall, D.J., Richardson, S.N., Shepard, M.K., and Charache, S. (1963). Hereditary persistence of fetal hemoglobin: A study of 79 affected persons in 15 Negro families in Baltimore. *Blood.* 21, 261-281.

64 Weatherall, D.J., and Clegg, J.B. (1975). Hereditary persistence of fetal haemoglobin. *Br. J Haematol.* 29, 191-198

65 Foeken, L.M., Green, A., Hurley, C.K., Marry, E., Wiegand, T., and Oudshoorn, M. (2010). Monitoring the international use of unrelated donors for transplantation: The WMDA annual reports. *Bone Marrow Transplant.* 45, 811-818.

66 Thomson, J.A., Itskovitz-Eldor, J., Shapiro, S.S., Waknitz, M.A., Swiergiel, J.J., Marshall, V.S., and Jones, J.M. (1998). Embryonic Stem Cell Lines Derived from Human Blastocysts *Science.* 282, 1145-1147.

67 Takahashi, K., and Yamanaka, S. (2006). Induction of pluripotent stem cells from mouse embryonic and adult fibroblast cultures by defined factors. *Cell.* 126, 663-676

68 Takahashi, K., Tanabe, K., Ohnuki, M., Narita, M., Ichisaka, T., Tomoda, K. and Yamanaka, S. (2007). Induction of pluripotent stem cells from adult human fibroblasts by defined factors. *Cell*. 131, 861-872.

69 Okita, K., Ichisaka, T. and Yamanaka, S. (2007). Generation of germlilne-competent induced pluripotent stem cells. *Nature.* 448, 313-317.

70 Wernig, M., Meissner, A., Foreman, R., Brambrink, T., Ku, M., Hochedlinger, K., Bernstein, B.E. and Jaemisch, R. (2007). In vitro reprogramming of fibroblasts into a pluripotent ES-cell-like state. *Nature.* 448, 318-324.

71 Yu, J., Vodyanik, M.A., Smuga-Otto, K., Antosiewicz-Bourrget, J., Frane, J.L., Tian, S., Nie, J., Vonsdottir, G.A., Ruotti, V., Stewart, R., Slukin, I.I. and Thomson, J.A. (2007). Induced pluripotent stem cell lines derived from human somatic cells. *Science.* 318, 1917-1920.

72 Stadtfeld, M., Nagaya, M., Utikal, J., Weir, G. and Hochedlinger, K. (2008). Induced pluripotent stem cells generated without viral integration. *Science*. 322, 945-949.

73 Lacoste, A., Berenshteyn, F. and Brivanlou, A.H. (2009). An efficient and reversible transposable system for gene delivery and lineage-specific differentiation in human embryonic stem cells. *Cell Stem Cell*. 5, 332-342.

74 Zhou, H., Wu, S., Joo, J.Y., Zhu, S., Han, D.W., Lin, T., Trauger, S., Bien, G., Yao, S., Zhu, Y., Siuzdak, G., Schöler, H.R., Duan, L. and Ding, S. (2009). Generation of induced pluripotent stem cells using recombinant proteins. *Cell Stem Cell*. 4, 381-384.

75 Ng, E.S., Davis, R.P., Azzola, L., Stanley, E.G., and Elefanty, A.G. (2005). Forced aggregation of defined numbers of human embryonicstem cells into embryoid bodies fosters robust, reproducible hematopoietic differentiation. *Blood.* 106, 1601-1603.

76 Choi, K.D., Yu, J., Smuga-Otto, K., Salvagiotto, G., Rehrauer, W., Vodyanik, M., Thomson, J., and Slukvin, I. (2009). Hematopoietic and endothelial differentiation of human induced pluripotent stem cells. *Stem Cells*. 27, 559-567.

77 Chang, C.J., Mitra, K., Koya, M., Velho, M., Desprat, R., Lenz, J., and Bouhassira, E.E. (2011). Production of embryonic and fetal-like red blood cells from human induced pluripotent stem cells. *PLoS. One.* **6**:10 doi: 10.1371/journal.pone.0025761.

78 Kobari, L., Yates, F., Oudrhiri, N., Francina, A., Kiger, L., Mazurier, C., Rouzbeh, S., El-Nemer, W., Hebert, N., Giarratana, M.C., François, S., Chapel, A., Lapillonne, H., Luton, D., Bennaceur-Griscelli, A., and Douay, L. (2012). Human induced pluripotent stem cells can reach complete terminal maturation: in vivo and in vitro evidence in the erythropoietic differentiation model. *Haematologica.* 97, 1795-1803.

79 Lu, S.J., Feng, Q., Park, J.S., Vida, L., Lee, B.S., Strausbauch, M., Wettstein, P.J., Honig, G.R., and Lanza, R. (2008). Biologic properties and enucleation of red blood cells from human embryonic stem cells. *Blood.* 112, 4475-4484.

80 Vodyanik, M.A., Bork, J.A., Thomson, J.A. and Slukvin, I.I. (2005). Human embryonic stem cell-derived CD34 + cells: efficient production in the coculture with OP9 stromal cells and analysis of lymphohematopoietic potential. *Blood.* 105, 617-626.

81 Vodyanik, M.A., Thomson, J.A. and Slukvin, I.I. (2006). Leukosialin (CD43) defines hematopoietic progenitors in human embryonic stem cell differentiation cultures. *Blood.* 108, 2095-2105.

82 Chadwick, K., Wang, L., Li, L., Menendez, P., Murdoch, P., Rouleau, A. and Bhatia, M. (2003). Cytokines and BMP-4 promote hematopoietic differentiation of human embryonic stem cells. *Blood.* 102, 906-915.

83 Chang, K.H., Nelson, A.M., Cao, H., Wang, L., Nakamoto, B., Ware, C.B., and Papayannopoulou, T. (2006). Definitive-like erythroid cells derived from human embryonic stem cells coexpress high levels of embryonic and fetal globins with little or no adult globin. *Blood.* 108, 1515-1523.

84 Lapillonne, H., Kobari, L., and Mazurier, C., Tropel, P., Giarratana, M.C., Cleon, I.Z., Kiger, L., Donzé, M.W., Puccio, H., Hebert, N., Francina, A., Andreu, G., Viville, S., and Douay, L. (2010). Red blood cell generation from human induced pluripotent stem cells: Perspectives for transfusion medicine. *Haematologica.* 95, 1651-1659.

85 Dias, J., Gumenyuk, M., Kang, H., Vodyanik, M., Yu, J., Thomson, J.A., and Slukvin, I.I. (2011). Generation of red blood cells from human induced pluripotent stem cells. *Stem Cells Dev.* 20, 1639-1647.

86 Qiu, C., Olivier, E.N., Velho, M., and Bouhassira, E.E. (2008). Globin switches in yolk sac-like primitive and fetal like definitive red blood cells produced from human embryonic stem cells. *Blood.* 111, 2400-2408

87 Zambidis, E.T., Park, T.S., Yu, W., Tam, A., Levine, M., Yuan, X., Pryzhkova, M. and Péault, B. (2008). Expression of angiotensin-converting enzyme (CD143) identifies and regulates primitive hemangioblasts derived from human pluripotent stem cells. *Blood.* 112, 3601-3614.

88 Keller, G. (2005). Embryonic stem cell differentiation: emergence of a new era in biology and medicine. *Genes and Development.* 19, 1129-1155.

89 Ng, E.S., Davis, R.P., Azzola, L., Stanley, E.G. and Elefanty, A.G. (2005). Forced aggregation of defined numbers of human embryonic stem cells into embryoid bodies fosters robust, reproducible hematopoietic differentiation. *Blood.* 106, 1601-1603

90 Kaufman, D.S., Hanson, E.T., Lewis, R.L., Auerbach, R., and Thomson J.A., (2001). Hematopoietic colony-forming cells derived from human embryonic stem cells. *Proc. Natl. Acad. Sci. USA.* 98(19), 10716-21.

91 Ledran, M.H., Krassowska, A., Armstrong, L., Dimmick, I., Renstrom, J., Lang, R., Yung, S., Santibanez-Coref, M., Dzierzak, E.,Stojkovic, M., Oostendorp, R.A.J., Forrester, L. and Lako, M. (2008). Efficient hematopoietic differentiation of human embryonic stem cells on stromal cells derived from hematopoietic niches. *Cell Stem Cell.* 3, 85-98.

92 Amit, M., Margulets, V., Segev, H., Shariki, K., Laevsky, I., Coleman, R and Itskovitz-Eldor, J. (2003). Human feeder layers for human embryonic stem cells. *Biology of Reproduction.* 68, 2150-2156.

93 Hovatta, O., Mikkola, M., Gertow, K., Stromberg, A.M., Inzunza, J., Hreinsson, J., Rozell, B., Blennow, E., Andang, M. and Ahrlund-Richter, L. (2003). A culture system using human foreskin fibroblasts as feeder cells allows production of human embryonic stem cells. *Human Reproduction.* 18, 1-6.

94 Koivisto, H., Hyvärinen, M., Strömberg, A.M., Inzunza, J., Matilainen, E., Mikkola, M., Hovatta, O., and Teerijoki, H. (2004). Cultures of human embryonic stem cells: serum replacement medium or serum-containing media and the effect of basic fibroblast growth factor. *Reproductive BioMedicine Online.* 9, 330-337.

95 Genbacev, O., Krtolica, A., Zdravkovic, T., Brunette, E., Powell, S., Nath, A., Caceres, E., McMaster, M., McDonagh, S., Li, Y., Mandalam, R., Lebkowski, J. and Fisher, S.J. (2005). Serum-free derivation of human embryonic stem cell lines on human placental fibroblast feeders. *Fertility and Sterility.* 83, 1517-1529.

96 Qiu, C., Hanson, E., Olivier, E., Inada, M., Kaufman, D.S., Gupta, S. and Bouhassira, E.E. (2005). Differentiation of human embryonic stem cells into hematopoietic cells by coculture with human fetal liver cells recapitulates the globin switch that occurs early in development. *Experimental Hematology.* 33, 1450-1458.

97 Olivier, E.N., Qiu, C., Velho, M., Hirsch, R.E. and Bouhassira, E.E. (2006). Large-scale production of embryonic red blood cells from human embryonic stem cells. *Experimental Hematology.* 34, 1635-1642.

98 Ran, D., Shia, W.J., Lo, M.C., Fan, J.B., Knorr, D.A., Ferrell, P.I., Ye, Z., Yan, M., Cheng, L., Kaufman, D.S., and Zhang, D.E. (2013). RUNX1a enhances hematopoietic

lineage commitment from human embryonic stem cells and inducible pluripotent stem cells. *Blood.* 121, 2882-2890.

99 Feng, Q., Lu, S.J., Klimanskaya, I., Gomes, I., Kim, D., Chung, Y., Honig, G.R., Kim, K.S., and Lanza, R. (2010). Hemangioblastic derivatives from human induced pluripotent stem cells exhibit limited expansion and early senescence. *Stem Cells.* 28, 704-712.

100 Chang, K.H., Nelson, A.M., Fields, P.A., Hesson, J.L., Ulyanova, T., Cao, H., Nakamoto, B., Ware, C.B., and Papayannopoulou, T. (2008). Diverse hematopoietic potentials of five human embryonic stem cell lines. *Exp. Cell. Res.* 314, 2930-2940.

101 Peyrard, T., Bardiaux, L., Krause, C., Kobari, L., Lapillonne, H., Andreu, G., and Douay, L. (2011). Banking of pluripotent adult stem cells as an unlimited source for red blood cell production; Potential applications for alloimmunized patients and rare blood challenges. *Transfus. Med. Rev.* 25, 206-216.

102 Zou, J., Mali, P., Huang, X., Dowey, S.N., and Cheng, L. (2011). Site-specific gene correction of a point mutation in human iPS cells derived from an adult patient with sickle cell disease. *Blood.* 118, 4599-4608.

103 Hanna, J., Wernig, M., Markoulaki, S., Sun, C.W., Meissner, A., Cassady, J.P., Beard, C., Brambrink, T., Wu, L.C., Townes, T.M., and Jaenisch, R. (2007). Treatment of sickle cell anemia mouse model with iPS cells generated from autologous skin. *Science.* 318, 1920-1923.

104Von Lindern, M., Zauner, W., Mellitzer, G., Steinlein, P., Fritsch, G., Huber, K., Löwenberg, B., and Beug, H. (1999). The glucocorticoid receptor cooperates with the erythropoietin receptor and c-Kit to enhance and sustain proliferation of erythroid progenitors in vitro. *Blood.* 94, 550-559.

105Bauer, A., Tronche, F., Wessely, O., Kellendonk, C., Reichardt, H.M., Steinlein, P., Schütz, G., and Beug, H. (1999). The glucocorticoid receptor is required for stress erythropoiesis. *Genes Dev.* 13, 2996-3002.

106Migliaccio, G., Di Pietro, R., Di Giacomo, V., Di Baldassarre, A., Migliaccio, A.R., Maccioni, L., Galanello, R., and Papayannopoulou, T. (2002). In vitro mass production of human erythroid cells from the blood of normal donors and of thalassemic patients. *Blood. Cells. Mol. Dis.* 28, 169-180.

107Migliaccio, G., Sanchez, M., Masiello, F. Tirelli, V., Varricchio, L., Whitsett, C., and Migliaccio, A.R. (2010). Humanized culture medium for clinical expansion of human erythroblasts. *Cell Transplant.* 19, 453-469.

108Carotta, S., Pilat, S., Mairhofer, A., Schmidt, U., Dolznig, H., Steinlein, P., and Beug, H. (2004). Directed differentiation and mass cultivation of pure erythroid progenitors from mouse embryonic stem cells. *Blood.* 104, 1873-1880.

109England, S.J., McGrath, K.E., Frame, J.M., and Palis, J. (2011). Immature erythroblasts with extensive ex vivo self-renewal capacity emerge from the early mammalian fetus. *Blood.* 117, 2708-2717.

110Huang, X., Shah, S., Wang, J., Ye, Z., Dowey, S.N., Tsang, K.M., Mendelsohn, L.G., Kato, G.J., Kickler, T.S., and Cheng, L. (2013). Extensive Ex Vivo Expansion of Functional Human Erythroid Precursors Established From Umbilical Cord Blood Cells by Defined Factors. *Mol. Ther.* **22**:2 doi:10.1038/mt.2013.201

111Kurita, R., Suda, N., Sudo, K., Miharada, K., Hiroyama, T., Miyoshi, H., Tani, K., and Nakamura, Y. (2013). Establishment of immortalized human erythroid progenitor cell lines able to produce enucleated red blood cells. *PLoS One.* **8:**3 doi:10.1371/journal.pone.0059890.

112Yoshioka, N., Gros, E., Li, H.R., Kumar, S., Deacon, D.C., Maron, C., Muotri, A.R., Chi, N.C., Fu, X.D., Yu, B.D., and Dowdy, S.F. (2013). Efficient generation of human iPSCs by a synthetic self-replicative RNA. *Cell Stem Cell.* 13, 246-254.

113Hou, P., Li, Y., Zhang, X., Liu, C., Guan, J., Li, H., Zhao, T., Ye, J., Yang, W., Liu, K., Ge, J., Xu, J., Zhang, Q., Zhao, Y., and Deng, H. (2013). Pluripotent stem cells induced from mouse somatic cells by small-molecule compounds. *Science.* 341, 651-654.

114Chou, B.K., Mali, P., Huang, X., Ye, Z., Dowey, S.N., Resar, L.M., Zou, C., Zhang, Y.A., Tong, J., and Cheng, L. (2011). Efficient human iPS cell derivation by a non-integrating plasmid from blood cells with unique epigenetic and gene expression signatures. *Cell Res.* 21, 518-529.

115Machlus, K.R., and Italiano, J.E. (2013). The incredible journey: From megakaryocyte development to platelet formation. *J Cell Biol*. **201**:6. doi: 10.1083/jcb.201304054.

116Christian, H., Rüster, B., Seifried, E., and Henschler, R. (2010). Platelet Precursor Cells Can Be Generated from Cultured Human CD34+ Progenitor Cells But Display Recirculation into Hematopoietic Tissue upon Transfusion in Mice. *Transfus. Med. Hemother.* 37, 185-190.

117Proulx, C., Boyer, L., Humanen, D.R., and Lemieux, R. (2003). Preferential *ex vivo* expansion of megakaryocytes from human cord blood CD34+-enriched cells in the presence of thrombopoietin and limiting amounts of stem cell factor and Flt-3 ligand. *J. Hematother. Stem. Cell. Res.* 12, 179-188.

118Proulx, C., Dupuis, N., Amour, I.S., Boyer, L., and Lemieux, R. (2004). Increased megakaryopoiesis in cultures of CD34-enriched cord blood cells maintained at 39 degrees *C.Biotechnol. Bioeng.* 88, 675-680.

119Cortin, V., Garnier, A., Pineault, N., Lemieux, R., Boyer, L., and Proulx, C. (2005). Efficient *in vitro* megakaryocyte maturation using cytokine cocktails optimized by statistical experimental design. *Exp. Hematol.* 33, 1182-1191.

120Mostafa, S.S., Papoutsakis, E.T., and Miller, W.M. (2001). Oxygen tension modulates the expression of cytokine receptors, transcription factors and lineage-specific markers in cultured human megakaryocytes. *Exp. Hematol.* 29, 873-883.

121Giamniona, L.M., Fuhrken, P.G., Papoustsakis, E.T., and Miller, W.M. (2006). Nicotinamide (vitamin B3) increases the polyploidisation and propletelet formation of cultured primary human megakaryocytes. *Br. J. Haemotol.* 135, 554-566.

122Guerriero, R., Mattia, G., Testa, U., Chelucci, C., Macioce, G., Casella, I., Samoggia, P., Peschle, C., and Hassan, H.J. (2001). Stromal cell-derived factor in increases polyploidization of megakaryocytes generated by human hematopoietic progenitor cells. *Blood.* 97, 2587-2595.

123Matsunaga, T., Tanaka, I., Kobune, M., Kawano, Y., Tanaka, M., Kuribayashi, K., Iyama, S., Sato, T., Sato, Y., Takimoto, R., Takayama, T., Kato, J., Ninomiya, T., Hamada, H., and Niitsu, Y. (2006). Ex Vivo Large-Scale Generation of Human Platelets from Cord Blood $CD34^+$ Cells *Stem Cells.* 24, 2877-2887.

124Sullenharger, B., Bhang, J.H., Gruner, R., Kotov, N., and Lasky, L.C. (2009). Prolonged continuous *in vitro* human platelet production using three-dimensional scaffolds. *Exp. Hematol.* 37, 101-110.

125Masuda, S., Li, M., and Izpisua Belmonte, J.C. (2013). In vitro generation of platelets through direct conversion: first report in My Knowledge (iMK). *Cell. Res*. **23**:2. doi: 10.1038/cr.2012.142.

126Ono, Y., Wang, Y., Suzuki, H., Okamoto, S., Ikeda, Y., Murata, M., Poncz, M., and Matsubara, Y. (2012). Induction of functional platelets from mouse and human fibroblasts by p45NF-E2/Maf. *Blood.* **120:**18. doi: 10.1182/blood-2012-02-413617.

127Matsubara, Y., Saito, E., Suzuki, H., Watanabe, N., Murata, M., and Ikeda, Y. (2009). Generation of megakaryocytes and platelets from human subcutaneous adipose tissues. *Biochem. Biophys. Res. Commun*. **378:**4. doi: 10.1016/j.bbrc.2008.11.117.

128Matsubara, Y., Suzuki, H., Ikeda, Y., and Murata, M. (2010). Generation of megakaryocytes and platelets from preadipocyte cell line 3T3-L1, but not the parent cell line 3T3, in vitro. *Biochem Biophys Res Commun*. **402:**4. doi: 10.1016/j.bbrc.2010.10.120.

129Takayama, N., Nishikii, H., Usui, J., Tsukui, H., Sawaguchi, A., Hiroyama, T., Eto, K., and Nakauchi, H. (2008). Generation of functional platelets from human embryonic stem cells in vitro via ES-sacs, VEGF-promoted structures that concentrate hematopoietic progenitors. *Blood.* **111:**11. doi: 10.1182/blood-2007-10-117622.

130Takayama, N., Nishimura, S., Nakamura, S., Shimizu,T., Ohnishi, R., Endo, H., Yamaguchi, T., Otsu, M., Nishimura, K., Nakanishi, M., Sawaguchi, A., Nagai, R., Takahashi, K., Yamanaka, S., Nakauchi, H., and Eto, K. (2010). Transient activation of c-MYC expression is critical for efficient platelet generation from human induced pluripotent stem cells. *J. Exp. Med*. **207:**13. doi: 10.1084/jem.20100844.

131Stroncek, D.F., and Rebulla, P. (2007). Platelet transfusions. *Lancet.* 370, 427-38.

132 Taylor, C.J., Peacock, S., Chaudhry, A.N., Bradley, J.A., and Bolton, E.M. (2012). Generating an iPSC bank for HLA-matched tissue transplantation based on known donor and recipient HLA types. *Cell Stem Cell.* **11:**2. doi: 10.1016/j.stem.2012.07.014.

133Okita, K., Matsumura, Y., Sato, Y., Okada, A., Morizane, A., Okamoto, S., Hong, H., Nakagawa, M., Tanabe, K., Tezuka, K., Shibata, T., Kunisada, T., Takahashi, M., Takahashi, J., Saji, H., and Yamanaka, S.A. (2011). More efficient method to generate integration-free human iPS cells. *Nat Methods.* **8:**5. doi: 10.1038/nmeth.1591.

134Dick, E.P., Rebecca, L., and Sabroe, P.I., (2008). Ex Vivo-Expanded Bone Marrow $CD34^+$ Derived Neutrophils Have Limited Bactericidal Ability. *Stem Cells* 26, 2552-2563.

135Saeki, K., Nakahara, M., Matsuyama, S., Nakamura, N., Yogiashi, Y., Yoneda, A., Koyanagi, M., Kondo, Y., and You, A. (2008). A feeder-free and efficient production of functional neutrophils from human embryonic stem cells. *Stem Cells.* 27, 59-67.

136Timmins, N. E., Nielsen, L. K.,(2009). Blood cell manufacture: current methods and future challenges. *Trends Biotechnol*, 27, 415–422.

137Zeuner A^1, Martelli F, Vaglio S, Federici G, Whitsett C, Migliaccio AR. (2012). Concise review: stem cell-derived erythrocytes as upcoming players in blood transfusion. *Stem Cells*, 30, 1587–1596.

138Ratcliffe E1, Glen KE, Workman VL, Stacey AJ, Thomas RJ (2012). A novel automated bioreactor for scalable process optimisation of haematopoietic stem cell culture. *J. Biotechnol*, 161, 387–390.

139Housler GJ1, Miki T, Schmelzer E, Pekor C, Zhang X, Kang L, Voskinarian-Berse V, Abbot S, Zeilinger K, Gerlach JC. (2012). Compart- mental hollow fiber capillary membrane-based bioreactor technol- ogy for in vitro studies on red blood cell lineage direction of hematopoietic stem cells. *Tissue Eng. Part. C Methods*, 18: 2. doi: 10.1089/ten.TEC.2011.0305. Epub 2011 Dec 28.

140Wang, Y., Ono, Y., and Ikeda, Y. (2011). Induction of megakaryocytes from fibroblasts by p45NF-E2fMaf. *Blood.* 11, 908

141England, S.J., McGrath, K.E., Frame, J.M., and Palis, J. (2011). Immature erythroblasts with extensive ex vivo self-renewal capacity emerge from the early mammalian fetus. *Blood.* 117, 2708-2717.

142Keel, S.B., Doty, R.T., Yang, Z., Quigley, J.G., Chen, J., Knoblaugh, S., Kingsley, P.D., De Domenico, I., Vaughn, M.B., Kaplan, J., Palis, J., and Abkowitz, J.L. (2008). A heme export protein is required for red blood cell differentiation and iron homeosiasis. *Science.* 319,825-828.

143Satchwell, T.J., Bell, A.J., Pellegrin, S., Kuziq, S., Ridgwell, K., Daniels, G., Anstee, D.J., van den Akker, E., and Toye, A.M. (2011). Critical band 3 multiprotein complex interactions establish early during human erythropoiesis. *Blood.* 118, 182-191.

144Carilli, A.R., Sugrue, M.W., Rosenau, E.H., Chang, M., Fisk, D., Medei-Hill, M., Williams, K., Wiggins, L., and Wingard, J.R. (2012). African American adult apheresis donors respond to granulocyte-colony-stimulatiflg factor with neutrophil and progenitor cell yields comparable to those of Cauc asian and Hispanic donors. *Transfusion.* 52, 166-172.

145Tirelli, V., Masiello, F., Sanchez, M., Ghinassi, B., Whitsett, C., Migliaccio, G., and Miliaccio, A.R.F. (2011). Effects of ontogeny, ethnicity, gender and loss of companion cells on ex-vivo expansion of erythroid cells for transfusion. *Blood.* 118, 563.

146Lapillonne, H., Kobari, L., Mazurier, C., Tropel, P., Giarratana, M.C., Zanella-Cleon, I., Kiger, L., Wattenhofer-Donze, M., Puccio, H., Hebert, N., Francina, A., Andreu, G., Viville, S., and Douay, L. (2010). Red blood cell generation from human induced

pluripotent stem cells; Perspectives for transfus ion medicine. *Haematologica*. 95, 165 l-l659.

147Keerthivasan, G., Small, S., Liu, H., Wickrema, A., and Crispino, J.D. (2010). Vesicle trafficking plays a novel role in erythroblast enucleation. *Blood*. 116, 3331-3340.

Figures' legends

Fig.1: Hierarchy of erythropoietic development in vertebrates: In adult Bone Marrow, committed progenitors arising from hematopoietic stem cells give rise to erythroblasts, and as the progeny of a stem cell progress through development, there is a loss of their multipotency while increasing lineage restriction. The various cellular stages in erythrocyte development are identified by their ability to form colonies in semisolid medium supplemented with specific cytokines and by cell surface markers

.

Fig.2: The various methods/protocols described so far for the Ex vivo RBCs Expansion: As discussed in the main text, manufacturing blood may involve various step which are to be categorized in three main phases as depicted in the figure. In phase 1: initial source material is to be collected from a variety of source material(s) on the basis of their availability, suitability and expansion potential and grown in medium generally supplemented with growth factors to enhance HSCs proliferation : subsequently these cells are cultured in the presence of Erythropoietin to induce their differentiation and maintenance into erythropoietic progenitor stage. Finally, in Phase 3 cultures these Erythropoietic progenitors may be co cultured with murine/ human stromal cell line support to induce their maturation and enucleation resulting into mature RBCs. These RBCs are evaluated for their biochemical properties and various antigenic profiles to ensure their nativeness.

Fig.3: An overview of the various approaches used for ex vivo Erythropoiesis: The different approaches are in use for develoing large amount of transfusable clinical grade RBCs include

$CD34^+$ HSPCs (from CB, PB, BM), ESCs/ IPSCs derived erythroid progenitors, and highly expanding erythroid progenitors due to stress erythropoiesis. All these approaches has been discussed in detail in text.

Table 1: Progression in the field of ex vivo RBCs expansion during last two decades

S. No.	Cell source & Culture time	Growth factors	Co-culture	Expansion	Units of blood	Enucleation Rate	Animal or human serum/plasma	Key points	Ref.
1	CB CD34+ 21 Days	FLT-3, SCF, TPO, EPO, IGF-1	**NO**	**NA**	**NA**	4% in vitro 99% in vivo	**No**	Basis for transfusion potential of ex vivo cultured RBCs in animal model	Neildez-Nguyen et al., 2002 [16])
2	Cord Blood 21 Days	SCF, IL-3, EPO Hydrocortisone	Murine Stromal mMS-5	$1.95X10^6$	4.6/CB	95%	No	First *in vitro* production of RBCs	Giarratana, M., et al 2005. [46]
3	Cord Blood 60 Days	EPO, SCF, IGF-1 Dex and lipid mix	No	10^9	-NA	-100%	Yes	Prolonged expansion protocol up to 60 days for adult globin switching	Leberbauer, C., 2005. [55]
4	Cord Blood 20 Days	SCF, IL-3, EPO VEGF, IGF-2	No	$7.2X10^5$	10^4/CB	77.5%	Yes	Low expansion & enucleation rates	Miharada, K., 2006. [59]
5	Cord Blood 21 Days	SCF, IL-3, EPO ,TPO, Flt-3	Human MSCs	$8X10^3$	.02/CB	64%	No	Less allogenicity, lower expansion & enucleation rates , replaced BM derived feeder cells with UCB derived cells	Baek, E.J., 2008. [53]
6	Cord Blood 38 Days	SCF+Flt-3+TPO IL-3+EPO	hTERT+ Macrophages	$3.5X10^6$	8.8/CB	100%	Yes	Impossible to scale up	Fujimi, A.,2008. [17]
7	hESCs 59 Days	Hydrocortisone, IL3, BMP-4, SCF, EPO , IGF-1	hMSCs, mMS-5 FH-B-hTERT	4×10^7 cells	NA	(6.5%, starting from CD34+ cells)	Yes	Globin switching	Qiu et al. 2008. [86]
8	hESCs 42 Days	SCF, Epo, BMP-4, VEGF , bFGF, TPO, FLT3 L	MEFs, OP9	10^{10}-10^{11} cells/6-well plate of hESCs	**NA**	10%–65%	No	Functional oxygen carrying capacity of ESCs derived RBCs	Lu et al. 2008. [79]
10	hiPSCs,(MR90, FD-136) hESCs(H1l) 46 Days	SCF,TPO, FLT3-L, TPO, BMP-4; VEGF- IL-3, IL-6		hIPSCs 4.4×10^8 hESCs 35×10^8	NA	4%–10% 52%–66%	NO	First time complete differentiation of hiPSCs cells into definitive erythrocytes capable of maturation up to enucleated RBCs (fetal hemoglobin in a functional tetrameric form)	Lapillonne et al. 2010. [84]
11	Cord Blood 33 Days	SCF, IL-3, EPO Hydrocortisone	No	$2.25X10^8$	-500 units/ UCB	>90%	No	First serum-free culture, First demonstration of RBC culture in a large-scale bioreactor	Timmins, N. E., 2011 . [62]

12	Cord Blood 18 days	SCF, EPO Hydrocortisone	No	$4.3X10^7$	75/CB	70%	Yes	Best yield to date	Giarratana, M., 2011. [15]
13	hiPSCs 59 Days	Hydrocortisone, IL-3 BMP-4, Flt3L, SCF, EPO, IGF-1	hMSCs/ Matrigel . hTERT immortalized fetal liver cells	0.5-8 x 10^6	NA	NA	YES	Production of large number of erythroid cells with embryonic and fetal-like characteristics regardless of the age of donor tissue	Chang et al.2011. [77]
14	hESCs hiPSCs 60-125 Days	iron saturated transferrin, dexamethasone, insulin, SCF, EPO, TPO, IL-3, IL-6	MEFs, mOP9 mMS-5	2×10^5 ESCs	NA	2%–10%	YES	RBCs production from transgenic and transgene-free iPSCs using the OP9 coculture method with efficiency comparable to hESCs	Dias et al.2011. [85]
15	hiPSCs 52 Days	holo-human transferrin recombinant human insulin heparin, and 5% human plasma SCF, TPO, FLT3 ligand , BMP4, VEGF- n-3, IL-Epo	MEFs	15-28.3×10^8	NA	20-26% RBC and 74-80% orthochromatic erythroblasts	5-10% Hu Plasma	First time in a normal and a pathological erythropoietic differentiation models that hiPSC are intrinsically able to mature into adult hemoglobin synthesizing cells.	Kobari et al. 2012. [78]

Figure 1.JPEG

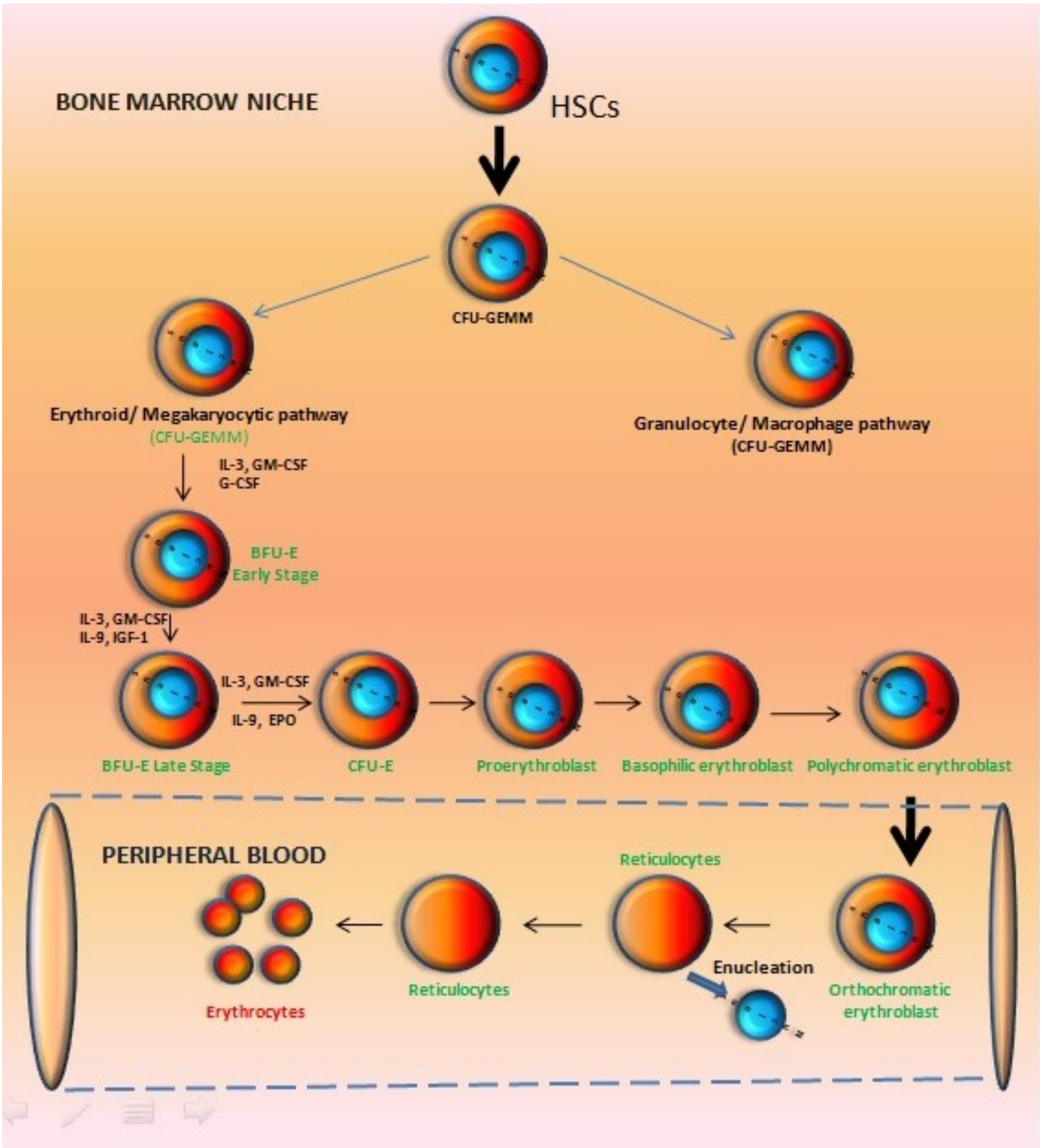

Figure 2.JPEG

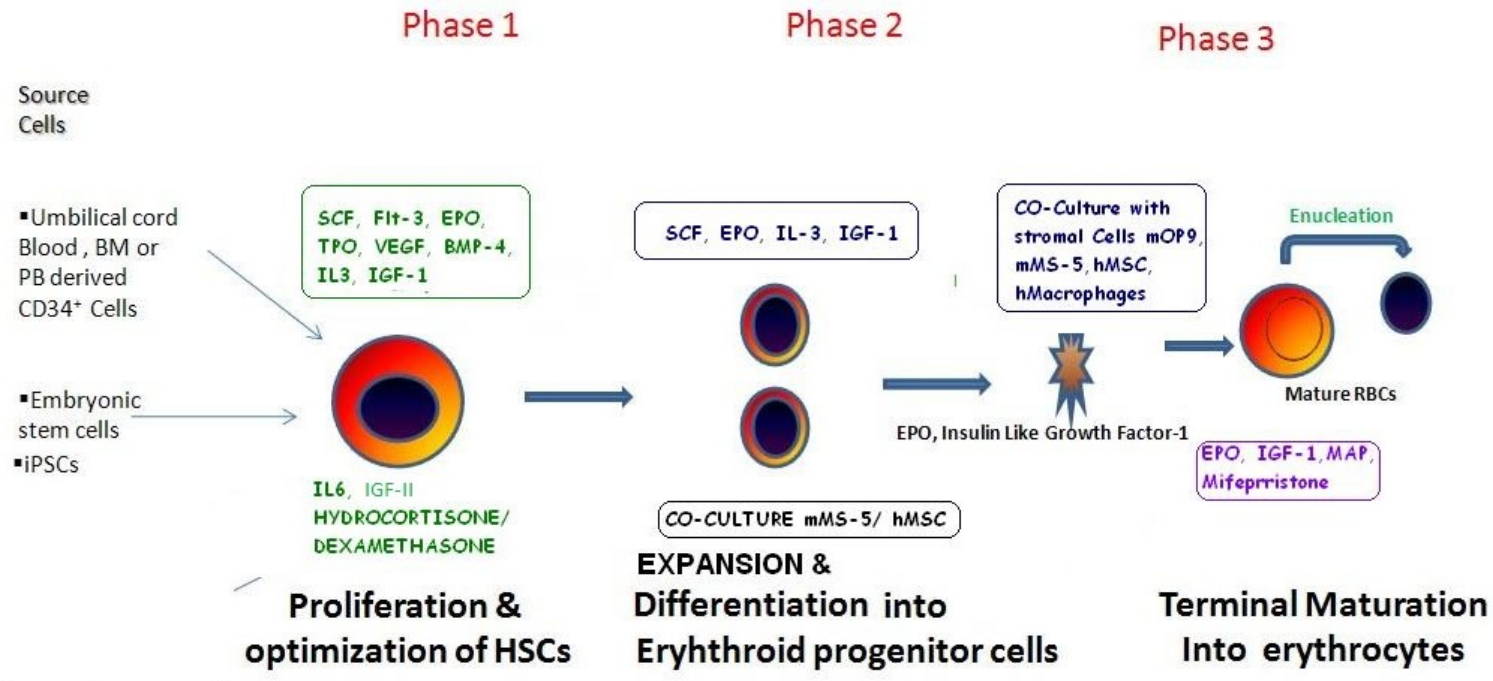

Figure 3.JPEG

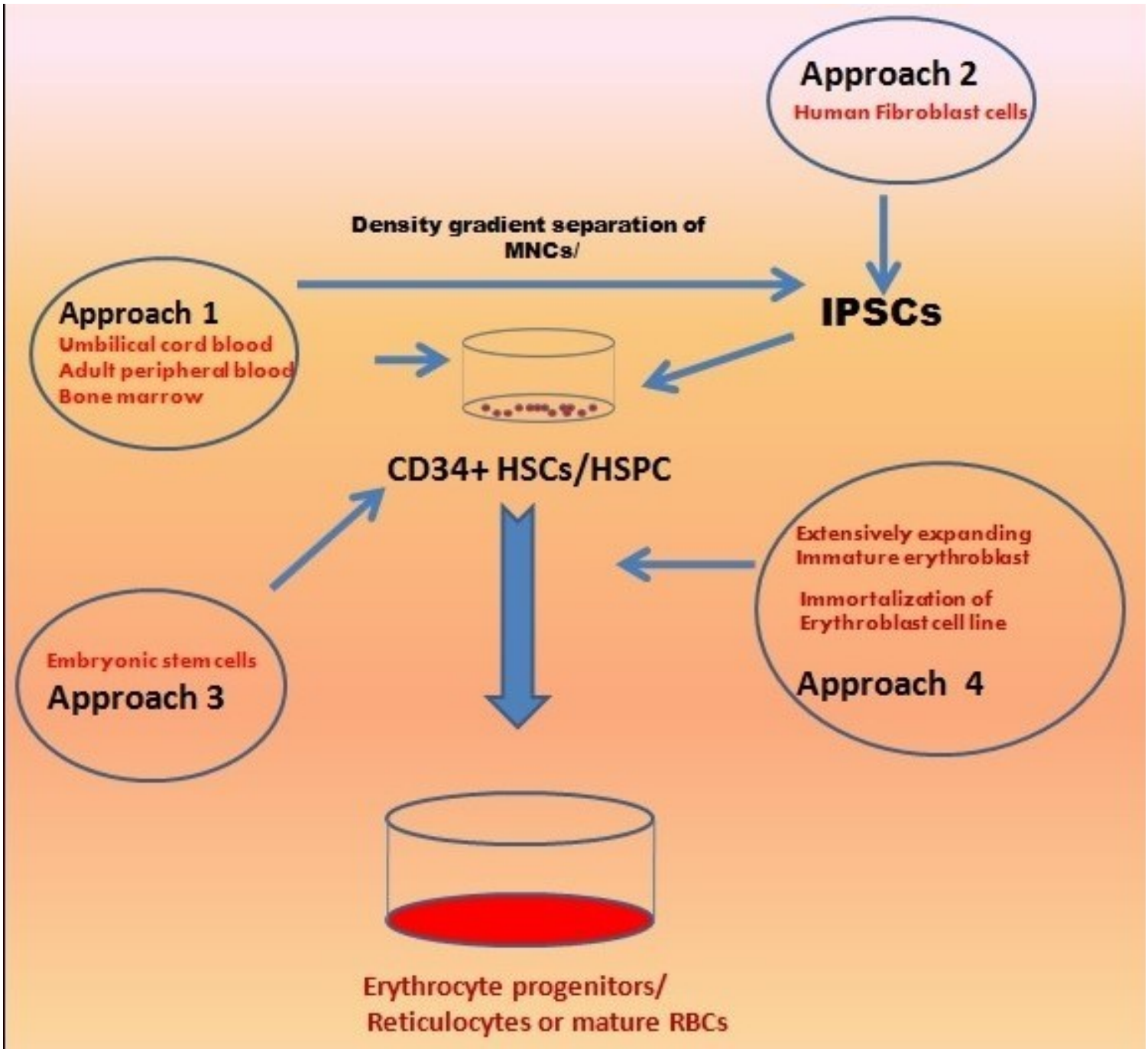

IRJSSE / Volume :2 / Issue: 4 / April 2014 | ISSN : 2347-6176

IRJSSE
Spreading Excellence

International Research Journal Of Sustainable Science & Engineering.

A Monthly Peer-Reviewed Journal

Method for improving thermal performance of Dual Pressure Linde system for liquefaction of gases using energy exergy analysis for reducing global warming and ozone depletion

Devender Kumar, [1]* .R.S Mishra[2]

Mechanical Department, Delhi Technological University, Shahabad, Delhi

Abstract:

The global warming creating inhabitant place on earth increasing temperature and reducing protective ozone layer of earth which various fatal skin diseases , the main cause of it using CFC refrigerant and other inefficient refrigeration method .In this paper ,exergy method is applied to Dual pressureLinde Hampson cycle to analyze the second law efficiency of system. Thermoanalysis of every component of the system is evaluated in detail. The effect of some various parameters like input pressure and temperature, compressor pressure, liquefaction temperature on system components are studied by applying computational numerical technique. The effect of intermediate pressure and intermediate mass flow ratio is studied of dual system considering five different gases for liquefaction. From study it notice that increasing intermediate pressure put positive effect upto some extent while increasing intermediate mass flow ratio show less good effect on system.

Keywords: Thermodynamics analysis linde dualsystem,COP, Exergy efficiency ,exergy

1 Research Scholar 2 Professor

**devenderdahiya@in.com*

Nomeculture:

m_i=Intermidiate mass flow rate

m=mass flow rate

m_f=Liquefaction mass

h=Enthalpy

s=Entropy

X=Dryness fraction

T=temperature

P =Pressure

$\eta_{2nd\ law}$=Second law efficiency

Ɛ =Effectiveness of heat exchanger (approx. 80%)

C = Specific heat capacity fluid or gas

W_{total}=Total Work of compression

W_c =Compressor work

1) Introduction:

Global Warming is the increase of Earth's average surface temperature due to effect of greenhouse gases, such as carbon dioxide emissions from burning fossil fuels or from deforestation, which trap heat that would otherwise escape from Earth. This is a type of greenhouse effect. The ozone depletion is due to using various harmful refrigerant and for this refrigerant sustainability by replacing more environmental friendly cryosystem which is more efficient than previous harmful cryosystems.

Ultility of Dual Pressure Linde system for liquefaction of gases for reducing global warming and ozone depletion. Air is already being liquefied on large industrial scale starting from atmospheric air. First vapour compression systems are used to achieve cryogenic temperature but used of these system worked is limited due to solidification temperature of the refrigerants .After this cryogenic industry find number of modes to achieve low temperature. Several liquefaction cycles exist [1]. The simplest cycle configuration is known as the Linde cycle, where compressed air is throttled over a valve and cooled due to the Joule Thomson effect. . There are two types of compression processes in liquefaction plants, isentropic compression and isothermal compression. In the present study isentropic compression is applied when the fluid temperature is lower than the ambient temperature. If the fluid temperature is higher than the ambient temperature, the process is considered as an isothermal

compression [2].Cryogenic process to liquefy air which is further extent to extract various particular gases like oxygen, nitrogen, feron etc. Liquefaction is currently done in more complex cycles, which require about 1080 kJ of energy for each liquefied kg [3].Linde Hampson cycle is enable to liquefy large number of gas but in a very inefficient way. Compression in one stage consumes more work than the work used in multi compression system. Exergy analysis is power full tool to find out the loop holes in the system .To make system more efficient it is optimal use of every component of system is necessary .Various method like use of Nano technology, ceramic technology also used to make a cryo-system them economical.

2) Thermo analysis of Dual Pressure Linde system:

First and second law analysis of dual pressure system is done by using computational numerical technique.In doing second law analysis following assumption are made:

i. All processes are steady state and steady flow with negligiblepotential and kinetic energy effects.

ii. There is no chemical reaction.

iii. Directions of the heat transfer to the system and work done on the system are positive.

iv. Heat transfer and refrigerant pressure drops in the pipeline are ignored

Dual pressure Linde system is a modification of simple Lindesystem. It modification based on the concept that multicompression is more efficient than the single stage compression system. In Dual compressorsLinde system two compressors L.P and H.P are used with two separationunits employing single heat exchanger unit as comparison of simple Linde system.The whole modification is done to get high output of liquefaction gas with high efficiency.Fig 1.1 shows the block diagram of Dual Pressure Linde system and Fig 1.2 show T-S diagram of Dual pressure Linde system.

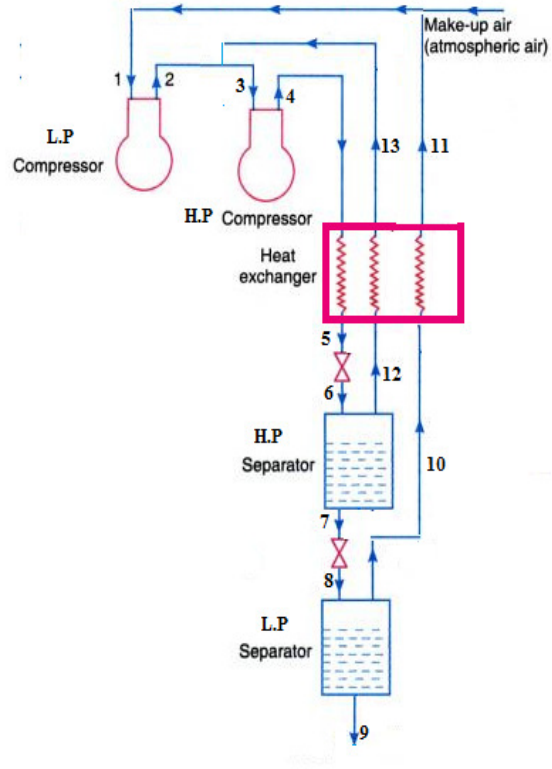

Fig 1:Dual pressure Linde system

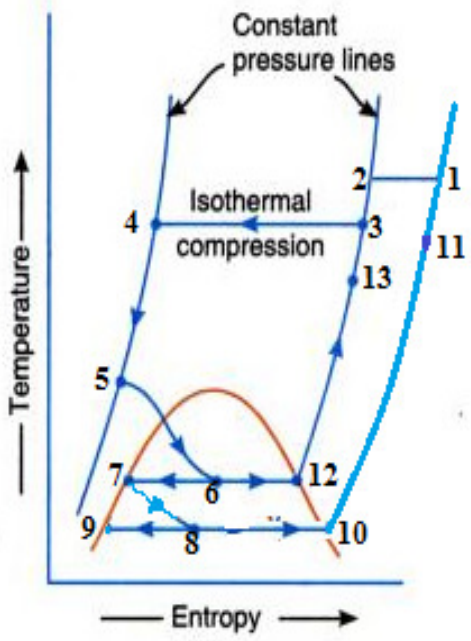

Fig 2: T-S diagram of Dual Pressure Linde system

Mixing Temperature

$$T_3 = \frac{m_2 * T_2 + m_{13} * T_{13}}{m_3} \quad (1)$$

$$0.80 = \frac{(T_4 - T_5)}{(T_4 - T_{10})} \quad (2)$$

Heat exchanger

$$m_4 * h_4 + m_{12} * h_{12} + m_{10} * h_{10} = m_5 * h_5 + m_{13} * h_{13} + m_{11} * h_{11} \quad (3)$$

First Expansion Valve

$$h_5 = h_6 \quad (4)$$

Energy balance of H.P separator

$$m_6 * h_6 = m_7 * h_7 + m_{12} * h_{12} \quad (5)$$

$$m_6 = m_7 + m_{12} \quad (6)$$

Second Expansion Valve

$$h_7 = h_8 \quad (7)$$

Energy balance of L.P separator

$$m_8 * h_8 = m_9 * h_9 + m_{10} * h_{10} \quad (9)$$

$$m_8 = m_9 + m_{10} \quad (10)$$

$$m_{13} = m_i \quad (11)$$

$$m_9 = m_f \quad (12)$$

$$m_1 = m \quad (13)$$

First law on control volume

$$m * h_3 = m_i * h_2 + (m - m_f - m_i) * h_1 + m_f * h_f \quad (14)$$

$$y = \frac{m_f}{m} \quad (15)$$

$$i = \frac{m_i}{m} \quad (16)$$

Work requirment for system

$$W_{total} = W_{c1} + W_{c2} \quad (17)$$

$$(m - m_i) * h_1 - W_{c1} = (m - m_i) * h_2 - Q_{r1} \quad (18)$$

$$Q_{r1} = (m - m_i) * T_1 * (s_2 - s_3) \quad (19)$$

$$-W_{c2} = m * T_1 * (s_2 - s_3) - (h_2 - h_3) \quad (20)$$

$$W_{comp\ for\ unit\ mass} = W_{total}/m \quad (21)$$

$$-\frac{W_{ideal}}{m} = T_1 * (s_1 - s_f) - (h_1 - h_f) \quad (22)$$

$$COP = \frac{(h_1 - h_f)}{W_{total}} \quad (23)$$

$$\eta_{2nd\ \%} = \frac{(h_f - h_1) - T_0 * (s_f - s_1)}{W_{total} * m_f} * 100 \quad (24)$$

3 Result and Discussion:

By computational mathematical technique various variable are noticed which are playing high role in optimizing dual system. To fully understand the effect of these variables on system various condition are given and graph are generated in respect of them considering five different gases. Fig 3 show that variation of liquefy mass to the intermediate pressure in between to low pressure and high pressure system. As the intermediate pressure increases the liquefaction mass ratio of system start decreasing. Fig 4 show the variation of total work of system to the intermediate mass flow ratio,as the ratio of intermediate mass increases the compressor work of system increases.Fig 5 show variation of compressors work with intermediate pressure it show inversely proportional behaviors and as the pressure increases the work of system start decreasing.Fig 6 show effect on liquefaction mass ratio to the intermediate mass flow ratio and it noticed that it show very minute effect and almost constant liquefaction mass ratio with respect to increasing intermediate mass flow ratio.Fig 7 shows directly proportional behavior of COP and intermediate pressure whereas Fig 8 show decrease in COP with increasing intermediate mass flow ratio. Fig 9 show effect on overall second law efficiency of system to the intermediate pressure ,it show increase in intermediate pressure also increasesas the efficiency of system and it reverse side Fig 10 show increases in intermediate mass flow ration there is decrease in overall second law efficiency of system.

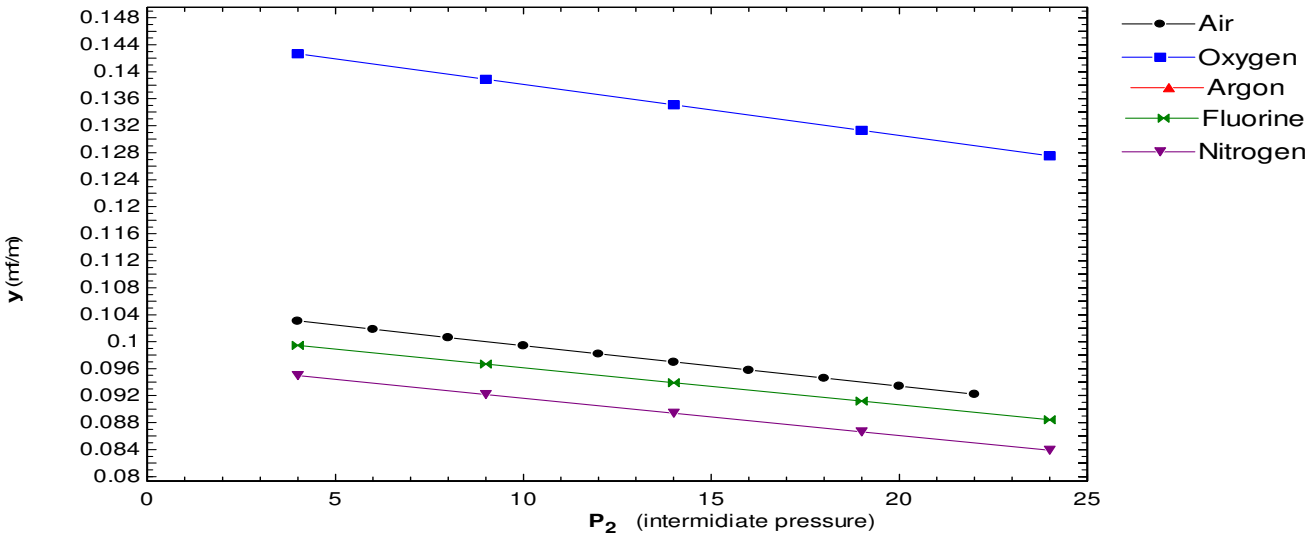

Fig:3Vairation of liquefaction mass ratio to intermediate pressure

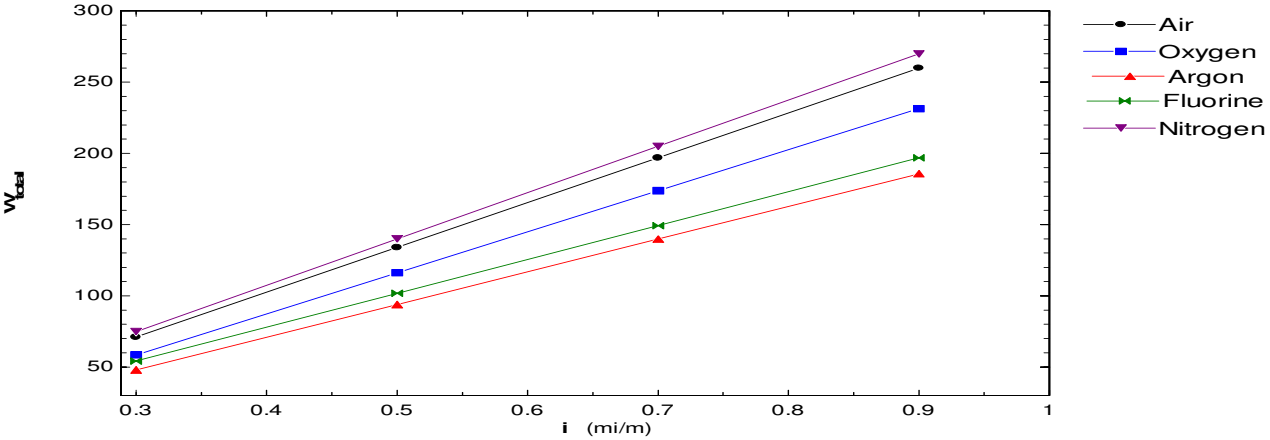

Fig:4 Variation of Total work system to intermediate mass flow ratio

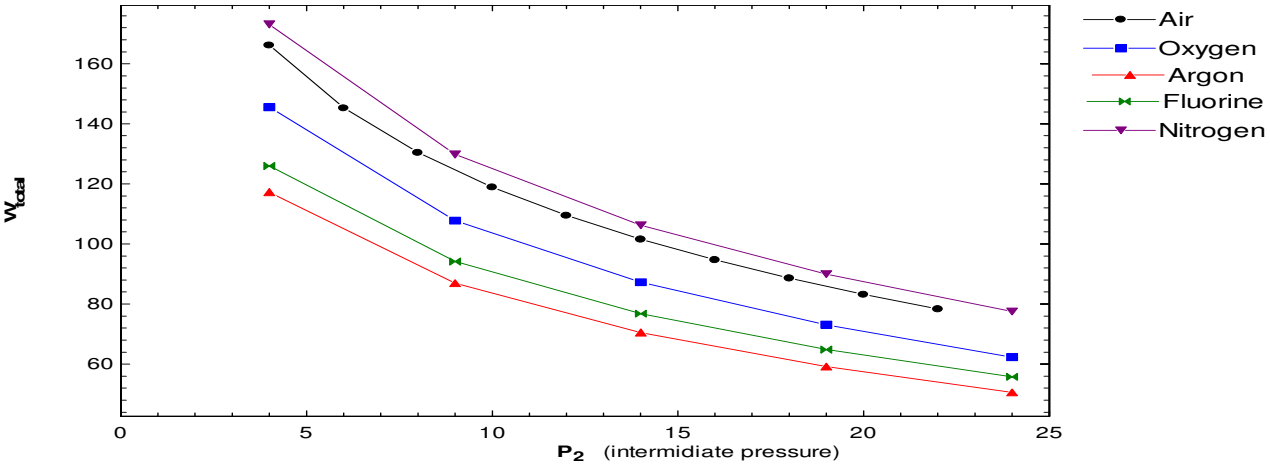

Fig:5 Variation of Total work system to intermediate pressure

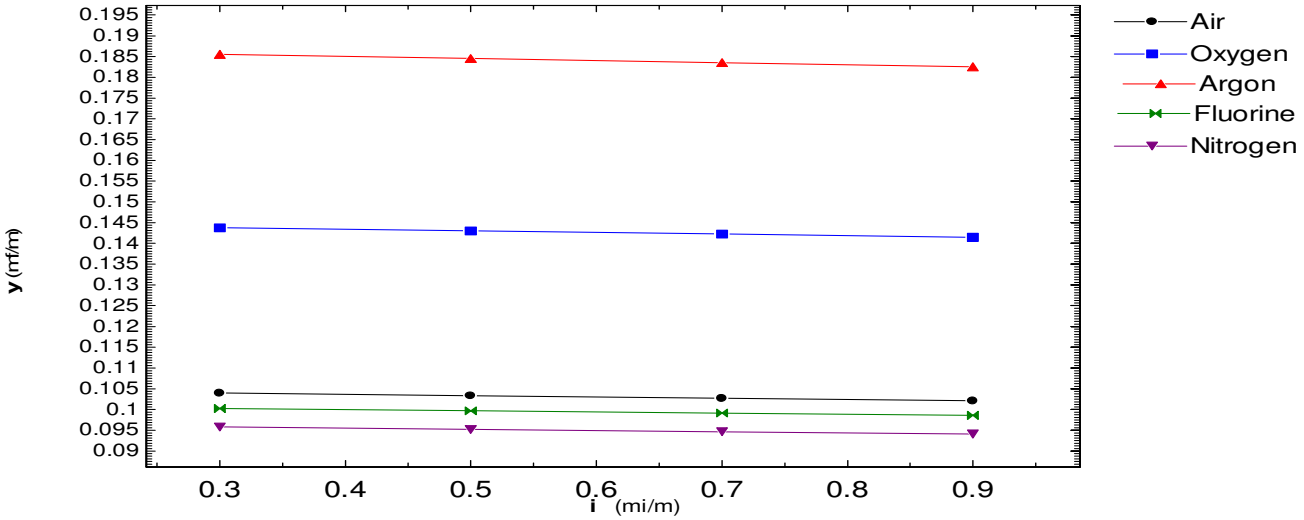

Fig:6Vairation of liquefaction mass ratio to intermediate mass flow ratio

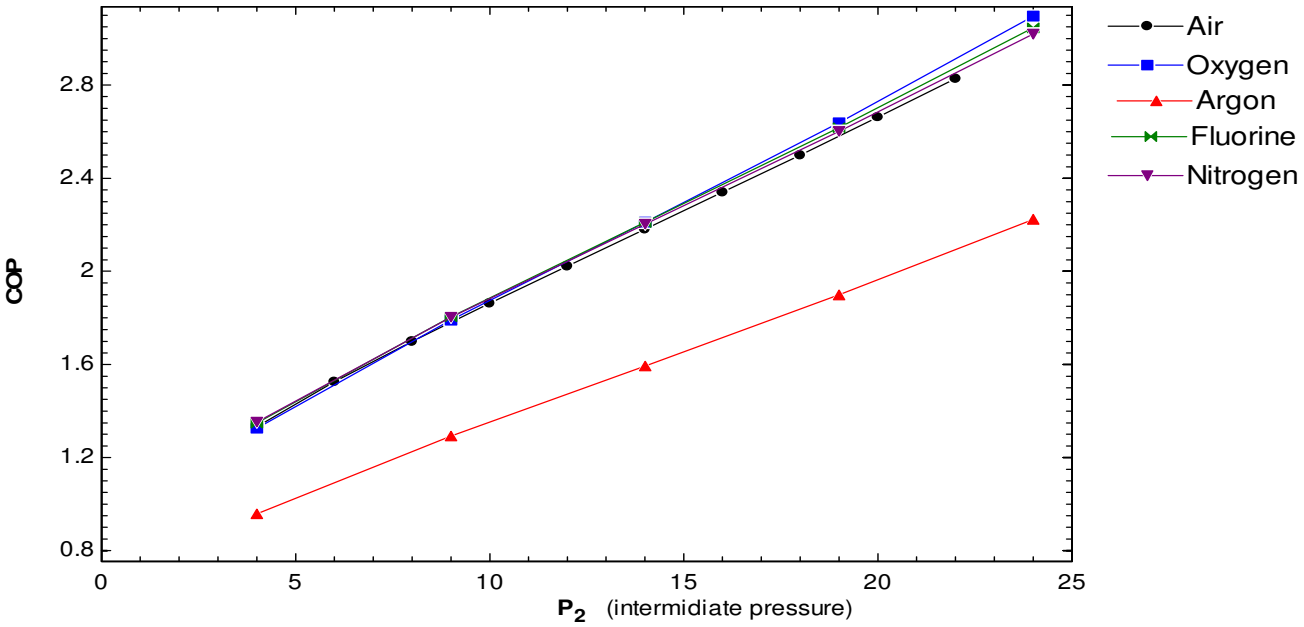

Fig:7 Variation of COP to intermediate pressure

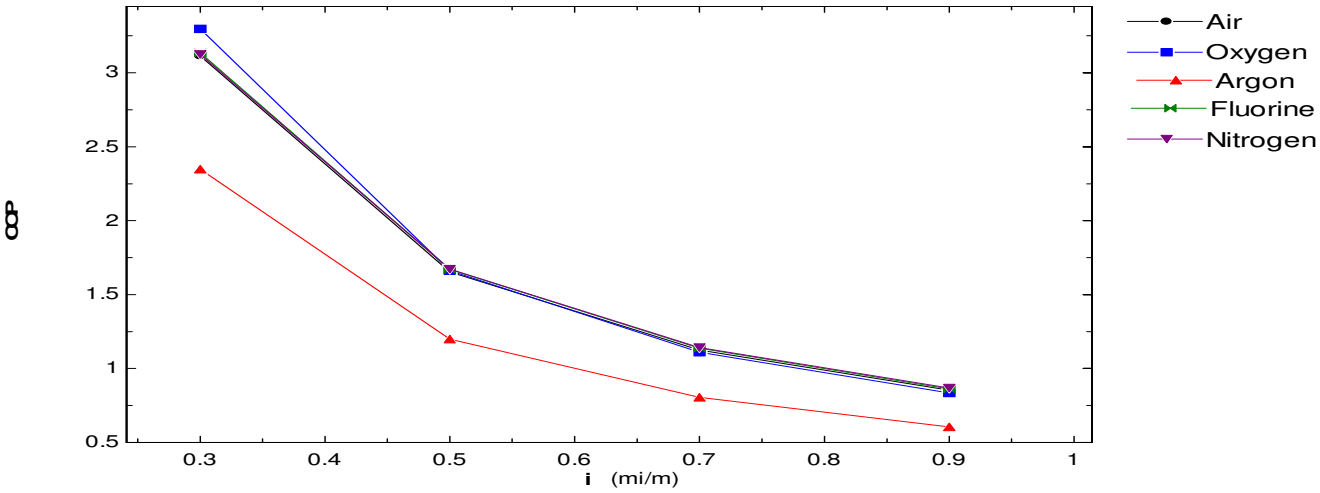

Fig:8 Variation of COP to intermediate mass flow ratio

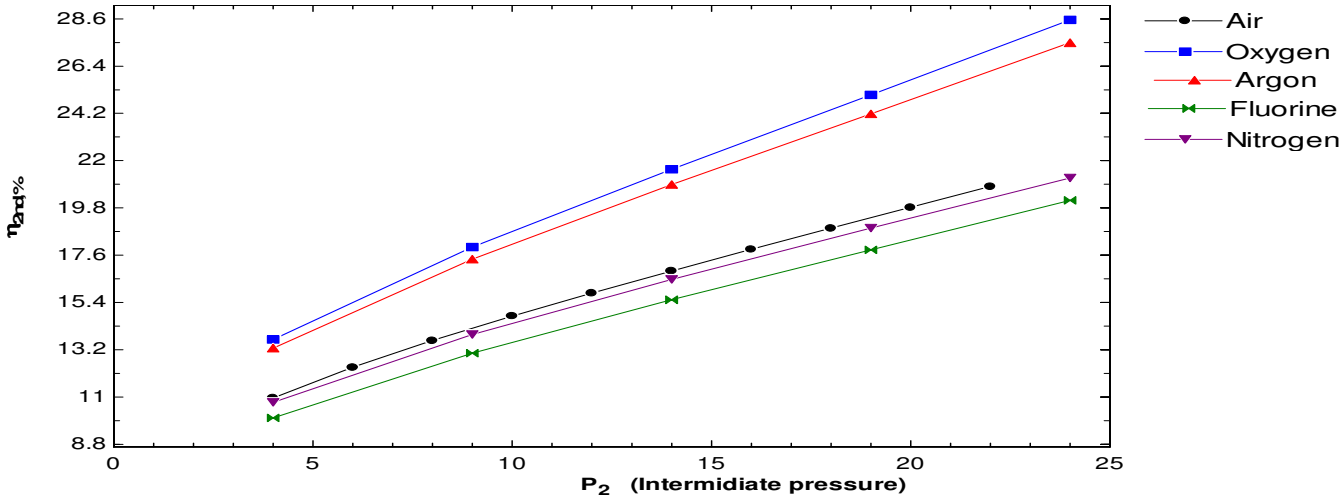

Fig:9 Variation of second law efficiency to intermediate pressure

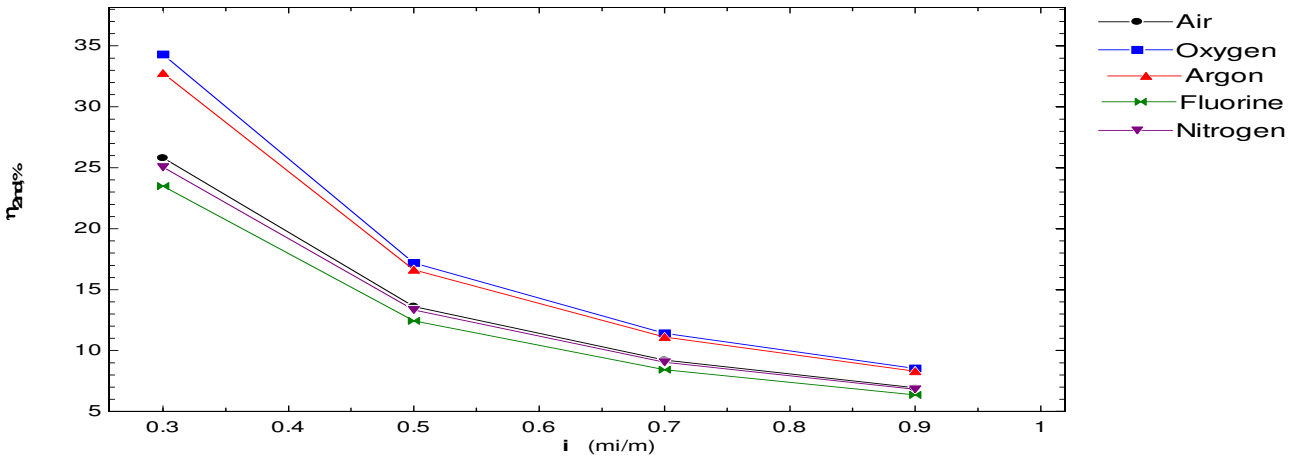

Fig:10 Variation of second law efficiency to intermediate mass flow ratio

Conclusion:

1) Increase in intermediate pressure put positive effect on system ,with increase in intermediate pressure there is decrease in compressor work increase in second law efficiency increase in COP and there very small scale dip in liquefaction mass for all five gases considered in system.

2) Increase in intermediate mass flow ratio show decrease in second law efficiency increase in total compressoe work decrease in COP and put a very negligible effect on liquefaction mass of system for all five gases.

Refrences:

[1] G. Venkatarathnam, Cryogenic Mixed Refrigerant Processes (2008). New York.

[2]Yongliang Li, Xiang Wang and Yulong Ding, "An optimal design methodology for large-scale gas liquefaction" , Applied Energy 99 (2012) 484–490.

[3] W.F. Castle, Air separation and liquefaction: recent developments and prospects
for the beginning of the new millennium, International Journal of
Refrigeration-Revue Internationale Du Froid 25 (Jan. 2002) 158e172.

Optimization of UPFC Controller Parameters Using Bacterial Foraging Technique for Enhancing Power System Stability

Poonam Singhal[*], S. K. Agarwal[*] and Narender Kumar[**]
*YMCA University of Science & Technology, Faridabad
**Delhi Technological University, Delhi

Abstract

To control the power flow,for increasing the transmission capacity & for power system stability,FACT devices are used.Unified Power Flow Controller is most widely used. This paper presents a novelBacterial foraging technique (BFO) for optimizing the PI controller parameters of UPFC for the transient stability enhancement of SMIB system .Complete modeling is done for SMIB system with UPFC controller.PI controller parameters computedbyconventional method [23] are usedas base for BFO, Bacterial Foraging Optimization Technique is applied for computing better optimized values.Results exhibit that BFO technique is able to find a better quality solution as compared to conventional technique for the proposed problem.

Keywords: *UPFC, Transient Stability, Bacterial Foraging Optimization Technique, SMIB (single machine on infinite bus bar), Synchronous MachineModeling.*

Nomenclature:

S=number of bacteria in the population,N_s=maximum number of swim length,N_c=chemotactic steps,N_{re}=number of reproduction steps,N_{ed}=elimination and dispersal events,P_{ed}=elimination and dispersal with probability.

1. INTRODUCTION

In recent years, power demand has increased substantially while there is a limited expansion of power generation and transmission due to limited resources and environmental restrictions. As a result some transmission lines get loadedheavily and the system stability becomes a power transfer limiting factor.In last two decades number of power devices have been developed and implemented and kept under the term Flexible AC Transmission System (FACTS) However, recent studies reveal that FACTS controllers could be used to enhance power system stability in addition to their main function of power flow control. FACT devices increase the reliability of AC grids and reduce power delivery costs. They improve transmission quality and efficiency of power transmission by supplying inductive or reactive power to the grid AUnified Power Flow Controller(or UPFC) is the most versatile member of the Flexible AC Transmission Systems (FACTS) family [1] for providing fast-actingreactive powercompensation onhigh-voltageelectricity transmissionnetworks. It uses a pair of three-phase controllable bridges to produce current that is injected into a transmission line using a series transformer. The controller can control active and reactive power flows in a transmission line. The UPFC is a combination of a static synchronous compensator (STATCOM) and a static synchronous series compensator (SSSC) coupled via a common DC voltage link as shown in fig.2. The UPFC concept was described in 1995 by L. Gyugyi of Westinghouse.It has an important function such as stability control to suppress power system oscillations & thus improving the transient stability of power system. Both voltage source converters can independently provide reactive power compensation & real power can flow freelyin either direction between the ac terminal of the two converters.The UPFC can provide simultaneous control of all or selected basic parameters of power system [5, 6] i.e. transmission voltage, line impedance and phase angle or any one of these and dynamic compensation of AC power system. Fig. 1 shows the equivalent circuit of the UPFC in which UPFC can be represented as a two port device with controllable voltage source V_{se} in series with line and controllable shunt current source I_{sh}. The voltage across the dc capacitor is maintained constant because the UPFC as a whole does not generate or absorb any real power.Requirement of the power quality is the today's major issue for the power utilities & their vital task is to reduce the transients. In this paper UPFC is used to damp the transients & improve the transient stability of the SMIB system. Proportional & Integral strategy is used for UPFC controller. The PI parameters of UPFC controller are optimized using Bacterial Foraging to attain desired results more speedly and thus making the system more reliable ,stable & secure.The present paper is laid out as follows: section I - Introduction, section II describes about the Unified Power Flow Controller. Section III explains theartificial intelligence techniquesfor power system stability.Section IV gives the description of thebacterial foraging optimization technique (BFO). SectionV describes the study system taken whereas section VI explains the mathematical modeling of the unified power flow controller. Section VIIdescribes the formulation of an objective function to be minimized .Section VIIIillustrates the simulation results of the system without UPFC

controller,with conventional UPFC controller & with BFO UPFC controller and section IX concludes and expresses the future scope of work.

2. UPFC DESCRIPTION

The general structure of UPFC consists of a back to back AC to DC voltage source converters operated from a common DC link capacitor. First converter is connected in shunt that operates as STATCOMand the second converter in series with the line which operates as SSSC. The main function of the shunt converter is to supply real power to the series converter through a common DC link. Series Converter has the main function of injecting the controlled voltage magnitude &phase angle in series with the line. Both converters can also generate or absorb reactive power, if desired, thereby provide independent shunt reactive power compensation for the line.

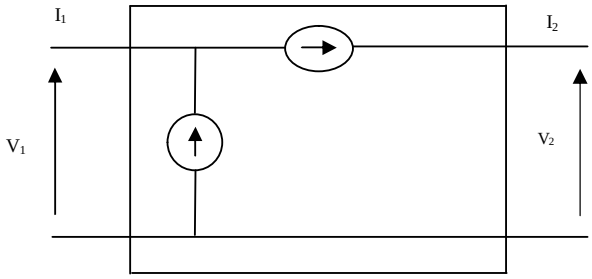

Fig. 1.Equivalent Circuit of UPFC

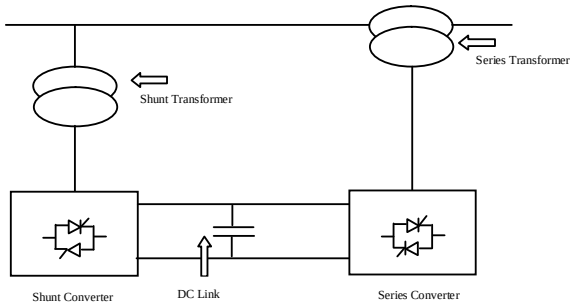

Fig 2: Basic block diagram of UPFC

3. AI TECHNIQUES FOR POWER SYSTEM STABILITY

A number of evolutionary techniques like Bacterial Foraging optimization, Genetic Algorithm, Particle Swarm optimization, Ant Colony optimization,and water droplet optimization technique have been proposed by many researchers [14-21] for optimizing parameters of FACTS controller.Though GA is much faster than PSO as PSO has the problem in trapping to local minima due to large computations. BFO technique has been proposed by passino [18, 19] in which the number of operations used for searching the total solution space is much higher compared to GA &PSO, hence better optimal solution can be achieved. Among various methods for the optimization, BF is selected because of its better capability of locating optimal solution and higher convergence rate. However it shall be too early to conclude that BF is the best optimization algorithm among rest others existing.

4. ABOUT BACTERIAL FORAGING OPTIMIZATION TECHNIQUE (BFO)

BFO is an effective AI technique to optimize the variables effectively and efficiently. BFO technique is inspired by the pattern exhibited by animal that have successful forging strategies (locating, handling &ingesting food). The author in [18, 22] explains the biology & physics of E. coli bacteria & applies that in adaptive controller.The control system of these E. coli bacteria can be explained by five operations: Chemotaxis, Swarming, Reproduction, Elimination and Dispersal. In this technique a group of bacteria moves in search of food and away from noxious elements. In chemotaxis step, the bacteria swim and tumble in its entire life span.

The nutrients concentration is computed at its initial position before tumbling with the help of flagella. If the bacteria gets more nutrients in that direction than it will swim in the same direction and if less, then tumbles and find new direction. Half of them which are weak, die out and healthier reproduce. The new born bacteria then also go under chemotaxis step &again healthier bacteria survive and weaker die out but bacteria population remains constant. During this process, the healthy bacteria attract other healthy bacteria which are quite away from them & repel those which are weaker; this takes the variable to best possible value.

4.1 Flow Chart

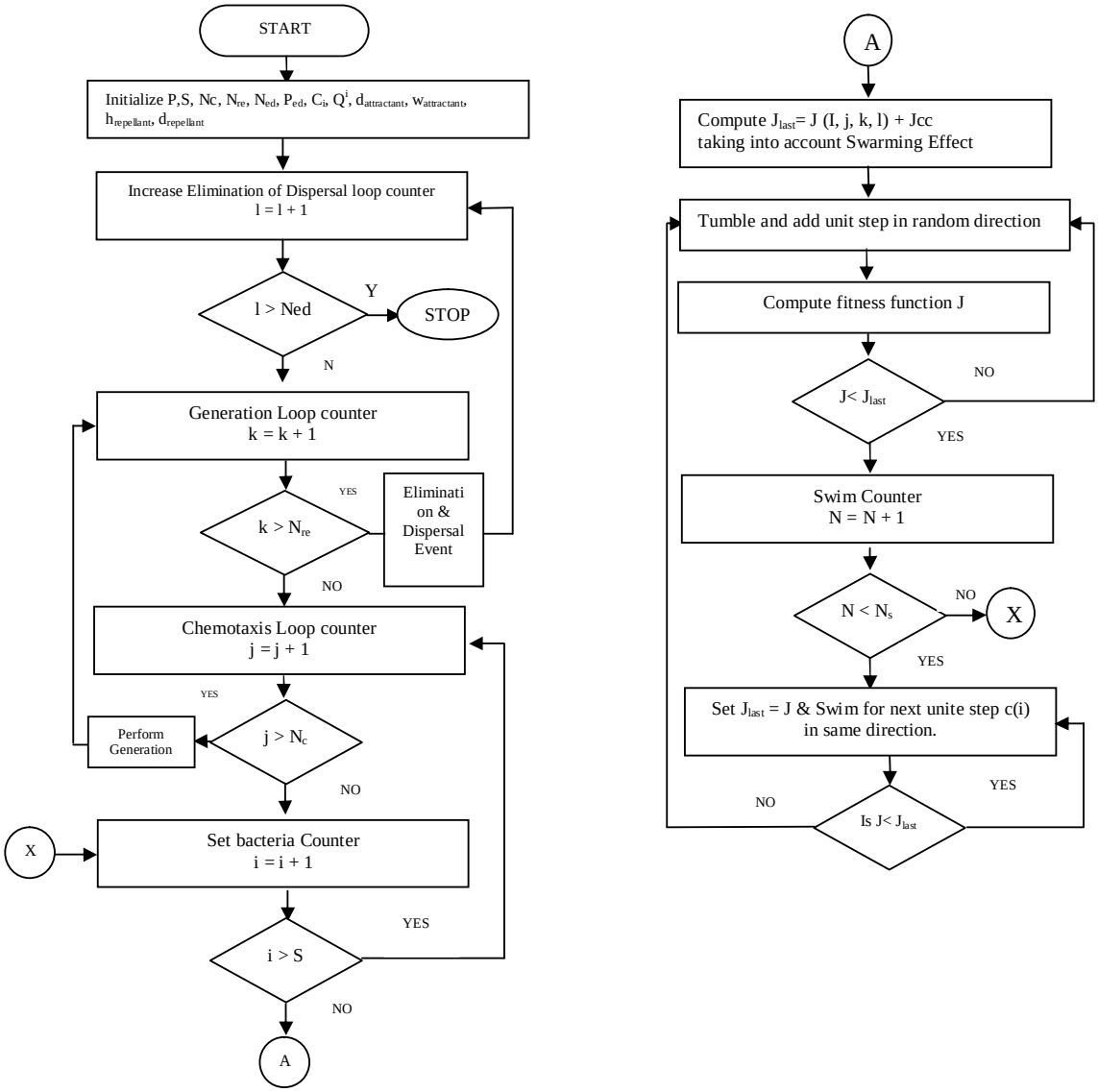

4.2. Algorithm

1) Initialize dimension of search space, number of bacteria, chemotaxis steps, swim steps, reproductionsteps, elimination & dispersal steps, probability of elimination & run length unit C(i)i=1,2,…..S), θ^i (initial position of bacterium). Cell to cell attractant & repellant parameters.
2) Initialize elimination dispersal loop control, l=l+1
3) Check l=N_{ed}, stop else continue
4) Initialize reproduction loop count k=k+1

5) Check $k<N_{re}$, continue else go to step 2
6) Initialize chemotaxis loop count j=j+1
7) Check $j<N_c$ continue else go to step 4
   a)Compute fitness value of objective function , J for each bacterium i,J(i,j,k,l) = J(I,j,k,l) + J_{cc}
   Where $J_{cc}= \Sigma[-d_{attaractant}\exp(-w_{attractant}\Sigma(\theta_m-\theta_m^i)^2]+\Sigma[h_{repellant}\exp(-w_{repellant}\Sigma(\theta_m-\theta_m^i)^2]$
   b)Check J (i, j, k, l) < J (i, j-1, k, l), save it.
   c)Tumble: Generate a random vector Δ (i) in range (-1,1).
   d)Move: $\theta^i(j+1,k,l) = \theta^i(j,k,l) +C_i\Delta(i)/(\Delta^T(i)\Delta(i))^{1/2}$.
   e)Again compute J(i, j+1, k, l) &compare, if least continue, else Tumble.
8) Initialize swim loop counter N=N+1
9) Check N<Ns go to 7(d) else tumble.
10)Perform Reproduction of healthy bacteria.
11) Perform Elimination & dispersal.
12) Continue the process till the maximum computations are over.

5. SYSTEM DESCRIPTION

For analysis of the UPFC for damping the power swings, parameters of the system like generator rotor angle, theta, terminal voltage, active power and reactive power are considered. A200MVA, 13.8KV, 50Hz generator supplying power to an infinite bus through two transmission circuits as shown in fig(3) is considered.The network reactance shown in fig. is in p.u. at 100 MVA base. Resistances are assumed to be negligible. The initial system operating condition, with quantities expressed in p.u. on 100MVA, 13.8 KV base are: P=0.4p.u.& Q=0.6p.u. The other generator parameters in p.u. are given in appendix. The three phase fault at infinite bus bar is created for 0.1 sec duration& simulation is carried out for 10sec. to examine the transient stability of the study system.

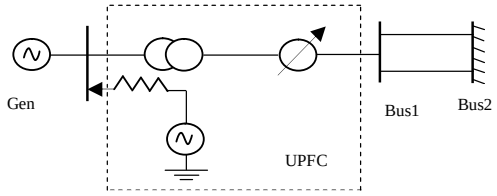

Fig. 3. Single Machine Infinite Bus system

6. MATHEMATICAL MODELING

6.1 Synchronous Machine Model

Mathematical models of synchronous machine vary from elementary classical model to more detailed one. Here, the synchronous generator is represented by third order machine model [2]. Different equations for stator, rotor, excitation system etc. are as follows:

Stator : $V_q = E'_q - r_s i_q - x'_d i_d$

$V_d = E'_d - r_s i_d - x'_q i_q$

$V_1 = v_d + jv_q \quad I = i_d + ji_q$

$S = V_1 I^*$

$P = v_d i_d + v_q i_q$

$Q = v_q i_d - v_d i_q$

Where,

$$\omega = \omega_o + \frac{d\delta}{dt}$$

$$\frac{\delta\omega}{dt} = \frac{P_m - P_e}{M}$$

Let D and K=0

r_s is rotor winding resistance

$x_d^{'}$ is d-axis transient reactance

$x_q^{'}$ is q-axis transient reactance

$E_d^{'}$ is d-axis transient voltage

$E_q^{'}$ is q-axis transient voltage

Rotor :

$$T_{do}^{'}\frac{dE_q^{'}}{dt} + E_q^{'} = E_f - (x_d - x_d^{'})i_d$$

$$\frac{dE_q^{'}}{dt} = \frac{E_f - E_q^{'} - (x_d - x_d^{'})i_d}{T_{do}^{'}}$$

Where, $T_{do}^{'}$ is d-axis open-circuit transient time constant $T_{qo}^{'}$ is q-axis open-circuit transient time constant E_f is field voltage

Torque Equation

$$T_e = E_q^{'}i_q + E_d^{'}i_d + (x_q^{'} - x_d^{'})i_d i_q$$

Excitation System

$$\frac{d(\Delta E_{fd})}{dt} = \frac{K_e(V_{ref} - V_t)}{T_e} - \frac{\Delta E_{fd}}{T_e}$$

Where $-0.6 \leq E_{fd} \leq 0.6$

6.2 UPFC Controller Structure

UPFC works in two modes: Voltage Regulation Mode and PQ Mode

In first case, the reactive power component of shunt converter is controlled to regulate the voltage magnitude at the bus as proposed for STATCOM by Schauder& Mehta [11].In this paper the proposed controller [23]can works in both voltage regulation mode and in PQ mode. Simulations are carried out for PQ mode only.P-Q demand on load side is met by controlling series voltage injection. In order to achieve the system stability, it is required to control the in phase & quadrature component of the series injected voltage after fault at infinite bus.

1. Series Converter

Let the voltage injected by the series converter isV_L. In d-q frame of reference,V_L can be written as

$V_{Ld} = V_L \sin(\theta - \varphi)$, $V_{Lq} = V_L \cos(\theta - \varphi)$

$$V_L = \sqrt{(V_{Ld})^2 + (V_{Lq})^2}$$

Where, $\theta = \tan^{-1}\frac{v_d}{v_q}$

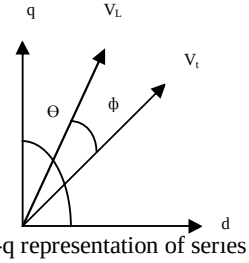

Fig. 4.d-q representation of series converter

In phase and quadrature components ofV_L are responsible for active and reactive power flow in line.

$$V_{Lp} = V_{Lpo} + \Delta V_p$$
$$V_{Lq} = V_{Lqo} + \Delta V_q$$
$$V_{bd} = V_{Ld} + \left(X_d^{'} + X_1\right) i_q - X_1 i_{sq}$$
$$V_{bq} = V_{Lq} + e_q^{'} - \left(X_d^{'} + X_1\right) i_d - X_1 i_{sd}$$
$$V_b = \sqrt{V_{bd}^2 + V_{bq}^2} \qquad (6)$$
$$P_{ref} = \left(V_d + V_{Ld}\right)\left(i_d - i_{sd}\right) + \left(V_q + V_{Lq}\right)\left(i_q - i_{sq}\right) \quad Q_{ref} = \left(V_q + V_{Lq}\right)\left(i_d - i_{sd}\right) - \left(V_d + V_{Ld}\right)\left(i_q - i_{sq}\right)$$

Where,

$$V_{Lpo} = V_{Ld} \sin\left(\tan^{-1}\frac{i_d - i_{sd}}{i_q - i_{sq}}\right) + V_{Lq} \cos\left(\tan^{-1}\frac{i_d - i_{sd}}{i_q - i_{sq}}\right)$$
$$V_{Lqo} = V_{Lq} \sin\left(\tan^{-1}\frac{i_d - i_{sd}}{i_q - i_{sq}}\right) + V_{Ld} \cos\left(\tan^{-1}\frac{i_d - i_{sd}}{i_q - i_{sq}}\right)$$

$$\Delta V_p = k_{p1}\Delta P + k_{i1}\int_0^T \Delta P \qquad \Delta V_q = k_{p2}\Delta Q + k_{i2}\int_0^T \Delta Q$$
$$\Delta P = P_{ref} - P \qquad \Delta Q = Q_{ref} - Q$$

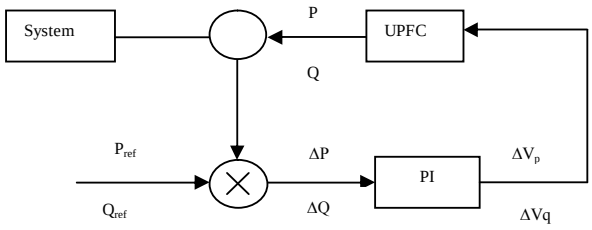

Fig.5. PI controller of the study system in PQ Mode

2. Shunt Converter

Let i_s be the current injected by shunt voltage source converter which is in same phase as that of generator terminal voltage, hence it will not supply or absorb reactive power & its aim is to provide the real power pdemand of series power voltage source converter.

Let lossless UPFC device is considered, then

$$R\left(\overline{V_1}\,\overline{I_1^*} - \overline{V_2}\,\overline{I}_2^*\right) = 0$$

And with losses, to maintain the voltage across the capacitor, shunt power should be equal to sum of series power and capacitor power.

$$V_t i_s = V_{Ld}\left(i_d - i_{sd}\right) + V_{Lq}\left(i_q - i_{sq}\right) + V_{dc} C \frac{dV_{dc}}{dt}$$

From the above equation, i_s can be obtained.

Where,

$$i_{sd} = i_s \sin\theta\,, \qquad i_{sq} = i_s \cos\theta$$

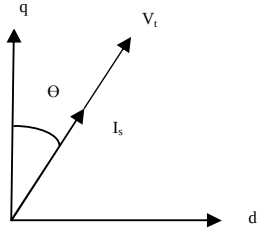

Fig.7.d-q representation of shunt converter

6.3 Transmission Line currents

The transmission line current i_t is split into d-q components represented as i_{td} and i_{tq}.

$$i_{td} = i_d - i_{sd} \quad , \qquad i_{tq} = i_q - i_{sq}$$

6.4 Capacitor Dynamics

The difference between the shunt power and series power is the capacitor power.
Mathematically,

Capacitor power=Shunt power– Series power $\left(C \frac{dV_{dc}}{dt} \right) V_{dc} = P_{sh} - P_{se}$

$$P_{sh} = V_t i_s$$

$$P_{se} = V_{Ld} i_{td} + V_{Lq} i_{tq} \qquad \left(C \frac{dV_{dc}}{dt} \right) V_{dc} = V_t i_s - \left(V_{Lp} i_{td} + V_{Lq} t_{tq} \right)$$

i_s then can be computed from the above equation

7. OBJECTIVE FUNCTION

It is worth mentioning that the UPFC controller isdesigned to minimize the power system oscillations after a disturbance so as to improve the stability. These oscillations are reflected in the deviations in the generator rotor speed(Δw), active power (ΔP)&reactive power(ΔQ). In the present study the objective function J is formulated as the minimization of:

$$J = \int_0^t \left[t \left(\Delta \omega (t, x) \right)^2 + t \left(\Delta P (t, x) \right)^2 + t \left(\Delta Q (t, x) \right)^2 \right] dt$$

In the above equations, Δw(t,x) denotes the rotor speed deviation,ΔPdenotes the change in Real Power flow & ΔQ denotes the change in Reactive Power flow for a set of controller parameters x(note that here xrepresents the parameters to be optimized; k_{p1}, $k_{i1,}$ $k_{p2,}$ k_{i2} are the parameters of UPFC controller), and tis the time range of the simulation. With the variation of theparameters x, the Δw(t,x), ΔP(t,x), ΔQ(t,x), will also be changed. For objective function calculation, the time-domain simulation of the power system model is carried out for the simulation period. It is aimed to minimize this objective function in order to improve the system response in terms of the settling time and overshoots.

8. SIMULATION

The SMIB system with UPFC is considered and system is modeled&simulated with conventional controller &BFO controller using MATLAB. The number of parameters to be optimized are four (k_{p1},k_{p2} , k_{i1}&k_{i2}). The analysis is carried out with 3 phase fault at Infinite bus for 0.1 sec& system is run for 10 sec. the result have been shown with PI controller parameters tuned by conventional method & PI controller parameters tuned by BFO (each bacterium is assigned with a set of 4 variables to be optimized and assigned with random value within the universe of disclosure).

The following are the simulation results of the system without controller, with conventional UPFC controller & with BFO based UPFC controller.

Simulation for P= 0.4p.u, Q=0.6 p.u and X_1= 0.3p.u (Figure 8 (a) to (g))

……Without Controller
------ With conventional UPFC controller
____With BFUPFC Controller

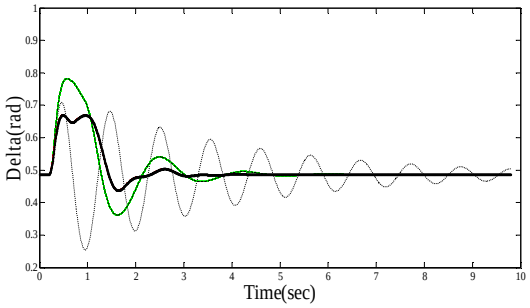

Fig. 8(a)

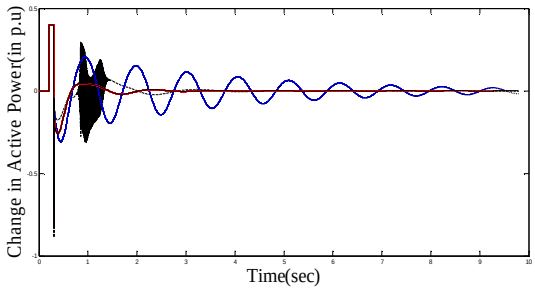

Fig. 8(b)

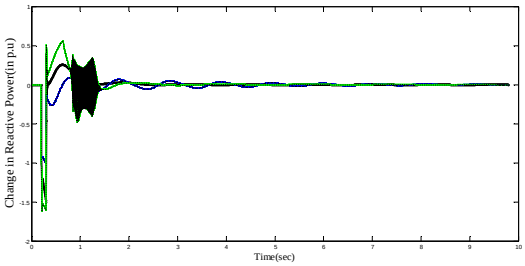

Fig. 8(c)

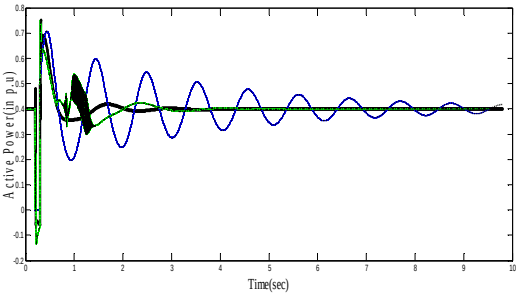

Fig. 8(d)

Curr Genet Med Rep
DOI 10.1007/s40142-014-0041-y

HOT TOPIC

Pharmacogenomics for Precision Medicine in the Era of Collaborative Co-creation and Crowdsourcing

Yasha Hasija · Jameel Ahmad Khan · Vinod Scaria

Abstract The whole gamut of new technologies in the past decade has revolutionized DNA sequencing, making it cheaper, efficient, and scalable. The consequent big-data in genomics have posed new challenges and opportunities. The transformation of internet as a fabric that intertwines multiple technological and social layers and the rise of platforms that can organize and integrate massively parallel human activities have transformed the workplaces in many industries and offers a new opportunity in the area of genomics. In this short review, we discuss the state-of-the art of crowdsourcing in genomics research with special focus on pharmacogenomics. We discuss the field, starting with an overview of technology and the major challenges. We also discuss a number of ongoing crowdsourcing approaches in the area of pharmacogenomics and personal genomics. We conclude with deliberating on the issues in genomics and how crowdsourcing could offer a plausible alternative to conventional approaches in genomics.

Keywords Personal genomes · Precision medicine · Pharmacogenomics · Crowdsourcing · Genomics · Clinical genomics

Y. Hasija
Department of Biotechnology, Delhi Technological University, Bhawana Road, Shahbad Daulatpur, New Delhi, India

J. A. Khan
Lifecode Technologies, B-1/E-24, Mohan Co-operative Industrial Estate, Mathura Road, New Delhi 110 044, India

V. Scaria (✉)
GN Ramachandran Knowledge Center for Genome Informatics, CSIR Institute of Genomics and Integrative Biology, Mathura Road, New Delhi 110025, India
e-mail: vinods@igib.in

Introduction

The sequencing and creation of the blueprint of the Human Genome [1, 2] offered promise toward creating groundbreaking advances in the understanding of the Human Genome and genetic diseases. The decade following the announcement of completion of the Human Genome sequencing has seen drastic improvements in the scale and consequent reduction in the costs of sequencing. This has been particularly contributed by advancements in technology and in scale of nucleic acid sequencing, brought about by a spectrum of novel methodologies to miniaturize and significantly improve the scale of sequencing: dubbed as next-generation sequencing technologies [3]. Moreover, methodologies like microarray have complemented the scale of querying genomic regions. There have also been tremendous developments in understanding genetic variations among populations [4]. Apart from providing valuable mechanistic insight into genetic diseases, it has also contributed to understanding genetic selection, human migration, and disease predisposition [5, 6]. These advancements have also illuminated the organization and architecture of functional elements in the genome, thus leading to a new understanding on the potential role of genetic variations in modulating phenotypes. A major contribution to this acumen has been provided by the Encyclopedia of DNA elements (ENCODE) consortium [7••] and other allied projects including the NIH Epigenomics Roadmap project [8].

Recent years have seen a number of Human genomes sequenced from multiple countries representing multiple ethnic groups. This includes personal genomes from many countries and ethnic populations spread across the globe. Besides, selected sets of population have been represented in the 1000 Genomes Project [9••]. Significant number of

Published online: 22 May 2014

the world population which resides in the Asian and African continents and their genomic diversity have been poorly represented in the 1000 Genomes initiative [10•]. Regional efforts have been initiated to fill in the gap of population genetic diversity. The Pan Asian Population Genomics Initiative (PAPGI) encompasses participants from over 17 countries aiming to create a high resolution map of population level genetic diversity within the Asian continent (www.papgi.org). The coming years would see a drastic improvement in resolution of genomic variations in these populations.

The advances in technology including miniaturization, parallelization, and improved methods of reading bases also promise to drastically reduce the cost of genome sequencing in near future, potentially enabling it as a clinical diagnostic tool. It is widely believed that the price of whole genome sequencing would drop approximately to USD 1000. This would have far-reaching implications in both the understanding of human genomic variations as well as the application of whole genome sequences in clinical applications. It has been speculated that the availability of high-quality human genomes at affordable costs could have far-reaching implications in clinical settings, and is widely believed to herald a new era of personalized medicine [11]. It has been argued that affordable clinical genome sequencing would enormously add to understanding genetic disorders, especially rare and inherited genetic diseases, and contribute largely to the genetic diagnosis of diseases. Moreover, Clinical genome sequencing can make a difference in better management of diseases based on evidence, otherwise called precision medicine.

The affordability and scale of genome sequencing and its application in clinical settings do not come without challenges. The major challenges include, first the management of humongous amount of data generated, which would require systematic efforts to store, organize, and annotate. Second, the analytics challenge, arising out of paucity of tools, resources and appropriate workforce to systematically parse and interpret the genomic information needs to be streamlined. A number of reviews have highlighted these issues in genomics. These two challenges are not unique to genomics and are shared by other data-intensive areas [3]. Many related industries, which rely on data-intensive tasks, have extensively used innovative approaches including crowdsourcing.

The developments in genomics have been in parallel with technological advances in many other areas including connectivity and the rise of collaboration as an enterprise at scale. The recent years have seen the transformation of internet from a communication platform to a fabric that intertwines multiple technological and social layers. This has impacted the way we gather, analyze, interpret data, and implement decisions. Rise of social media and platforms that can organize and integrate massively parallel human activities has transformed the workplaces in many industries and offers a new opportunity in the area of genomics. It has been widely discussed how massive parallelization of human tasks could be a viable alternative to traditional approaches for collecting, analyzing, interpreting data, and resources [12]. These approaches, involving tasks which are distributed among a large number of individuals, have been popularly called crowdsourcing [13]. A variant of this methodology which includes analytical tasks spawned among a large group of individuals has been popularly called crowd-computing [14].

In this short review, we discuss the state-of-the art of crowdsourcing in genomics research with special focus on pharmacogenomics and precision medicine. We discuss the field in three distinct headings, starting with an overview of technology and the major challenges. We take cues from other areas of technologies where crowdsourcing and crowd-computing have been successfully applied. We also discuss a number of ongoing crowdsourcing approaches in the area of pharmacogenomics and personal genomics. We conclude with deliberating on the issues in genomics and how crowdsourcing could offer a plausible alternative to conventional approaches in genomics.

New Technologies

A number of recent technologies have provided the much needed starting point toward generating the required knowledge base for implementing translational application of genomics. Broadly, these technologies could be grouped into Genotyping technologies and the consequent genome-wide association studies; next-generation sequencing; and third, the computational analysis capability, curation of data sets, and other tools of functional genomics.

The availability of microarray technology that has enabled querying of large number of genetic variants at an ample scale has revolutionized the way we look at genetic variants and their association with diseases. This has led to hypothesis-free, genome-wide estimates of genetic associations with traits or disease phenotypes and discovery of novel/unknown genes related to a particular disease. Recently, the NHGRI GWAS Catalog has compiled over 5,000 variants from over 1,300 publications which have shown evidence of genotype–phenotype correlations using Genome Wide Association Studies [15]. Presently, these datasets encompass over 17 general traits, including a large number of distinct Human traits and diseases. A number of them are of pharmacological relevance with high odds-ratios. Easy availability of genetic variations from genome-scale association studies offers a new opportunity toward

applying them in clinical settings by detecting not only the susceptibility of an individual toward a particular disease/disorder at an early stage in life, but also prioritizing specific health and medical regimens best suited to the individual.

One of the major technological advancements, which followed the Human genome sequencing, is the availability of fast, efficient, and cheap methodologies for re-sequencing human genomes. These gamut of technologies have been based on massively parallel sequencing of short reads. These technologies have been popularly dubbed as Next Generation Sequencing technology. This has also been complemented by availability of faster algorithms and dwindling compute and storage costs. The initial years have seen sequencing of a number of individual genomes from different countries, populations, and ethnic groups. These include genomes from China [16], Japan [17], Korea [18], India [19], Sri Lanka [20], and Malaysia [21]. The 1000 Genome initiative includes 13 population groups in Phase I and additional 7 population groups in Phase II. Other regional initiatives aimed at covering regions/populations that have not been covered by the 1000 Genome initiative have taken shape. For example, the ambitious Pan-Asian Population Genomics Initiative encompasses the entire population of Asia [6]. These initiatives are expected to provide essential raw material for sequence level, and genome wide studies at global level. Together, these advances would pave the way for a new era of evidence-based medicine, known as precision medicine, based on pharmacological landscape of the individual to provide precise dosage and treatment schedule.

Recent years have also seen a paradigm shift in the drug discovery process. Traditional drug discovery processes were heavily dependent on chance and involved tedious screening of large compound libraries. Such methods usually take more than 10 years for the chance discovery of drugs. Also, they utilize a lot of resources, sometimes without giving any productive results. Computational modeling of biological activities has increasingly been used to prioritize molecules for screening [22–24]. Recent research, including from our lab, has extensively used data from previous high-throughput screens of large molecular libraries to create highly accurate in silico structure activity relationship models for prioritizing molecules with requisite activity. Such computational methods of molecular modeling and drug design have the potential to accelerate, automate, and make the drug discovery more successful and less expensive.

New Challenges

The availability of new technologies, both for the discovery of new genetic variants and associations with human traits and the possibility of re-sequencing human genomes in clinical settings, have also created newer challenges in a number of fields ranging from data management and analysis, methodologies for prediction of phenotypes/traits and interpretation based on genomic data and of course, making technology affordable and easy to use. These challenges should also be seen in context with other challenges generally faced by the pharmaceutical companies on the ever-rising cost of drug discovery and rapidly dwindling rate of discovery of new drugs [25]. Technological challenges apart, the major challenge, which has not been sufficiently discussed, is making advancements in genomic technologies affordable, thus significantly improving the reach and utility of these technologies in improving the quality of life of large underprivileged populations in under-developed and developing worlds.

The availability of affordable whole genome or exome sequences at clinical settings is widely believed to impact healthcare and disease management, but also has been widely discussed to pose new challenges in the area of data management, mining, interpretation, and integration with health care systems. This is primarily contributed by the fact that functional correlates to a majority of human variations are unknown [26]. A large proportion of the markers revealed from Genome-wide association studies, especially for complex traits, do not have enough predictive power to be applied in clinical settings [27]. These studies nevertheless have significantly contributed to the understanding of biological pathways [28]. Furthermore, the numbers of genetic variants that show additional phenotypic correlates have been growing at an exponential phase. This necessitates constant re-mining and re-interpretation of the data necessary in real-time.

Another major challenge is the availability of a systematic-curated resource for genetic variants and their associations. This has majorly been a challenge in past since the datasets and reports are scattered in thousands of publications, and in non-standardized formats and different genome builds and versions. It would be an impossible task for researchers to compile and manually curate this vast information from literature sources, though there have been ample efforts to curate it using computational tools and methods. The creation of locus-specific variation databases (LSDBs), pioneered by the Human Genome Variation Society [29, 30] along with standard guidelines to report and disseminate various variations, has been a major effort toward systematic curation of information in a standardized format. Recent availability of tools and aggregators, including efforts from the NCBI and the Gen2Phen consortium [31], is worth mentioning. Fortunately, in the area of pharmacogenomics, a number of resources like DrugBank [32] and PharmGKB [33] curate complementary evidence for genetic markers and traits. Nevertheless, it has

not escaped our attention that neither of the databases has been able to cope with the deluge of information on pharmacogenetic markers and reports being published in the scientific literature. Apart from the availability of highly curated datasets, appropriate tools to systematically mine and compare variations from personal genomes is a necessity. Integration of the knowledge from various parts of the world, in different formats and versions, has posed a huge challenge in the pharmacogenomics research. It is a herculean task to manually curate such large amount of data and make it available in standardized formats for efficient mining and analysis.

Innovation Through Crowdsourcing and Open Source

The recent years have seen the development of a new organizational framework which is popularly called as crowdsourcing. The crowdsourcing taps into collective competence of the network of large number of individuals present outside of physical organizational frameworks. It is a paradigm shift from the traditional organizational structure and is particularly accelerated by the ubiquitous internet and connectivity. These organizational frameworks or rather networks have been increasingly tapped for tasks that were earlier considered impossible. For example, using crowdsourcing model, Amazon Mechanical Turk (http://www.mturk.com) could organize large human networks and spawn activities across the networks. In fact, crowdsourcing has presently become norms in many industries including software development and testing and marketing.

Crowdsourcing may be defined as a product or service delivery pipeline outsourced to volunteers, often amateurs. The defining characteristic of crowdsourcing is that the task is carried out by people unknown to the initiator. In crowdsourcing, initiator (whether individual, companies, or non-profit organizations) do not need to hire many employees to accomplish the task. Instead, major portion of the task is carried out by volunteers in their spare time. Usually, the volunteers may not be even paid for the task they do. Instead, the primary motivators for the participation in crowdsourcing projects are intrinsic factors like peer recognition, social contact, intellectual stimulation, skill development, and autonomy. Therefore, crowdsourcing is turning out to be a very low cost method to accomplish highly complex tasks [13].

Innovative solutions are being achieved through crowdsourcing in areas as diverse as genomics, engineering, predictive analytics, software development, video games, mobile apps, and marketing. The innumerable numbers of apps in Apple, Android, and Nokia stores are probably the best examples of crowdsourcing. The crowdsourced solutions are not limited to low end product development. In fact, it has been shown that, in terms of novelty and customer benefit, the crowd-sourced solutions may surpass those of professionals. It is being recognized that only limitation in crowdsourcing is posing right challenges and taking it to the right crowd of volunteers. Successful launch of many businesses based on crowdsourced design at OpenIDEO is a glaring example of the power of crowdsourcing. A lot can be learned from success stories of other fields and applied into biomedical research.

Crowdsourcing in Biomedical Research

Last few decades have seen steady increase in healthcare costs without significant improvement in clinical outcomes. The condition is even more complex in case of the so-called "neglected diseases" which primarily affect people in the third-world countries. While it is very difficult for Pharma companies to develop drugs for these diseases, which will return the investments, the academic R&D is too fragmented to develop drugs on their own [25, 34]. It shows that the cost burden of traditional model of drug development is not sustainable, anymore. The situation appears to have reached to an inflection point where paradigm shifts in traditional approaches to biomedical research for drug discovery are inevitable.

The researchers in biomedical sciences and the volunteers in crowdsourcing share a lot in common, in terms of motivation to accomplish the tasks. In both fields, the primary motivators are intangible intrinsic factors like peer recognition, intellectual stimulation, skill development, etc. Therefore, biomedical research is one of the ideal areas to explore crowdsourcing model for accomplishing complex tasks. It is not surprising that it is already being used in many areas of biomedical research, especially those in which tasks can be accomplished online. It is becoming an increasingly popular approach to solve highly complex biomedical problems and emerging as a powerful, low cost alternative to the traditional approaches of biomedical research.

Crowdsourcing has been innovatively utilized to accomplish many low cost biomedical solutions. For example, David Baker's group at University of Washington, have developed a protein-folding video game Foldit. The game utilizes human problem-solving skills to solve complex crystal structures of proteins. The Foldit volunteers, many of them with no training in biology, have produced accurate model of M-PMV retroviral protease [35]. It is claimed that gamers accomplished this task in just 3 weeks which eluded researchers for 15 years. The structure can provide new insights for development of anti-HIV drugs. In another recent accomplishment of Foldit, the users were challenged to computationally remodel the

Diels-Alderase enzyme backbone, for better enzymatic activity. The gamers came up with a 13-residue insertion that could increase enzyme activity by more than 18-fold. Through an approach similar to crowdsourcing the image analysis program, ImageJ [36] (known as NIH Image in its previous incarnation) has emerged as a powerful alternative to many commercial image analysis software. The power of ImageJ relies in its user contributed plugins. The ImageJ and many of its curated plugins are freely available as an Open Source software. In terms of utility, they match or even surpass most commercially available image analysis software which cost thousands of dollars.

As stated earlier, the crowdsourcing model has been especially successful for projects amenable to online collaborations. Therefore, it is not surprising that paradigm of crowdsourcing has shown immense potential in the area of genomics or rather the omics sciences, one of the largest big-data enterprises in life sciences. The Genomics organizations like 23andMe (www.23andme.com), PatientsLikeMe (http://www.patientslikeme.com/), Quantified Self (www.quantifiedself.com), DIYgenomics (www.diygenomiocs.org) have pioneered crowd-sourced research. They have started publishing data on disease research, drug response, and user experience for consumer Genomics products. Many researcher-organized genome annotation projects have been successfully completed at a fraction of cost and in significantly less time by large number of voluntary curators. These success stories are just the beginning. As mentioned earlier, the crowdsourcing has unimaginable potential for innovations, limited only to posing right challenges and taking it to the right crowd of volunteers. Some successful examples in Genomics field in more detail are elaborated below.

Crowdsourcing Genomics and Genomic Analysis

The present scale and throughput of genome sequencing far exceeds the analysis capability, and has been increasingly discussed as the next major challenge in this area. Harnessing the power of genomics would require careful and large-scale integration of seemingly disparate datasets derived from multiple-omics technologies to provide insights and further integrate insights or models to provide knowledge [37]. Open initiatives like the ones for Ash Dieback [38] aim at harnessing the expertise and speed of crowd-sourced analysis on Openly available genome and transcriptome datasets. One of the earliest initiatives include the annual Genetic Analysis Workshops (http://www.gaworkshop.org/) where genetic analysis methodologies of a given genetic problem and dataset have been crowd-sourced and compared to identify the best possible methodology.

Similar efforts, with the help of large-number of students and custom web tools, have been explored for metagenomic analysis. In addition, crowd-sourced mycobacteriophage identification has been recently explored. Recently, microbiome collection and analysis have been crowd-sourced through probably the first citizen science driven Human microbiome analysis (www.ubiome.com/). In the area of Human genomics, recent report shows an elegant example of crowd-sourced and self-reported traits and genomic datasets could be extensively used for discovering novel associations.

SNPedia and OpenPGx

Annotation and interpretation of personal genomes would also require standardized and well-curated evidence from the peer-reviewed literature. Single-nucleotide polymorphisms (SNPs) have been long known to confer phenotypic changes and hence medically important consequences. Systematic curation and collection of these SNPs is an important part of analyzing personal genomes, and a number of projects largely involving collaborative editing and contribution similar to the Wikipedia model have been spearheaded. SNPedia is one such wiki-based resource which collects information on SNPs from peer-reviewed journals and provides it in a semantic web form for easy access and interpretation [39•]. While this manuscript was being written, SNPedia houses 38,492 SNPs in its database presently. SNPedia is already used by many resources for clinical interpretation of data from genome sequencing and other test. While SNPedia only provides genotypic information related to any SNP, OpenPGx [40], in addition to giving genotypic information, also curates and stores pharmacogenomically significant information regarding that SNP. Similar analytical challenges for omics data have been attempted recently including the DREAM challenges (www.the-dream-project.org/). A similar effort for genomic data analysis has been put forward by the Boston Children's Hospital called the CLARITY (Children's Leadership Award for the Reliable Interpretation and appropriate Transmission of Your genomic information) challenge (http://www.childrenshospital.org/research-and-innovation/research-initiatives/clarity-challenge) for interpretation of genomic data, with the vision to be able to identify best analytic methodologies for genome interpretation. Similar approaches for technological innovations, not limited to genomics, have also been attempted as part of the X-prize (http://www.xprize.org/) Initiative.

Personal Genome Project

Notwithstanding the privacy concerns, human genome sequence and analysis have also been amenable to crowdsourcing. The personal genome project (PGP) [41] aims to create a publicly available and crowd-sourced

repertoire of human genome information associated with self-reported traits and medical records. The present repertoire encompasses a total of 1,000 volunteers; a small subset of whose genomic information is also available to the public.

OpenSNP

Another such crowd-sourced effort is OpenSNP (www.opensnp.org) where a user freely shares their genotype information over the web for everyone to access. One can simply upload their genotype file from any Direct-to-consumer (DTC) genetic testing company and have their genotypes analyzed. Annotation of the genotypes is done using a host of resources like SNPedia and the peer-reviewed literature.

The Pan-Asian Population Genomics Initiative

The Pan-Asian population genomics initiative (www.papgi.org) is a unique experiment of a loosely knit community of researchers, strongly motivated by the spirit of collaboration and sharing of resources toward realizing the application of genomics to improve the quality of life and health care through understanding genome diversity of Asia. Incidentally, Asia is home to a fifth of world population and home to a rich pool of ethnically, socially, linguistically, and genetically diverse populations with a vivid history of migration and admixture. The open consortium is built upon the strong network of over 100 collaborators from over 16 countries and aims to create one of the most comprehensive curated catalogs of genetic variations in Asian populations. The closely-knit consortium is built on the principles of mutual trust, cooperation, sharing of resources, transparency, and accountability, without the binding of formal memoranda or legal obligations, and thus reflects the true spirit of scientific collaboration in genomics.

The Impact of Crowdsourcing in Clinical Genomics and Precision Medicine

Crowdsourcing of genome data is increasingly been adopted by individuals, though it has not become the mainstream yet. One example worth mentioning is the crowd-sourced "*Corpasome*," where the genomic and metagenomic data of individuals of a family have been made available for crowd-sourced analysis and interpretation [42•]. The idea stemmed from the fact that no single organization or individual is in a position to provide the most comprehensive analysis and interpretation of personal genome data. The diverse skillsets of the genomics community could provide ways of richly annotating and interpreting genomic variations. Another example has been the involvement of crowd-sourced cohorts of individuals and genomic datasets for personalized medicine. The impact of such approaches is two-fold; on one end they make use of the rich knowledge base of the community, which was not possible before, and on the other end, they could access the resource at a fraction of cost of the service if it was existent [13]. This would possibly impact the field in distinct ways. The researchers would immensely benefit from the availability of well-curated and characterized genome-scale information for integration, development, and standardization of new methods and baseline data sets for scientific discovery at minimal costs. The individuals/participants and their doctors and care-givers gain from saving significantly on the cost of analysis, while being able to tap an enormous knowledge base and skill set, which was previously not accessible. The funders also stand to gain from saving cost on duplication of efforts, primarily caused by de-identified data sets generated by multiple researchers, while gaining immense benefit from the possibility to integrate datasets for discovery. The planning bodies also stand to gain from the ready availability of epidemiological data which could help make accurate and precise decisions. The drawbacks of crowdsourcing approaches would also worth mentioning. The major ones include intentional malicious activity, inadvertent errors, and data inconsistencies which could potentially affect the quality of the final resource, methodology or product. Many internal correction systems, including automated bots for consistency checks and manual regular scanning of articles, have been implemented in many large crowd-sourced and collaborative editing platforms like Wikipedia. It should also be noted that the success of the crowdsourcing initiative would also depend largely on the incentive system and motivation of the stakeholders involved. It should be emphasized that the field has a fair share of examples for failures due the lack of a proper incentive system and draining motivation.

Future Perspective

The future of pharmacogenomics for personalized disease management would see creation of pharmacogenomic maps with different granularities being created. On one end, population-scale genome sequencing would provide the much necessary baseline for population-scale differences in pharmacogenetic markers and would provide for disease management strategies for clinicians and policy-makers alike. Personal genome maps for population-scale applications could be created by genotyping or sequencing large number of individuals in the population.

Another major area where pharmacogenomic maps could be potentially used would be to rationalize therapies, especially cost-effective regimens and keep low-cost drugs in the market. This approach would attain more significance in coming years, with the increasingly dwindling drug pipelines and increasing cost of research and development in the drug industry. In a more futuristic scenario, computational models could be used to plan combination regimens in silico or even used to model effects of new and investigational drugs even before human clinical trials. The computational power made available by volunteers through crowd-computing approaches may be utilized to reduce the costs of in silico modeling. This would also have the potential to drastically reduce the cost of failures and subsequently reduce the cost of drug discovery as a whole.

The major impact of pharmacogenomic maps would be in how they could be potentially integrated into Electronic Medical Records, Decision Support Systems and Research Databases [43]. The future could see new standards enabled with the highest encryption, offering tiered release of relevant information to all stakeholders- the patient, physicians, researchers, and planners. Such integration also offers an immense opportunity to provide real-time evidence-based assessment and planning of the disease prevention and management. It has also not escaped our attention that data integration and tiered access to data and crowd-sourced or participatory research could provide for a new framework of collaborative co-creation of knowledge potentially at a fraction of the cost incurred today, while providing enormous health benefits to the community as a whole.

These futuristic developments are not without concerns of privacy. It is imperative that new frameworks for consultative and collaborative ethical and regulatory frameworks emerge, and would increasingly be one of the major challenges in the coming years, as the public knowledge and perception on access to genomic information improve. Nevertheless this could also be compounded by the improving accuracy of predictions of phenotypes based on computational heuristics and well-curated datasets. Keeping the technological challenges aside, the public perception of genomics and its utility to improve quality of life and health care is of significant importance. We also foresee the regional or rather the east–west differences in perceptions of privacy to impact the acceptability of crowdsourcing in genomics.

Acknowledgments The authors acknowledge discussions with Dr. Sridhar Sivasubbu and Dr. S Ramachandran and members of the OpenPGx consortium and PAPGI consortium, which have significantly enriched the content of the Manuscript. This work was funded by the Council of Scientific and Industrial Research, India, through Grant CARDIOMED (BSC0122).

Disclosure Y Hasija, JA Khan, and V Scaria all declare no conflicts of interest.

Human and Animal Rights and Informed Consent This article does not contain any studies with human or animal subjects performed by any of the authors.

References

Papers of particular interest, published recently, have been highlighted as:
- • Of importance
- •• Of major importance

1. Venter JC, Adams MD, Myers EW, et al. The sequence of the human genome. Science. 2001;291:1304–51.
2. Consortium" "the International Human Genome Sequencing. Initial sequencing and analysis of the human genome. Nature. 2001;409:860–921.
3. Metzker ML. Sequencing technologies—the next generation. Nat Rev Genet. 2010;11:31–46.
4. International T, Consortium H. A haplotype map of the human genome. Nature. 2005;437:1299–320.
5. Article R. Genetic landscape of the people of India: a canvas for disease gene exploration. Genome. 2008;87:3–20.
6. Abdulla MA, Ahmed I, Assawamakin A, et al. Mapping human genetic diversity in Asia. Science. 2009;326:1541–5.
7. •• ENCODE Project Consortium. An integrated encyclopedia of DNA elements in the human genome. Nature. 2012;489:57–74 *The ENCODE consortium paper discusses the outline and major results from the large international collaborative initiative.*
8. Bernstein BE, Stamatoyannopoulos JA, Costello JF, et al. The NIH Roadmap Epigenomics Mapping Consortium. Nat Biotechnol. 2010;28:1045–8.
9. •• The 1000 Genomes Project Consortium. An integrated map of genetic variation from 1,092 human genomes. Nature. 2012;491:56–65 *This landmark paper provides a glimpse of the population level variability of humans.*
10. • Lu D, Xu S. Principal component analysis reveals the 1000 Genomes Project does not sufficiently cover the human genetic diversity in Asia. Front Genet.2013. doi:10.3389/fgene.2013.00127. *This paper discusses the issues of comprehensiveness of the 1000 Genomes Project in uncovering the Human genetic diversity.*
11. Highnam G, Mittelman D. Personal genomes and precision medicine. Genome Biol. 2012;13:324.
12. Nicholson N (2012) Crowdsourcing. Manag Today 18.
13. Malone TW, Laubacher R, Dellarocas C (2009) Harnessing crowds: mapping the genome of collective intelligence. Elements 1–20.
14. Murray DG, Yoneki E, Crowcroft J, Hand S (2010) The case for crowd computing. In: MobiHeld '10 Proceedings of the second ACM SIGCOMM workshop on Networking, systems, and applications on *mobile handhelds*.
15. Hindorff LA, Sethupathy P, Junkins HA, Ramos EM, Mehta JP, Collins FS, Manolio TA. Potential etiologic and functional implications of genome-wide association loci for human diseases and traits. Proc Natl Acad Sci USA. 2009;106:9362–7.
16. Wang J, Wang W, Li R, et al. The diploid genome sequence of an Asian individual. Nature. 2008;456:60–5.

17. Fujimoto A, Nakagawa H, Hosono N, et al. Whole-genome sequencing and comprehensive variant analysis of a Japanese individual using massively parallel sequencing. Nat Genet. 2010;42:931–6.
18. Ahn S-M, Kim T-H, Lee S, et al. The first Korean genome sequence and analysis: full genome sequencing for a socio-ethnic group. Genome Res. 2009;19:1622–9.
19. Patowary A, Purkanti R, Singh M, Chauhan RK, Bhartiya D, Dwivedi OP, Chauhan G, Bharadwaj D, Sivasubbu S, Scaria V. Systematic analysis and functional annotation of variations in the genome of an Indian individual. Hum Mutat. 2012;33:1133–40.
20. Dissanayake VHW, Samarakoon PS, Scaria V, Patowary A, Sivasubbu S, Gokhale RS. The Sri Lankan Personal Genome Project: an overview. Sri Lanka J Bio-Med Informatics. 2011;2:4–8.
21. Salleh MZ, Teh LK, Lee LS, et al. Systematic pharmacogenomics analysis of a malay whole genome: proof of concept for personalized medicine. PLoS One. 2013;8:e71554.
22. Jamal S, Periwal V, Consortium OSDD, Scaria V. Predictive modeling of anti-malarial molecules inhibiting apicoplast formation. BMC Bioinformatics. 2013;14:55.
23. Jamal S, Periwal V, Scaria V. Computational analysis and predictive modeling of small molecule modulators of microRNA. J Cheminform. 2012;4:1–9.
24. Periwal V, Rajappan JK, others. Predictive models for anti-tubercular molecules using machine learning on high-throughput biological screening datasets. BMC Res Notes. 2011;4:504.
25. Munos B. Lessons from 60 years of pharmaceutical innovation. Nat Rev Drug Discov. 2009;8:959–68.
26. Scriver CR. After the genome—the phenome? J Inherit Metab Dis. 2004;27:305–17.
27. Goldstein DB. Common genetic variation and human traits. N Engl J Med. 2009;360:1696–8.
28. Hirschhorn JN. Genomewide Association Studies—illuminating biologic pathways. N Engl J Med. 2009;360:1699–701.
29. Cotton RGH, Horaitis O (2000) Human Genome Variation Society. eLS.
30. Horaitis O, Cotton RGH. The challenge of documenting mutation across the genome: the human genome variation society approach. Hum Mutat. 2004;23:447–52.
31. Thorisson GA, Lancaster O, Free RC, Hastings RK, Sarmah P, Dash D, Brahmachari SK, Brookes AJ. HGVbaseG2P: a central genetic association database. Nucleic Acids Res. 2009;37:D797–802.
32. Wishart DS, Knox C, Guo AC, Cheng D, Shrivastava S, Tzur D, Gautam B, Hassanali M. DrugBank: a knowledgebase for drugs, drug actions and drug targets. Nucleic Acids Res. 2008;36:D901–6.
33. Sangkuhl K, Berlin DS, Altman RB, Klein TE. PharmGKB: understanding the effects of individual genetic variants. Drug Metab Rev. 2008;40:539–51.
34. Munos B. Can open-source drug R&D repower pharmaceutical innovation? Clin Pharmacol Ther. 2010;87:534–6.
35. Eiben CB, Siegel JB, Bale JB, Cooper S, Khatib F, Shen BW, Players F, Stoddard BL, Popovic Z, Baker D. Increased Diels-Alderase activity through backbone remodeling guided by Foldit players. Nat Biotech. 2012;30:190–2.
36. Schneider CA, Rasband WS, Eliceiri KW. NIH Image to ImageJ: 25 years of image analysis. Nat Methods. 2012;9:671–5.
37. Editor. Community engagement. Nat Rev Microbiol. 2013;11:219.
38. Maclean D, Yoshida K, Edwards A, et al. Crowdsourcing genomic analyses of ash and ash dieback—power to the people. Gigascience. 2013;2:2.
39. • Cariaso M, Lennon G. SNPedia: a wiki supporting personal genome annotation, interpretation and analysis. Nucleic Acids Res. 2012;40:D1308–D1312. *An open source resource for variant annotation.*
40. Pasha A, Scaria V. Pharmacogenomics in the era of personal genomics: a quick guide to online resources and tools. In: Barh D, Dhawan D, Ganguly NK, editors. Omics for personalized medicine. Springer; 2013. p. 187–211.
41. Church GM. The personal genome project. Mol Syst Biol. 2005;1(2005):0030.
42. • Corpas M. Crowdsourcing the corpasome. Source Code Biol Med. 2013;8:13. *An example for crowdsourcing genome analysis.*
43. Kawamoto K, Lobach DF, Willard HF, Ginsburg GS. A national clinical decision support infrastructure to enable the widespread and consistent practice of genomic and personalized medicine. BMC Med Inform Decis Mak. 2009;9:17.

International Journal of Current Engineering and Technology
E-ISSN 2277 – 4106, P-ISSN 2347 - 5161

Available at http://inpressco.com/category/ijcet

Research Article

Production and Performance Testing of Waste Frying Oil Biodiesel

Amit Pal[À*], Shashank Mohan[À] and Dhananjay Trivedi[Ḃ]

[À]Department of Mechanical Engineering, Delhi Technological University,Bawana Road, Delhi-110042, India
[Ḃ]Department of Mechanical Engineering, JSS Academy of Technical Education, Sector-62, Noida, India

Accepted 01 May 2014, Available online 01 June2014, **Vol.4, No.3 (June 2014)**

Abstract

Due to rapidly diminishing petroleum resources and the escalating environmental pollution from the use of the fossil fuels, there is a gigantic search for alternative sources of fossil fuels. Biodiesel demonstrates to be the best appropriate substitute for the diesel fuel because it can be used in any existing diesel engine without incorporating any adaptation. Waste Frying Oil (WFO), which is not suitable for human utilization, and whose safe disposal is a challenge, may be suitably used for biodiesel production. The present paper deals with the details of conversion of WFO into biodiesel through cavitation techniques followed by its performance testing on a diesel engine.

Keywords: *Waste Frying Oil, Cavitation, Transesterification, Biodiesel, Smoke Opacity*

1. Introduction

The worldwide dependence of transport systems on fossil fuels is continuously increasing as well as price of crude oil is also rising day by day. The economical growth of any developing country is based on agriculture and industrial sector. The basic power source of industrial sector as well as agriculture sector is diesel fuel. Also the emissions produced by these fuels are creating a threat to our existence. (Ramesh, and Sampatraja, 2008). Majority of the world's energy needs are abounding through petrochemical sources, coal and natural gases, the exception of hydroelectricity and nuclear energy. It is understood that within four decades, the present reserves of petroleum fuel including diesel will be exhausted fully (Nabi, *et al*, 2009). Also, petroleum fuels are at present the principal global source of CO_2 and posing a stronger threat to clean environment. Depleting reserves of crude petroleum, uncertainty in availability, environmental degradation and speedy hike in petroleum prices has necessited search of alternate fuels (Lin, *et al*, 2011). The prerequisite for an alternative fuel is that it should be easily available, renewable, environment friendly and techno-economically competitive. India is a developing country and its energy requirement is growing day by day. Most of the country's oil demands are met by import from the foreign countries. Bio-diesel is an alternative to petroleum-based fuels derived from vegetable oils or animal fats which can substitute them locally (Murugesan, *et al*, 2008).Lower cost feed stocks, such as waste Frying oil, grease, soap stocks are preferred because of their economic viability, since feedstock costs are about more than 85% of the total cost of biodiesel production (Pal, and Kachhwaha, 2013). The biodiesel produced from vegetable oil or animal fat is usually more expensive than petroleum based diesel fuel from 10 to 50 %. Many vegetable oils like Soybean, Groundnut, Rapeseed, Palm, Olive etc. are wildly used for a number of food items. But once they are heated above a critical temperature for deep, they become unfit for eating, as their further use may lead to cholesterol formation. Thus they need to be disposed in an environment friendly manner. In developing countries like India, the significant amount of WCOs may be collected from catering industry. Their use for biodiesel production offers solution to a growing problem of the increased WFO generation from household and industrial sources all around the world. Biodiesel can be produced by various conventional methods such as: alkali catalysis, acid catalysis, lipase catalysis etc. Acid catalyzed process is helpful when a high amount of free fatty acids are present in the vegetable oil, but the reaction time is very long (48–96 h), even at the boiling point of the alcohol, and a high molar ratio of alcohol is needed (20:1 wt/wt to the oil). In the base catalyzed procedure, some soap is formed and it acts as phase transfer catalyst, thus helping the mixing of the reactants. Presently, mechanical stirring is the commonly adopted process in worldwide industrial applications. Considering these limitations, there is a strong quest to develop an efficient, time-saving, economically functional and environmental friendly biodiesel production process at industrial scale having superiority over the classical procedure.

Recently developed biodiesel production technologies such as hydrodynamic cavitation and power ultrasound may prove very good for biodiesel production at industrial scale due to their easy scale-up property. (Pal, *et al*, 2013).presented the details of thumba biodiesel production test rig based on hydrodynamic cavitation followed by

*Corresponding author: **Amit Pal**

results of experimental investigation carried out on a CI engine. The transesterification reaction of vegetable oils using base catalyst and short-chain alcohols was studied by Gogate, and Pandit, 2005),by the method of hydrodynamic cavitation. This is a rapid technique for preparing alkyl esters from triglycerides at pilot plant scale operation. The transesterification reaction of vegetable oils using base catalyst and short-chain alcohols using the method of hydrodynamic cavitation was studied by (Gogate*et al*, 2006) Cavitation results in the generation of local turbulence and liquid micro- circulation (acoustic streaming) in the reactor, enhancing the rates of transport processes. The generation, subsequent growth and collapse of cavities results in very high energy densities of the order of 1x 10^{18} kW/m^3.

Hydrodynamic Cavitation

In hydrodynamic cavitation method mixing of two phases of reaction is carried out by cavitation conditions, produced by pressure variation, which in turn obtained by using the geometry of system to create velocity variation. Cavitation is generated by the flow of liquid under controlled conditions through simple geometries such as venturi tubes & orifice plates. When the pressure at the throat falls below the vapour pressure of liquid, the liquid flashes, generating a large number of cavities which subsequently oscillate and then give rise to pressure & temperature pulses. (Pal, *et al*, 2013). It is reported that hydrodynamic cavitation can be successfully applied to transesterification reaction for more than 90% yield of the product according to stoichiometry in as low as 15 minute of the reaction time.

2. Biodiesel Production: Material and Methods

Biodiesel production through cavitation technology

In this work the WFO is collected from Hotel Paris Hilton of Delhi. The filtered WFO (3kg) is taken in a beaker and then it is heated up to 110^{0}C in order to remove any water content in the oil. This oil is then brought down to 55^{0}C temperature so that after mixing the reactants the mixture temperature is limited to 50^{0}C. Simultaneously methyl alcohol (CH_3OH) is taken in molar ratio of (1:4.5 & 1:6) and Catalyst (KOH) is taken as (0.5%, 0.75% and 1% by weight of the oil).The mixer of methyl alcohol and KOH is stirred until KOH dissolves in methyl alcohol. Experiments have been conducted with the main objectives of converting the WFO in to biodiesel by both types of cavitation technique and to compare both the methods in terms of biodiesel production time and yield (%). Table1 presents the details of ingredients used for biodiesel production. Experiments were carried out for molar ratio of 4.5:1 and 6:1. Results for biodiesel production yield and time are shown in Fig 1 to Fig. 3 respectively. It is observed that the Hydrodynamic cavitation can be successfully applied to transesterification reactions, more than 90% yield of the product for molar ratio 4.5:1 and minimum catalyst percentage of 0.5%. Changing molar ratio to 6:1 does not give any appreciable increase in yield %.

Table 1: Oil, alcohol and catalyst used for mechanical stirring

Molar ratio (alcohol/oil)	WFO(g)	methanol (g)	Catalyst (KOH)		
			0.5%	0.75%	1.0%
6:1	3000 g	660 g	15 g	22.5 g	30 g
4.5:1	3000 g	492 g	15 g	22.5 g	30 g

Experimental results

As shown in figures 1 and 2, biodiesel yield increases as reaction time increases and eventually it becomes constant after 75 min of reaction time. The yield is more for molar ratio 6:1 and 1 % catalyst as compared to molar ratio 4.5:1 and 0.75% catalyst.

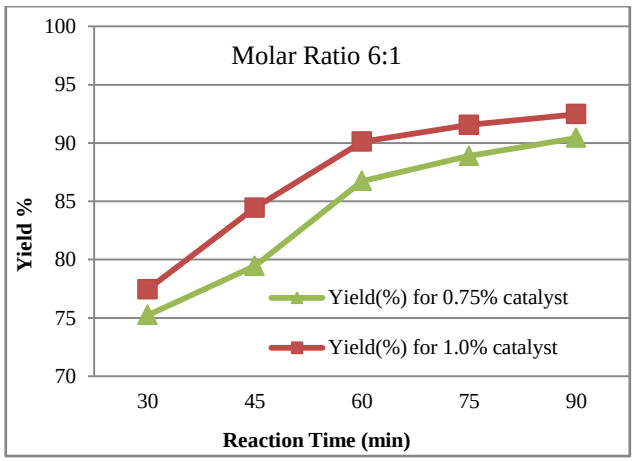

Figure 1 Time v/s Yield (%) for molar ratio 6:1 and different catalyst percentage

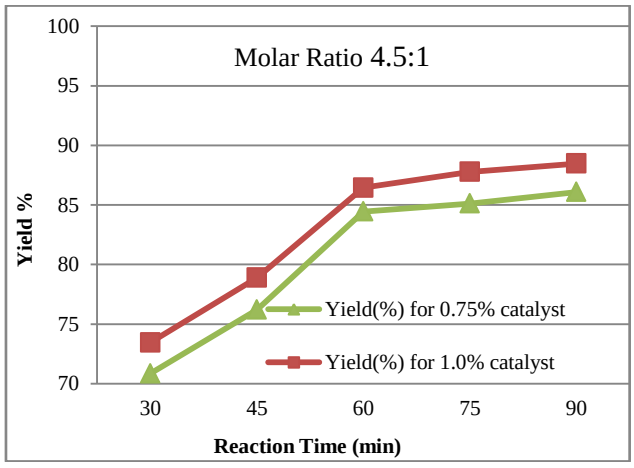

Figure 2 Time v/s Yield (%) for molar ratio 4.5:1 and different catalyst percentage

Hydrodynamic cavitation

The schematic diagram of the hydrodynamic cavitation test rig developed is shown in Figure 4. Like cavitation in turbines and pumps, hydrodynamic cavitation can be generated by the passage of the liquid through a

constriction such as throttling valve, orifice plate etc. As the liquid passes through the orifice plates, the velocities at the orifice increase due to the abrupt reduction in the flow area, resulting in a decrease in the pressure. If the local pressure goes below the medium vapour pressure under operating conditions (at constant temperature), vapour bubbles are formed. At the downstream of the orifice, however, due to an increase in the area of cross-section, the velocities decrease giving rise to increasing pressures and pressure fluctuations, because of which bubbles collapse and local cavities are formed at a number of locations. This process generates conditions of very high temperatures and pressures locally. The collapse of the cavitation bubbles disrupts the phase boundary and impinging of the liquids create micro jets, leading to intensive emulsification of the system, which result in increase of reaction rate at much faster rate. This process is carried again and again until all the mixture is converted into biodiesel.

Experimental results

As shown in figures 3 and 4, the yield is more for molar ratio 6:1 and 1 % catalyst (max value is 98.12%) as compared to molar ratio 4.5:1 and 0.75% catalyst (max value is 95.14%).

3. Experimental Work on Performance and Emission in CI Engine

The setup consists of four cylinders, four stroke, Tata Indica diesel engine connected to eddy current type dynamometer for loading. It is provided with necessary instruments for combustion pressure and crank-angle measurements. The signals are interfaced to computer through engine indicator for p-θ diagrams. Provision is also made for interfacing airflow, fuel flow, temperatures and load measurement.

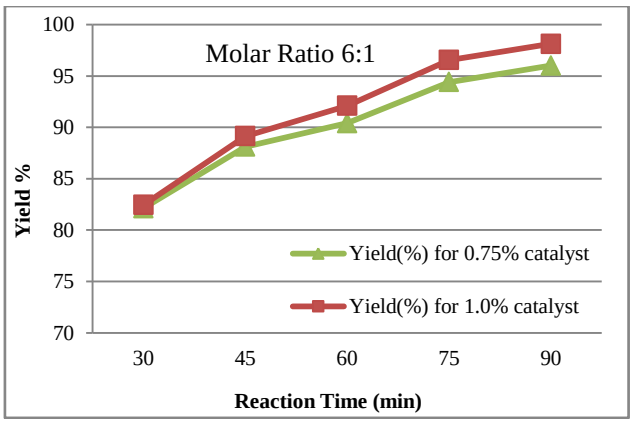

Figure 3 Time v/s Yield (%) for molar ratio 6:1 and different catalyst percentage

The set up has stand-alone panel box consisting of air box, fuel tank, manometer, fuel measuring unit and transmitters for air and fuel flow measurements. Experiment has been performed by taking WFO biodiesel blends diesel in proportion of volume 20%, 40% and 60% respectively and following parameters has been obtained. The main aim of this experiment is to investigate the suitability and effect on performance of blending of biodiesel in comparison to the petroleum diesel fuel.

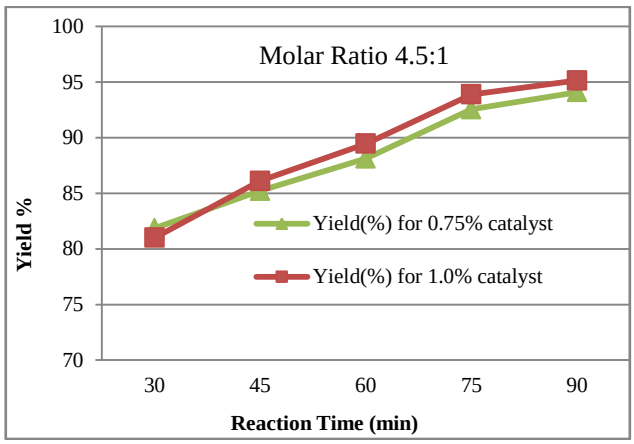

Figure 4 Time v/s Yield (%) for molar ratio 4.5:1 and different catalyst percentage

Brake thermal efficiency v/s brake power

Figure 5 shows comparison of Brake thermal efficiency v/s brake power for different blends in comparison to diesel. For WFO-B20 AND WFO-B40 blend brake thermal efficiency values are higher as compared to diesel at higher load. This is due to better combustion efficiency of blends caused by presence of extra amount of oxygen. The maximum thermal efficiency achieved by WFO-B40 is around 40.33 % at 4.0 kW.

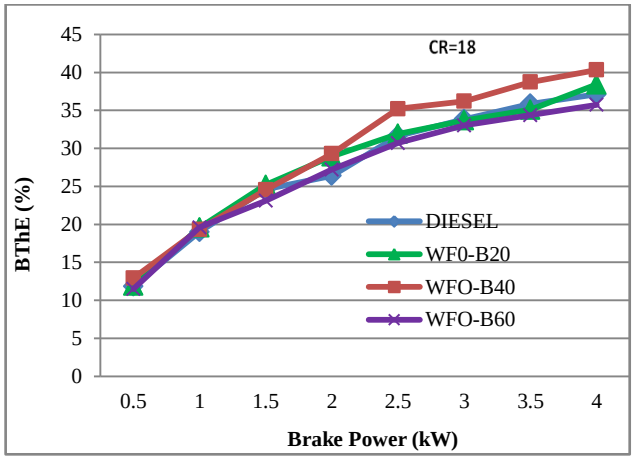

Figure 5 Comparison of brake thermal efficiency v/s brake power

Brake specific fuel consumption v/s brake power

The variation of specific fuel consumption vs. brake power is shown in figure 6 for blends and diesel. For all cases the bsfc initially decreases sharply with increase in brake power and afterward remains stable. In case of blends bsfc values are higher at the beginning because of higher viscosity. Once the required temperature is attained inside the engine cylinder the values are comparable with diesel but little bit higher specifically for WFO-B20 and WFO-B40 as compared to diesel.

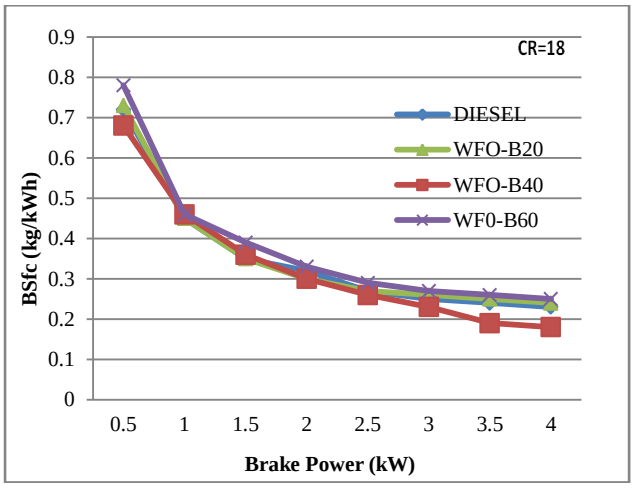

Figure 6 Comparison of specific fuel consumption v/s brake power

Exhaust gas temperature v/s brake power

Exhaust Temperature of the blends such as WFO-B20, WFO-B40 and WFO-B60 at various brake powers compared to diesel are shown in the Figure 7. The Ex. Temperature values are higher for blends because of better combustion efficiency. This high temperature is also indication of more NOx emission in case of blends.

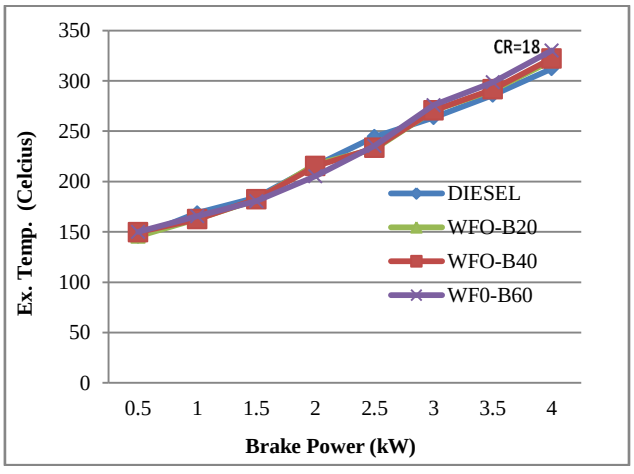

Figure 7 Comparison of exhaust gas temperature v/s brake power

Smoke opacity v/s brake power

To understand the pollution aspect of WFO and diesel blends the variation of opacity v/s brake power are shown in Figure 8 for blends in comparison to pure diesel. The opacity value for pure diesel is higher as compared to all type of blends for wide range of Brake power. At all brake power condition the opacity of all blends has less value than diesel oil. Maximum value of opacity has obtained at 59.21 at 4.0 kW brake power for pure diesel and for blends 45.7 at 4.0 kW for B-20.

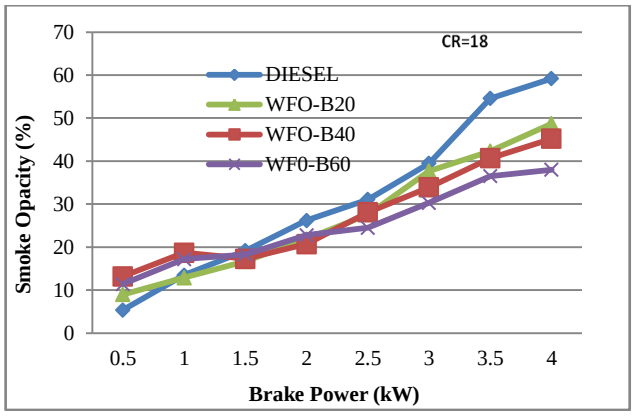

Figure 8 Comparison of smoke opacity v/s brake power

Conclusions

The production and performance testing of biodiesel from low-cost waste Frying oil have been investigated. The experimental study performed in this work has demonstrated that the hydrodynamic cavitation method is more efficient than the conventional mechanical stirring method with better yield in less reaction time**.** Waste Frying oil can be a good source of biodiesel production especially in Indian condition where large amount of waste oil is produced and then dumped either into land or river causing environmental pollution. As per performance testing performed in this work it can be seen that waste Frying oil biodiesel blends give better thermal efficiency and have got safer impact on environment as compared to diesel fuel. Thus present Experimental study on performance and emissions prove that WFO biodiesel can be easily used through blending it with diesel in existing diesel engines for better combustion and greener exhaust emissions.

References

Gogate, P. R., Pandit, A. B. (2005), A review and assessment of hydrodynamic cavitation as a technology for the future. Ultrasounds Sonochemistry, (12), pp 21–27.

Gogate, P. R., Pandit, A. B. andTayal, R. K. 2006. Cavitation: a technology on the horizon,*Current Science*, (91), pp35–46.

Lin, L., Cunshan, Z., Vittayapadung, S., Xiangqian, S., Minutesgdong, D., (2011), Opportunities and challenges for biodiesel fuel, *Applied Energy*, (88), pp 1020–31.

Murugesan, A., Umarani, C. Chinnusamy, T. R. Krishnan, M., Subramanian, R., Neduzchezhain, N. (2008), Production and analysis of bio-diesel from non-edible oils—A Review.Renewable and Sustainable Energy Reviews, 13(4), pp825-834.

Nabi, M.N., Rahman, M.M., Akhtar, M.S., (2009), Biodiesel from cottonseed oil and its effect on engine performance and exhaust emissions. Applied thermal engineering (29), pp2265-2270.

Pal, A., Verma, A., Kachhwaha, S. S., Maji, S. (2010), Biodiesel production through hydrodynamic cavitation and performance testing, *Renewable Energy*, 35(3), pp 619–624.

Pal, A., and Kachhwaha, S. S., (Jun 2013), Waste Cooking Oil: A Promising Feedstock for Biodiesel Production through Power Ultrasound And Hydrodynamic Cavitation, *Journal of Scientific and Industrial Research India*, Vol 72 pp387-192

Ramesh, D. and Sampatraja, A., (2008), Investigation on Performance and emission characteristics of diesel engine with Jatropha biodiesel and its blends, *.AgricEnggInt: CIGR e-J Sci Res Develop*, 10 EE 07 01.

International Journal of Research in Electrical and Electronics Technology (IJREET)
Volume 1 - Issue 1 April 2014

Renewable Energy Advancements in India

M. Rizwan, N. Kumar, A. H. Quadri
Department of Electrical Engineering, Delhi Technological University, Delhi-110042, India
Email: rizwan@dce.ac.in, dnk_1963@yahoo.com, arshad_quadri@yahoo.com

***Abstract*— In India, the demand of electricity is increasing exponentially due to urbanization and population growth. The gap between demand and supply is also increasing day by day due to depletion of fossil fuels. Further, the power generated from fossil fuel becoming source of green house gas emissions. To bridge the gap and environment friendly power generation, renewable energy sources (RES) plays an important role. In this paper, the advancements of renewable energy during last 20 years is presented. From this study, it is concluded that there is a huge progress in the development of power plants based on RES. In March 1992, the contribution of RES was 32 MW i.e. 0.05% only; whereas the installed power capacity as on 31.12.2013 is 29989 MW i.e. 13%. In addition, the projected installed capacity by 2022 would be 72400 MW, which can contribute significantly to fulfill the demand of electricity.**

Keywords: **Renewable energy sources, Photovoltaic systems, Solar energy, power generation.**

I. INTRODUCTION

In the last six decades, India's energy use has increased 16 times and the installed energy capacity by 84 times, still India is facing the problem of acute power deficit [1]. The present scenario indicates that India's future energy requirements are going to be extremely high. In order to meet the ever increasing power requirements, huge amount of power needs to be generated in the existing power sector. According to Ministry of Power statistics, the installed power generation capacity of India as on December 31, 2013 was 234456 MW and with per capita energy consumption of 917 kWh as on March 2013. Further, the total demand for electricity in India is expected to cross 950,000 MW by 2030 [2, 3] and it is beyond doubt that a substantial contribution would be from renewable energy. As on 31st December 2013, the current installed capacity of thermal power is 159794 MW which is 68% of total installed capacity. Current installed capacity of coal based thermal power is 138213 MW which comes to 59% of total installed base and current installed base of gas based thermal power is 20382 MW which is 9% of total installed base, while oil based thermal power is 1,200 MW which is 0.5% of total installed base. In addition, 39893 MW of power is generated through large hydro and 4780 MW and 29989 MW of power is generated from nuclear energy and renewable energy resources respectively [3, 4]. The graphical representation of Indian power sector as on December 31, 2013 is presented in Fig. 1.

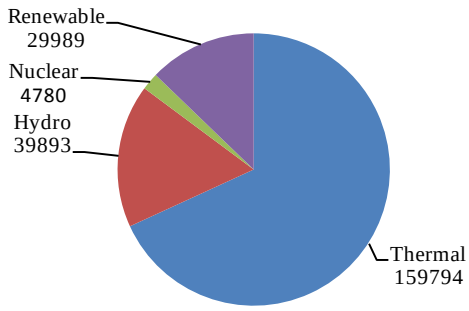

Figure 1: Installed Power Capacity (MW) of India

As renewable energy is concerned, the current installed base of renewable energy is 29989 MW. The power generation through wind is 20150 MW; small hydro contributes 3763 MW while the power generated from biomass and solar photovoltaic technology is 3896 MW and 2180 MW respectively [4]. The potential of above mentioned resources is huge and this could be sufficient to meet the future requirements of power in the country.

The graphical representation of contribution of renewable energy resources in Indian power sector as on 31st December, 2013 is shown in Fig. 2.

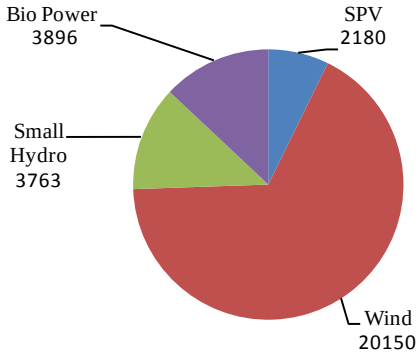

Figure 2: Contribution RES in Indian Power Sector(MW)

II. RENEWABLE ENERGY IN INDIA

Renewable energy is an effective option for meeting the ever-increasing energy demands. Renewable energy sources are attracting more attention as conventional fossil - fuel energy sources will get exhausted eventually in the next century and worldwide environmental concern about global warming. The following are the major sources of renewable power generation in India.

A. Solar Energy

India is blessed a vast solar energy potential, which is about 5000 trillion kWh/year (MNRE). Out of which we are able to exploit the small amount of power i.e. 2180 MW as on 31st December 2013. Solar energy can be utilized with the help of two technologies i.e. solar thermal technology and solar photovoltaic technology. In India, solar thermal technology for power generation is limited. However there is a drastic advancement in photovoltaic technology. The power generated from PV system can be expressed using the following equation [5]:

$$P = Ax^2 + Bx + C \quad \text{(Watts)} \qquad (1)$$

Where, P = power generation (watts), x = solar radiation and A, B, C are the constants, which may be derived from the measured data.

B. Wind Energy

Due to the geographical location in the tropics wind energy is the powerful resource available in abundance in India. However fluctuation in the speed and intermittent availability is the main concern for the production of electricity with this clean source of renewable energy. Though India is the fifth largest in the world to have installed wind power capacity of more than 20 GW, which is much less than the potential available for wind power generation i.e. 300 to 400 GW as per Lawrence Berkley National Laboratory (LBNL) [6]. Wind Energy Conversion System is capable of producing electrical power from 500 watt to 5 kW with daily electrical energy output of 4-10 kWh under average speed of wind 5-10 m/s.
The output power of turbine is proportional to the cube of the wind velocity, so as power output increases drastically with increase of wind velocity. According to the Betz limit only 59% of wind power can be converted in to electricity. The output power of wind generator can be expressed as [5, 7]:

$$P = \left(\frac{1}{2}\right) \times \rho \times A \times v^3 \quad \text{(Watts)} \qquad (2)$$

Where, P = power generation (watts), A = swept area of blades (m^2), ρ ρ = density of air (kg/m^3), v = wind velocity (m/s).

C. Biomass

India is privileged with abundant biomass resource potential i.e. 23 GW [8]. According to World Bank report of 2011, 60% of land area in India is used for agricultural purposes. Biomass power plants in India are based mostly on agricultural wastes. For providing grid based power 8-15 MW thermal bio plants are suitable. Only 20% of biomass potential had been utilized to generate electrical power as on 31st December 2013. It is projected to achieve 32% biomass power from the available bio potentials by 2022 [9]. Biomass energy includes energy from fores, residues rice husk, dead trees, branches, yard clippings, wood chips, and even municipal solid waste, sugarcane etc.

D. Biogas

Biogas can be produced by digestion pyrolysis or hydro gasification. Digestion is a biological process that occurs in the absence of oxygen and in presence anaerobic organism at atmospheric temperature and pressure of 35°C-70°C. Biogas contains (55%-65%) methane, (30%-40%) CO_2 and remainder are impurities like H_2S, H_2, N_2 gases. The main sources of production of biogas are crop residues, wet cow dung, vegetable waste, algae, poultry or piggery droppings, human waste, bagasse, rice husk etc. Cattle dung can produce $0.037m^3$ of biogas per kg of cow dung [10].
Assuming 34-40% conversion efficiency from biogas to electricity, it can be expressed as [5]:

$$e_{biogas} = E_{biogas} \times \eta \quad \text{(BTUs)} \qquad (3)$$

Where, e_{biogas} = generated electricity from biogas (BTUs), E_{biogas} = unconverted raw energy in biogas (BTUs), η = overall conversion efficiency
Total electricity produced from biogas including unit conversions in kWh is given by the equation [5]:

$$e_{biogas} = E_{biogas}[BTU] \times 0.00293 \left[\frac{kWh}{BTU}\right] \times \eta \quad \text{(kW)} \qquad (4)$$

E. Small Hydro

Hydropower is one of the most established renewable energy source for electricity generation from stored water at a given height. There is a vast scope of hydro power development in India as around 15 GW of potential available today [4] and only 25% of hydropower is exploited till 31st December 2013. The power generation from hydropower is projected to 44% of its available potential by 2022 [9]. Electrical power from hydro power can be obtained by the following expression [5, 11]:

$$P = H \times Q \times g \quad \text{(kW)} \qquad (5)$$

Where, P = Power generated (kW), H = Water head (m), g = Acceleration due to gravity (9.81 m/s^2).

III. Government of India Initiatives

As per the statistics of MNRE, the power generation through solar photovoltaic technology has increased around 25 times during the last one year. However, the Government of India is planning to add 20000 MW of power through solar energy under Jawaharlal Nehru National Solar Mission (JNNSM). The National Solar Mission is one of the major initiatives of the Government of India and as well as State Governments to promote ecologically sustainable growth while addressing India's energy security challenge. It also constitutes a major contribution by India to the global effort of meeting the challenges of climate changes. India has tropical climate, where sunshine is available for longer hours per day and in great intensity. As solar energy is one of the most promising and more predictable than other renewable sources and less vulnerable to change in seasonal weather, it has great potential as future energy source. It also has the advantage of permitting the decentralized distribution of energy; thereby empowering people at the grassroots level. The Government of India also gives incentives for solar power generation in the form of subsidies for various solar applications; and has set a goal that use of solar energy should contribute 7% of India's total power production by 2022. With such high targets, solar energy is

going to play a key role in shaping the future of India's power sector.

IV. CONTRIBUTION OF INSTALLED POWER GENERATION CAPACITY

India has been making continuous progress in renewable power generation. The trajectory growth of installed capacity since year 2002 and at present as on 31st December, 2013 is given in Table 1 [3, 4].

Table1: Contribution of Installed Power Generation Capacity

Source	Time Period			
	1.4.02	1.4.07	30.06.12	30.09.13
Thermal (MW)	74429	87015	136436	155969
Hydro (>25MW)	26269	34654	39291	39788
Nuclear (MW)	2720	3900	4780	4780
Renewable(MW)	1628	10258	24833	28184

It is observed that the renewable energy capacity has increased around 8 times from 1.6% to 12.8% during last 11 years and is contributing around 4.4% electricity generation mix. In 2022, the projected share of renewable energy resources and the electricity mix would be around 16% and 6.4% respectively. From this data, it is clearly seen that the role of renewable energy resources in meeting the future energy demand would be significant.

The projected contribution of grid interactive renewable power along with the conventional power is shown in Table 2 [9].

Table2: Projected Contribution of Grid Interactive Power

Source	Capacity/Total Projected Capacity (MW)			
	30.06.2012	30.9.2013	31.03.2017	31.03.2022
Conventional	180507.58	200537.39	283000	383000
Wind	24832.68	28184.34	27300	38500
Small Hydro			5000	6600
Biomass			5100	7300
Solar Power			4000	20000
Total	205340.26	228721.73	324300	455100

The projected contribution of renewable energy and conventional power as on 31st March 2022 is also presented in Fig. 3.

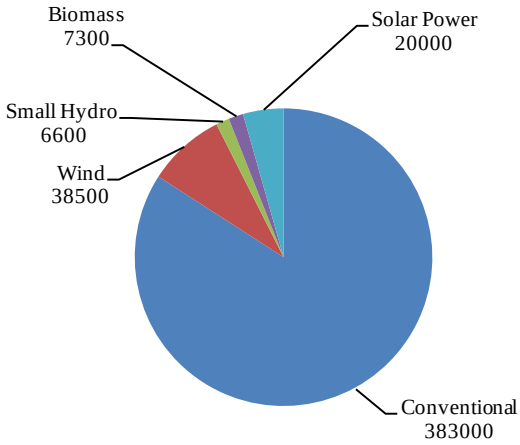

Figure 3: Renewable and Conventional Power in Future Power System

The growth of installed capacity and share of RES in total installed generation capacity is shown in Fig. 4. The contribution of renewable power in early nineties was just 0.05% of total installed capacity. In 1997 renewable power shared 1% of total installed power.

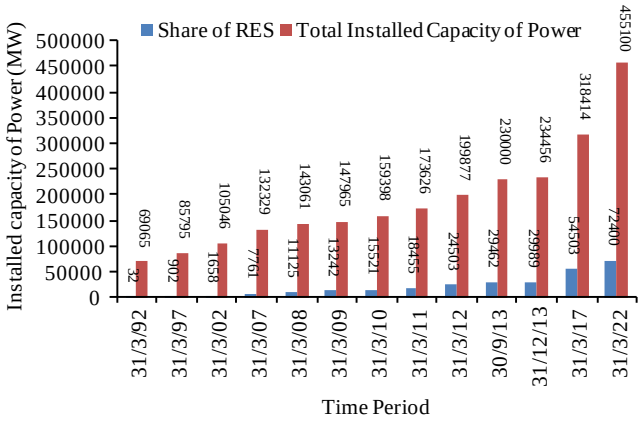

Figure 4: Growth of RES in Total Installed Capacity in India

This chart is showing the continuous growth of renewable energy share in total installed generation capacity of India. It is clearly seen from the Fig. 4 that during the last few years, there is a drastic change in this share. Presently renewable energy shares 13% of the total generating capacity as on 31st December 2013.The future share of renewable power is projected 16% as on 31st March 2022. The contribution of renewable power in India is shown in Fig. 5. This bar chart clearly indicates that wind and solar will be the main source of renewable power to contribute in Indian power sector. However due to unavailability of wind and continuous variation in velocity, wind power generation is restricted in coastal areas of the country only. As India is blessed with a vast solar energy potential, it is the better option to utilize the solar power to meet the future demands. In last few years, it is observed that solar power is increasing drastically as compared to other energy sources with the new advancements in solar technology.

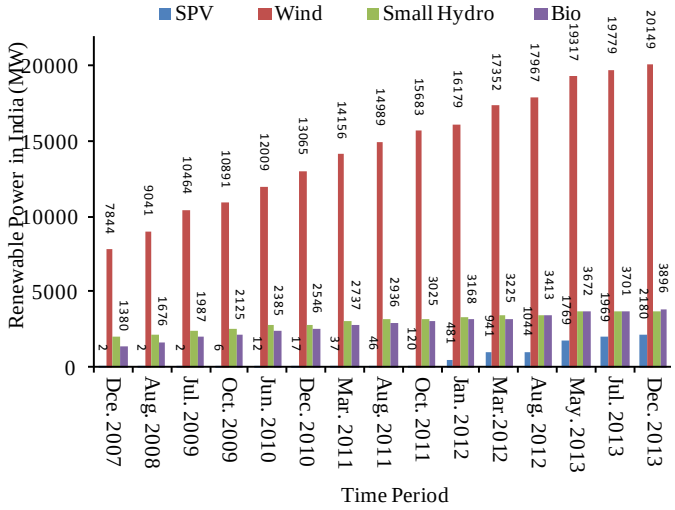

Figure 5: Contribution of Renewable in India

The growth of solar power in India is shown in Fig. 6. Solar power in Indian power sector had contributed just only 2 MW up to July 2009. A little growth was shown in December 2010, with a generation capacity of around 17 MW. A significant change in solar power sector had occurred in October 2011. In last two years solar power generation capacity had increased rapidly and reached to 2180 MW, which is around 18 times of the previous generation capacity. At present solar power shares more than 7% of the total renewable power capacity of India.

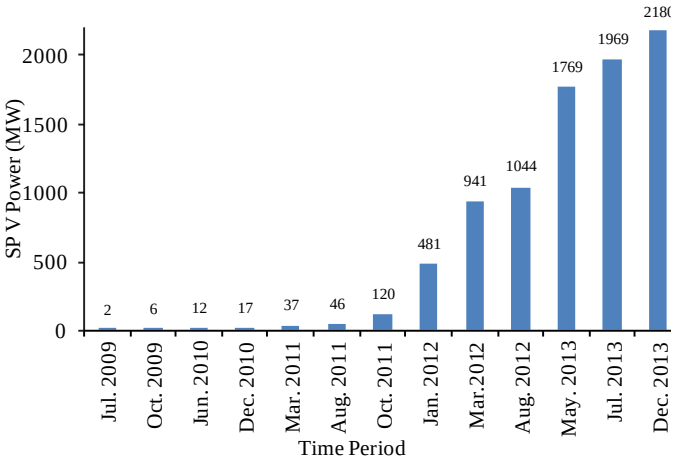

Figure 6: Growth of Solar Power in India

V. CONCLUSION

From this analysis, it is concluded that the demand of power is increasing drastically. The demand of power would increase to about 5 times of the present installed capacity by 2030. The gap is to be bridged by using renewable energy resources to be harnessed at maximum level with improved conversion efficiency. It is also observed that photovoltaic technology will play an important role in the future power sector.

REFERENCES

[1] P. Garg, "Energy scenario and vision 2020 in India,"*Journal of Sustainable Energy & Environment*, vol. 3, pp. 7-17, 2012.

[2] India Power Corporation Limited:
http://www.ipclindia.com/IPCLCorporateProfile_March-2011.pdf

[3] Ministry of Power:
http://www.cea.nic.in/reports/monthly/executive_rep/dec13.pdf

[4] Ministry of New and Renewable Energy (MNRE):
http://mnre.gov.in/file-manager/akshay-urja/september-december-2013/EN/52.pdf .

[5] N. R. Chowdhary, , S. E. Reza, T. A. Nitol, A. F. I. Mahabub, "Present scenario of renewable energy in bangladesh and a proposed hybrid system to minimize power crisis in remote areas," *International Journal of Renewable Energy Research*, vol. 2, 2012.

[6] Indian Wind Turbine Manufacturers Association :
http://www.indianwindpower.com/news_views.html

[7] M. N. Ambia, N. K. Islam, M. A. Shoeb, M. N. I. Maruf, A. S. M. Mohsin, "An analysis & design on micro generation of a domestic solar-wind hybrid energy system for rural and remote areas-perspective Bangladesh," *ICMEE*, vol. 2, pp. 107-110, 2010.

[8] R. Singh, A. D. Setiawan, " Biomass energy policies and strategies: Harvesting potential in India and Indonesia", *Renewable and Sustainable Energy Reviews*, vol. 22, pp. 332-345, 2013.

[9] Ministry of Power: http://powermin.nic.in/

[10] H. S. Sorathia, D. P. P. Rathod, A. S. Sorathiya, "Bio-gas generation and factors affecting the Bio-gas generation – a review study," *International Journal of Advanced Engineering Technology*, vol. 3, pp. 72-78, 2012.

[11] M. A. Wazed, S. Ahmed, "Micro hydro energy resources in Bangladesh: A review," *Australian J of Basic and Applied Sc.*, vol. 2, pp. 1209-1222, 2008.

Reptiles Inspired Biomimetic Materials and Their Novel Applications

Kishor Kalauni and K. M. Gupta
Department of Applied Mechanics, Motilal Nehru National Institute of Technology, Allahabad -211004, India
Email: kishor.kalauni@gmail.com, kmgupta@mnnit.ac.in

Isha Bharti
Teaching-cum-Research Fellow, Department of Applied Physics, Delhi Technological University, Delhi-110042, India

***Abstract*—For all nature's sophistication, many of its clever devices are made from simple materials like keratin, calcium carbonate, and silica which nature manipulates into structures of fantastic complexity, strength, and toughness. In the past few decades, materials scientists have shown increasing interest in studying the whole variety of biological materials including hard and soft tissues, and to use discovered concepts to engineer new materials with unique combinations of properties. This paper aims at elaborating the development of such biomimetic materials by compiling the ongoing researches. In this regard, the research developments of some newer materials by other investigators have been presented here. Brief details of the development of Gecko feet inspired sticky-bot, Mini-viper model robot, Clothes that change colour, Snakes imitating robot, Robot scorpion are discussed. In these elaborations, it is shown that these biomimetic materials can be effectively used in a large variety of application in near future.**

***Index Terms*—gecko feet inspired sticky-bot, mini-viper model robot, clothes that change colour, snakes imitating robot, robot scorpion**

I. Introduction

Biomimetics is the word most frequently used in scientific and engineering literature that is meant to indicate the process of understanding and applying (to human designs) biological principles that underlie the function of biological entities at all levels of organization. Among the many fields of study of biomimetic, one area is the Mobile Robot. Biomimetics and bio-mimicry are both aimed at solving problems by first examining, and then imitating or drawing inspiration from models in nature. Biomimetics is the term used to describe the substances, equipment, mechanisms and systems by which humans imitate natural systems and designs, especially in the fields of defence, nanotechnology, robot technology, and artificial intelligence. Designs in nature ensure the greatest productivity for the least amount of materials and energy. They are able to repair themselves, are environmentally friendly and wholly recyclable. They operate silently, are pleasing in aesthetic appearance, and offer long lives and durability. Biomimetic materials inspired by biology from molecules to materials and from materials to machines. Some of mimicking of natures are adhesives that mimic gecko fingers, heat-sensing system that mimic viper, colour-changing clothes that mimic chameleons and constant state of balance inspired by snake. They are presented as examples of next generation bio-inspired materials. Biomimetic articulated robots are robots that imitate living creatures and have many modules. Various forms of bio-inspiration and related examples are listed below for a ready reference.

TABLE I. Various Forms of Bio-Inspiration and Related Examples

Biological example	Type of analogy	Biomimetic Materials
Gecko	Adhesion	Dry adhesives
Snakes	Sensing system, and Balancing system	Shape memory alloys (SMAs), Piezoelectric materials, and Electro-active polymers.
Chameleons	Colour changing	Choleric liquid crystals (CLCs)
Scorpion	Behavioural	Central pattern generators

II. Gecko Feet Inspired Biomimetic Products and Materials

Small lizards are able to run very fast up the walls and walk around clinging to the ceiling, very comfortably. Until recently, we could not understand as to how it could be possible for any vertebrate animal to climb up walls like the cartoon and film hero Spiderman. Now, years of research have finally uncovered the secret of their extraordinary ability. Little steps by the gecko have led to enormous discoveries with tremendous implications, particularly for robot designers. A few of them can be summarized as follows:

- Researchers in California believe that the lizard's "sticky" toes can help in developing a dry and self-cleaning adhesive.
- Geckos' feet (Fig. 1a) generate an adhesive force 600 times greater than that of friction. Gecko-like

Manuscript received December 1, 2013; revised February 25, 2014.

doi: 10.12720/ijmse.2.2.122-125

robots could climb up the walls of burning buildings to rescue those inside.

- Dry adhesives could be of great benefits in smaller devices, such as in medical applications and computer architecture.
- Their legs act like springs, responding automatically when they touch a surface. This is a particularly appropriate feature for robots, which have no brain. Geckos' feet never lose their effectiveness, no matter how much they are used; they are self-cleaning and they also work in a vacuum or underwater.
- A dry adhesive could help hold slick body parts in place during Nano surgery.
- Such an adhesive could keep car tires stuck to the road.
- Gecko-like robots could be used to repair cracks in ships, bridges and piers, and in the regular maintenance of satellites.
- Robots modelled after the geckos' feet could be used to wash windows, clean floors, and ceilings. Not only will they be able to climb up flat vertical surfaces, but overcome any obstacles they meet on the way.

(a) (b)

Figure 1. (a) Gecko feet, and (b) Sticky-bot: Gecko inspired wall climbing robot [1]

The water's spreading out incredibly fast as drops fell on to the lizard's back and vanished. Its skin is far more hydrophobic. There may be hidden capillaries, channelling the water into the mouth. A subsequent examination of the thorny lizard's skin with an instrument called a micro-CT scanner confirmed, revealing tiny capillaries between the scales evidently designed to guide water towards the lizard's mouth. With this in mind, Cutkosky [2] endowed his robot with seven-segmented toes that drag and release just like the lizard's, and a gecko-like stride that snugs it to the wall. He also crafted Sticky-bot's legs and feet with a process, which combines a range of metals, polymers, and fabrics to create the same smooth gradation from stiff to flexible that is present in the lizard's limbs and absent in most man-made materials. Stickybot (Fig. 1b) is a four-legged robot capable of climbing smooth surfaces. He subsequently embedded a branching polyester cloth "tendon" in his robot's limbs to distribute its load in the same way evenly across the entire surface of its toes. Sticky-bot now walks up vertical surfaces of glass, plastic, and glazed ceramic tile, though it will be some time before it can keep up with a gecko. For the moment it can walk only on smooth surfaces, at a mere four centimetres per second, a fraction of the speed of its biological role model. The dry adhesive on Sticky-bot's toes isn't self-cleaning like the lizard's either, so it rapidly clogs with dirt. "There are a lot of things about the gecko that we simply had to ignore".

III. Viper as a Model in Its Defense

Dr. John Pearce, of the University of Texas Electrical and Computer Engineering Department, has studied Crotalines [3], better known as pit vipers. His research focused on the pit organs of these snakes. In front of the snake's eye (Fig. 2a) is a tiny nerve-rich depression, called the pit, which is used in locating warm-blooded prey. It contains a sophisticated heat-sensing system—so sensitive, that the snake can detect a mouse several meters away in pitch darkness. The researchers stated that when they unravel the secrets of the pit viper's search-and-destroy mechanism, the methods the snake employs can be adapted more widely to protect the country from enemy missiles.

The snake's pit is a thin membrane rich in blood vessels and nerve bundles. The membrane is so sensitive, and the variations in responses so minute that, to catch and study these signals has proved exceedingly difficult. To understand the functioning of the pit organ, it is necessary to work with delicate measurements and photomicrographs. The Mini-VIPER model robot in (Fig. 2b) weighs around 3.5 kilograms and is equipped with an array of sensors. Most of these conventional sensors, are strain sensors, thermal sensors, and optical sensors. More advanced actuation concepts are typically employed using active materials such as Shape memory alloys (SMAs), piezoelectric materials, and electroactive polymers. Small enough to move through tunnels and narrow alleys, it can be thrown into a building through a window and automatically begins scanning its environment. The robot is designed to protect infantry soldiers from explosives, booby traps and hostile forces lying in ambush.

(a) (b)

Figure 2. (a) Snake, and (b) the mini-viper model [4] photo: Elbit

IV. Chameleons Inspired Colour Changing Clothes

The impressive ability that chameleons (Fig. 3a-Fig. 3b) have to change colours to match their surroundings is both astonishing and aesthetically pleasing. The chameleon can camouflage itself at a speed that quite amazes people. With great expertise, the chameleon uses its cells called chromatophores which contain basic yellow and red pigments, the reflective layer reflecting blue and white light, and the melanophores containing the black to dark brown pigment melanin, which darkens its colour. The technology in colour-changing clothes (Fig. 3c) and the chameleon's ability to change colour may

appear similar, but are in fact very different. Even if this technology can change colour, still it entirely lacks the chameleon's camouflage ability that lets it match its surroundings in moments. For instance, place a chameleon into a bright yellow environment, and it quickly turns yellow. In addition, the chameleon can match not only one single colour, but a mixture of hues.

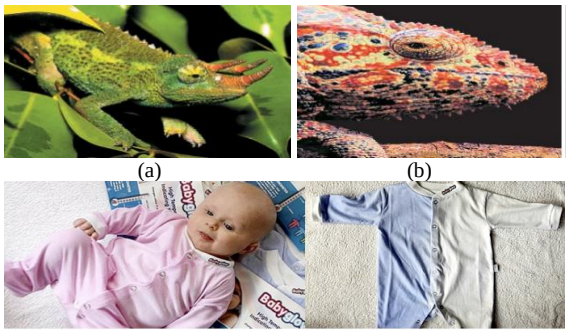

(a) (b) (c)

Figure 3. (a-b) Chameleon's body with a system that lets it change colour to match its surroundings, and (c) Baby clothes that change colour with temperature [5].

The secret behind this lies in the way pigment-containing cells under the camouflage's skin expand or contract to match their surroundings. God has created the chameleon's body with a system that lets it change colour to match its surroundings, endowing it with a considerable advantage. Chameleons inspired for making clothes, bags and shoes that are able to change colours the same way as the chameleon does. Researchers envision clothing made from the newly developed fibre, which can reflect all the light that hits it, and equipped with a tiny battery pack. This technology will allow the clothing to change colours and patterns in seconds by means of a switch on the pack. Yet this technology is still very expensive. Scientists have designed choleric liquid crystals (CLCs) to alter the visible colour of an object to create the thermal and visual camouflage in fabrics. The colour of CLCs can be changed with temperature sensitive thermocouples [6]. The heating-cooling ability of thermocouples can be used to adjust the colour of the liquid crystals to match the object's background colour, providing camouflage or adaptive concealment.

V. Snakes Imitating Robot to Overcome the Problem of Balance

For those engaged in robotics, one of the problems they encounter most frequently is of maintaining equilibrium. Even robots equipped with latest technology can lose their balance when walking. Robot experts attempt to build a balance-establishing learning that the snake (Fig. 4a) never loses its balance. Unlike other vertebrates, snakes lack a hard spine and limbs, and have been created in such a way as to enter cracks and crevices. They can expand and contract the diameter of their bodies, can cling to branches and glide over rocks. Snakes' properties inspired for a new robotic, interplanetary probe developed by NASA's Ames Research Centre which they called the "snake-bot" (Fig. 4b). This robot thus was designed to be in a constant state of balance, without ever getting caught up by obstacles.

(a) (b)

Figure 4. (a) Snake, and (b) Snake-bot [3]

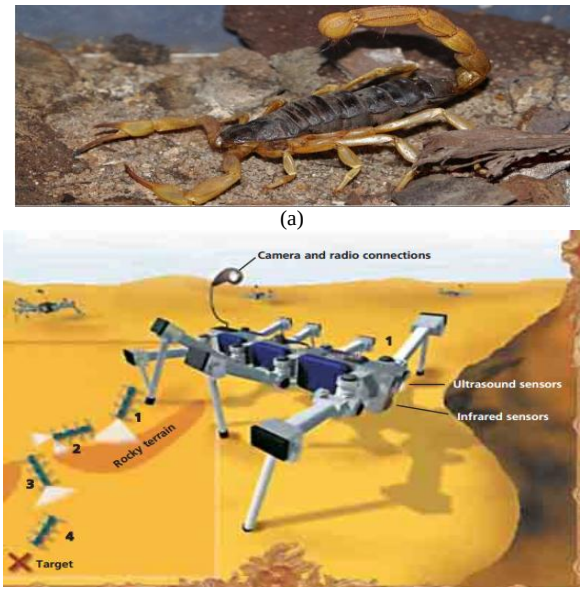

(a) (b)

Figure 5. (a) Scorpion, and (b) Scorpion Robot [3]

VI. A Robot Scorpion Can Work in Harsh Desert Conditions

Sand or other abrasive particles have a way of eroding anything they encounter. Scorpions (Fig. 5a) have been able to survive harsh desert conditions ever since their creation. They live their entire lives subjected to blowing sand, yet they never appear to well, to erode. As a result, items such as helicopter rotor blades, airplane propellers, rocket motor nozzles and pipes regularly wear out and need to be replaced. A group of scientists recently set out to discover their secret, so it could be applied to man-made materials. In the United States, Defence Advanced Research Projects Agency (DARPA) is working to develop a robot scorpion (Fig. 5b) [3]. The reason the project selected a scorpion as its model is that the robot was to operate in the desert. The scientists subsequently applied what they observed in the scorpions' exoskeletons to man-made surfaces. They determined that the effects of erosion on steel surfaces could be significantly reduced, if that steel contained a series of small grooves set at a 30-degree angle to the flow of abrasive particles [7]. But another reason why DARPA selected a scorpion was that along with being able to move over tough terrain very easily, its reflexes are much simpler than those of mammals and can be imitated.

Before developing their robot, the researchers spent a long time observing the movements of live scorpions using high-speed cameras, and analysed the video data. Later, the coordination and organization of the scorpion's legs were used as a starting point for the model's creation. The robot is controlled using a biomimetic approach of ambulation control. The approach is based on two biological control primitives, Central Pattern Generators and Reflexes. Using this approach, omni-directional walking and smooth gait transitions can be achieved. Additionally, the posture of the robot can be changed while walking. The robot was successfully tested in rough terrain with obstacles as high as the robot's body and in different terrains such as sand, grass, concrete and rock piles.

VII. Conclusions

From the above studies, the following conclusions have been drawn.

- Gecko feet inspires in developing a dry, and self-cleaning adhesive. A dry adhesive could help hold slick body parts in place during Nano surgery. Sticky-bot walks up vertical surfaces of glass, plastic, and glazed ceramic tile and also used repair cracks in ships, bridges and piers, and in the regular maintenance of satellites.
- After inspiring from viper a mini robot is designed to protect infantry soldiers from explosives, booby traps and hostile forces lying in ambush. Viper's search-and-destroy mechanism, the methods the snake employs can be adapted more widely to protect the country from enemy missiles.
- Smart and intelligent textiles are important developing area in science and technology because of their major commercial viability and public interest. Chameleons inspired for making clothes, bags and shoes able to change colours.
- Snakes' properties inspired for a new robotic interplanetary probe, which has a constant state of balance, without ever getting caught up by obstacles. The balancing problem can be overcome.
- By mimicking the scorpion, a robot is made for withstand harsh desert conditions. The robot can be asked to go to a specific region and, with a camera in its tail, send back to base images of the location

References

[1] K.-J. Cho, J.-S. Koh, *et al.*, "Review of manufacturing processes for soft biomimetic robots," *International Journal of Precision Engineering and Manufacturing*, vol. 10, no. 3, pp. 171-181, Jul. 2009.

[2] T. Mueller, "Biomimetics: design by nature," *National Geographic Magazine*, vol. 213, no. 4, pp. 68-91, 2008.

[3] H. Yahya, "Biomimetics: Technology imitates nature," *Global Publishing*, Mar. 2006.

[4] Y. Lappin, "Elbit unveils new defense products," in *Proc. Latrun Conference*, Latrun, Israel, Jul. 2010.

[5] Brian, "Baby clothes that change color with temperature," *Stories, Elemental/Exposing the Positive*, Oct. 14, 2010.

[6] A. V. Singh, *et al.*, "Bio-inspired approaches to design smart fabrics," *Materials & Design*, vol. 36, pp. 829-839, 2011.

[7] B. Coxworth, "Wear-resistant surfaces inspired by scorpions," *American Chemical Society journal Langmuir*, Jan. 26, 2012.

Kishor kalauni is a postgraduate student of Material Science and Engineering discipline in the Department of Applied Mechanics of Motilal Nehru National Institute of Technology, Allahabad, India. He obtained Degree in Mechanical Engineering in 2010. He has authored 3 research papers in reputed International Conferences. His major fields of study are Bio-composites and Biomimetic Materials.

Dr. K.M. Gupta is a Professor in the Department of Applied Mechanics, Motilal Nehru National Institute of Technology, Allahabad, India. He has over 35 years of teaching, research and consultancy experience. He obtained Postgraduation (M.E. with Honours) in 1977, and completed his Doctorate (Ph.D.) degree from University of Allahabad.

He has authored 30 books and edited 2 books on Engineering subjects, and a chapter in Scrivener Wiley published 'Handbook of Bio-plastics and Bio-composites Engineering Applications'. He has also authored 106 research papers in reputed International and National journals to his credit. He has presented his research papers in 16 International conferences abroad has also chaired 7 International Conferences in China, Singapore, Dubai, Bangkok etc.

Professor K. M. Gupta has acted as Editor-in-Chief of The International Journal of Materials, Mechanics and Manufacturing (IJMMM), has edited many International Journals and International Conferences. He has worked as reviewer for various International and National Journals, and has acted as Member of several Editorial Board. In recognition to his academic contribution at International level, Marquis Publication (USA) has included him in the list of 'World Who's Who in Science and Engineering 2007' and 'Who's Who in the World 2008'. The International Biographical Centre, a leading research institute (Great Britain) has also selected him as one of the '2000 Outstanding Scientists 2009' from across the world; and Rifacimento International Publisher has included his biographical-note in 'Reference Asia: Asia's Who's Who of Men and Women of Achievement. Earlier, he has served as Dean of Research & Consultancy, Head of the Applied Mechanics Department at Motilal Nehru National Institute of Technology Allahabad. He has acted as Chairman of various Research Selection Committees, of Research Project Monitoring Committees and other Administrative Committees of his Institute and other Universities. He has also served as Chairperson, Community Development Cell (CDC) of MNNIT for several years. Presently, Dr. Gupta is teaching Materials Science, Engineering Mechanics, Thermodynamics of Materials, Electrical and Electronic Materials etc. His research interests are in the fields of Materials Science, Composite Materials, Stress Analysis, Solid Mechanics etc.

Isha Bharti is from New Delhi, India, currently working as Teaching-cum-Research Fellow in the department of Applied Physics, Delhi Technological University. She completed her Masters (M.Tech.) in Nanoscience and Technology with specialization in Nanobiotechnology from Delhi Technological University in 2011. Her major field of study is synthesis and fabrication of Nanobiotechnological materials, luminescent materials for novel biomedical applications and diagnostic therapies, etc.

Risk Management in Supply Chain using PetriNet

[1]Pranay Bhardwaj, [2]Prateek Singh, [3]Girish Kumar

Delhi Technological University
Email: [1]prnybhrdwj@gmail.com, [2]Prateek.dce14@gmail.com

Abstract- This paper is aimed at formalising an objective method to analyse and assess operational risk in a Supply Chain network. The proposed method exploits the analogy between the supply chain network and dynamical systems. We wish to identify the risky events characterising a general supply chain by constructing and studying its Petri Net. Here we have tried to simulate the Petri Net of the network through MATLAB so we can analyse the results to identify the risky events in the network and more importantly, the contribution of these risky events towards disruption of the system, i.e. stock-outs at the retailer end. We have applied the method to a single item, 3-stage Supply Chain and have tried to make the model more relevant by adding events such as partial-fulfilment of demand at the retailer stage and complete non-availability of transportation resources during scheduled servicing at the distributor and manufacturer stage, thereby making the model more robust and closer to reality.

Index Terms—MATLAB, Petri Net, Risk, Supply Chain

I. INTRODUCTION

With the spread of Globalization and the advances in the field of communication and IT, this world has become a very small place, with various inter-connections. What it means for businesses around the world is that even small incidents in one part of the world can have big impacts on another part or the world at large. The well-known terrorist event of September 11, 2001 in USA led to the closure of US Air space, Hurricane Floyd flooded a Daimler Chrysler plant leading to closure of the company's 7 other plants across North America, Toyota was forced to shut down 18 plants for almost 2 weeks following a fire in 1997 at one of its brake fluid supplier, and many other such examples are present which have cost companies major losses in business because of small events that disrupted the supply chain. Managing supply chains in today's competitive world is increasingly challenging. "The greater the uncertainties in supply and demand, globalisation of the market, shorter and shorter product and technology life cycles, and the increased use of manufacturing, distribution and logistics partners resulting in complex international supply network relationships, have led to higher exposure to risks in the supply chain." [11]

With the broad aim of studying these risks inherent in a supply chain, our team decided to focus on the supply chain in its simplest form and study the areas where a disruption will have maximum effect on the whole supply chain at large. Being engineering graduates, we are trying to model a distributed system like supply chain by adding mathematical rigour to it. For the same purpose, we have modelled a simple 3-tier supply chain through Petri Net. Later we realized that the present work available on the same is considering only complete fulfilment of the demand as the basis of measurement of supply-demand dynamics. However, in real world, we also have partial fulfilment of demand as an alternative for lack of supply in comparison to demand. Keeping that in mind, our team tried to re-model the Petri Net to include partial fulfilment of the orders. The same has been presented in this project report. The attempt still lacks mathematical rigour as the model is very complex. However, we have succeeded in getting a graphical representation of the same that satisfies the basics.

MATLAB has been used to simulate the Petri Net model. The report presents the findings of the simulation of the model with partial-fulfilment. Our results have shown a considerable decrease in the total number of completely unsatisfied customers and the results are consistent over a large number of iterations.

We would also like to bring to the attention of the readers of this report that while Supply Chain risk management includes various kinds of risks, we, with the aim of simplifying the whole thing for simulation, are focussing only on Stock-outs and Bull-whip effect due to information distortion, transport line breakage and production disruption. The elements considered in this simplified 3-tier supply chain are restricted to Customer-Retailer-Manufacturer-Supplier and the Transport system connecting them all..

II. METHOD

In real life, a customer is not always necessarily classified as 'satisfied' or 'unsatisfied'. In many industries, the customer orders for partial fulfilment of demand in case the stock level is low for complete fulfilment. This is an important aspect that will give a better picture of the risks inherent in Supply Chain.

Moreover, the transport model linking the manufacturer-wholesaler and wholesaler-retailer also can be made closer to reality by adding the fact that availability of transport also varies because the need for servicing and the rate of failure varies with time. These problems are the main points of concerns that have been addressed by this project report.

The Proposed Approach

The proposed approach for simulating the Supply Chain operating without any biased deficiencies consists of applying Petri Net and then simulating it in MATLAB. Firstly, the Petri Net corresponding to the theoretical supply chain under study is built. The disruptions the system can suffer are of two kinds. The more harmful disruptions are in the form of totally unmet demand. The less harmful disruption to the system comes from partially met demand. While building the Petri Net, it is important to put in the net some places which do not correspond to any physical element of the network but record, through the tokens they contain, the number of times the disruptions of each kind has occurred. By means of the reachability graph of the considered Petri Net, sequences of fired transitions which enable marks characterized by tokens in the above mentioned places can be determined and hence, risky events can be identified.

Phase	Technique	Tool
Risk Analysis	Dynamic System modeling and control	Petri Net Reachability Graph (MATLAB)
Risk Assessment	Simulation Statistical Analysis	Event Driven Simulation ANOVA/MATLAB

Table No. 3

If there are n risky events the network can suffer from, n+ 1 experimental campaign have to be performed on the network. Once when no risky event happens and then in other n experiments, each risky event is taken into account separately.

THE NETWORK

To contain the level of complexity, a single item 3-stage supply chain is considered. In particular network consists of 1 retailer, 1 distributor and one manufacturer. Concerning the retailer, it should be noted that the replenishment policy referred to is the EOQ model modified according to the forecast system.

The elements characterizing the retailer are:

1. Daily demand (Given by the customer arrival time and the customer demand. Customer arrival time fits into an exponential distribution. Customer demand is probabilistically chosen from a set of empirical data)

2. Level of partial satisfaction of customer (In case of failure at the end of the retailer to meet the customer demand, a random number X is generated from a distribution. X ε (1,100). X gives the percentage of original demand acceptable to the customer. The value of acceptable quantity A is given by: A = (Xxd)/100, where d represents the original demand. If A<= M(P6), the entire inventory is emptied and the goods are given to the customer)

3. Economic reorder quantity (Depends upon retailer forecast)

4. Reorder point (Depends upon retailer forecast)

5. Safety stock (Depends upon retailer forecast)

6. Standard and increased delivery time (represented by the probability distribution of the time the retailer has to wait to receive goods both under normal circumstances and when some problems occur)

7. Forecast horizon

8. Forecast accuracy

The distributor too manages his inventories according to the EOQ model. The difference at the level of the distributor comes when we have to model transportation availability. Moreover, the distributor does not get a daily demand. The demand is given by retail orders. The parameters to be considered at the level of the distributor are:

- Initial inventory
- Economic Reorder Quantity (EOQ)
- Reorder point
- Safety stock
- Transportation availability (failure of transportation and the subsequent repair is built into the structure)

- Standard and increased delivery lead time (From the manufacturer)
- Forecast horizon
- Forecast accuracy
- The manufacturer produces goods through predefined production campaigns. The important parameters for the manufacturer are:
- Availability of transportation (Failure and repair is built into the Petri Net)
- Availability of production resources
- Lot sizing policy
- Production lead time
- Time interval two production campaigns
- Inventory

SUPPLY CHAIN PETRI NET

The place P1 and the transition T1 allow customer arrival to be modelled. Whenever there is a token in P1, T1 fires after a duration drawn from the probability distribution of customers' inter-arrival times. The firing of T1 removes the token from P1, generates a token in P2 with an attribute d, a value drawn from the empirical distribution of the number of items bought by a single customer and it simultaneously also generates a token in P1. The transition T3 is fired if the number of tokens in P6 is greater than or equal to d, i.e. if $M(P6) \geq d$. If T3 fires, one token is removed from P2 and one token is generated in P4, recording the number of satisfied customers and one token is created in P5. As soon as the token is generated in P5, T7 fires, removing one token from P5, d tokens are removed from P6 and one token is generated in P8. T9 fires when the marking of P6 (the number of tokens in P6) is less than ROP, i.e. the Re-order Point, creating a token in P12 and removing the token from P8. Otherwise T8 fires and removes the token from P8, dumping the token in P11.

If the demand created by the customer is more than the number of tokens in P6 ($M(P6)<d$), T2 fires creating a token in P3. Depending upon whether the stock level is acceptable to the customer or not, T4 or T6 fires. The probability of acceptance of stock level is proportional to the percentage of demand being fulfilled. T4 fires if the customer accepts the stock level and T6 fires if it is not.

When T4 fires, it removes the token from P3 and creates one in P7. Whenever there is a token in P7, T5 fires instantaneously removing M(P6) tokens from P6, generating a token in P10, which records the number of partially satisfied customers and one token in P12, indicating that it has placed an order with the distributor when T6 fires, it removes the token in P3 and creates one in P9, which records the number of dissatisfied customers.

Whenever there is a token in P12, P23 (indicating availability of transportation) and the EOQr (Economic Order Quantity of the Retailer) quantity is present in the distributor warehouse P13, T10 fires, removing the token from P12, EOQr tokens from P13, and creates one token in P27 and EOQr tokens in P6 after a duration drawn from the distribution of distributor delivery lead times. Simultaneously, it creates a token in P24, which records the number of trips completed since the delivery vehicle underwent its scheduled servicing. If the delivery vehicle hasn't been taken in for servicing (there is a token in P23), the availability of transportation resource is 0.8 M(P24) (equal to the number of trips completed since the last scheduled servicing) is greater than 1 and less than 10. Otherwise, it is 0.7. If the vehicle is deemed unavailable even if there is a token in P23, the delivery time generated is normally distributed with mean equal to 2 days and standard deviation 0.6 days. If the transportation resource is available, the delivery time generated is normally distributed with mean equal to 2 days and standard deviation 0.5 days. T10 fires after the delivery time generated in this process.

The transportation availability of the distributor is modelled in the Petri Net. When a token is in P23 and no token is present in P12 (indicating the retailer hasn't placed an order), T20 after 90 days creating a token in P25. Whenever there is a token in P25, T19 fires after a time which is normally distributed with mean equal to 2 days and mean 0.5 days (to model the time taken up in servicing the vehicle). This removes M(P24) token from P24, thereby resetting the trip meter, one token from P25 and generates one token in P23 and one token in P26 which counts the number of times the vehicle underwent scheduled servicing.

	Element	**Expression Value**
Retailer	Customers inter-arrival time	Exp(0.0069) [days]
	Items bought by the single customer	Disc(0.5,1,0.8,2,0.95, 3,1, 10) [units]
	Initial inventory (R)	650 [units]
	Economic order quantity (EOQr)	(2*100*Dr/3.5*0.005)1/2
	Re-order point (ROPr)	(Dr/15)*2+SS
	Safety stock (SSr)	1.96*[(Dr/15)2*0.52 +2*(1.25*MAD)2]1/ 2
	Supplier delivery lead time	norm(2,0.5) [days]

	(standard)	
	Supplier delivery lead time (non-standard)	norm(2.5,0.6) [days]
	Forecasting horizon	15 [days]
	Forecast accuracy	0.9
Distributor	Initial inventory (S)	1100 [units]
	Economic order quantity (EOQd)	(2*100*Dd/2.5*0.015)1/2
	Re-order point (ROPd)	(Dd/3)*0.13+SS
	Safety stock (SSd)	1.96*[(Dr/3)2*0.032 +0.13*(1.25*MAD)2]1/2
	Transportation resource availability	0.8
	Supplier delivery lead time (standard)	norm(0.13,0.03) [15days]
	Supplier delivery lead time (non-standard)	norm(0.17,0.04) [15days]
	Forecasting horizon	45 [days]
	Forecast accuracy	0.9
Manufacturer	Initial inventory (U)	20000 [units]
	Lot size (LS)	30000 [units]
	Time intervals among 2 campaigns (IC)	40 [days]
	Production lead time	5 [days]
	Production resource availability	0.8
	Transportation resource availability	0.8

Table No. 4 – Synthetic view of considered supply chain [7]

T11 fires when there are less than ROP_D tokens in P13. It eliminates M(P27) tokens from P27 and generates a token in P14. T12 fires whenever there is a token in P14, P16 (representing availability of transportation at the manufacturer end) and more than EOQ_D number of tokens in P19 after a duration drawn from the manufacturer delivery lead times generating EOQ_D tokens in P13, one token in P15, removes one from P14 and EOQ_D tokens from P19. The transportation availability at the manufacturer is modelled as it was at the distributor.

The modeling of the production campaign of the manufacturer is as follows. Whenever there is a token in P22 (implying availability of raw materials for manufacturing), T18 fires after a 5 days (which is the production lead time). The firing creates LS (Lot Size) tokens in P19, and one token in P20. This activates T15 which fires after IC(40) days. IC is the number of days between successive production campaigns. Firing of T15 generates a token in P21. Depending upon whether production resources are available or not, T16 or T17 fires. T16 fires if the resources are not available and T17 fires if they are. The probability of T17 firing is 0.8. Otherwise T16 fires after one minute generating a token in P21 again. Firing of T17 creates a token in P22 indicating that production resources are now available.

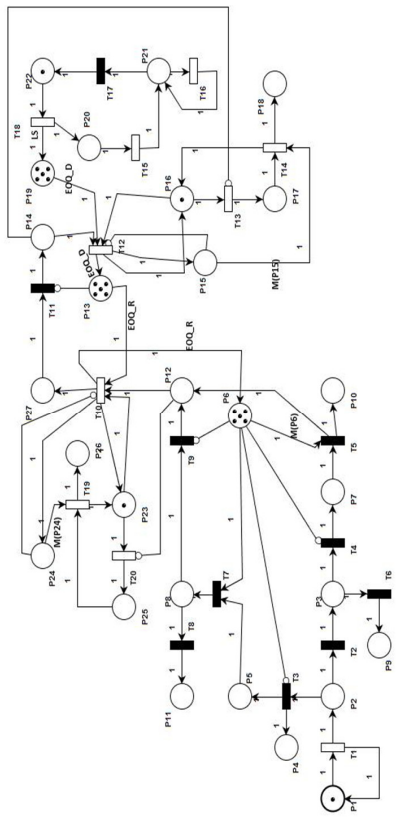

Figure 10

Algorithm Used

1. Customer arrives at the retail store. Arrival interval is distributed exponentially.
2. Customer creates a demand d.
3. Retailer checks the warehouse level to see if the demand can be fulfilled.

4. If the demand can be fully met, the customer is satisfied; warehouse level goes down by the value of his demand.
5. If the demand cannot be fully met, the percentage of demand being fulfilled is equal to the probability of acceptance of warehouse stock by the customer.
6. If the customer in such a case finds the warehouse stock acceptable, he is assumed to be partially satisfied. Otherwise, he is assumed to be a dissatisfied customer.
7. The retailer compares his warehouse level after every customer with his re-order value. If he finds it less, he places an order with the distributor provided he hasn't done so already.
8. The distributor, on receiving an order from the retailer, checks his inventory level and transportation availability. If the demand can be met and the delivery vehicle has not been sent for scheduled servicing, a normally distributed delivery time is generated.
9. When the time elapsed since the retailer re-ordered becomes equal to the delivery time generated, the retailer demand is fulfilled. The distributor inventory reduces by the same level.
10. After every order, the distributor checks his warehouse. If the inventory level is less than his re-order point, he places an order with the manufacturer provided he hasn't done so already.
11. The manufacturer on receiving an order from the distributor looks at his inventory level and transportation availability. If the inventory level is sufficient to meet the demand and the delivery vehicle has not been sent for scheduled servicing, a normally distributed delivery time is generated.
12. When the time elapsed since the distributor re-ordered becomes equal to the delivery time generated, the distributor demand is fulfilled. The manufacturer inventory reduces by the same level.
13. The manufacturer runs a production campaign every 40 days provided production resources are available. The lot size is 30000 and the campaign lasts 5 days.
14. Running simultaneously are the models for transportation availability at the distributor and the manufacturer. They are scheduled for servicing once every 90 days provided their customer in the Supply Chain hasn't placed an order. After every delivery, the trips completed by the delivery vehicle are increased by 1. The number of trips completed is reset after servicing. The availability of transportation resource is 0.8 if the trips completed lie between 1 and 10. Otherwise it is 0.7.
15. This Supply chain model is run for 180 days an n number of times and the number of satisfied, partially satisfied and dissatisfied customers are plotted against the number of iterations. The number of dissatisfied customers gives a measure of the inefficiency of the system.

III. RESULTS

The modified Petri Net with the addition of partial fulfilment of customers improves the efficiency of the supply chain. The percentage of 'dissatisfied' customers comes down from 2.193% to 1.461%. Therefore the efficiency of the supply chain improves by 0.718% and the level of 'dissatisfied' customers is reduced by 32.89%. Not being able to meet the customer demand at the level of the retailer is the only disruption the supply chain is supposed to refer to.

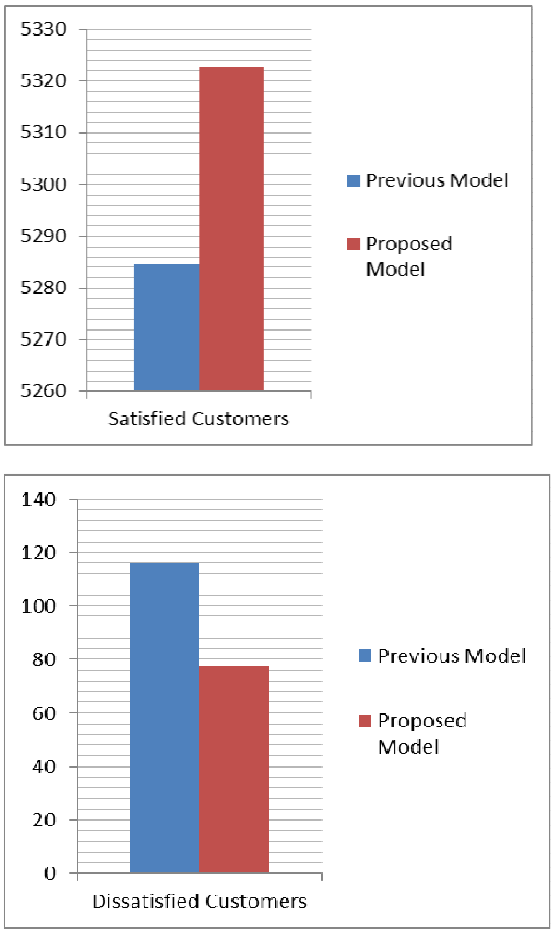

Figure 11 Comparison of models for number of satisfied customers and unsatisfied customers at the end of simulation

Comparison of the previous model and the proposed model has been done using Monte Carlo simulations. Satisfied, Unsatisfied and Partially-satisfied customers have been plotted against time interval in a 180 day campaign. Simulation Results from MATLAB are given below.

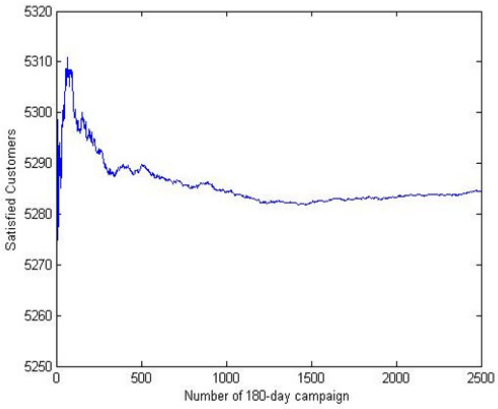

(1) Satisfied customers in previous model

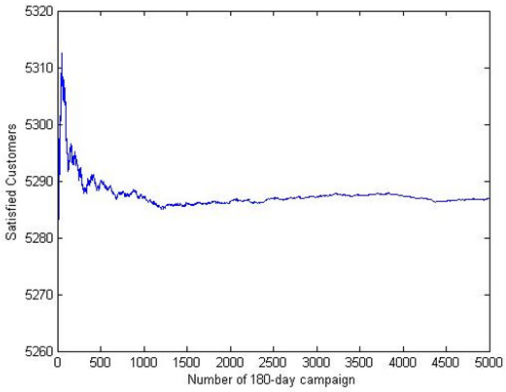

(2) Satisfied customers in proposed model

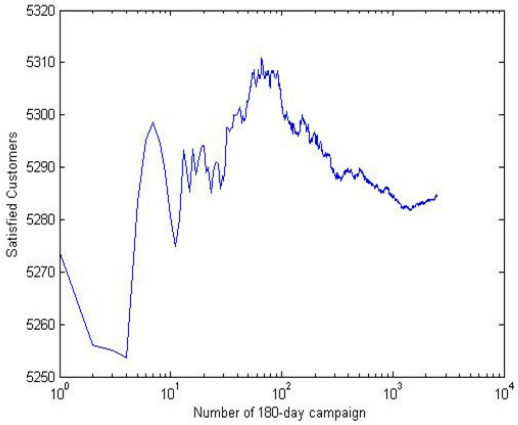

(3) Semi log plot of previous model

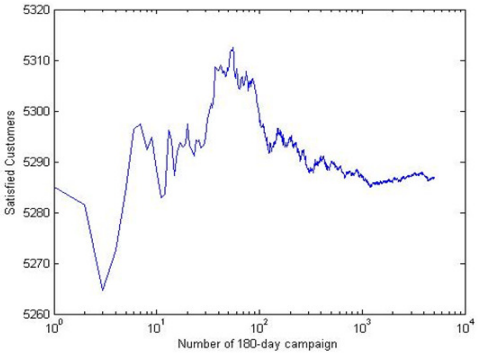

(4) Semi log plot of proposed model

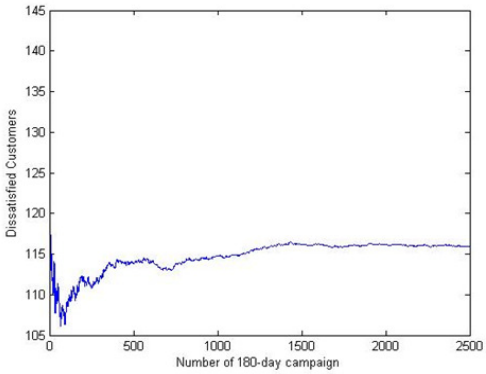

(5) Dissatisfied customers in previous model

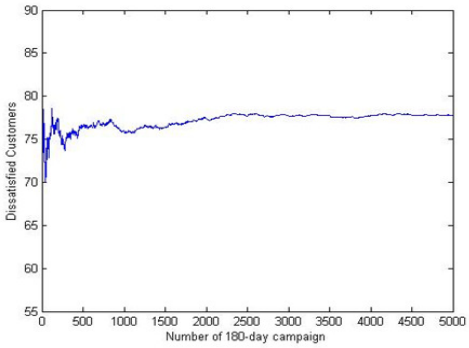

(6) Dissatisfied customers in proposed model

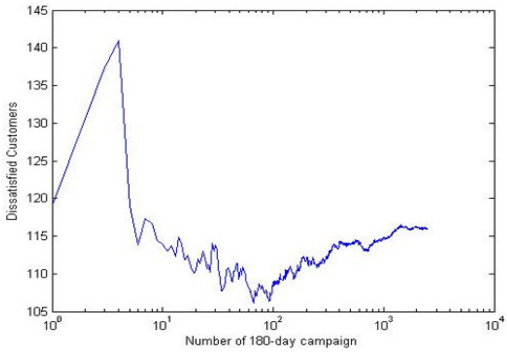

(7) Semi log plot of previous model

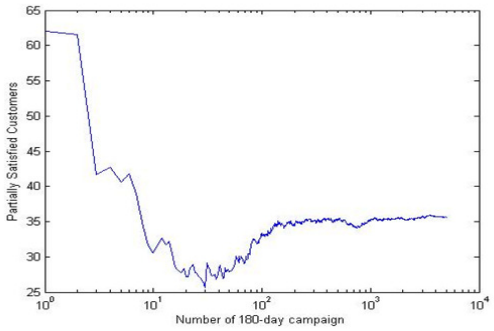

(8) Semi log plot of proposed model

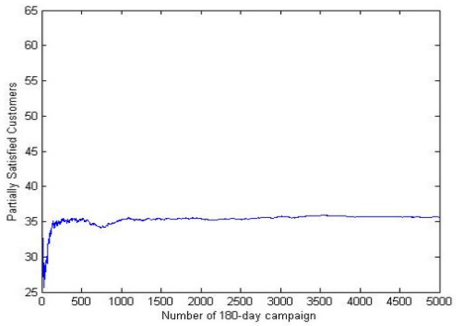

(9) Partially satisfied customers

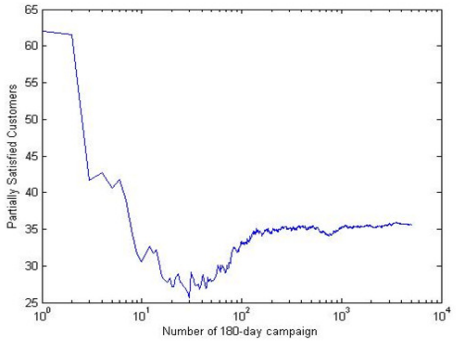

(10) Semi log plot of partially satisfied customers

Figure 12 Comparison of MATLAB simulation graphs for 180-day campaign

IV. CONCLUSION

The model we built for the supply chain mirrors the actual world better than the models available previously. Therefore the risk factors identified by our model will be more relevant in the real world and would be a better diagnosis of the problems that the Supply Chain faces. The efficiency of the supply chain increases by introducing the clause of partial fulfilment of demand at the retailer stage but delivery times get worse by making the model more real as we have incorporated scheduled servicing of delivery vehicles. Overall, the Supply chain has become more efficient by 0.7% (approximately) and relatively, the efficiency of the supply chain goes up by about 33%.

REFERENCES

[1] P. Biljana, V. Mirko and M. Dragan, "A Supply Chain simulation model based on hierarchical Coloured Petri Net," Competitivness In The EU – Challenge For The V4 Countries, Faculty of Economics and Management SAU, Nitra, May 17-18, 2006

[2] C. Papanagnou and G. Halikias, "Analysing different ordering policies in a series Supply Chain by using Coloured Petri Nets," Control Engineering Research Centre City University, EC1V 0HB, London, UK.

[3] F. Strozzi, C. Noè and J. Zaldívar, "Stability control in a Supply Chain: Total costs and Bullwhip effect reduction," Engineering Faculty, Carlo Cattaneo University (LIUC), Castellanza, Italy European Commission, Joint Research Centre, Ispra, Italy

[4] Y. Narahari, "overview and foundations," Petri Nets, Resonance, Aug. 1999

[5] E. Liu, A. Kumar and W. van der Aalst, "A formal modeling approach for Supply Chain event management."

[6] M. Dragan, P. Biljana and V. Mirko, "Bullwhip effect and Supply Chain modeling and analysis using CPN tools," Operations Research Laboratory, Faculty of Organizational Sciences, University of Belgrade.

[7] T. Rossi, A. Sianesi and C. Noe, "Analyzing and assessing operational risk in Supply Chains through Petri Nets and simulation techniques".

[8] J. Reeb and S. Leavengood, "Simulating a manufacturing system: An introduction," 2003.

[9] R. Lummus and R. Vokurka, "Defining Supply Chain management: A historical perspective and practical guidelines," Industrial Management & Data Systems, Vol. 99(1), 1999

[10] W. Lucato and M. Júnior, "Solving actual production problems through Monte-Carlo simulations," POMS 22nd Annual Conference Reno, Nevada, USA, 2011.

[11] M. Christopher and H. Lee, "Mitigating Supply Chain risk through improved confidence," International Journal of Physical Distribution & Logistics Management, 2004

[12] A. Cox , J. Sanderson , G. Watson, "Power Regimes: A new perspective on managing Supply Chains and Networks, 2004.

[13] B. Sarkar, S. Sanyal, N. Chaki, "A Stochastic Net Model for controlling Bullwhip Effect in virtual Multitier Retail Network", University of Calcutta, 2011

[14] R. Landeghem, C. Bobeanu, "Formal Modelling of Supply Chain: An incremental approach using Petri Net", Ghent University, Department Industrial Management, Belgium

◈◈◈

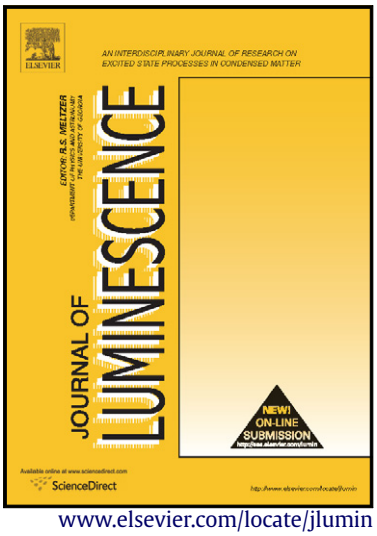

www.elsevier.com/locate/jlumin

Spectral characterization of Sm^{3+} ions doped Oxy-fluoroborate glasses for Visible Orange Luminescent Applications

Sk. Mahamuda, K. Swapna, M. Venkateswarlu, A. Srinivasa Rao, Suman Latha Shakya, G. Vijaya Prakash

PII: S0022-2313(14)00300-7
DOI: http://dx.doi.org/10.1016/j.jlumin.2014.05.017
Reference: LUMIN12702

To appear in: *Journal of Luminescence*

Received date: 18 March 2014
Revised date: 4 May 2014
Accepted date: 19 May 2014

Cite this article as: Sk. Mahamuda, K. Swapna, M. Venkateswarlu, A. Srinivasa Rao, Suman Latha Shakya, G. Vijaya Prakash, Spectral characterization of Sm^{3+} ions doped Oxy-fluoroborate glasses for Visible Orange Luminescent Applications, *Journal of Luminescence,* http://dx.doi.org/10.1016/j.jlumin.2014.05.017

Spectral Characterization of Sm^{3+} ions doped Oxy-fluoroborate Glasses for Visible Orange Luminescent Applications

Sk. Mahamuda[1], K. Swapna[1], M. Venkateswarlu[1], A. Srinivasa Rao*[1, 2], Suman Latha Shakya[3] and G. Vijaya Prakash[3]

[1]Department of Physics, K L University, Green Fields, Vaddeswaram-522 502, Guntur (Dt.), A P, India
[2]Department of Applied Physics, Delhi Technological University, Bawana Road, New Delhi-110 042, India
[3]Nanophotonics Laboratory, Department of Physics, Indian Institute of Technology-Delhi, Hauz Khas, New Delhi-110 016, India
Corresponding author, **E-mail: drsrallam@gmail.com, Tel: +91 85860 39007, Fax: +91 01127871023.*

Abstract

Oxy-fluoroborate (OFB) glasses doped with different concentrations of Sm^{3+} ions have been prepared by using conventional melt quenching technique and characterized for their lasing potentialities using the spectroscopic techniques such as FTIR, optical absorption, emission and emission decay measurements. The FTIR spectrum has been recorded to know the various functional groups present in the OFB base glass. From the absorption spectra, the bonding parameters (δ) were evaluated to find the bonding nature present between Sm^{3+} ions with its neighbouring ligands. The Judd-Ofelt intensity (J-O) parameters (Ω_λ, where λ=2, 4, and 6) measured from the experimental oscillator strengths of the absorption spectral futures, are used to evaluate the radiative parameters for the fluorescent transitions $^4G_{5/2}\rightarrow{}^6H_{5/2}$, $^4G_{5/2}\rightarrow{}^6H_{7/2}$, $^4G_{5/2}\rightarrow{}^6H_{9/2}$ and $^4G_{5/2}\rightarrow{}^6H_{11/2}$ of Sm^{3+} ions in OFB glasses. The asymmetric ratio has been evaluated to understand the local disorder of Sm^{3+} ions in the glass network. The experimental lifetimes (τ_{exp}) measured from the decay curves are coupled with radiative lifetimes (τ_{rad}) to measure quantum efficiency (η) of the prepared glasses. The experimental lifetimes (τ_{exp}) for $^4G_{5/2}$ emission state are decreasing with increase in Sm^{3+} ion concentration due to energy transfer. In order to elucidate the nature of energy transfer mechanism, the non-exponential decay curves are well fitted to Inokuti-Hirayama model for S=6, which indicates that the energy transfer mechanism is of dipole-dipole type. The branching ratio (β_R), stimulated emission cross-section (σ_{se}) and quantum efficiency (η) values measured for the most intense emission transition $^4G_{5/2}\rightarrow{}^6H_{7/2}$ (598 nm) optimises the concentration of Sm^{3+} ions as 1 mol% to produce bright visible orange lasing emission from these OFB glasses.

Keywords: *Amorphous materials, optical materials, optical properties, luminescence*

1. Introduction

Quite recently, glasses doped with transition metal and rare earth ions have attracted a great deal of attention because of their memory and photo conducting properties. They also find potential applications in diversified fields such as solid state lasers, luminescent solar energy concentrators, optical detectors, waveguide lasers, optical fiber amplifies, hole burning high density memories and optoelectronic devices [1-7]. It is well known that, a glassy host with phonon energies at lower end patronages radiative transitions rates very much and is much useful for the design and development of the optical devices such as up-convertors, light emitting diodes (LEDs) and memory devices [8-10]. Since the luminescence quantum efficiency and emission transitions band widths of the doped rare earth ions strongly depends on the structural changes of the host matrices, apt selection of a suitable host material is very much essential in order to obtain better luminescence efficiency needed for the design and development of an optical devices. Among various optical glasses available, borates are the most important glassy systems owing to their peculiarities such as low melting point, high optical transparency, high chemical stability and good rare earth ion solubility. They are also found to be robust and inexpensive. All the aforementioned novel characteristic features possessed by the borate glasses makes them to act as an exalting host matrices and the best choices for RE ions doping for the applications where the flexibility of size and compositions of the material are necessary. On the other hand, the high phonon energies (~1300-1500 cm^{-1}) possessed by borate glasses encourage non radiative emission process very much and cannot acts as good laser host. From this point of view, fluoride hosts are found to be superior to borates as the former hosts need not encourage non-radiative transitions. However fluoride hosts are found to be toxic, corrosive and needs to be synthesizing in absence of oxygen under controlled atmosphere. Owing to all these difficulties, fluoride hosts are not used commonly. But the addition of alkali/alkaline earth oxide/fluoride converts the boron coordination and the structural groups from one to another depending on the type and concentration of the alkali/alkaline earth oxide/fluoride. Among the oxide and mixed oxy-fluoride glass compositions, lead borate glasses doped with RE ions seems to be very attractive systems for applications in laser technology. Not only this but also the addition of fluoride compounds to borate glasses as network modifiers can reduce the redundant phonon energies of borate glasses considerably and eventually increases their mechanical strength [11-18]. Especially the fluoride compounds such as BaF_2 and CaF_2 with their less phonon energies

(~346 cm^{-1}) added to borate host as network modifiers, can strongly reduce the phonon energies of borates (~1300-1500 cm^{-1}) to a relatively lower values [19]. Moreover, the solubility of RE ions is also larger in the fluoride medium than in the oxide [20] and the fluoride compounds present in borates helps in reacting and removing the –OH group from the borate glass. Over and above, the fluoride compounds in a glass can reduce scattering and dispersion losses which are very much required for the construction of LEDs.

In recent years, glasses containing ZnO are playing a vital role in technology and attracting many researchers, because, ZnO being a non-toxic and non-hygroscopic in nature possesses excellent optical, electrical and magnetic properties. ZnO based glasses are very much useful in developing the optoelectronic devices, luminescent solar energy converters, gas sensors and ultraviolet emitting lasers [21]. ZnO enters in to a glass as a network modifier and breaks the B-O-B bonds (normally the oxygen's of ZnO breaks the local symmetry while Zn^{2+} ions occupies the interstitial positions) and forms co-ordinate defects known as dangling bonds. However, when ZnO forms covalent bond with four oxygen atoms in glass network, it may form ZnO_4 structural units [22, 23]. The presence of Al_2O_3 in a borate glass network will decrease the tendency of crystallization and improves the stability of the glass structure [24] besides its action as an intermediate in a glass. It is well known that intermediates have mid-position between network former and network modifier. Because of this intermediate nature aluminium may either form tetrahedral and so reinforce the network with co-ordination number 4 or loosen the network in analogy to network modifiers with co-ordination number 6. In $BaO-Al_2O_3-B_2O_3$ glass system, it was reported that [25-27], Al_2O_3 co-ordinated with the oxygen atoms and forms AlO_4 or AlO_6 units in the glass structure. It was also assumed that aluminium ions enter the glass in the form of triclusters, where the triclusters consist of three tetrahedral BO_4 and/or Al_2O_3 in the form of AlO_4 having an oxygen in common [27]. For $MO-Al_2O_3-B_2O_3$; (M = Sr, Ca and Ba) glassy system Owen [28] proposed that some of the M atom associate themselves with Al_2O_3 forming AlO_4 and the rest by reacting with B_2O_3 produces BO_4 or non-bridging oxygen ions. The influence of alkaline earth oxides (Ca, Sr and Ba) as network modifiers on the structural and insulating strength of a glass matrix $RO-Na_2O-B_2O_3$ [R=Ca,Sr and Ba] was discussed in detailed by Yusub et al.[29]. Sakka et. al [30] concluded that the ratio of Al_2O_3 / CaO can affects the glassy structure where AlO_4 is dependent on B_2O_3 content. Pernice et al. [31] reported that, in BaO-

Al_2O_3-B_2O_3 glassy system against devitrification process the stability of the glass was increased by Al acting as a good glass former.

In the backdrop of the above discussion, contemplating on all the scientific patronages offered by B_2O_3, BaF_2, CaF_2, ZnO and Al_2O_3, for the present investigation, we prepared a germane oxy-fluoroborate (OFB) glassy system using the aforementioned chemicals as constituent elements. As explained earlier, a good glass former like B_2O_3 added with BaF_2, CaF_2, ZnO and Al_2O_3 as network modifiers can give a better glassy system, since they combine the transparency, mechanical and chemical resistance and the feasible production with the low phonon energy of the fluoride matrices.

Among all the rare earth ions, Sm^{3+} ions are having their applications in diversified fields such as high density optical memory storage devices, under sea communication, colour display systems, solid state lasers in visible region, lasers needed for next generation nuclear fusion and gain media in the microchip laser at higher doping levels [32-34]. Sm^{3+} doped glasses give high power lasers in reddish-orange visible region, having applications in pre-clinical radiation treatment for cancer known as micro beam radiation therapy (MRT) [35]. In Sm^{3+} doped materials an efficiency gap existing around 560 nm known as "yellow gap" [36, 37] is falling in the wavelength range called amber range (590-600 nm) produced by efficient diodes made up of either III-nitrides or III phosphides. These amber LEDs are best suited for automotive applications such as day-time-running lights used in vehicles for tuning and also traffic signals. Moreover, it is impossible for the multi-phonon non-radiative decay process to exit in the host materials having high phonon energies such as borate glasses and do not affect the reddish-orange emission at ~600 nm because of the huge energy gap (~7250 cm^{-1}) existing between $^4G_{5/2}$ fluorescent level and the lower lying level $^6F_{11/2}$ of Sm^{3+} ions. Further due to the lack of lower lying excited states, Sm^{3+} doped laser materials are found to be superior to the other rare earth doped materials from the point of view of concentration quenching effect with no excited state absorption and up conversion losses.

The present paper reports the results obtained on the "spectroscopic and stimulated emission characteristics of Sm^{3+} ions in Oxy-fluoroborate (OFB) glasses" thoroughly studied by us using the spectroscopic techniques such as absorption, photoluminescence and decay measurements. The Judd-Ofelt (J-O) intensity parameters Ω_λ (λ = 2, 4, 6) determined from the measured oscillator strengths (f_{exp}) are used in evaluating the radiative properties such as

spontaneous transition probabilities (A_R), total transition probabilities (A_T), radiative branching ratios (β_R) and radiative lifetimes (τ_R) for the observed fluorescent levels of Sm^{3+} ions in OFB glasses. The laser characteristic parameters namely the experimental branching ratios (β_{exp}), stimulated emission cross-sections (σ_{se}), gain bandwidths (σ_{se} x $\Delta\lambda_P$), optical gain (σ_{se} x τ_R) and quantum efficiency were evaluated to optimise the doped rare earth ion concentration in OFB glasses for solid state lasers and optical fibre amplifiers in visible region.

2. Experimental

2.1. Synthesis

In the present work, the glass samples with the selected chemical composition of 15 ZnO – (5-x) Al_2O_3 –10 BaF_2 – 10 CaF_2 – 60 B_2O_3 –x Sm_2O_3 (further known as OFBSm1, OFBSm5, OFBSm10, OFBSm15, OFBSm20 and Sm25 for x = 0.1, 0.5, 1.0, 1.5, 2.0 and 2.5 mol %) were prepared by conventional melt quenching technique. The stoichiometric compositions of the batch materials about 8g were taken into an alumina crucible and heated at 1200^oC in an electrical furnace for 40-60 min until the homogeneous melt was obtained. This melt was then poured rapidly on a pre-heated brass mould and compressed rapidly with another brass mould to obtain globular shaped glass samples with uniform thickness. To eliminate thermal strains produced in glass samples, annealing was done at 400°C for 2 hrs.

2.2. Characterization

The densities of the prepared glasses were measured by using Archimedes's method with water as an immersion liquid. The XRD measurement were taken using XPERT-PRO diffractometer with CuKa radiation (k=1.54°A) in the 2θ angle range 0° - 80° with step size 0.02° s^{-1}. By using the Brewster's angle method (He-Ne laser with a wavelength 650 nm line), the refractive indices for these glasses were measured. The FTIR spectrum for an undoped OFB glass has been recorded using a Thermo scientific make Nicolet-380 spectrometer. The room temperature optical absorption spectra of these glass samples were recorded by using JASCO model V-670 UV-vis-NIR spectrometer in the spectral wavelength range 350-2000 nm with a spectral resolution of 0.1 nm. RF-5301 PC Spectrofluorophotometer was used to record the photoluminescence excitation and emission spectra for all these glasses at room temperature. Using 410 nm CW laser as an excitation source, the time-resolved photoluminescence (PL) measurements were carried out using a home-built set up. The emission from sample was coupled into a monochromator (Acton SP2300) coupled to CCD (charge coupled detector)

through the appropriate lenses and filters. For time-resolved PL measurements, a frequency generator (5 Hz), lock-in amplifier, digital storage oscilloscope and a monochromator (Acton SP2300) coupled to a photo multiplier tube (PMT) were employed. A laser scanning confocal microscope (Olympus, BX51) equipped with XY-piezo stage and excited with 410 CW laser was used to record PL images given by the OFB glasses.

3. Results and Discussion

3.1 XRD Spectral Analysis

Fig. 1 shows the XRD pattern of an undoped OFB glass. A broad hump at lower angles ($2\theta=28°$) authenticates the presence of Short Range Ordering (SRO) in glasses. The featureless XRD spectrum obtained confirms the non-crystalline nature of the prepared OFB glasses.

3.2 Physical properties

From the experimentally measured densities and refractive indices different physical properties of OFB glasses have been evaluated, by considering the relevant equations given in the reference [38] and are presented in Table 1. Density is an effective tool to investigate the degree of structural compactness, modifications of geometrical configurations of the glass network, change in co-ordination and the variation of dimensions of interstitial holes. Another important property for the optical materials is refractive index. Many researchers tried to bring the relation between refractive index and glass composition. In the present system of glasses the refractive index decreases with the increase of Sm^{3+} ion concentration. This is due to the dual nature of ZnO because it acts as a network modifier at very low concentrations of Sm^{3+} ion and occupies the network former positions with the increase of Sm^{3+} ion concentration. From Table 1, it can be observed that density of the glasses increasing with increase in Sm^{3+} ion concentration representing the replacement of B_2O_3 by the addition of Sm_2O_3. Molar volume also increases with increase of density and Sm_2O_3 concentration. Fig. 2 shows the variation of density and molar volume with the Sm^{3+} ion concentration. Linear relationship can be observed between Sm^{3+} ion concentration with density and molar volume. These increasing values of density and molar volume indicates that the non-bridging oxygen's (NBO's) increases in the glass network. Hence the glass network expands with the addition of Sm_2O_3 because Sm_2O_3 enters into the glass network as a network modifier, occupies the interstitial space in the network and finally generates the NBO's in the glass structure [39]. The bonding condition in the glass can be measured by using the molar refraction, which is the sum of the contributions given by cationic and oxygen ionic refractions. The high solubility of rare earth ions in the glass can be decided on the basis of low field strength values. The non-linearity response of the materials was governed by the one of the most important property like polarizability. Whenever a material is exposed for intense beam of light, the optical non-linearity will be produced by the electronic polarization. Molecular electronic polarizability of a material is an important physical property for any material as it plays a vital role in deciding the properties possessed by the material such as

optical absorption, chemical stability and dielectric properties. In the present work, the OFB glasses are showing low molecular electronic polarizability values indicating stability of the prepared glass. The theoretical value of optical basicity (Λ_{th}) is expressed in terms of the electron density carried by oxygen can be evaluated by using the following expression which was proposed by Duffy and Ingram [40]

$$\Lambda_{th} = \sum_i \frac{Z_i r_i}{2\gamma_i}, \gamma_i = 1.36(x_i - 0.26)$$

Here Z_i is the oxidation number of the cation i, r_i is the ionic ratio with respect to the total number of oxides γ_i is the basicity moderating parameter and is given from the Pauling electro negativity x_i. The optical basicity denotes the average electron donating power of the medium to the oxide atoms present in that medium. Increasing in optical basicity value indicates increasing covalency in the cation-oxygen bonding.

3.3 FTIR Spectral Analysis

Fig. 3 shows the FTIR spectrum of OFBSm10 glass in the region 400–4000 cm^{-1} which is used to know the functional groups involved and the local structure present in OFBSm10 glass. The bands and their assignments are given Table 2. The FTIR spectral absorption peaks can be divided into three main groups in the ranges 400–700 cm^{-1}, 800-1200 cm^{-1} and 1200–1600 cm^{-1} related to B-O-B linkages or vibrational modes produced by a network modifier or metal oxygen bonds, the asymmetric stretching relaxation of the B-O bond stretching of trigonal BO3 units and B-O stretching of the BO_4 units respectively. The bands observed in the region 1600 to 4000 cm^{-1} are due to hydrogen bonding and stretching vibrations of OH groups. The band observed at 401cm^{-1} is attributed to metal oxygen bond vibrations of Ca-O, Al-O, Ba-O [41, 42]. This band also signifies the presence of fluorine in the glass matrix. The absorption band at 451 cm^{-1} related to the "isolated" AlO_4 tetrahedral groups [43]. The band at 550 cm^{-1} attributed to Al_2O_3 that enters the glass network mainly as both AlO_6 octahedral in modifying position and also as AlO_4 tetrahedral groups [44]. The presence of stretching vibrations of B-O-B linkages can be confirms from the band at 609 cm^{-1}. The band at 673 cm^{-1} attributed to the combined B-O stretching vibrations of tetrahedral BO_4 units and AlO_4 tetrahedral groups [43, 45]. The band at 887 cm^{-1} is due to the B–O stretching vibrations in BO_4 units from di-borate groups [45]. The peak observed around 1382 cm^{-1} is attributed to the asymmetric stretching modes of BO_3, BO_2O^- borate triangles and various networks consisting six membered borate planar groups [45, 46]. The B-O bond stretching vibrations of borate units in which boron atoms are co-ordinated with

three oxygen atoms leads to the formation of a band around 1623 cm^{-1} [47, 48]. The bands at 2843 and 2917 cm^{-1} are attributed to hydrogen bonding in the present OFB glass. The Characteristic infrared absorption band at 3433 cm^{-1} can be assigned to the fundamental vibrations of OH group. The large amount of OH content present in a glass leads to more non-radiative losses in the glass matrix and decreases the efficiency of the materials doped with rare earth ions. From Fig. 3 it can be seen that, the intensity of OH band in OFB glasses is low. The coefficient of OH vibration (α_{OH}) at 3000 cm^{-1} is used as a measure for the OH content [49]. The content of OH in a glassy material can be estimated using the relevant expression given in our previous paper [50]. For the OFBSm10 glass, the estimated value of OH content is 16.73 ppm , which is found to be smaller than OFPrG (25ppm), OFPrGC04 (30ppm), OFPrGC24 (32 ppm) [51], ZnAlBiB (65.48ppm) [50], LBTAF (123.00 ppm) [52], LHG-8L (128ppm) [53], KBS (133 ppm) [54] and GeS2 (175.5 ppm) [55]. Comparatively, a smaller amount of OH content present in OFB glasses indicates that these materials are aptly suitable for efficient visible lasers.

3.4 Absorption Spectral Analysis

The room temperature absorption spectrum of OFB10 glass in UV-vis-NIR regions is shown in Fig. 4(a) and it consists of several in homogeneously broadened bands assigned to f-f transitions from the ground state $^6H_{5/2}$ to various excited states of Sm^{3+} ions in the host glass. Because of inhomogeneous line broadening, the crystal field fine structure is not well resolved so that only few absorption bands between limited numbers of $^{2S+1}L_J$ manifolds are clearly observed. These absorption bands are observed at 360, 374, 388, 402, 416, 435, 460, 475, 942,1079, 1226, 1405, 1471, 1523, 1585, 1882 nm and are assigned as $^6H_{5/2} \rightarrow {}^4D_{3/2}+({}^4D, {}^6P)_{5/2}$, $^6P_{7/2}$, $^4G_{11/2}$, $^6P_{3/2}+{}^4F_{7/2}$, $({}^6P, {}^4P)_{7/2}$, $^4I_{15/2}$, $^4I_{13/2}$, $^4I_{11/2}$, $^6F_{11/2}$, $^6F_{9/2}$, $^6F_{7/2}$, $^6F_{5/2}$, $^6F_{3/2}$, $^6H_{15/2}$, $^6F_{1/2}$ and $^6H_{13/2}$ transitions respectively. The absorption spectra for the remaining OFB glasses are quite similar and observed at the same wavelength with some variations in their band intensities and hence they were not shown in Fig. 4(a). All these bands are assigned as per the data given by Carnal et al. [56]. Most of the transitions observed in the spectrum were originate from electric dipole induced interactions with selection rule $\Delta J \leq 6$. Some transitions are found to be containing magnetic dipole contribution with selection rule $\Delta J = 0, \pm 1$. The visible absorption bands are appearing as weak in their intensity as they are spin forbidden. The overlap of different $^{2S+1}L_J$ levels made it difficult in assigning the absorption bands in UV-vis region. The presence of fluorides such as PbF_2 and BaF_2 in the present glasses leads to lesser intensity for the observed absorption transitions [57]. The bands observed in infrared region with energies less than 11000 cm^{-1} are found to be sharp and intense, may be because of the effective shielding provided by 5s and 5p shells on the 4f electrons. These transitions are spin allowed ($\Delta S=0$) from the $^6H_{5/2}$ ground state to ^6H and ^6F terms and are assigned to $^6H_{5/2} \rightarrow {}^6F_J$ manifolds with J=1/2, 3/2, 5/2, 7/2, 9/2 and 11/2 respectively.

3.4.1 Nephelauxetic effect–Bonding parameter

The nephelauxetic effect which is designated to measure the covalency of rare earth-oxygen bond in the host matrix arises because of partially filled f-shell. Whenever a rare earth ion enters into a host matrix, the electronic orbitals present in 4f configuration are deformed in the host ligand field due to the nephelauxetic effect. The overlap produced between the oxygen orbitals and the 4f orbitals, the energy level structure of the rare earth ions contracts and lead to the wavelength shift. To get an idea about the nature of Sm^{3+} ligand bond in the present work, the nephelauxetic ratios (β) and bonding parameters have been evaluated and are given in Table 3. The nephelauxetic ratio (β) is calculated by using the following relation [38].

$$\beta = \frac{\vartheta_c}{\vartheta_a} \text{ ---------- (1)}$$

Where ϑ_c is the wave number (in cm^{-1}) of a particular transition for the rare earth ion under investigation and ϑ_a is the wave number (in cm^{-1}) for the same transition of an aqua-ion. The bonding parameter δ is calculated using the formula [38, 58].

$$\delta = \frac{1-\bar{\beta}}{\bar{\beta}} \text{ ---------- (2)}$$

where $\bar{\beta}$ is the average value of β. Depending on the field of environment, the bonding parameter (δ) may be positive or negative indicating covalent or ionic bonding. In the present work, the negative values obtained for the bonding parameter (δ) indicates the bonding nature between Sm-O bond is ionic, which gradually decreases as the Sm^{3+} ion concentration increases. This result observed for the present OFB glasses are inconsistent with other Sm^{3+} doped borate, fluoroborate [59] and phosphate [32] glasses.

3.4.2 Oscillator strengths

The energies of an absorption transitions originating from the ground state of rare earth ions in a host matrix can be expressed in terms of oscillator strengths. Such experimental oscillator strengths can be measured by taking the integrated areas under the absorption peaks of the absorption spectrum by using the following expression [60, 61].

$$f_{exp} = \frac{2.303mc^2}{N\pi e^2} \int \varepsilon(\vartheta) d\vartheta \text{ ---------- (3)}$$

Here m and e are mass and charge of an electron, c is the velocity of light; N is the Avogadro's number and $\varepsilon(\vartheta)$ is the molar absorptivity of a band at a wave number ϑ (cm^{-1}).

By applying the J-O theory [62, 63] the calculated oscillator strengths (f_{cal}) of an electric dipole transition from an initial state (ψ_J) to an excited state ($\psi'_{J'}$) which depends on three J-O intensity parameters Ω_λ (λ=2, 4 and 6) have been determined from the least square fit between f_{exp} and f_{cal} values.

$$f_{cal} = \left[\frac{8\pi^2 mc\nu}{3h(2J+1)}\right]\left[\frac{(n^2+1)^2}{9n}\right]\sum_{\lambda=2,4,6}\Omega_\lambda(\psi_J \| U^\lambda \| \psi'_{J'})^2 \text{ ---------- (4)}$$

Where ν is the wave number (cm^{-1}) of the transition from ground state (ψ_J) to an excited state ($\psi'_{J'}$), c is the velocity of light in vacuum, m is the rest mass of an electron and $\left\|U^\lambda\right\|^2$ is square reduced matrix elements. The square reduced matrix elements needed for the present work were collected from literature as they are host invariant. The quality of the fit is usually measured by root mean square deviation (δ_{rms}) between the experimental and calculated oscillator strengths by using the following expression

$$\delta_{rms} = \left[\frac{\sum(f_{exp}-f_{cal})^2}{n}\right]^{1/2} \text{ ------ (5)}$$

Here n is the total number of energy levels included in the fitting procedure. The values of f_{exp} and f_{cal} together with the r.m.s deviation are given in Table 3. In the present system, OFBSm10 possesses highest oscillator strengths for all the transitions when compared with other glasses. From Table 3 it can be seen that, relatively small change in rare earth ion concentration in OFB glasses brings changes in the oscillator strengths and modifies the local structure around the Sm^{3+} ions.

3.4.3 Hypersensitive Transitions

According to Jorgenson and Judd [62], for some of the electric dipole transitions of rare earths called hypersensitive transitions, the position and intensity of the bands are found to be sensitive to the environment around the rare earth ions These hypersensitive transitions obey the selection rules of quadrupole transitions $|\Delta S| = 0, |\Delta L| \le 2$ and $|\Delta J| \le 2$ [64, 65]. Calculations have exposed that the intensities of these hypersensitive transitions are larger in magnitude. The polarizability also plays an important role in the hypersensitive transitions. Judd [66] noticed that the hypersensitive transitions are associated with the large values of the reduced matrix elements $\| U^2 \|$ and hence the hypersensitiveness is mainly described by the Ω_2 parameter only. In contrast to it, the $\| U^4 \|$ and $\| U^6 \|$ matrix elements for the hypersensitive transitions are small. The degree of hypersensitivity exhibited by the rare earth ion can be measured from the relative

variation of Ω_2 parameter for a rare earth ion in different host environments. This could also be understood from the Fig. 4(b) which shows the variation of oscillator strength of hypersensitivity transition and $\sum\Omega_\lambda$ with the concentration of Sm^{3+} ion in the OFB glasses. From the Fig. 4(b) it can be seen that, the magnitude of J-O intensity parameters depends upon the intensity of hypersensitive transition. The intensity of hypersensitive transition and $\sum\Omega_\lambda$ varies in the same manner with the variation of Sm^{3+} ion concentration. The hypersensitive transitions show differences which are the characteristic features for the co-ordination and symmetry [67]. The qualitative indication of the site symmetry can be known from the band shape and intensity of hypersensitive transitions [68]. From Table 3 it is observed that, the hypersensitive transitions $^6H_{5/2}\rightarrow{}^6P_{3/2}$, $^6H_{5/2}\rightarrow{}^6F_{7/2}$ possesses highest intensity for all the glasses.

3.4.4 J-O theory & Estimation of J-O intensity parameters

The J-O theory is the most well recognized method used to measure the three phenomenological spectroscopic parameters Ω_2, Ω_4 and Ω_6 of rare earth ions in various environments. These parameters are very helpful to know the information about efficiency and performance of the luminescent material. The Ω_2 J-O Parameter is associated with the covalency of the metal-ligand bond and can be employed to check the covalency changes in glasses [69]. The amount of covalency present in the rare earth ligand bonds can be known from the intensity and nature of the hypersensitive transitions. The magnitude of Ω_2 is also depends upon the crystal field variations of the rare earth ion from the cubic symmetry. The magnitude of intensity parameters Ω_4 and Ω_6 are interrelated to the rigidity of the host medium in which the rare earth ions are located [70]. For the present Sm^{3+} doped OFB glasses, the evaluated J-O intensity parameters are given in Table 4 along with the reported values [62, 63, 71-75]. From Table 4, it is seen that the J-O intensity parameters follow the same trend ($\Omega_6 > \Omega_4 > \Omega_2$) for all the OFB glasses and their magnitudes increases up to 1 mol% of Sm^{3+} ions and beyond decreases. The magnitudes of J-O intensity parameters are found to be high for OFBSm10 glass. The magnitude of Ω_2 is found to be lower than Ω_4 and Ω_6. Reisfeld et al [70, 76] have observed that several rare earth doped oxide glasses and chalcogenide glasses possess high magnitude of Ω_2 parameter than fluoride glasses and crystals. In fluoride glass systems, the symmetry of the sites in which the rare earth ions are situated is very large but the number such sites are very small. Additionally, they exhibit very low covalent bonding than oxide glasses. So the Ω_2 parameters obtained for fluoride glassy systems are smaller than that of oxide glassy systems. This may be due to narrow absorption and emission spectral futures observed in fluoride glasses than in oxide glasses. For chalcogenide glasses, the Ω_2 parameters were observed to be very high among all the glasses may be due to their highest covalency [76]. This implies that rare earth-oxygen covalency decreases when pure oxide glasses modified with fluorine content, which is also reflected from the bonding

parameters. These J-O intensity parameters are also depend upon the polarizabilities of the neighbouring ions and nature of the chemical atmosphere. From the 100% ionic model of the ligand field interaction, it is observed that the charge of fluorine and chlorine ions is -1 and their dipolar isotropic polarizabilities are 1Å^3 and 3 Å^3 respectively. This is one of the main reasons, for the existing of hypersensitive transitions which are generally dominated by the one of the J-O intensity parameter Ω_2.

3.5 Photoluminescence spectral properties

Fig. 5 shows the excitation spectrum of OFBSm glasses in the region 350-525 nm at an emission wavelength 599 nm. The inset in Fig.5 shows the excitation spectrum with wavenumber (cm^{-1}) scale. The excitation spectra have nine excitation bands at 360, 374, 388, 402, 416, 438, 461, 477, 500 nm corresponding to the transitions $^6H_{5/2}\rightarrow{}^4D_{3/2}$, $^6F_{7/2}$, $^4L_{15/2}$, $^4F_{7/2}$, $(^6P, {}^4P)_{5/2}$, $^4M_{19/2}$, $^4I_{13/2}$, $^4I_{11/2}$ and $^4G_{7/2}$ respectively. Among all these transitions, the transition $^6H_{5/2}\rightarrow{}^4F_{7/2}$ at 402 nm is very intense and hence used to record the photoluminescence spectra of Sm^{3+} doped OFB glasses. This intense excitation wavelength observed at 402 nm also indicates that the commercially available UV-blue laser diodes and blue-bluish-green light emitting diodes (LEDs) are aptly suitable to act as pumping sources for the Sm^{3+} doped oxy-fluoride glasses [77]. Though the excitation band related 402 nm is more intense than other transitions, the emission spectra in the present work were recorded at 410 nm using CW laser source because a laser source can excite the atoms to the desired level much effectively than the conventional excitation sources. As we don't have a laser source at 402 nm, we have used the nearest wavelength CW laser source (410 nm) for excitation. Fig. 6 shows the photoluminescence spectra of Sm^{3+} doped OFB glasses using 410 nm CW laser diode as an excitation source with wavenumber (cm^{-1}) scale on X-axis. The left side inset in Fig. 6 shows the photoluminescence spectra of Sm^{3+} doped OFB glasses using 410 nm CW laser diode as an excitation source with wavelength scale on X-axis. However, we have also recorded the emission spectra for Sm^{3+} doped OFB glasses by fixing the excitation wavelength at 402 nm using a commercial Spectrofluorophotometer to know the difference between the emission spectra given by 402 nm (commercial source) and 410 nm (CW laser) excitation sources. The right side inset in Fig. 6 shows the photoluminescence spectra of Sm^{3+} doped OFB glasses at an excitation wavelength 402 nm. Both the inset photoluminescence spectra shown in Fig. 6 consists of four emission bands in yellow, orange, red and NIR regions at 563, 598, 646 and 708 nm corresponding to the transitions $^4G_{5/2}\rightarrow{}^6H_{5/2}$, $^4G_{5/2}\rightarrow{}^6H_{7/2}$, $^4G_{5/2}\rightarrow{}^6H_{9/2}$ and $^4G_{5/2}\rightarrow{}^6H_{11/2}$ respectively with slight difference in their intensities. The intensity

of the photo luminescent bands produced by 410 nm CW laser excitation is slightly more that its counterparts produced at 402 nm using conventional excitation source. This is obvious because, the CW laser source can effectively excite the atoms to the desired level than the conventional excitation source. As shown in Fig. 6, an emission transition observed in orange region $^4G_{7/2}\rightarrow{}^6H_{7/2}$ is highly intense than the remaining transitions for all glasses. From Fig. 6 it can also be observed that, in both the photoluminescence spectra, the concentration quenching occurs at 1 mol% of Sm^{3+} ions in OFB glasses. This concentration quenching may be due to efficient energy transfer between rare earth ion sites or due to cross- relaxation mechanism produced at higher dopant concentrations.

The optical transitions $^6H_{5/2}\rightarrow{}^6F_{9/2}$ and $^6H_{5/2}\rightarrow{}^6F_{7/2}$ occurring in the absorption spectra in the NIR region are hypersensitive. In the emission spectra, the transition $^4G_{5/2}\rightarrow{}^6H_{9/2}$ at 646 nm is also recognized as hypersensitive transition. A careful observation of these absorption and emission spectra further indicate that the transition $^6H_{5/2}\rightarrow{}^6F_{7/2}$ is a threefold triplet. The reason for splitting of this transition may be due to the degeneracy produced in $^6H_{5/2}$ ground state in the crystal field [78] due to certain self-adjustment of Sm^{3+} environment in the glass network. The quenching of luminescence in the OFBSm10 glass is low due to the high intensity of the luminescence bands in Sm^{3+} ion in that glass. The high luminescence of this OFBSm10 glass is also a representation of less cross relaxation i.e. the transfer of energy in between the Sm^{3+} ions from the excited state to the ground state is low for this OFBSm10 glass when compared with other glasses due to dipole-dipole or dipole-quadrupole interactions. In the emission spectra, the transition $^4G_{5/2}\rightarrow{}^6H_{7/2}$ with the selection rule $\Delta J = \pm 1$ is a magnetic dipole (MD) allowed whereas the transition $^4G_{5/2}\rightarrow{}^6H_{9/2}$ is purely electric dipole. The intensity ratio of electric dipole to magnetic dipole transitions gives the magnitude of the asymmetry of the local environment of Sm^{3+} ions. If the intensity ratio of the electric dipole transition to the magnetic dipole transition (Asymmetry Ratio = $^4G_{5/2}\rightarrow{}^6H_{9/2}$/ $^4G_{5/2}\rightarrow{}^6H_{7/2}$) is high then the asymmetry of Sm^{3+} ions in the network is high [79]. For the present glasses the asymmetric ratios are OFBSm1=0.4464, OFBSm5=0.4786, OFBSm10=0.4313, OFBSm15=0.4899, OFBSm20=0.5019 and OFBSm25=0.5824 respectively. This asymmetric ratio is high for OFB25 glass and low for OFBSm10 glass; indicate that OFB25 glass has more local disorder and OFB10 glass have less local disorder for the Sm^{3+} ions in the present glass network. For all these glasses, asymmetric

ratio values are found to be less than one which is a representation of occupation of Sm^{3+} ions at inverse symmetry site.

3.6 Radiative properties

From the evaluated J-O parameters, the radiative properties such as radiative transition probability (A_R), total radiative transition probability (A_T), branching ratio (β_R), radiative lifetime (τ_R) and stimulated emission cross-section (σ_{se}) for the Sm^{3+} ions corresponding to the transitions $^4G_{5/2}\rightarrow{}^6H_{5/2}$, $^4G_{5/2}\rightarrow{}^6H_{7/2}$, $^4G_{5/2}\rightarrow{}^6H_{9/2}$ and $^4G_{5/2}\rightarrow{}^6H_{11/2}$ have been measured by using the equations in the literature [80] and these evaluated values are given in Tables 5 and 6. From Table 5, it is observed that, the radiative transition probability (A_R) values for the transition $^4G_{5/2}\rightarrow{}^6H_{7/2}$ are found to be higher than other emission transitions. The luminescence branching ratio is one of the important characteristic parameter used to describe the possibility of attaining stimulated emission from any specific transition. One can identify a potential laser transition if that transition possesses a branching ratio ≥ 0.50 [81]. The experimental branching ratio (β_{exp}) values obtained from the relative areas of the emission lines and these values are found to be in good agreement with the radiative branching ratios (β_R). From Table 5, it is observed that all the glasses have higher radiative branching ratios (β_R) (≥ 0.50) for the transition $^4G_{5/2}\rightarrow{}^6H_{7/2}$. These radiative branching ratio values [50.5% (OFBSm1), 50.6% (OFBSm5), 53.9% (OFBSm10), 52.1% (OFBSm15), 51.6% (OFBSm20) and 50.9% (OFBSm25) respectively] suggest that the glass OFBSm10 have a possibility to be used as a luminescent material for laser applications. Larger stimulated emission cross-section (σ_{se}) value is an attractive feature for low threshold, high gain laser applications, which are used to get continuous wave (CW) laser action [82]. From the observed luminescence bands, the stimulated emission cross-section σ_{se} can be evaluated by using the equation

$$\sigma_{se}\left(a_J, b_{J'}\right) = \frac{\lambda_P{}^4}{8\pi c n^2 \Delta\lambda_P} A_R\left(a_J, b_{J'}\right)$$

Here $\Delta\lambda_P$ is the emission peak wavelength and $\Delta\lambda_P$ is known as full width at half maximum which can be evaluated by integrating the intensity at the peak wavelength [82]. Out of all the radiative parameters, full width at half maximum ($\Delta\lambda_P$), stimulated emission cross-section (σ_{se}), gain bandwidths ($\sigma_{se}\times\Delta\lambda_P$), optical gain parameters ($\sigma_{se}\times\tau_R$) and quantum efficiencies (η) are the five most crucial parameters for a laser designer. These parameters calculated for the

transitions $^4G_{5/2} \rightarrow {}^6H_J$ (J=5/2, 7/2, 9/2, 11/2) are given in Tables 6 and 7. From Table 6, it can be seen that, Glass OFBSm10 exhibits highest values of stimulated emission cross-section (σ_{se}), gain bandwidths ($\sigma_{se} \times \Delta\lambda_P$) and optical gain parameters ($\sigma_{se} \times \tau_R$) for the transition $^4G_{5/2} \rightarrow {}^6H_{7/2}$. These radiative properties of the electric dipole transitions are liable for orange emission in Sm^{3+} doped glasses. Hence, OFBSm10 is most suitable for solid state lasers as well as fiber amplifiers in visible Orange region.

3.7 Decay measurements, cross-relaxation rates (non-radiative decay rates) and quantum efficiency

The Logarithmic decay curves recorded for $^4G_{5/2}$ level of Sm^{3+} ions in OFB glasses are shown in Fig. 7(a-f). As shown in Fig. 7(a-f), the decay curves are finely fitted to a single exponential function at lower concentrations (up to 1.0 mol % of RE) and non-exponential at higher concentrations (≥ 1.0 mol % of RE). Normally, when the concentration of the RE ion is low enough, they can act as an isolated centres and the decay from any excited level can be described by a single exponential function. When the concentration of the RE ion increases, the distance between the RE ion centres will decrease and the interaction between them increases. Such strong interactions existing between two active ions are able to transfer excitation energy from one RE ion to the other [57]. The overlap between absorption and emission bands and the existence of the trap centres around the Sm^{3+} ion are also responsible for energy transfer. The non-exponential nature of decay curves observed at higher concentration of Sm^{3+} ions in OFB glasses are due to such energy transfer process [57]. The effective decay time can be determined by the expression

$$\tau_{exp} = \frac{\int tI(t)dt}{\int I(t)dt}$$

Here I (t) is the emission intensity at time‘t’. The experimental lifetimes of the excited $^4G_{5/2}$ level have been obtained by taking first e-folding times of the decay curves and are given in Table 7 along with the radiative lifetimes. The experimental lifetimes are found to be decreasing with increase in Sm^{3+} ion concentration in these OFB glasses.

The phenomenon of photoluminescence quenching, the non-exponential nature of decay curves observed at higher concentrations and hence decrease in experimental lifetimes can be understood clearly from the possible cross-relaxation channels of emission shown in energy level

diagram (Fig. 8). For photoluminescence quenching the closely spaced large number of Sm^{3+} ion energy levels are also responsible. In general, the photoluminescence quenching observed can be understood through two important mechanisms. The first one is due to the energy transfer between the rare earth ions through cross-relaxation and the second one is through migration of excitation energy to the structural defects acting like energy sinks through the mechanism called multi-phonon relaxation [45]. The multi-phonon relaxation rate of an excited state depends on the energy separation of that level with the next lower lying level and phonon energy of the host material.

The exponential energy-gap law for the multi-phonon relaxation rate is given by [83].

$$W_{MPR} = \beta \exp\left(-\alpha \Delta E\right), where\, \alpha = (a\hbar\omega)^{-1}$$

Here the parameters $\beta = 6.30 \times 10^{-10} s^{-1}$, $\alpha = 420\ \ cm^{-1}$ and $\Delta E = 7211 cm^{-1}$ are host dependent and need not depends on the chosen rare earth ion. By using above equation the multi-phonon relaxation rate is evaluated and it is equal to almost zero. Hence, in the present work, for OFB glasses the multi-phonon relaxation rate is almost negligible and the non-radiative relaxation process involved in photoluminescence quenching is mainly due to the energy transfer through cross-relaxation phenomenon as shown in Fig. 8. From the energy level diagram shown in Fig. 8, the following emission and absorption channels can be identified for photoluminescence quenching through cross-relaxation mechanism at higher concentrations of the doped rare earth ion.

Emission Channels	***Absorption channels***
ET₁: $^4G_{5/2} \rightarrow {}^6F_{5/2}$ *(10551 cm^{-1})*	***AT₁:*** $^6H_{5/2} \rightarrow {}^6F_{11/2}$*(10523 cm^{-1})*
ET₂: $^4G_{5/2} \rightarrow {}^6F_{7/2}$ *(9691 cm^{-1})*	***AT₂:*** $^6H_{5/2} \rightarrow {}^6F_{9/2}$ *(9257 cm^{-1})*
ET₃: $^4G_{5/2} \rightarrow {}^6F_{9/2}$ *(8567 cm^{-1})*	***AT₃:*** $^6H_{5/2} \rightarrow {}^6F_{7/2}$ *(8133 cm^{-1})*
ET₄: $^4G_{5/2} \rightarrow {}^6F_{11/2}$ *(7301 cm^{-1})*	***AT₄:*** $^6H_{5/2} \rightarrow {}^6F_{5/2}$ *(7273 cm^{-1})*

The cross-relaxation rate (W_{CR}) can be measured from the following expression and are given in Table 6.

$$W_{CR} = \frac{1}{\tau_{exp}} - \frac{1}{\tau_R}$$

The large cross-relaxation rates at higher concentrations (≥ 1 mol %) are responsible for energy transfer process. Due to these increased cross-relaxation rates (non-radiative decay process) the quantum efficiencies also decreases at higher concentrations. Quantum efficiency is a crucial

factor that can control the performance of the material and these materials further can be used in lasers, optical fibers and planar waveguides.

The quantum efficiency for the present OFB glasses can be evaluated by using the following expression and these values are presented in Table 7.

$$\eta = \frac{\tau_{exp}}{\tau_R}$$

In the present investigation, the glass OFBSm10 has highest quantum efficiency and low cross-relaxation rates (non-radiative decay rates) than other glasses. Hence the glass OFBSm10 is most reliable lasing material to exhibit efficient visible lasing emission in the orange spectral region. The most crucial parameters like branching ratios (β_R), stimulated cross-section (σ_{se}) and quantum efficiencies (η) along with cross-relaxation rates of OFBSm10 glass are compared with other reported values in Table 8 [45, 78, 84- 89].

***3.8 Inokuti-Hirayama model analysis*.**

It is well known that, the lifetime of an excited state energy level refer to the average time for which the molecule/ion can stay in that excited state before coming down to the lower energy level by emitting a photon [90]. The excited (donor) ions can relax to lower energy state through two different methods. One method is direct energy transfer to other active ion (acceptor) and another method is energy migration among the donor ions before such energy reaches to the accepter ion [71]. If the donor and the acceptor ions are homogeneously distributed in the host matrix and the energy migration among the donor ions are negligible, then the decay curves can be fitted to the frame work of Inokuti-Hirayama (IH) model [91] to disclose the dominant mechanism of energy transfer. Therefore the IH model is explicitly applicable when the energy transfer between the donor and accepter is faster than the energy migration between the donor ions and the luminescence decay intensity in such a case is given by

$$I(t) = I_0 \exp\left\{-\frac{t}{\tau_0} - Q\left(\frac{t}{\tau_0}\right)^{\frac{3}{S}}\right\}$$

Here't' is the time after excitation, 'τ_0' is the intrinsic decay time of the donors in absence of acceptors. 'Q' is the energy transfer parameter defined as

$$Q = \frac{4\pi}{3}\Gamma\left(1-\frac{3}{S}\right)N_0 R_0^{\,3}$$

Depend on the value of S and the gamma function $\Gamma(X)$, which is equal to 1.77 for dipole-dipole (S=6), 1.43 for dipole-quadrupole (S=8) and 1.3 for quadrupole-quadrupole (S= 10) interactions, respectively. N_0 is the acceptor ion concentration and R_0 is the critical transfer distance which is defined as the donor-acceptor separation when the rate of energy transfer between a donor and acceptor ion is equal to the rate of intrinsic decay τ_0^{-1}.

The donor-acceptor interaction parameter C_{DA} and the energy transfer probability W_{ET} are calculated using the expressions

$C_{DA} = R_0^{(S)}\tau_0^{-1}$ and $W_{ET} = C_{DA}R_0^{(S)}$.

The energy transfer parameter (Q), critical energy transfer distance (R_0) and donor-acceptor interaction parameter (C_{DA}) are calculated by fitting the IH model are given in Table 9. The study of non-exponential behaviour of decay curves shows an increase in magnitude of energy transfer parameter (Q) and donor-acceptor interaction parameter (C_{DA}) with the increase in Sm^{3+} ion concentration which is similar to other reported Sm^{3+} doped glasses [33, 57, 71, 72, 92]. From Fig.7 (a-f), it is observed that for IH fitting model, s = 6 is well fitted with the non-exponential decay curves which authenticates that the energy transfer between the Sm^{3+} ions is due to dipole-dipole interaction. From the Table 9 it is observed that, the magnitude of Q, R_0 and C_{DA} are strongly depends on the Sm^{3+} ion concentration and these values are increasing with increase in Sm^{3+} ion concentration and found to be higher than the values reported for other glasses [33, 57, 71, 72, 92].

3.9 CIE Chromaticity Co-ordinates & Confocal Images.

Fig. 9 shows the site of colour chromaticity co-ordinates evaluated for OFB glasses doped with different concentrations of Sm^{3+} ions and are displayed in Table 7 numerically. In general, the colour purity or colour saturation can be estimated from the distance between the colour coordinates of present investigated Sm^{3+} doped OFB glasses and the colour co-ordinates of equal-energy point (0.33, 0.33), divided by the distance between the equal-energy point to the dominant wavelength point [93]. The colour co-ordinates evaluated using the above said

procedure for the present Sm^{3+} doped OFB glasses are situated on the border of the colour chromaticity figure which comes into view to be very closest to the bright orange colour (590–635 nm). Normally, the colour purity is 100% for the monochromatic light sources located on the border of the chromaticity diagram and 0% for white light illuminates [93]. The orange emission given by OFB glasses are also further confirmed in principle by the confocal photoluminescence images recorded under the excitation of 410 nm CW laser. Such confocal images recorded for all the OFB glasses are also shown in Fig. 9. From Fig.9 it is conspicuous that, the orange emission exhibited by OFB glasses increases with RE ion concentration up to 1 mol% and then decreases beyond. This result is inconsistent with the CIE chromaticity coordinates possessed by the glasses. Thus the CIE coordinates measured and confocal images recorded for Sm^{3+} ions in OFB glasses are complimenting to each other.

4. Conclusions

Oxy-fluoroborate (OFB) glasses doped with different concentration of Sm^{3+} ions were prepared and investigated using the spectroscopic techniques such as XRD, FTIR, absorption, emission and decay curve measurements to characterize and optimise the doped rare earth ion for visible lasing emission. Featureless XRD spectrum recorded for an undoped OFB glass confirms the amorphous nature of the prepared glasses. The FTIR spectral studies, confirms the various fundamental functional groups present in these glasses. The bonding parameters measured confirms the ionic nature of the Sm^{3+} ions with its neighbouring ligands and the degree of iconicity decreases gradually with the increase of rare-earth ion concentration. The photoluminescence spectra recorded for OFB glasses gives four emission bands in yellow, orange, red and NIR regions at 563, 598, 646 and 708nm corresponding to the transitions $^4G_{5/2}\rightarrow{}^6H_{5/2}$, $^4G_{5/2}\rightarrow{}^6H_{7/2}$, $^4G_{5/2}\rightarrow{}^6H_{9/2}$ and $^4G_{5/2}\rightarrow{}^6H_{11/2}$ respectively. In the present investigation, luminescence quenching was observed at 1 mol% of Sm^{3+} ion concentration and beyond 1 mol% the decay curves of the Sm^{3+} doped OFB glasses changes from exponential to non-exponential nature. The non-exponential decay curves are well fitted to the Inokuti-Hirayama model for S=6, indicating that the nature of interaction between Sm^{3+} ions for energy transfer through cross-relaxation is dipole-dipole type. Under 410 nm CW laser excitation, an intense orange emission has been observed at 598 nm ($^4G_{5/2}\rightarrow{}^6H_{7/2}$) in all these OFB glasses, for

which the branching ratio, stimulated emission cross-section and quantum efficiency values are measured and found to be maximum for OFBSm10 glass. From all these studies, it is concluded that OFB glass with 1 mol% of Sm^{3+} (OFBSm10) can act as efficient lasing material to produce intense visible orange emission at 598 nm in principle. Visible orange emission possessed by these glasses is also further confirmed by CIE chromaticity coordinates and the confocal images recorded under 410 nm CW laser excitation.

Acknowledgements

Two of the authors, Mahamuda Shaik (File No: SR/WOS-A/PS-53/2011) and Swapna Koneru (File No: SR/WOS-A/PS-35/2011) are very much thankful to Department of Science and Technology (DST), Government of India, New Delhi, for awarding them with a Women Scientist's scheme under DST-WOS (A) programme. This work is also partly supported by High-impact Research initiative of IIT-Delhi, UK-India Education Research Initiative (UKIERI) and DST, Govt. of India, New Delhi.

References

[1] M. Srinivasulu, A. S. Rao, J. Mater. Science Letter 20 (2001) 737-740.

[2] M. Venkateswarlu, M. V. V. K. S. Prasad, K. Swapna, Sk. Mahamuda, A. Srinivasa Rao, A. Mohan Babu, D. Haranath, Ceram. Int. 40 (2014) 6261-6269.

[3] R. Rama Kumar, A. S. Rao, B. C. Venkata Reddy, Opt. Mater. 4(1995) 723-728.

[4] K. Swapna, Sk. Mahamuda, A. Srinivasa Rao, T. Sasikala, L. Rama Moorthy, J. Lumin. 146 (2014) 288-294.

[5] K. Swapna, Sk. Mahamuda, A. Srinivasa Rao, S. Shakya, T. Sasikala, D. Haranath, G. Vijaya Prakash, Spectrochim. Acta. Part A 125 (2014) 53-60.

[6] Sk. Mahamuda, K. Swapna, P. Packiyaraj, A. Srinivasa Rao, G. Vijaya Prakash, J. Lumin. 153(2014) 382-392.

[7] A. Srinivasa Rao, J. L. Rao, R. Ramakrishna Reddy, T. V. Ramakrishna Rao, Opt. Mater. 4 (1995) 717-721.

[8] K. Swapna, Sk. Mahamuda, A. Srinivasa Rao, M .Jayasimhadri, T. Sasikala, L. Rama Moorthy, J .Lumin. 139 (2013) 119-12

[9] A. Srinivasa Rao, B. Rupa Venkateswara Rao, M.V.V.K.S. Prasad, J. V. Shanmukha Kumar, M. Jayasimhadri, J. L. Rao, R. P. S. Chakradhar, Physica B 404(2009) 3717-3721.

[10] Sk. Mahamuda, K. Swapna, A. Srinivasa Rao, T. Sasikala, L. Rama Moorthy, Physica B 428(2013)36-42.

[11] Y. Divwedi, S. B. Rai, Opt. Mater. 31 (2008) 87-93.

[12] Sd. Zulfiqar Ali Ahamed, C. Madhukar Reddy, B. Deva Prasad Raju, Opt. Mater. 35 (2013) 1385-1394.

[13] G. Dominiak-Dzik, W. Ryba-Romanowski, J. Pisarska, W.A. Pisarski, J. Lumin. 122-123 (2007) 62-65.

[14] M. V. Vijaya Kumar, K. Rama Gopal, R.R. Reddy, G.V. Lokeswara Reddy, B.C.Jamalaiah, J. Lumin. 142 (2013) 128-134.

[15] I. Arul Rayappan, K. Marimuthu, J. Phys. Chem. Solids 74 (2013) 1570-1577.

[16] W.A. Pisarski, G. Dominiak-Dzik, W. Ryba-Romanowski, J. Pisarska, J. Alloys Compd. 451 (2008) 220-222.

[17] J. Pisarska, R. Lisiecki, W. Ryba-Romanowski, G. Dominiak-Dzik, W.A. Pisarski, J. Alloys. Compd. 451 (2008) 226-228.

[18] C. Madhukar Reddy, N. Vijaya, B. Deva Prasad Raju, Spectrochim. Acta A 115 (2013) 297-304.

[19] S. A. Pollack, D. B. Chang, J. App. Phys. 64 (1988) 2885-2893.

[20] A. Lucca, M. Jacquemet, F. Druon, F. Balembois, P. Georges, P. Camy, J. L. Doulan, R. Moncorge, Opt. Lett. 29 (2004) 1879-1881.

[21] Sk. Mahamuda, K. Swapna, A. Srinivasa Rao, M. Jayasimhadri, T. Sasikala, K. Pavani, L. Rama Moorthy, J. Phys. Chem. Solids 74 (2013) 1308-1315.

[22] P. Subbalakshmi, N. Veeraiah, Ind. J. Eng. Mater. Sci. 8 (2001) 275-284.

[23] R. K. Brow, D. R. Tallent, S. T. Myers, J. Non-Cryst. Solids 191 (1995) 45-55.

[24] L. Van Wullen, W. Muller Warmth, J. Solid State NMR, 2 (1993) 279-284.

[25] H. Scholze, "Glass : Nature, Structure and Properties", Springer, New York, (1991).

[26] J. E. Shelby, Introduction to "Glass Science and Technology", The Royal Society of Chemistry, Cambridge, (1997).

[27] A. Naruse, Y. Abe, Takami, Yogyo- Kyokai-Shi 79 (1971) 225.

[28] A. E. Owen, Phys. Chem. Glasses 2 (1961) 152-162.

[29] S. Yusub, Ch. Rajyasree, A. Ramesh Babu, P.M. Vinaya Teja, D. Krishna Rao, J. Non-Cryst. Solids 364 (2013) 62-68.

[30] S. Sakka, Yogyo- Kyokai- Shi 85 (1977) 299-302.

[31] P. Perince, S. Esposito, A. Aronne and V. N. Sigaev, J. Non-Cryst. Solids 258 (1999) 1- 10.

[32] V. Venkatramu, P. Babu, C. K. Jayasankar, Th. Troester, W. Sievers, G. Wortmann, Opt. Mater, 29 (2007) 1429-1439.

[33] J. Suresh kumar, K. Pavani, T. Sasikala, A. Srinivasa Rao, Neeraj Kumar, S. B. Rai, L. Rama Moorthy, Solid. Stat. Sci. 13 (2011) 1548-1553

[34] C. K. Jayasankar, V. Venkatramu, J. Appl. Phys. 97 (2005) 093523-093527.

[35] D. N. Slatin, P. Spanne, F. A. Dilmanin, M. Sandborg, Med. Phys. 19 (1992) 1395-1400.

[36] Regina Muellar-Mach, Gerd O. Mueller Michal R. Krames, Oleg B. Shchekin, Peter J. Schmidt, Helmut Bechtel, Ching-Hui Chen, Oliver steigelmann, Phys. Status Solidi RR1. 3(7-8) (2009) 215-217.

[37] Michal R. Krames, Oleg B. Shchekin, Regina Mueller-Mach, Gerd O. Mueller, Ling Zhou, Gerard Harbers, M. George craford, J. disp. Technol. 3 (2) (2007) 160-175.

[38] A. S. Rao, Y. N. Ahammed, R. R. Reddy, T.V.R. Rao, Opt. Mater. 10 (1998) 245-252.

[39] S. Rakpinch, J. Kaewkhao, N. Sresittipokakun, K. Boonin, J. M. Park, H. J. Kim, P. Limsuwan, Physics International 4 (2013) 81-87.

[40] J. A. Duffy, M. D. Ingram, J. Inorg. Nucl. Chem. 37 (1975) 1203-1206.

[41] Y. H. Zhou, J. Lin, S. B. Wang, H. J. Zhang, Opt. Mater. 20 (2002)13-20.

[42] D. Boyr, G. Bertrand-Chadeyron, R. Mahiou, Opt. Mater. 26 (2004) 101-105.

[43] P. Tarte, Spectrochim. Acta: Part A 23 A (1967) 2127- 2143.

[44] S. Kojima, M. Kodama, Jpn. J. Appl. Phys, 33 (1994) 2886-2889.

[45] K. Maheshvaran, K. Linganna, K. Marimuthu, J. Lumin. 131 (2011) 2746-2753.

[46] Madhukar Reddy, G.R. Dillip, K. Mallikarjuna, Sd. Zulifiqar Ali Ahamed, B. Sudhakar Reddy, B. Deva Prasad Raju, J. Lumin. 131 (2011) 1368-1375.

[47] H. Scholze, Glass Ind. 47 (11) (1966) 622-628.

[48] M. Kaur1, S.P. Singh, D. S. Mudahar, G. S. Mudahar, Materials Physics and Mechanics 15 (2012) 66-73.

[49] H. Ebendorff-Heidepriem, W. Seeber, D. Ehrt, J. Non-Cryst. Solids 163 (1)(1993) 74-80.

[50] Sk. Mahamuda, K. Swapna, P. Packiyaraj, A. Srinivasa Rao, G. Vijaya Prakash, Opt. Mater. 36 (2013) 362-371.

[51] K. Biswas, A. D. Sontakke, J. Ghosh, K. Annapurna, J. Am. Ceramic. Society, 93 (4) (2010) 1010-1017.

[52] T. Suhasini, B. C. Jamalaiah, T. Chengaiah, J. Suresh Kumar, L. Rama Moorthy, Physica B 407 (2012) 523-527.

[53] T. I. Suratwala, R.A. Steele, G.D. Wilke, J.H. Campbell, K. Takeuchi, J. Non-Cryst. Solids 263–264 (2000) 213-227

[54] B.B. Kale, A. Jha, S.K. Apte, P.V. Adhyapak, D.P. Amalnerkar, Mater. Chem. Phys.78 (2002) 330-336.

[55] Tirtta Som, Basudeb Karmakar, Spectrochim. Acta Part A 79 (2011) 1766-1782.

[56] W. T. Carnall, P. R. Fields, K. Rajnak, J. Chem. Phys. 49 (1968) 4424-4442.

[57] S. Arun Kumar, K. Marimuthu, J. Alloys. Compd. 565 (2013) 104-114.

[58] S.P. Sinha, Complexes of the Rare Earths, Pergamon, Oxford, 1966.

[59] C. K. Jayasankar, P. Babu, J. Alloys Compd. 307 (2000) 82-95.

[60] W.T. Carnall, in: K.A. Gschneidner, L.R. Eyring (Eds.), Handbook on the Physics and Chemistry of Rare Earths, vol. 3, North-Holland, Amsterdam, 1979 (Chapter 24).

[61] R.R. Jacobs, M.J. Weber, IEEE J. Quant. Electron. QE-12 (1976) 102-111.

[62] B. R. Judd, Phys. Rev. 127 (1962) 750-761.

[63] G.S. Ofelt, J. Chem. Phys. 37 (1962) 511-520.

[64] C. K. Jorgensen, B. R. Judd, Mol. Phys. 8 (1964) 281-290.

[65] S. Tanabe, T. Ohyagi, N. Soga, T. Hanada, Phys. Rev. B 46 (1992) 3305-3310.

[66] S.N. Misra, J. Sci. Ind. Res. 44 (1985) 366-375.

[67] D. G. Karraker, Inorg. Chem. 6 (1967) 1863-1868.

[68] G. R. Choppin, D. E. Henrie, K. Buijs, Inorg. Chem. 5 (1966) 1743-1748.

[69] B. G. Wybourne, Spectroscopic Properties of Rare earths, Interscience, New York, 1975.

[70] C. K. Jorgenson, R. Reisfeld, J. Less-Common Met. 93 (1983) 107-112.

[71] B. C. Jamalaiah, M. V. Vijaya Kumar, K. Rama Gopal, Opt. Mater. 33(2011)1643-1647.

[72] B. C. Jamalaiah, J. Suresh Kumar, A. Mohan Babu, T. Suhasini, L. Rama Moorthy, J. Lumin. 29 (2009) 363-369.

[73] M. Jayasimhadri, L. R. Moorthy, S. A. Saleem, R. V. S. S. N. Ravi Kumar, Spectrochim. Acta Part A 64 (2006) 939-944.

[74] R. Praveena, V. Venkatramu, P. Babu, C.K. Jayasankar, Physica B 403 (2008) 3527-3534.

[75] Ch. Srinivasa Rao, C.K. Jayasankar, Optics Communications 286 (2013) 204-210.

[76] R. Reisfeld, J. Less-Common Met. 112 (1985) 9-18.

[77] B. J. Chen, L. F. Shen, E. Y. B. Pun, H. Lin, Opt. Express 20 (2012) 2802-2809.

[78] H. Ahrens, M. Wollenhaupt, P. Frobel, J. Lin, K. Barner, G. S. Sun, R. Braunstein, J. Lumin. 82 (1999) 177-186.

[79] A. Kurita, T. Kushida, T. Izumitani, M. Matsukawa, Opt. Lett. 19 (1994) 314-316.

[80] K. Swapna, Sk. Mahamuda, A. Srinivasa Rao, M. Jayasimhadri, T. Sasikala, L. Rama Moorthy, Ceram. Int. 39 (2013) 8459-8465.

[81] L. Rama Moorthy, T. S .Rao, K. Janarthanam, A. S. Rao, Y. Subramanyam, Opt. Mater. 12 (1999) 459-465

[82] S. A. Saleem, B. C. Jamalaiah, M. Jayasimhadri, A. Srinivasa Rao, Kiwan Jang, L. Rama Moorthy, JQSRT 112 (2011) 78-84.

[83] R. Reisfeld, C.K. Jorgensen, Handbook on the Physics and Chemistry of Rare Earths, in: K.A. Gschneidner, L. Eyring (Eds.), Excited state phenomena in vitreous materials, North-Holland, Amsterdam, 1987, pp. 41–44. Chapter 58.

[84] T. Suhasini, J. Suresh Kumar, T. Sasikala, Kiwan Jang, Ho Sueb Lee, M. Jayasimhadri, Jung Hyun Jeong, Soung Soo Yi, L. Rama Moorthy, Opt. mater. 31 (2009) 1167-1172.

[85] I. Arul Rayappan, K. Selvaraju, K. Marimuthu, Physica B 406 (2011) 548-555.

[86] K. Selvaraju, K. Marimuthu, J.Alloys.Compd. 553 (2013) 273-281.

[87] T. Sasikala, L. Rama Moorthy, A. Mohan Babu, Spectro. Chimica. Acta. Part A 104 (2013) 445-450.

[88] K. S. V. Sudhakar, M. Srinivasa Reddy, L. Srinivas Rao, N. Veeraiah, J. Lumin 128 (2008) 1791-1798.

[89] Y. K. Sharma, S. S. L. Surina, R. K. Singh, J. Rare earths 27 (2009) 773-780.

[90] A.G. Souza Filho, J. Mendes Filho, F.E.A. Melo, M.C.C. Custodio, R. Lebullenger, A.C. Hernandes, J. Phys. Chem. Solids 61 (2000) 1535-1542.

[91] M. Inokuti, F. Hirayama, J. Chem. Phys. 43 (1965) 1978-1989.

[92] C.R. Kesavulu, C.K. Jayasankar, J. Lumin. 132 (2012) 2802-2809.

[93] E. Fred Schubert, Light Emitting Diodes, 2nd ed., Cambridge University Press, New York, USA, 2006.

Table 1:

Various physical properties of Sm^{3+} ions in OFB glasses

Physical Property	**OFBSm01**	**OFBSm05**	**OFBSm10**	**OFBSm15**	**OFBSm20**	**OFBSm25**
Refractive index (n_d)	1.619	1.617	1.615	1.613	1.611	1.599
Density, d (gm/cm^3)	3.385	3.399	3.418	3.436	3.454	3.472
Average molecular weight, $\bar{M}$ (g)	84.66	85.65	86.88	88.12	89.35	90.58
Molar Volume (V_m) (cm^3/mol)	25.00	25.19	25.41	25.64	25.86	26.08
Sm^{3+} ion concentration, N(10^{22} ions/cm^3)	0.241	1.200	2.370	3.520	4.660	5.770
Mean atomic volume (g/cm^3/atom)	5.683	5.725	5.777	5.828	5.878	5.928
Dielectric constant (ϵ)	2.621	2.614	2.608	2.601	2.595	2.588
Optical dielectric constant ($\epsilon - 1$)	1.621	1.614	1.608	1.601	1.595	1.588
Reflection losses (R %)	5.580	5.550	5.531	5.503	5.476	5.448
Molar refraction (R_m)(cm^{-3})	8.773	8.814	8.871	8.926	8.979	9.032
Polaron radius (r_p) (Å)	3.060	1.790	1.430	1.250	1.140	1.060
Inter-atomic distance (r_i) (Å)	7.580	4.440	3.540	3.100	2.830	2.630
Molecular electronic polarizability α ($10^{-23}cm^3$)	34.80	6.960	3.520	2.360	1.780	1.430
Field strength ,F ($10^{15}cm^{-2}$)	3.210	9.360	14.70	19.20	23.10	26.60
Optical basicity ,(Λ_{th})	0.487	0.536	0.537	0.539	0.541	0.543

Table 2:

The FTIR band positions and their assignments in an undoped OFB glass

Band Positions (cm^{-1})	**Assignments**
401	Metal oxygen bond vibrations (Ca-O, Al-O, Ba-O)
451	Stretching vibrations of AlO_4 tetrahedral groups
550	Stretching vibrations of AlO_6 octahedral groups
609	Bending vibrations of O–B–O linkages
673	Combined vibrations of BO_4 and AlO_4
887	B–O bonds stretching vibration in BO_4 tetrahedra from diborate groups
1062	B–O bonds stretching vibrations in BO_4 units
1384	B–O Stretching containing planar 6 member borate groups
1623	Stretching vibrations of BO_3 triangles
2843	Hydrogen Bonding
2917	Hydrogen Bonding
3433	Fundamental stretching of OH group

Table 3:

Experimental (f_{exp} x 10^{-6}), calculated (f_{cal} x 10^{-6}) oscillator strengths, their rms deviation, nephelauxetic ratios ($\bar{\beta}$) and bonding parameters (δ) of Sm^{3+} ions in OFB glasses

Transitions from	OFBSm01		OFBSm05		OFBSm10		OFBSm15		OFBSm20		OFBSm25	
$^6H_{5/2}$→	f_{exp}	f_{cal}	f_{exp}	f_{cal}	f_{exp}	f_{cal}	f_{exp}	f_{cal}	f_{exp}	f_{cal}	f_{exp}	f_{cal}
$^6H_{13/2}$	0.44	0.21	0.48	0.36	0.50	0.39	0.25	0.34	0.18	0.30	0.14	0.21
$^6F_{1/2}$	0.16	0.02	0.19	0.18	0.23	0.19	0.13	0.08	0.12	0.08	0.01	0.02
$^6H_{15/2}$	0.17	0.01	0.31	0.02	0.40	0.03	0.20	0.02	0.15	0.02	0.12	0.01
$^6F_{3/2}$	0.39	0.59	1.18	1.06	1.22	1.18	0.84	0.75	0.75	0.67	0.61	0.51
$^6F_{5/2}$	1.33	1.25	1.49	2.03	1.88	2.27	0.87	1.51	0.74	1.34	0.72	1.08
$^6F_{7/2}$	2.81	2.90	4.53	4.75	4.86	5.25	4.38	4.32	3.85	3.79	2.59	2.76
$^6F_{9/2}$	2.16	2.08	3.73	3.42	4.23	3.77	3.26	3.26	2.85	2.84	2.31	2.03
$^6F_{11/2}$	0.37	0.34	0.81	0.56	1.52	0.62	0.82	0.54	0.66	0.47	0.54	0.33
$^4I_{11/2}$	0.31	0.14	0.34	0.23	0.41	0.25	0.28	0.22	0.29	0.19	0.24	0.13
$^4I_{13/2}$	0.21	0.34	0.27	0.57	0.39	0.63	0.15	0.53	0.14	0.46	0.11	0.33
$^4I_{15/2}$	0.23	0.02	0.35	0.04	0.65	0.05	0.28	0.04	0.24	0.04	0.19	0.02
$(^6P, ^4P)_{5/2}$	0.32	0.39	0.42	0.62	0.63	0.69	0.18	0.46	0.14	0.41	0.01	0.33
$^6P_{3/2}$	3.01	2.59	7.48	4.15	7.52	4.63	6.43	3.11	5.88	2.76	4.40	2.23
$^4G_{11/2}$	0.31	0.01	0.44	0.02	0.57	0.03	0.37	0.02	0.14	0.02	0.13	0.01
$^6P_{7/2}$	0.98	1.27	1.38	2.09	1.70	2.31	1.16	2.01	0.93	1.75	0.84	1.24
$^4D_{3/2}$+ $(^4D, ^6P)_{5/2}$	0.50	0.43	1.30	0.69	2.29	0.77	1.98	0.51	1.54	0.45	1.12	0.37
δ_{rms} (x10^{-6})	±0.19		±0.90		±0.91		±0.96		±0.87		±0.60	
$\bar{\beta}$	1.0252		1.0153		1.0152		1.0146		1.0142		1.0090	
δ	–0.2461		–0.1510		–0.1500		–0.1448		–0.1407		– 0.0964	

Table 4:

Comparison of Judd-Ofelt Parameters ($\Omega_\lambda X10^{-20}cm^2$) and their trend for Sm^{3+}ions in OFB glasses with different hosts.

Glass System	Ω_2	Ω_4	Ω_6	Trend	References
OFBSm01	0.08±0.001	2.34±0.003	2.35±0.002	$\Omega_6 > \Omega_4 > \Omega_2$	present work
OFBSm05	0.56±0.007	3.74±0.007	3.87±0.002	$\Omega_6 > \Omega_4 > \Omega_2$	present work
OFBSm10	0.59±0.025	4.18±0.006	4.27±0.002	$\Omega_6 > \Omega_4 > \Omega_2$	present work
OFBSm15	0.27±0.008	2.81±0.021	3.74±0.001	$\Omega_6 > \Omega_4 > \Omega_2$	present work
OFBSm20	0.24±0.007	2.50±0.006	3.26±0.002	$\Omega_6 > \Omega_4 > \Omega_2$	present work
OFBSm25	0.06±0.012	2.03±0.011	2.31±0.003	$\Omega_6 > \Omega_4 > \Omega_2$	present work
0.1SmPbFB	0.39	3.66	2.44	$\Omega_4 > \Omega_6 > \Omega_2$	[62]
0.5SmPbFB	0.32	3.62	2.04	$\Omega_4 > \Omega_6 > \Omega_2$	[62]
1SmPbFB	0.31	3.28	1.92	$\Omega_4 > \Omega_6 > \Omega_2$	[62]
L5FBS	2.34	7.54	5.40	$\Omega_4 > \Omega_6 > \Omega_2$	[63]
PbF_2-TeO_2-B_2O_3	0.21	1.42	1.87	$\Omega_6 > \Omega_4 > \Omega_2$	[71]
LBTAF	0.27	2.52	2.47	$\Omega_4 > \Omega_6 > \Omega_2$	[72]
LiTFP	0.04	3.49	2.36	$\Omega_4 > \Omega_6 > \Omega_2$	[73]
(PPNSm10)	3.42	2.80	1.85	$\Omega_2 > \Omega_4 > \Omega_6$	[74]
P_2O_5– PbO– Nb_2O_5					
PKMASm	6.83	2.97	2.03	$\Omega_2 > \Omega_4 > \Omega_6$	[75]
K–Mg–Al phosphate					

glass

Table 5:

Transition probabilities (A_R) (s^{-1}), total transition probability (A_T) (s^{-1}), radiative and experimental branching ratios (β_R & β_{exp}) for the prominent emission transitions of Sm^{3+} ions in OFB glasses

Transition	OFBSm01		OFBSm05		OFBSm10		OFBSm15		OFBSm20		OFBSm25	
	A_R											
$^4G_{5/2}\rightarrow{}^6H_{5/2}$	20.16		22.53		23.14		20.77		20.21		19.31	
$^4G_{5/2}\rightarrow{}^6H_{7/2}$	101.27		156.53		181.52		134.94		119.89		93.21	
$^4G_{5/2}\rightarrow{}^6H_{9/2}$	36.22		66.33		73.03		49.37		43.63		31.62	
$^4G_{5/2}\rightarrow{}^6H_{11/2}$	22.13		35.60		39.50		28.76		25.31		19.57	
A_T	200.23		308.79		336.68		258.75		232.21		183.05	
	β_R	β_{exp}	β_R	β_{exp}	β_R	β_{exp}	β_R	β_{exp}	β_R	β_{exp}	β_R	β_{exp}
$^4G_{5/2}\rightarrow{}^6H_{5/2}$	0.100	0.119	0.073	0.160	0.068	0.163	0.080	0.172	0.087	0.156	0.105	0.150
$^4G_{5/2}\rightarrow{}^6H_{7/2}$	0.505	0.415	0.506	0.436	0.539	0.455	0.521	0.440	0.516	0.383	0.509	0.380
$^4G_{5/2}\rightarrow{}^6H_{9/2}$	0.180	0.251	0.214	0.255	0.216	0.322	0.190	0.272	0.187	0.240	0.172	0.232
$^4G_{5/2}\rightarrow{}^6H_{11/2}$	0.110	0.103	0.115	0.128	0.117	0.152	0.111	0.135	0.109	0.130	0.106	0.115

Table 6:

Emission peak wavelength (λ_P) (nm), effective band widths ($\Delta\lambda_P$) (nm), stimulated emission cross-sections (σ_{se}) ($\times 10^{-22}$) (cm^2), gain band width ($\sigma_{se} \times \Delta\lambda_P$) ($\times 10^{-28}$) ($cm^3$) and optical gain ($\sigma_{se} \times \tau_R$) ($\times 10^{-25}$) ($cm^2$ s) for the prominent emission transitions of Sm^{3+} doped OFB glasses.

Spectral parameters	OFBSm01	OFBSm05	OFBSm10	OFBSm15	OFBSm20	OFBSm25
$^4G_{5/2} \rightarrow {}^6H_{5/2}$ ($\lambda_P = 563$ *nm*)						
$\Delta\lambda_P$	8.09	8.09	7.35	9.56	10.3	11.0
σ_{se}	1.27	1.42	1.61	1.11	1.01	0.90
$\sigma_{se} \times \Delta\lambda_P$	1.03	1.15	1.18	1.06	1.04	0.99
$\sigma_{se} \times \tau_R$	6.33	4.60	4.78	4.30	4.34	4.92
$^4G_{5/2} \rightarrow {}^6H_{7/2}$ ($\lambda_P = 598$ *nm*)						
$\Delta\lambda_P$	11.o	10.3	8.09	11.8	13.2	13.2
σ_{se}	5.94	9.87	14.6	7.48	5.92	4.62
$\sigma_{se} \times \Delta\lambda_P$	6.56	10.2	11.8	8.80	7.84	6.11
$\sigma_{se} \times \tau_R$	29.7	32.0	43.4	28.9	25.5	25.2
$^4G_{5/2} \rightarrow {}^6H_{9/2}$ ($\lambda_P = 646$ *nm*)						
$\Delta\lambda_P$	13.2	10.3	10.3	14.7	16.2	17.6
σ_{se}	2.41	5.69	6.29	2.98	2.40	1.60
$\sigma_{se} \times \Delta\lambda_P$	3.19	5.86	6.47	4.39	3.88	2.82
$\sigma_{se} \times \tau_R$	12.0	18.4	18.7	11.5	10.3	8.74
$^4G_{5/2} \rightarrow {}^6H_{11/2}$ ($\lambda_P = 708$ *nm*)						
$\Delta\lambda_P$	22.1	14.7	14.0	25.0	35.3	35.3
σ_{se}	1.28	2.14	2.51	1.02	0.63	0.49
$\sigma_{se} \times \Delta\lambda_P$	2.82	3.15	3.50	2.55	2.25	1.75
$\sigma_{se} \times \tau_R$	6.37	6.93	7.44	3.95	2.75	2.70

Table 7:

Experimental (τ_{exp}) (μs), radiative (τ_R) (μs) lifetimes, quantum efficiencies (η), multi phonon relaxation rates (W_{NR}) (μs^{-1}) and colour co-ordinates of Sm^{3+} ions in OFB glasses.

Name of the sample	$^4G_{5/2} \rightarrow {}^6H_{7/2}$				Colour co-ordinates λ_{exc}=410 nm	
	τ_{exp}	τ_R	η (%)	W_{NR}	X-Co-ordinates	Y-Co-ordinates
OFBSm01	2802±1.9μs	4994	56.1	156.6	0.5623	0.4376
OFBSm05	2548±3.4 μs	3238	78.6	83.63	0.5813	0.4023
OFBSm10	2467±3.8 μs	2970	83.0	68.65	0.5945	0.4065
OFBSm15	2150±5.7 μs	3864	55.6	206.3	0.5831	0.3985
OFBSm20	1564±9.6 μs	4306	36.3	407.1	0.5764	0.3723
OFBSm25	1186±9.3 μs	5462	21.7	660.0	0.5623	0.3746

Table 8:

Comparison of branching ratio (β_R), stimulated emission cross-section (σ_{se}), quantum efficiency (η) and cross-relaxation rates (W_{CR}) of OFBSm10 glass for the prominent emission transition $^4G_{5/2} \rightarrow {}^6H_{7/2}$ (λ_p = 598 nm) with other glasses.

Name of the material	β_R	σ_{se} (x10^{-22} cm^2)	η (%)	W_{CR} (μs^{-1})	Reference
OFBSm10	0.520	14.6	83	68.65	Present work
B1TS	0.500	9.24	26	747	[45]
LiTFP	0.500	6.91	-	197	[78]
NaTFP	0.501	6.23	-	195	[78]
KTFP	0.484	4.76	-	217	[78]
PKFBASm	0.080	0.99	75	76	[84]
Sm^{3+}:BNNS	0.596	9.15	85	57	[85]
Sm^{3+}:BCNS	0.402	11.8	86	56	[85]
1SLBTZ	0.624	16.0	24	1201	[86]
TZKCSm10	0.380	6.68	47	694	[87]
CaSm	0.511	5.00	-	-	[88]
PbSm	0.510	5.73	-	-	[88]
ZnSm	0.505	7.12	-	-	[88]
NCS:Sm^{3+}	0.360	3.07	-	-	[89]

Table 9:

Energy transfer parameter (Q), critical transfer distance (R_0) (Å), donor–acceptor interaction parameter ($C_{DA,}$ $10^{-41}cm^6 s^{-1}$) of Sm^{3+} doped OFB glasses.

Name of the Glass	Q	R_0	C_{DA}	References
OFBSm01	-	-	-	Present System
OFBSm05	-	-	-	Present System
OFBSm10	0.240	5.150	0.666	Present System
OFBSm15	0.725	6.526	2.758	Present System
OFBSm20	2.234	8.648	14.93	Present System
OFBSm25	3.320	9.191	21.52	Present System
CFB1.0	0.150	4.390	0.302	[33]
1SmPbFB	2.173	6.850	3.730	[57]
PKFBASm1.0	0.217	4.850	0.402	[71]
LBTAF1.0	0.430	5.130	13.08	[72]
PBFPSm10	0.950	7.550	0.690	[92]

Fig. 1 : XRD spectrum of an undoped OFB glass.

Fig. 2 : Variation of density and molar volume with Sm^{3+} ion concentration in OFB glasses.

Fig. 3 : FTIR spectrum of an undoped OFB glass.

Fig. 4(a): Absorption spectrum of 1 mol% of Sm^{3+} ions doped OFB glass in UV-vis-NIR region.

Fig. 4(b): Variation of intensity of hypersensitive transition and $\sum \Omega_\lambda$ with Sm^{3+} ion concentration in OFB glasses.

Fig. 5 : Excitation spectra of Sm^{3+} ions in OFB glasses in terms of wavelength (nm). The inset figure shows the excitation spectra of Sm^{3+} ions in OFB glasses in terms of wavenumber (cm^{-1}).

Fig. 6 : Photoluminescence spectra of Sm^{3+} doped OFB glasses recorded using 410 nm CW laser in terms of wavenumber (cm^{-1}). The right inset figure shows the photoluminescence spectra of OFBSm glasses at 402 nm excitation in terms of wavelength (nm). The left inset figure shows the photoluminescence spectra of OFBSm glasses at 410 nm excitation in terms of wavelength (nm).

Fig. 7 : The decay curves for $^4G_{5/2} \rightarrow {}^6H_{7/2}$ (598 nm) emission of Sm^{3+} ions in OFB glasses when excited at 410nm.

Fig. 8 : Partial energy level diagram showing the absorption, excitation and emission mechanism and cross-relaxation channels involved in Sm^{3+} ions in OFB glasses.

Fig. 9 : CIE chromaticity co-ordinates of Sm^{3+} ions in OFB glasses having different concentrations located in the CIE 1931 chromaticity diagram along with the confocal photoluminescence images recorded at an excitation wavelength 410 nm (CW Laser).

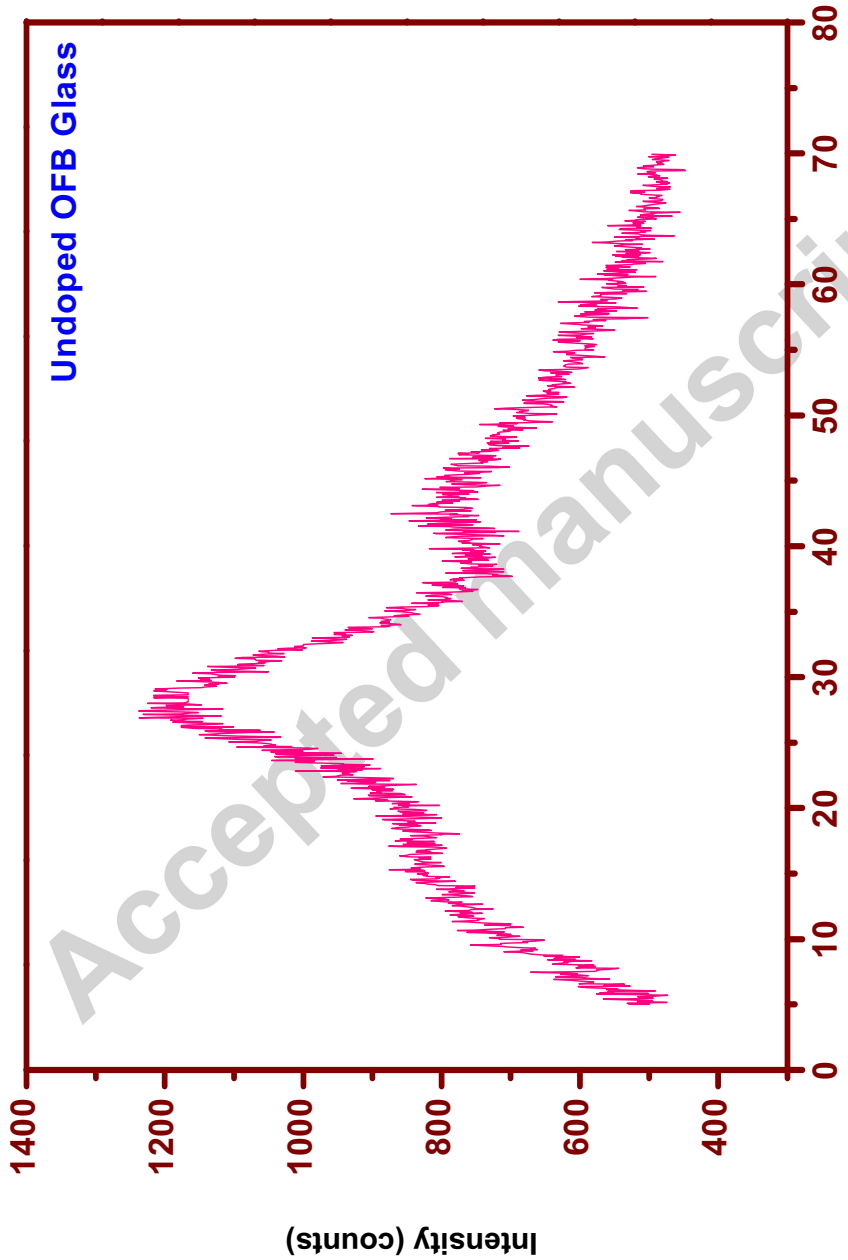

Fig. 1

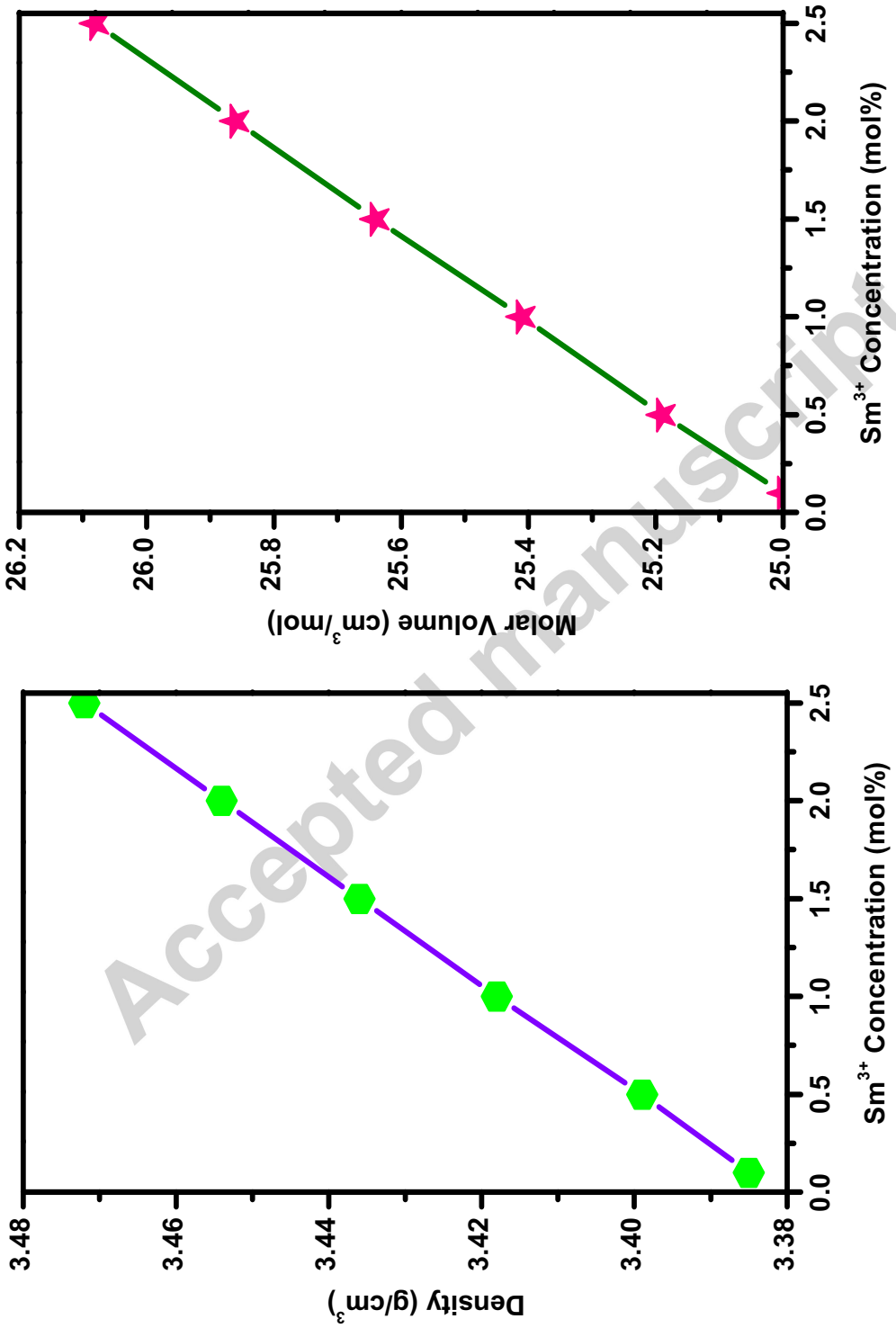

Fig. 2

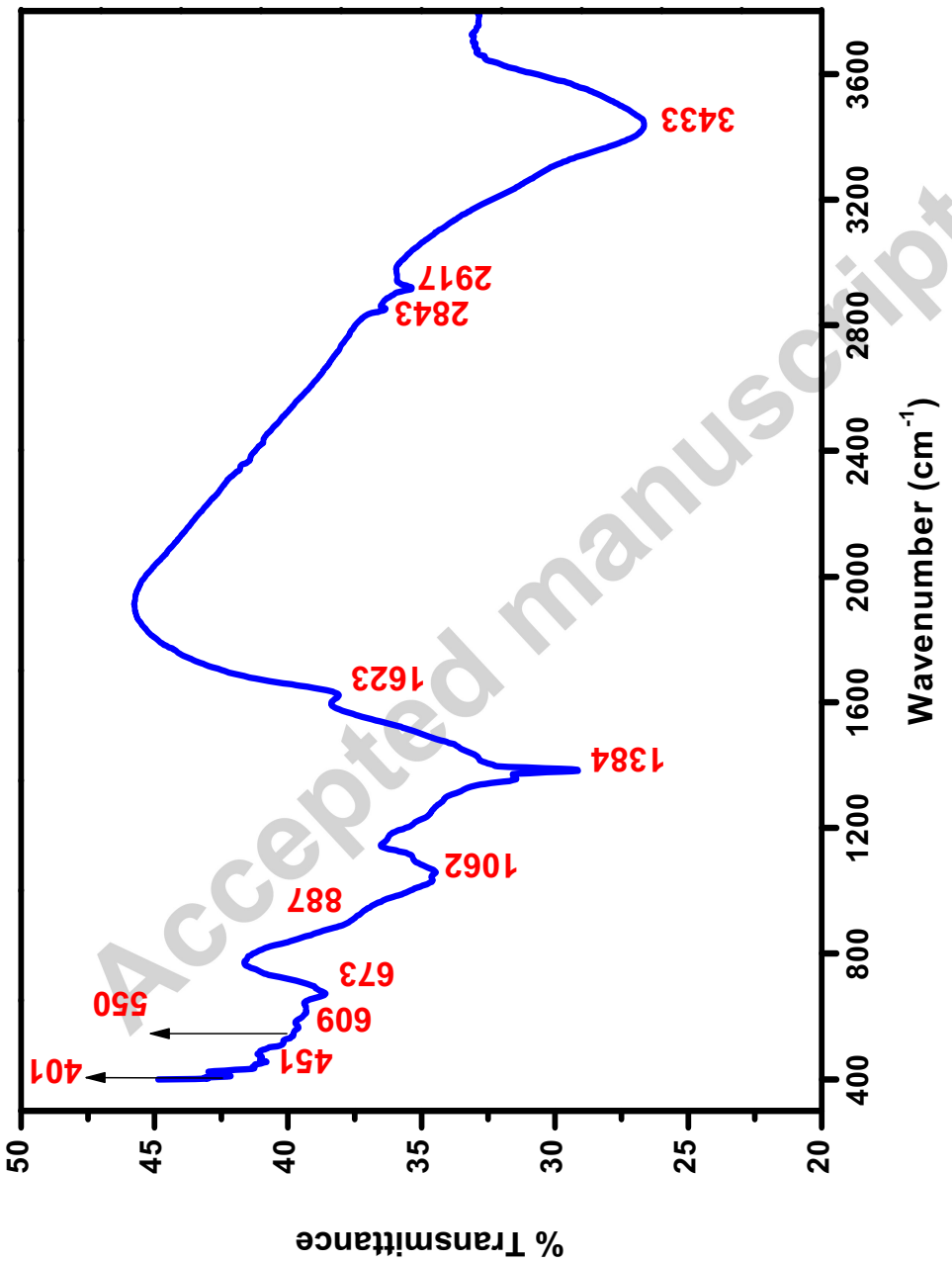

Fig. 3

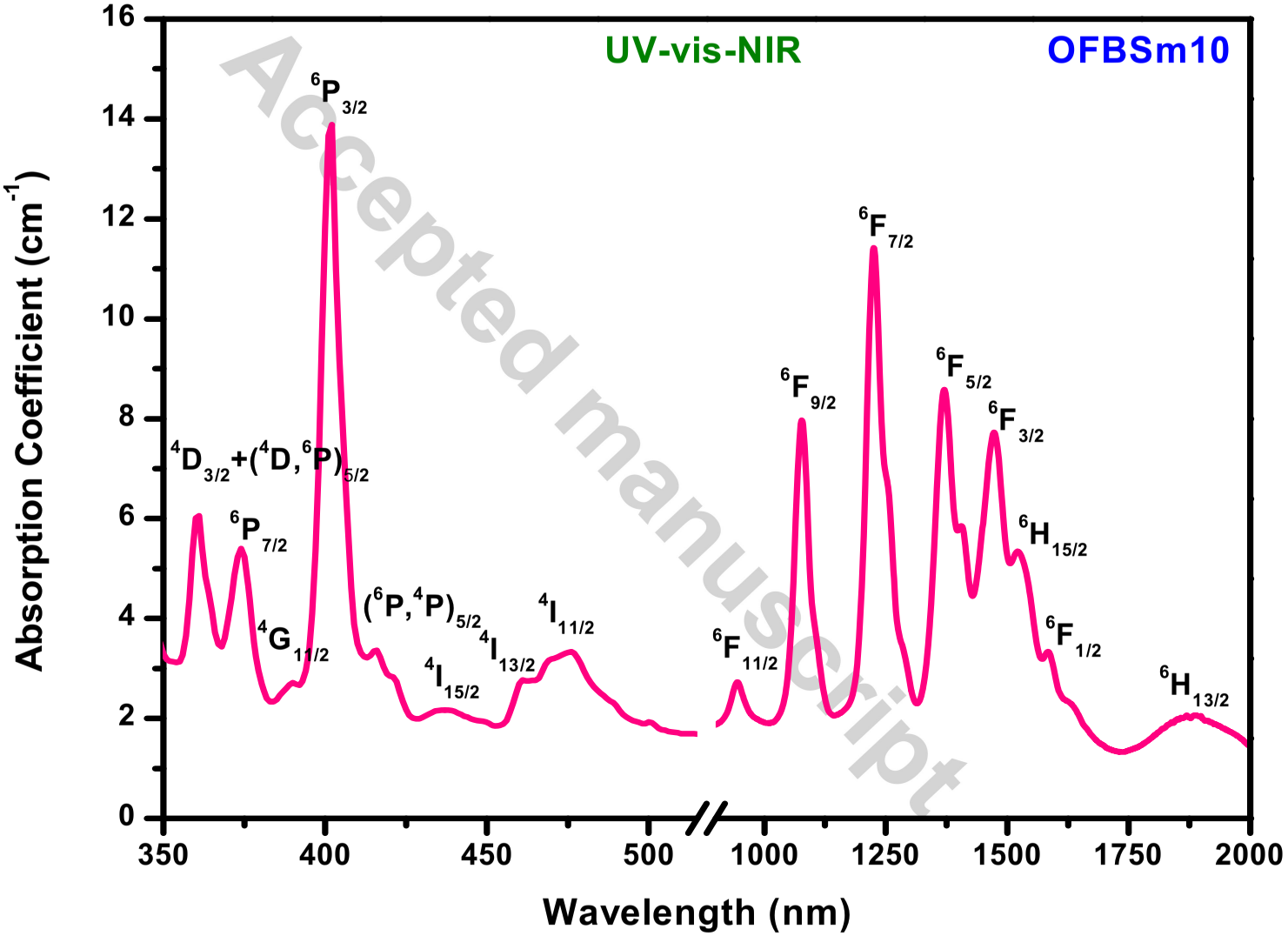

Fig. 4(a)

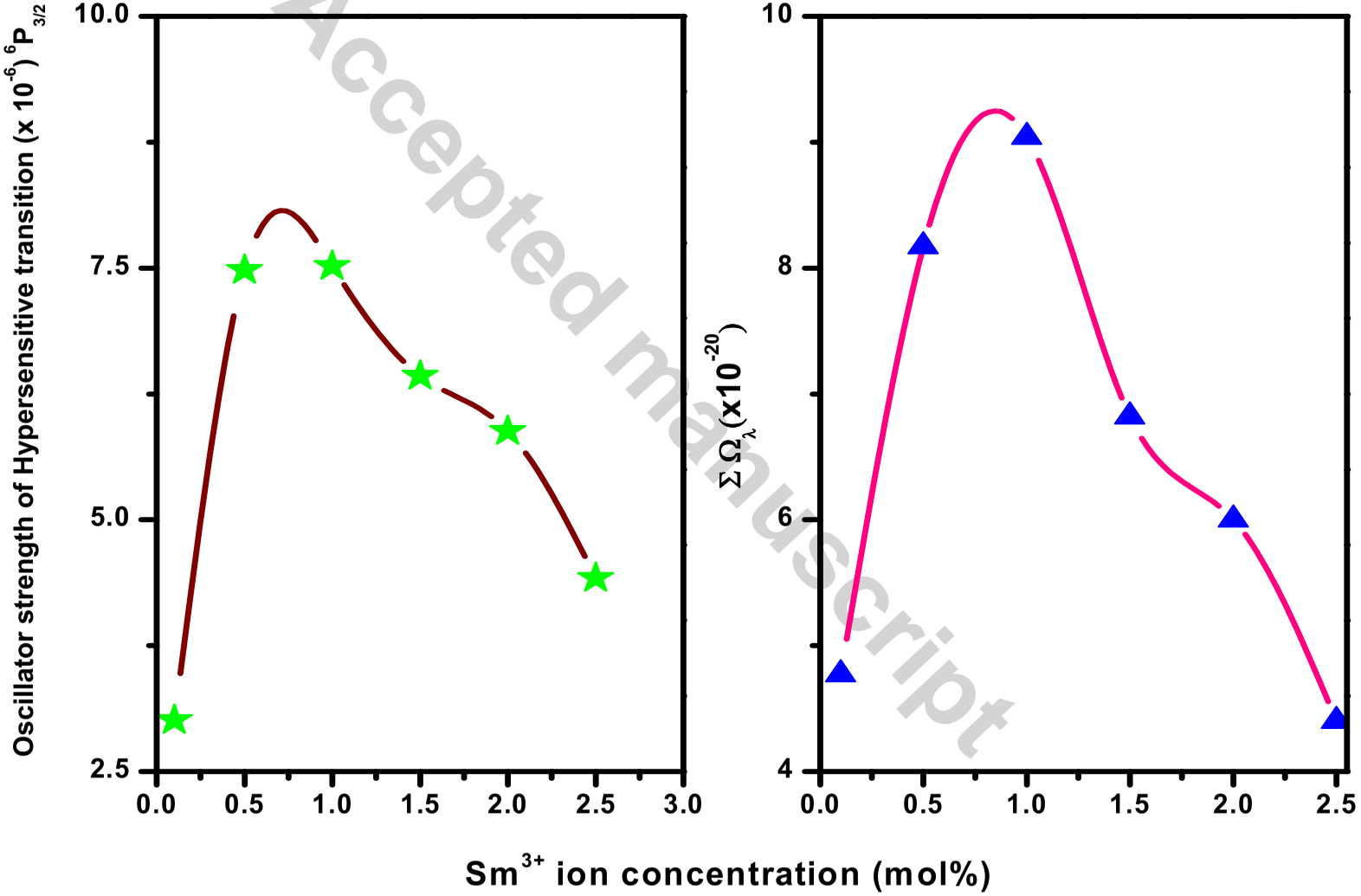

Fig 4. (b)

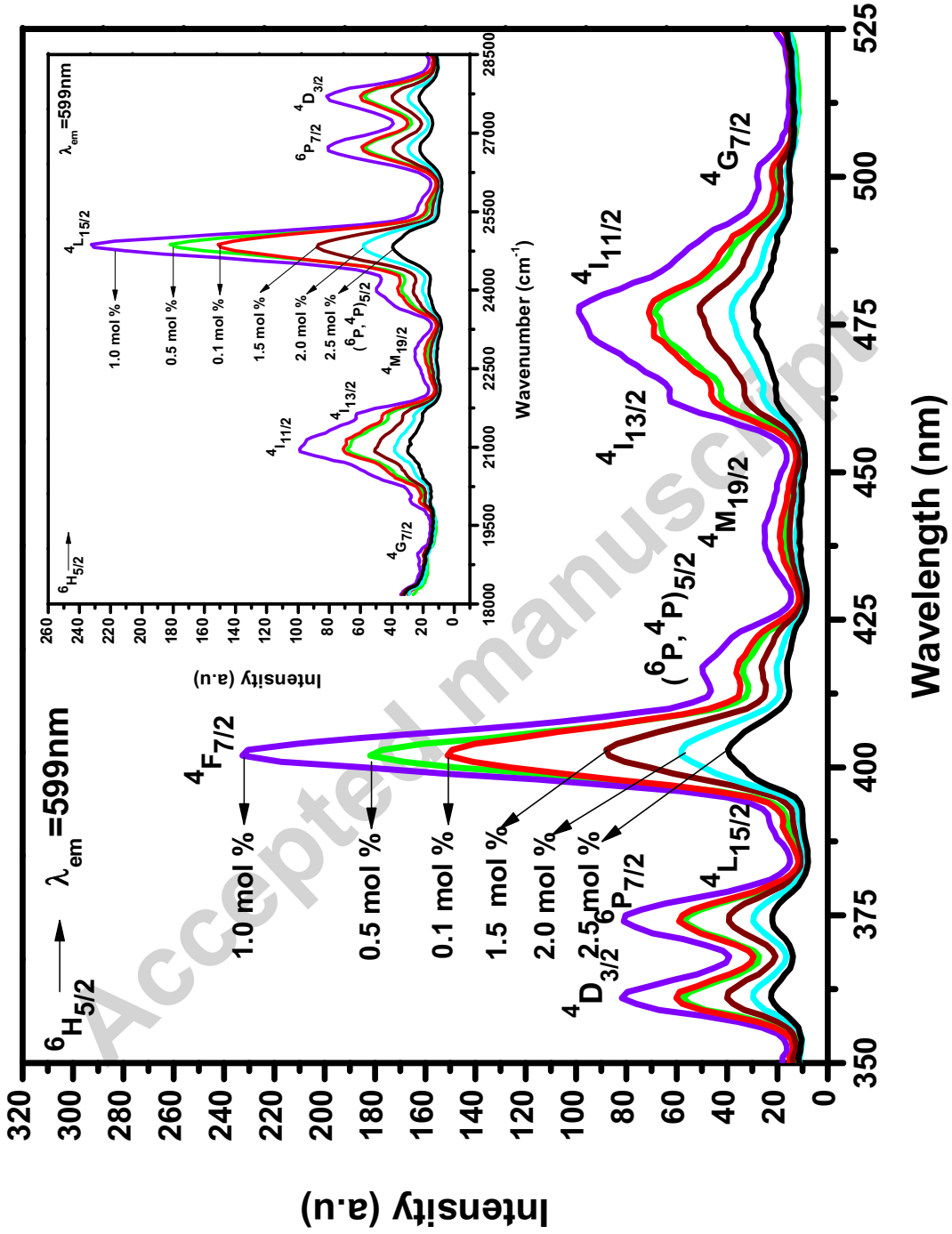

Fig. 5

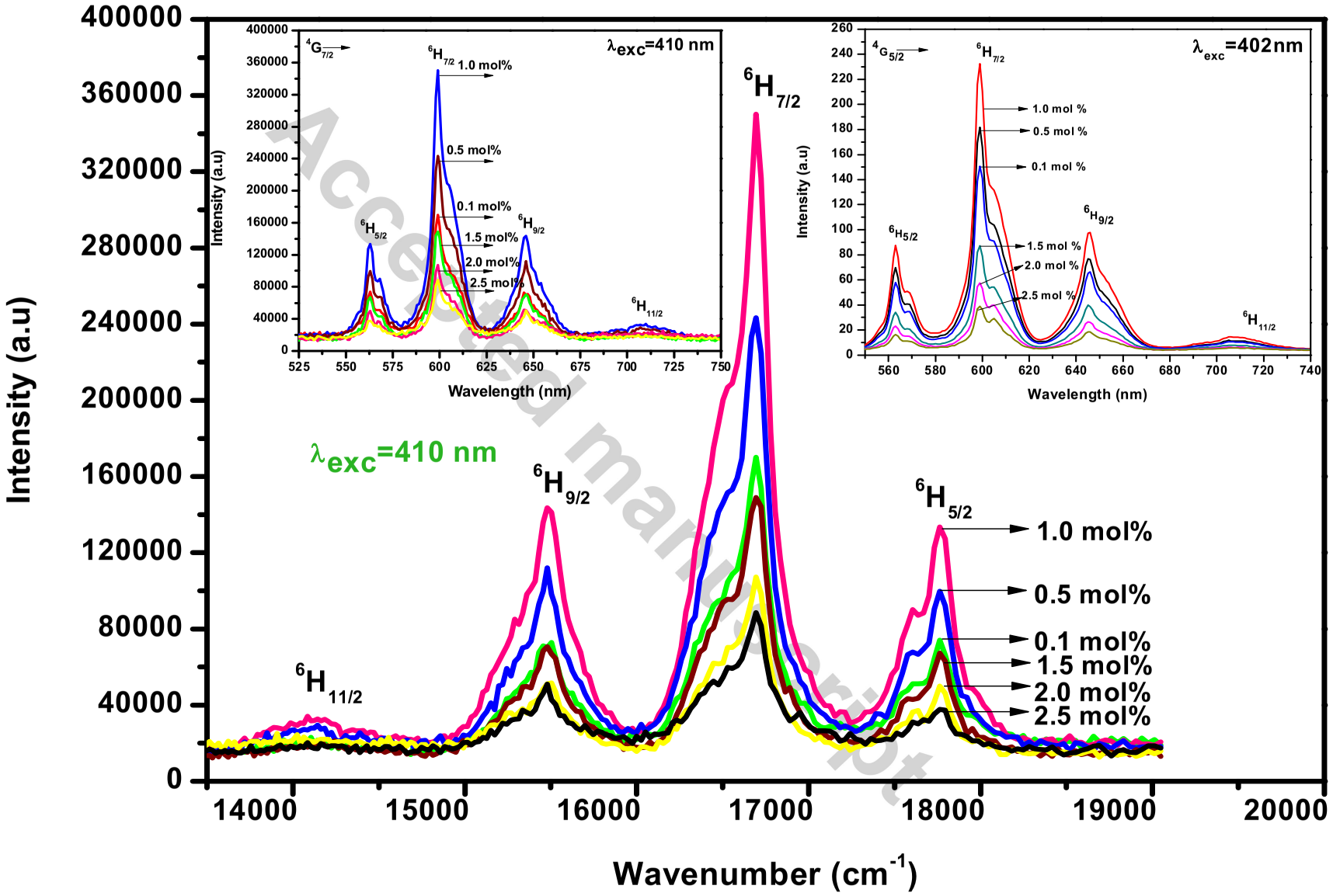

Fig. 6

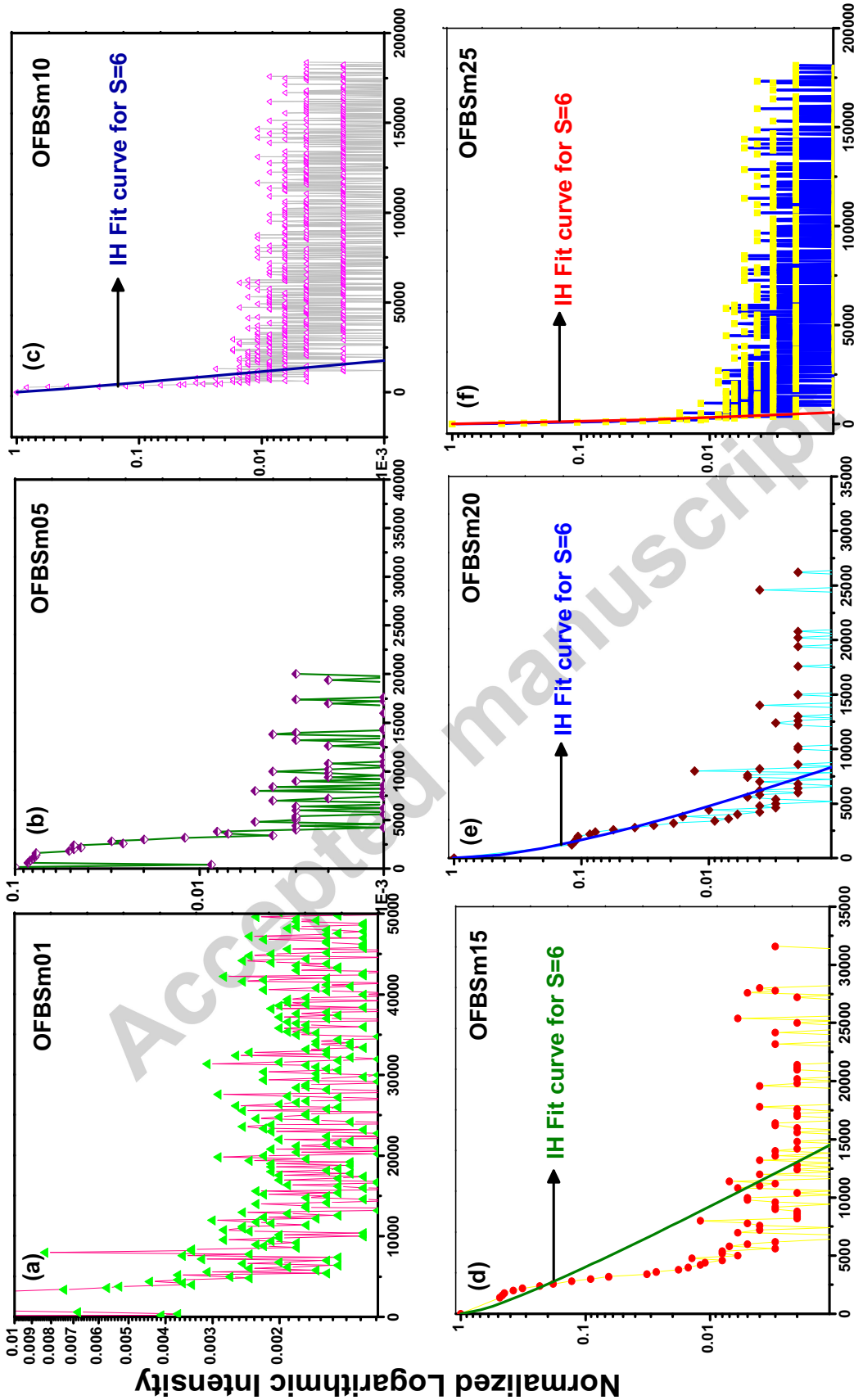

Fig. 7

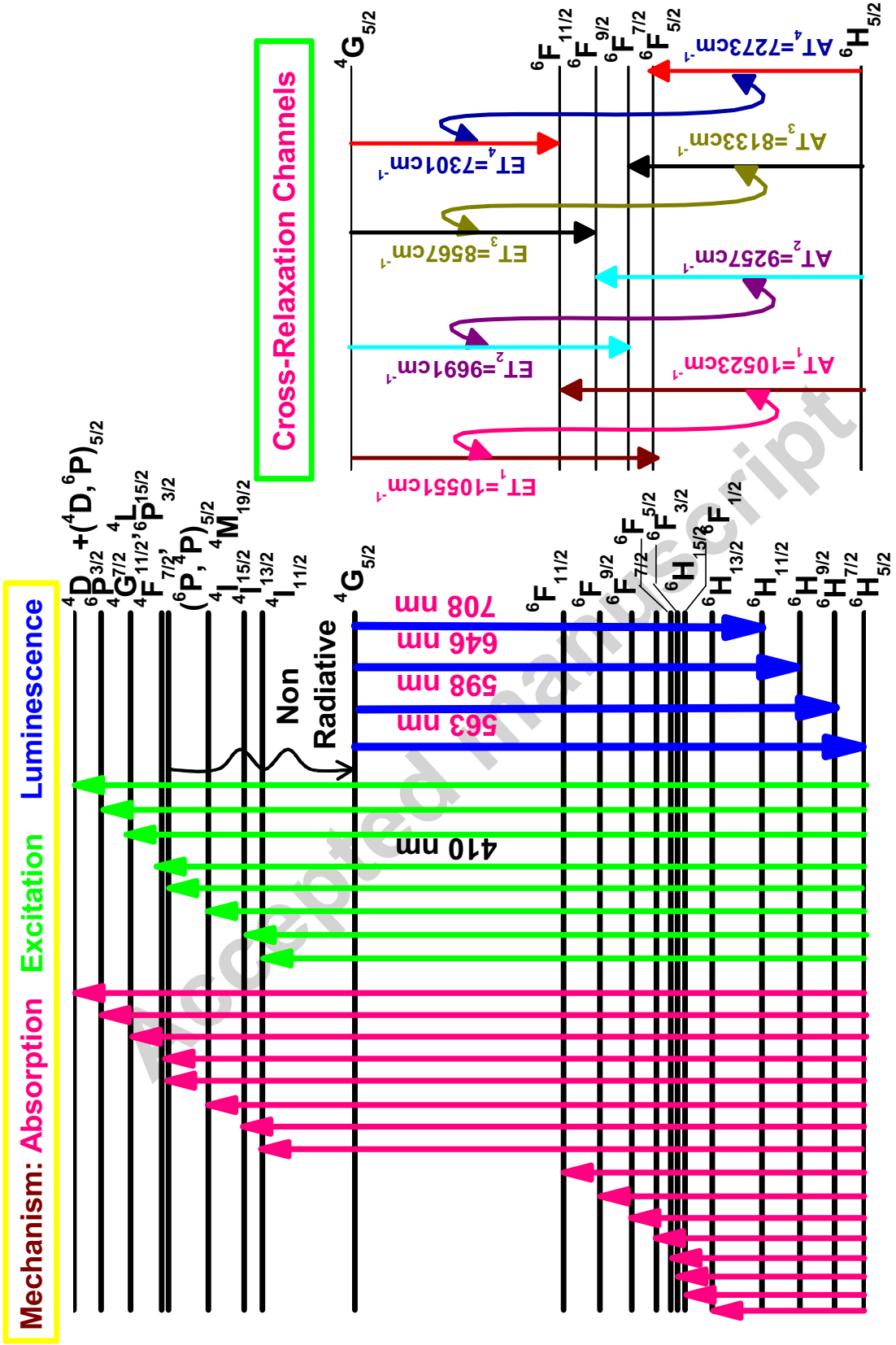

Fig. 8

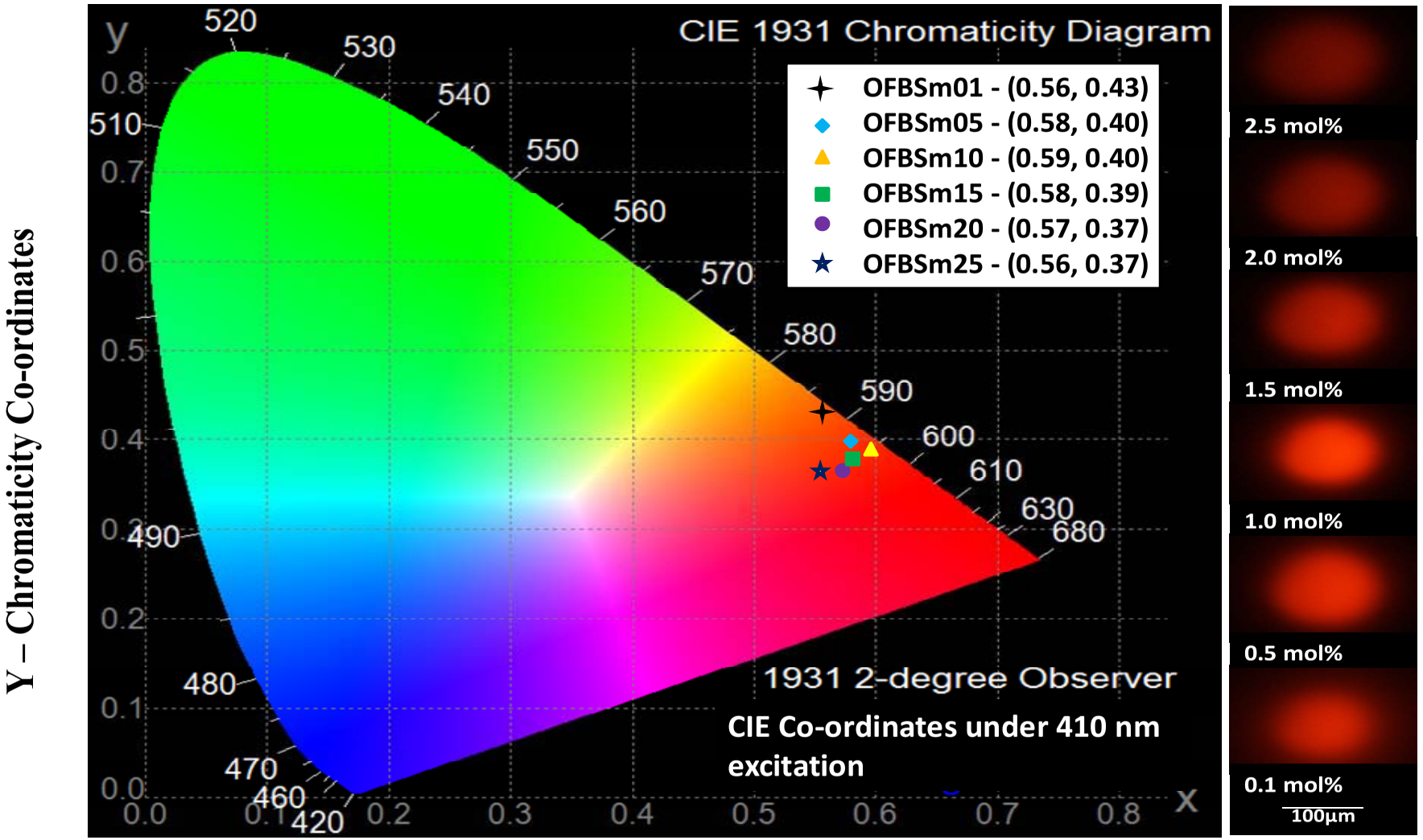

Fig. 9

High Lights

1. Sm^{3+} doped OFB glasses have been synthesized using melt quenching technique.
2. From the absorption spectra, J-O parameters have been calculated using J-O theory.
3. Emission cross-sections & efficiencies are calculated for laser transitions.
4. CIE colour co-ordinates were evaluated using emission spectra.
5. OFBSm1.0 glass was found to be the best for laser action in visible orange region.

Supercooling transition in phase separated manganite thin films: An electrical transport study

Sandeep Singh, Pawan Kumar, P. K. Siwach, Pawan Kumar Tyagi, and H. K. Singh

Citation: Applied Physics Letters **104**, 212403 (2014); doi: 10.1063/1.4880725
View online: http://dx.doi.org/10.1063/1.4880725
View Table of Contents: http://scitation.aip.org/content/aip/journal/apl/104/21?ver=pdfcov
Published by the AIP Publishing

Supercooling transition in phase separated manganite thin films: An electrical transport study

Sandeep Singh,[1,2] Pawan Kumar,[1,3] P. K. Siwach,[1] Pawan Kumar Tyagi,[2] and H. K. Singh[1,a)]

[1]*National Physical Laboratory (Council of Scientific and Industrial Research), Dr. K. S. Krishnan Marg, New Delhi 110012, India*
[2]*Department of Applied Physics, Delhi Technological University, Delhi 110042, India*
[3]*Inter-University Accelerator Centre, Aruna Asaf Ali Marg, New Delhi 110067, India*

(Received 19 March 2014; accepted 18 May 2014; published online 29 May 2014)

The impact of variation in the relative fractions of the ferromagnetic metallic and antiferromagnetic/charge ordered insulator phases on the supercooling/superheating transition in strongly phase separated system, $La_{5/8-y}Pr_yCa_{3/8}MnO_3$ ($y \approx 0.4$), has been studied employing magnetotransport measurements. Our study clearly shows that the supercooling transition temperature is non-unique and strongly depends on the magneto-thermodynamic path through which the low temperature state is accessed. In contrast, the superheating transition temperature remains constant. The thermo-magnetic hysteresis, the separation of the two transitions and the associated resistivity, all are functions of the relative fraction of the coexisting phases. © *2014 AIP Publishing LLC*. [http://dx.doi.org/10.1063/1.4880725]

Phase separation (PS) is believed to be the key ingredient of the physics of doped rare earth manganites.[1–3] It dominates the composition-temperature (x-T) diagram of intermediate and low bandwidth manganites like $Nd_{1-x}Sr_xMnO_3$,[3,4] $Sm_{1-x}Sr_xMnO_3$,[5,6] and $La_{1-x-y}Pr_yCa_xMnO_3$.[7–10] Amongst these materials, $La_{1-x-y}Pr_yCa_xMnO_3$ has emerged as the prototypical phase separated system and its different variants like bulk single crystal, polycrystals, and thin films have been investigated.[7–16] The strong nature of the phase separation has been established by the observation of (i) strong divergence of the zero filed cooled (ZFC) and field cooled warming (FCW) magnetization, (ii) pronounced hysteresis between the field cooled cool (FCC) and FCW magnetization, and (iii) prominent thermomagnetic hysteresis in the temperature and magnetic field (H) dependent resistivity (ρ) measured in cooling-warming cycles.[7–16] A study by Uehara *et al.*[7] has shown the coexistence of sub-micrometer scale ferromagnetic metallic (FMM) and antiferromagnetic/charge ordered insulator (AFM/COI) clusters and that the latter is explicit in magnetotransport measurements only at $y \geq 0.3$. Consequently, the electrical transport becomes percolative, which is evidenced by huge residual resistivity (ρ_0) for $y \approx 0.4$ in the metallic regime.[7] The study of Ghivelder and Parisi[8] on bulk $La_{5/8-y}Pr_yCa_{3/8}MnO_3$ ($y \approx 0.4$) has shown that COI phase appears at $T_{CO} \sim 230$ K and subsequently acquires AFM and FM spin order $T_N \sim 180$ and $T_C \sim 80$ K, respectively. Due to the rapid spatial and temporal variations in the relative fraction of the FMM and AFM/COI phases, large relaxation effects are also observed.[8] Further, the theoretical study by Ghivelder and Parisi[8] has predicted that interplay between temperature and separation of the system from equilibrium could create multiple blocked states. Sharma *et al.*[9] studied the same material and have established the existence of a liquid like magnetic phase in the phase separated regime, which transforms cooperatively to a randomly frozen glass like phase at low temperature. The frozen glass like phase (termed as strain glass) is believed to arise from the presence of martensitic accommodation strain.[9] Wu *et al.*[10] have demonstrated that in $La_{5/8-y}Pr_yCa_{3/8}MnO_3$ ($y \approx 0.4$) thin films the magnetic liquid like phase exhibits a supercooled glass transition. This glass transition is believed to arise due to the presence of the accommodation strain caused by distinct structural symmetries of FMM and AFM/COI phases. Their study has also provided evidence in favour of the non-ergodic nature of the magnetic liquid. Wu *et al.*[10] have shown that non-ergodicity appears when the long range cooperative strain interactions hinder the cooperative dynamic freezing of the first-order AFM/COI–FMM transition.[9,10]

The FCC-FCW and thermoresistive hysteresis are regarded as signatures of supercooling and superheating transition of the magnetic liquid formed by competing FMM and AFM phases in the presence of martensitic of accommodation strain and long range cooperative strain interactions.[8–10] Despite the exhaustive investigations on different variants of the $La_{1-x-y}Pr_yCa_xMnO_3$, the nature of the supercooling/superheating transitions, e.g., their dependence on relative fractions of FMM and AFM phases has not been probed through electrical transport measurements. The different relative fractions of the FM/AFM phases at the beginning of the magneto-thermodynamic process are expected to lead to different thermodynamic paths and yield different supercooling transition temperatures. Hence, it is important to investigate the signature of different magneto-thermodynamic paths in electrical transport. In this Letter, we report the electrical transport studies on $La_{5/8-y}Pr_yCa_{3/8}MnO_3$ ($y \approx 0.4$) epitaxial thin films. Our results demonstrate that of the two observed insulator-metal transitions (IMTs), the lower one caused by the supercooling of a magnetic liquid is non-unique, while the upper on remains constant.

The $La_{5/8-y}Pr_yCa_{3/8}MnO_3$ ($y \approx 0.4$) thin films were grown by RF magnetron sputtering of a stoichiometric (2 in.)

a)Author to whom correspondence should be addressed. Electronic mail: hks65@nplindia.org.

target in 200 mTorr of Ar + O_2 (80 + 20) mixture on single crystal (001) $SrTiO_3$ (STO) substrates maintained at ~800 °C. The lattice mismatch (ε) between the target and substrate is ≈−1.93% ($\varepsilon = (a_t - a_s)_{x100}/a_s$ where a_t and a_s are the lattice parameters of the bulk target and substrate, respectively) and hence the strain is tensile. In order to achieve optimum oxygen content, the films were annealed at ≈900 °C for 10 h in flowing oxygen.

The film thickness estimated from the X-ray reflectivity data is ~41 nm. The high resolution X-ray diffraction (HRXRD; 2θ-ω scan, ϕ-scan, and ω-2θ scan) confirmed the epitaxial nature of the films and also showed that the film is under tensile strain. The significantly reduced out-of-plane lattice constant of the film is $a_f = 3.7988$ Å ($a_{bulk} = 3.831$ Å), which confirms the presence of appreciable tensile strain. The occurrence of the step-terrace features in the surface topography further confirms the epitaxial nature of the films.

The temperature dependent magnetization (M-T) was measured using ZFC, FCC, and FCW protocols. The ZFC, FCC, and FCW data plotted in Fig. 1 show several interesting features, viz., (i) huge irreversibility in the ZFC and FCW curves, (ii) pronounced hysteresis between the FCC and FCW curves, (iii) reversible behavior of FCC and FCW curves below T ≈ 26 K, (iv) a peak in the FCW M-T around $T_P \sim 43$ K, and (v) sharp drop in ZFC M-T curve around T_P. The ZFC-FCW irreversibility, which is distinct from that of a representative spin glass state,[17] is invariably observed in phase separated manganites as a signature of cluster glass state.[18–20] The cluster glass state is prevalent in the intermediate bandwidth manganites having $x \sim 1/2$[18] or over a wide range of divalent doping (x) in low bandwidth manganites[19,20] and originates due to the coexistence of FMM and AFM/COI phases below the Neel temperature T_N. The sharp drop in the ZFC curve observed at temperature marked T_P is a signature of cluster freezing. The prominent FCC-FCW hysteresis is signature of the different magneto-thermodynamics of the system in the two protocols and arises due to the global frustration created by the AFM/COI phase that increases the energy

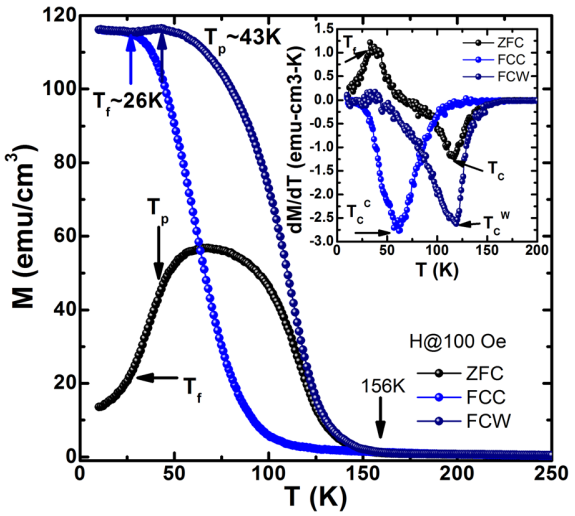

FIG. 1. The temperature dependence of ZFC, FCC, and FCW magnetization measured at H = 100 Oe. The inset shows the temperature derivative of the ZFC, FCC, and FCW curves. Various transitional features are marked in the figure.

of the system and also the degeneracy of the energy minima. Hence, the origin of the non-ergodicity is traceable to the AFM/COI phase, which alone can create frustration. The low temperature (T < 26 K) reversible behavior of the FCC and FCW has been regarded as a signature of an equilibrium state attained in the FCC protocol by Ghivelder and Parisi[9] and could be related to the blocking of system or freezing of the cluster glass. The increase in magnetization at T > 26 K is the signature of unblocking of the system states, and hence, the peak at $T_P \sim 43$ K can be regarded as the onset of cluster freezing.

The FM transition, determined from the derivative of M-T data (inset of Fig. 1), occurs at $T_C \approx 117$ K, $T_C^C \approx 63$ K, and $T_C^W \approx 120$ K in the ZFC, FCC, and FCW protocols, respectively. The protocol dependence of FM transition temperature could be regarded as evidence of non-ergodicity. A significantly lower value of FM transition temperature in FCC protocol can be considered as a consequence of supercooling,[10] whereas the FCW FM transition at $T_C^W \approx 120$ K can be taken as the equilibrium FM transition. The COI and AFM transitions are not explicit in the M-T data. This could be attributed to defect induced quenching of AFM/COI in thin film form.[12–16]

The drastic difference between the FM transition temperatures in FCC and FCW protocols can be understood in terms of the accommodation strain arising due to the distinct structural symmetry of the coexisting FM (pseudocubic) and AFM/COI (orthorhombic) phases.[11,21] The accommodation strain and the magnetic frustration induced by AFM order would create multiple minima in the energy landscape of the system and hence could hinder the nucleation of the equilibrium low temperature state. Such a scenario in turn could give rise to a liquid like magnetic phase.[9] The electrical transport characteristics of the magnetic liquid phase should depend on the relative fractions of FM and AFM/COI phases at the instant from where the low temperature state is arrived. Hence, IMT temperature (T_{IM}) corresponding to liquid like magnetic phase should be non-unique and depend on the magneto-thermodynamic path used to access the low temperature state of the system. In view of the variation in the relative fractions of FM and AFM/COI phases across T_C^W, T_{IM} must be a function of the temperature (T*) corresponding to the initial state of the magneto-thermodynamic process. This was experimentally verified by temperature dependent resistivity (ρ-T) measurement using a protocol in which the magneto-thermodynamic cycle was started from a temperature (T*), which was achieved by cooling the sample from room temperature to 6 K and subsequent warming up to T*. ρ-T was measured during cooling and warming employing the cycle T* → 6 K → T ($T > T_{IM}^W$) at H = 0 and H = 10 kOe. In view of the M-T data present above, it is obvious that each T* corresponds to a distinct ratio of FMM and AFM/COI phases. Here, we would like to mention that the impact of thermal cycling on the thermoresistive hysteresis, IMT, and peak resistivity in phase separated manganites has also been studied previously.[22,23] Mahendiran *et al.*,[22] employing a protocol of measurement different from the one used in the present case, have shown that (i) the resistivity close to and just below IMT is unstable, (ii) the resistivity increases with respect to thermal cycling, and (iii) the ρ-T

behaviour is hysteretic even when the sample is warmed from just above the IMT. These studies have outlined the important role of strain and percolation in electrical transport in phase separated manganites.

The full cycle (300 K → 6 K → 300 K) ρ-T taken during cooling and warming (cooling and warming rate 1 K/min) is plotted in Fig. 2(a). In the cooling cycle IMT occurs at $T_{IM}^{C} \approx 64$ K, where ρ drops by more than four orders of magnitude within a narrow temperature window. This is generally attributed to the abrupt enhancement in the FMM fraction at the cost of the AFM/COI.[3] During the warming cycle, the ρ-T curve shows a minimum at $T_m \approx 45$ K and IMT appears at $T_{IM}^{W} \approx 123$ K. The rapid rise in resistivity just below T_{IM}^{W} corresponds to the enhanced fraction of the AFM/COI. The huge thermo-resistive hysteresis in the ρ-T curve and large $\Delta T_{IM} = T_{IM}^{W} - T_{IM}^{C} \approx 59$ K unravels the strongly phase separated nature of the system. The T_{IM}^{C} almost coincides with the FCC $T_C^{C} \approx 63$ K, while $T_{IM}^{W} \approx 123$ K is very close to $T_C^{W} \approx 120$ K. It is believed that the drastically lowered T_{IM}^{C} and T_C^{C} is caused by supercooling of the phase separated magnetic liquid consisting of FMM and AFM/COI sub-lattices.[7–13]

The zero filed cooling and warming cycle ρ-T data acquired after cooling from different T* is plotted in Figs. 2(b)–2(f). When the film is cooled down from T* ≈ 97 K, IMT not is observed in the cooling cycle. However, for all higher values of T*, IMT appears in the cooling cycles at temperature that we denote by which we denote by $T_{IM}^{C^*}$. The value of $T_{IM}^{C^*}$ for T* ≈ 105 K, 113 K, 117 K, 122 K, and 143 K are observed to be 103 K, 95 K, 88 K, 79 K, and 69 K, respectively. For values of T* ≥ 170 K, the $T_{IM}^{C^*}$ saturates to

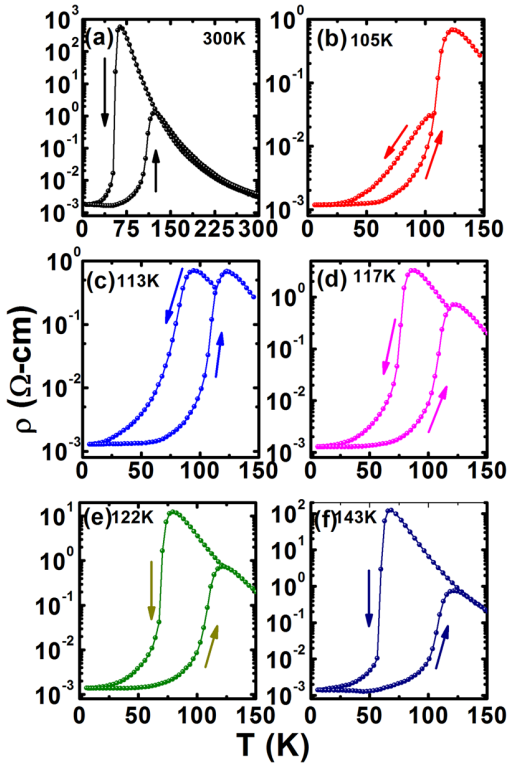

FIG. 2. Temperature dependence of resistivity measured in zero magnetic field in cooling and warming cycles after initial cooling to 6 K and subsequent warming to different T*.

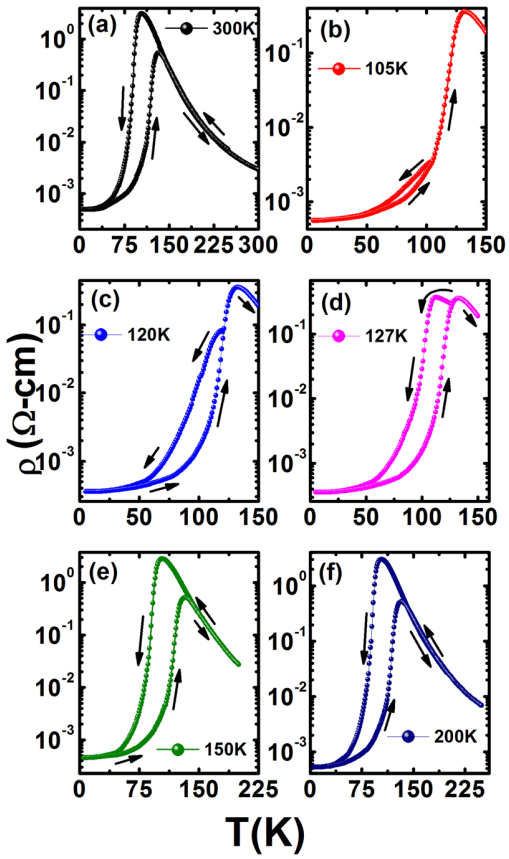

FIG. 3. Temperature dependence of resistivity measured in a magnetic field of H = 10 kOe in cooling and warming cycles after initial cooling to 6 K and subsequent warming to different T*.

$T_{IM}^{C} \approx 64$ K, the full cycle value. Interestingly, the warming cycle IMT, $T_{IM}^{W^*}$ remains independent of T*. The field (H = 10 kOe) cooling and warming cycle ρ-T data acquired after cooling from different T* are plotted in Fig. 3. The full cycle ρ-T shows $T_{IM}^{C} \approx 104$ K and $T_{IM}^{W} \approx 133$ K. At H = 10 kOe, the cooling cycle IMT shows an increase of 40 K, which, however, is only 10 K in the warming cycle. This could be attributed to the substantial suppression of AFM induced frustration in the phase separated regime. For T* = 105 K, no IMT was observed in cooling cycle, while in warming cycle IMT was observed at $T_{IM}^{W^*} \approx 133$ K. The absence of IMT for T* = 105 K shows that at this temperature the film has a dominant FMM fraction. For higher T* ($<T_{IM}^{W}$), e.g., 120 K and 127 K, IMT occurs at $T_{IM}^{C^*} \sim 119$ K and 112 K, respectively, was observed in the cooling cycle but the warming cycle IMT remained constant at $T_{IM}^{W^*} \approx 133$ K (Fig. 3). For further higher values of T* = 150 K, 200 K, and 300 K, both $T_{IM}^{C^*}$ and $T_{IM}^{W^*}$ remain constant at 104 K and 133 K, respectively. The variation of $T_{IM}^{C^*}$ and the corresponding peak resistivity measured in the cooling cycle (ρ_{IMC}) are plotted in Figs. 4(a) and 4(b), respectively. From Fig. 4, it is clear that the relative fraction of the FMM and AFM phases also controls the resistivity (ρ_{IMC}) at $T_{IM}^{C^*}$. The difference of more than two orders of magnitude in ρ_{IMC} measured at H = 0 and 10 kOe clearly reflects the colossal magnetoresistance effect. Another interesting feature seen in the zero field warming ρ-T data is the appearance (disappearance) of resistivity minimum ρ_m (T_m)

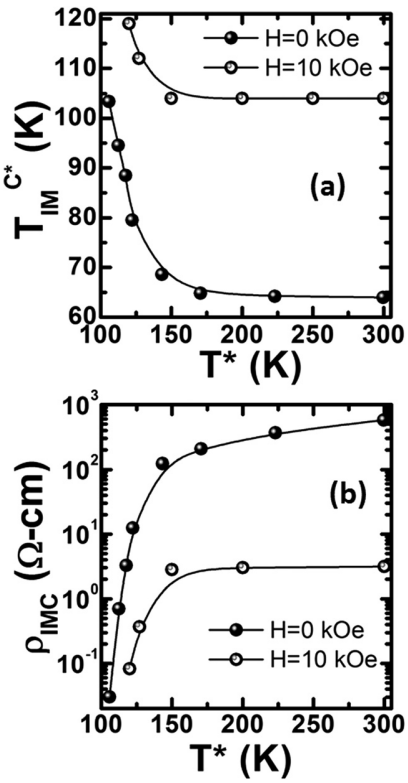

FIG. 4. (a) The variation of the T_{IM}^{C*} as a function of the characteristic temperature T^* measured at H = 0 and 10 kOe. (b) The variation of the peak resistivity measured in the cooling cycle as a function of T^*.

for all $T^* \geq 143$ K ($\leq$122 K). In the measurements carried out at H = 10 kOe, no ρ_m (T_m) is observed at all. When the sample is cooled from a T* at which the either FMM is in minority or absent, T_{IM}^{C*} saturates to the lowest value $T_C^C \approx 64$ K and the resistivity minimum reappears. This clearly shows that the AFM fraction is a key to the occurrence of resistivity minimum and is probably related to the freezing of the strain glass state.

The existence of different T_{IM}^{C*} for different $T^* < T_{IM}^W$ is an unambiguous signature of non-ergodicity, which in the present case arises due the existence of different energy configuration for each magneto-thermodynamic path. At $T^* > T_{IM}^W$, the fraction of FMM (AFM/COI) phase decreases (increases), leading to dilution of the competitive phase coexistence tendency and therefore no modulation of the IMT. The results presented above clearly show that the supercooling transition temperature is strongly dependent on T*, i.e., on the relative fraction of the two coexisting phases (FMM and AFM/COI) and hence the degree of magnetic frustration at the temperature from where the system is cooled down to access the low temperature state.

To conclude, we have shown that the electrical transport in a strongly phase separated manganite thin film is extremely sensitive to the relative fraction of the coexisting FMM and AFM/COI phases and has inherent non-ergodicity. The phase separation tendency is weakened when the fraction of AFM/COI phase is reduced. The supercooling insulator-metal transition is non-unique and depends on the relative fractions of the FMM and AFM phases at the start of the magneto-thermodynamic process. In contrast, the superheating transition has equilibrium characteristic and remains independent of the ratio of the two ordered phases.

Authors are grateful to Professor R. C. Budhani for his persistent encouragement. Dr. Anurag Gupta and Dr. V. P. S. Awana are thankfully acknowledged for magnetic (MPMS-DST facility) and magnetotransport measurement, respectively.

[1]E. Dagotto, T. Hotta, and A. Moreo, Phys. Rep. **344**, 1 (2001).
[2]E. Dagotto, New J. Phys. **7**, 67 (2005).
[3]Y. Tokura, Rep. Prog. Phys. **69**, 797 (2006).
[4]H. Kuwahara, Y. Tomioka, A. Asamitsu, Y. Moritomo, and Y. Tokura, Science **270**, 961 (1995).
[5]Y. Tomioka, H. Hiraka, Y. Endoh, and Y. Tokura, Phys. Rev. B **74**, 104420 (2006).
[6]M. K. Srivastava, A. Kaur, K. K. Maurya, V. P. S. Awana, and H. K. Singh, Appl. Phys. Lett. **102**, 032402 (2013).
[7]M. Uehara, S. Mori, C. H. Chen, and S.-W. Cheong, Nature **399**, 560 (1999).
[8]L. Ghivelder and F. Parisi, Phys. Rev. B **71**, 184425 (2005).
[9]P. A. Sharma, S. B. Kim, T. Y. Koo, S. Guha, and S.-W. Cheong, Phys. Rev. B **71**, 224416 (2005).
[10]W. Wu, C. Israel, N. Hur, S. Park, S.-W. Cheong, and A. de Lozanne, Nature Mater. **5**, 881 (2006).
[11]V. Podzorov, B. G. Kim, V. Kiryukhin, M. E. Gershenson, and S.-W. Cheong, Phys. Rev. B **64**, 140406R (2001).
[12]T. Dhakal, J. Tosado, and A. Biswas, Phys. Rev. B **75**, 092404 (2007).
[13]H. Jeen and A. Biswas, Phys. Rev. B **88**, 024415 (2013).
[14]T. Z. Ward, S. Liang, K. Fuchigami, L. F. Yin, E. Dagotto, E. W. Plummer, and J. Shen, Phys. Rev. Lett. **100**, 247204 (2008).
[15]V. G. Sathe, A. Ahlawat, R. Rawat, and P. Chaddah, J. Phys. Condens. Matter **22**, 176002 (2010).
[16]S. Singh, M. R. Fitzsimmons, H. Jeen, A. Biswas, and M. E. Hawley, Appl. Phys. Lett. **101**, 022404 (2012).
[17]J. A. Mydosh, *Spin Glasses: An Experimental Introduction*, 2nd ed. (Taylor & Francis, London, 1993).
[18]R. Prasad, M. P. Singh, P. K. Siwach, A. Kaur, P. Fournier, and H. K. Singh, Appl. Phys. A **99**, 823 (2010).
[19]V. Agarwal, R. Prasad, M. P. Singh, P. K. Siwach, A. Srivastava, P. Fournier, and H. K. Singh, Appl. Phys. Lett. **96**, 052512 (2010).
[20]M. K. Srivastava, P. K. Siwach, A. Kaur, and H. K. Singh, Appl. Phys. Lett. **97**, 182503 (2010).
[21]P. Littlewood, Nature **399**, 529–530 (1999).
[22]R. Mahendiran, A. Maignan, M. Hervieu, C. Martin, and B. Raveau, J. Appl. Phys. **90**, 2422 (2001).
[23]J. Fan, L. Pi, and Y. Zhang, J. Magn. Magn. Mater. **307**, 186 (2006).

Uncertain Supply Chain Management 2 (2014) **–**

Contents lists available at GrowingScience

Uncertain Supply Chain Management

homepage: www.GrowingScience.com/uscm

Implementation of 5S practices: A review

Jagtar Singh[a], Vikas Rastogi[b] and Richa Sharma[c*]

[a]*Mechanical Engineering Department, SLIET Longowal-148106, Distt. Sangrur, Punjab, India*
[b]*Department of Mechanical &Production Engineering, Delhi Technological University Delhi-110042, India*
[c]*PhD. Research Scholar, Mechanical Engineering Department, SLIET Longowal- 148106, Sangrur, Punjab,India*

C H R O N I C L E

Article history:
Received December 10, 2013
Received in revised format
16 March 2014
Accepted April 29 2014
Available online
May 2 2014

Keywords:
5S
Efficiency
Housekeeping
Total Productive Maintenance
Total Quality Management
Availability

A B S T R A C T

5S is a systematic technique used by organizations come from five Japanese words; Seiri (Sort), Seiton (Set in order), Seiso (Shine), Seiketsu(standardize) and Shitsuke (sustain). This system helps to organize a workplace for efficiency and decrease non value added activities and optimize quality and productivity through monitoring an organized environment. This paper aims to review previous studies about benefits of 5S Implementation and its efficiency in organizations. The results show that 5S is an effective tool for improvement of organizational performance, regardless of organization type, size, its production or its service. Consequently, 5S technique would strongly support the objectives of organization to achieve continuous improvement in performance and productivity.

1. Introduction

Nowadays, in this dynamic and technological world, the secret of surviving for any kind of organization is to be competitive and pioneer in its products or services. Normally, this improvement has been achieved through implementation of best practices, which are chosen to meet a particular objective. With increasing of the competition in the world, two major challenges are in front of organizations' managers: First, in this competitive environment, managers have to make the best decisions and choose the best methods to achieve their objectives and not to lose very finite opportunities. Second, lack of knowledge is one of the most important problems of managers about familiarity with an appropriate method to improve the performance of organization, successfully. In addition, the quality of performance also is vital to be evaluated and recognized. Such an evaluation can help managers identify the improvement of performance. 5S is a way to improve the performance and to organize the whole system, which has been used first time by Japanese. It comes from five Japanese words start with S, which is translated into English words to give the best explanation for them.

* Corresponding author. Tel: +8130857467
E-mail address: richasahnivirgo@gmail.com (R. Sharma)

doi: 10.5267/j.uscm.2014.5.002

2. 5S technique

The 5S concept comes from Japan. The original purpose of the 5S is to make the workplace orderly to improve safety and efficiency, reducing the product defects rate. It is expressed by five Japanese words that express cleaning and order at the company and accepting this as work discipline as shown in Fig. 1. These words are (Patra et al., 2005; Mora, 2007):

i.) Seiri: Sort
ii.) Seiton: Set in Order/Straighten
iii.) Seiso: Shine/Sweep
iv.) Seiketsu: Standardize
v.) Shitsuke: Sustain/Self-discipline

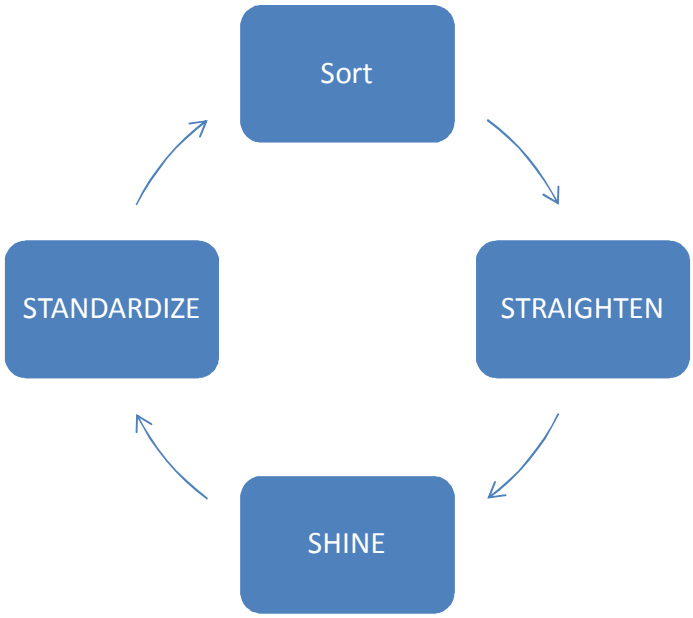

Fig. 1. 5S Technique

2.1 Seiri (Sort)

Sorting necessary and unnecessary materials is called “sort”. The arrangement used for keeping each material in the company at correct place is named as Sort (Mora, 2007). The defective or rarely used material and equipment in the company cause the demolishment of the workplace’s order and decrease in the work efficiency (Sancoban, 2006). Therefore, the necessary and unnecessary materials available in the workplace should be sorted and classified. In order to improve the availability of the working machine and hardware; some workstations such as the machines, tools, hand machines, materials to be used etc. should be kept available in an order and at places where can be easily accessed (Celebi, 1997; Kocalam, 1999). For this reason, when this first basic principle is well applied, the problems and complaints through the work flow will decrease and the communication between the personnel will be simplified. In addition to this, since serious savings will be obtained in the size of the required working environment, important drops will be observed in the operation cost (Sarıcoban, 2006).

2.2 Seiton (Set in Order)

According to this purpose, a localization order is designed for easily accessing to the necessary materials at required times and the materials are put their own places again after utilization (Patra et al., 2005). As a result of the arrangement performed at the work stations (machines, tools, hand tools, materials to be used, etc.), these should be kept at a place where can be accessed easily due to the case of requirement (Kocalan, 1999). The place where the operation is actually realized, material transition paths and the storage method are the points that should be considered in this step. Some points that can be controlled during regulation can be summarized as following (Celebi, 1997):

i.) Stock areas should be used at top level. Solutions such as a shelf order in proportion to the height of the classified material and drawers instead of big sized cupboards and boxes can gain efficiency in terms of stocking.

ii.) In cases where "First in first out" principle is used, it should be avoided that stocking is deep

iii.) The stock areas, shelf and drawers as well as materials should be labeled.

iv.) In case if the dimension and kind of the product change, then special vehicles may be used in machine adjustments.

2.3 Seiso (Shine/Sweep)

In order to realize effective tasks, it is essential to create a clean and regular working and living environment (Patra et al., 2005). This is because dust, dirt and wastes are the source of untidiness, indiscipline, inefficiency, faulty production and work accidents (Anon, 2007). We can handle cleaning practices as a two stepped approach; "general cleaning of workplace and availability of dirtiness sources" and "machine, hardware, tool cleanliness" referred as detailed cleaning (Celebi, 1997). In case of detailed cleaning, some advantages can be obtained. These can be summarized as following (Karabulut, 1999):

i.) Dirt and dust causes bad operation, corrosion and early demolishment of machine and its components. Therefore, dirt and dust sources are removed.
ii.) As a result of making the workplace more proper to the working conditions, the morale of the personnel improves.
iii.) The abnormal cases such as lubricant leakage, wastes, etc. are recognized immediately.
iv.) As a result of psychological impact, the reactions and performances of the personnel get better.
v.) Through providing a safer working environment, the danger contained works decrease.

In order to realize shining through an effective system, the names of the personnel who are responsible from the cleaning of each zone, each department and each point of the factory should be clearly determined and written at the proper places. The shining time should be very short in order to obtain effective utilization. The best times for cleaning are the beginning of shift, end of shift or after meal. All personnel should be well trained about cleaning and participate in cleaning.

2.4 Seiketsu (Standardize)

Following the application of first 3S principles, the necessary systems are formed in order to maintain the continuance of these good practices at the workplace. In order to do this, these activities should be written according to the procedures and the memorization of these procedures by the personnel as well as the functionality of the rules should be obtained. Providing the visual control that will enable the revealing of the problems that may negatively affect the conducted cleaning and the order is very

important here. The methods which can be recognized by anyone at the workplace, not only by the relevant person, should be developed. It will be appropriate to write down performance monitoring labels, control lists, tables and some procedure for visual understanding on TPM board that will be formed in order to control the activities. Following the visual control, the following activities are realized in standardize (Celebi, 1997; Kocaalan, 1999):

i.) Allocation of workplace in terms of area or machine based regions.
ii.) Determination of representatives for each region.
iii.) Identification of points required to be controlled in each region (formation of cleaning-order lists).
iv.) Removal of negativities recognized as a result of controls.

For full application and development of the standards, the participation of all personnel is required. Therefore, standardization means to make correct attitude and behaviors as daily habits and assure their full application in order to get over the handicaps in the first three basic principles.

2.5 Shitsuke (Sustain/Self discipline)

The last step of 5S program covers the improvement of the methods directed to the adaptation of 5S as habit by all personnel. The task here is undertaken by the leader directors. The directors should explain the importance of 5S to the personnel through various trainings and the knowledge of the personnel about 5S should be kept. Updated through the 5S boards to be formed at the workplace. Through various campaigns with easy participation, the dissemination of 5S should be targeted (Celebi, 1997). The objectives of these studies can be summarized as following (Karabulut, 1999):

i.) Formation of a disciplined company.
ii.) Removing small faults through the aid of cleaning.
iii.) Providing the execution of visual control.
iv.) Granting the responsibility of the machine to the worker
v.) Providing the performance of protective activities.
vi.) And granting the responsibility of the workplace to the personnel.

3. Review on 5S

5S is a useful method for founding an organization and spread out a design and can improve communication and help employees to develop their characteristics to decrease downtime, lead time, inventory, defect and associated cost (Van Patten, 2006).. Result of the study indicates that 5S technique is an effective way to improve health and safety standards, environmental performance and housekeeping (Rahman, et al., 2010). 5S is a method for development of companies, change and training. Hirano in 1995 regards 5S as an industrial practice that distinguishes an organization from the others (Osada, 1991). According to the Japanese organizations 5S have two components, a high level of management and organizational system with complexity meaning and it translates to perfect performance and the other one is management provision tools position (Gapp et al., 2008). Even though the 5S housekeeping program aids production (Eckhardt, 2001) but the 5S technique is one of the most known in industrial and business environment and there are few proofs about its adoption in organizations (Bayo-Moriones et al., 2010). Other studies still accept 5S as a method of housekeeping (Eckhardt, 2001; Becker, 2001; Ahmed & Hassan, 2003; Chin & Pun, 2002). However, there are other ideas that believe 5S is a supportive way for Lean and TQM (Kumar et al., 2006).

From the quality management point of view, order and cleanliness have been considered as a part for continuous improvement (Yusof & Aspinwall, 2001) and a point to start continuous improvement and more advancement in organizations. 5S can link with total productive maintenance (TPM) (Ahuja &

Khamba, 2008) and Japanese management approaches such as TPM, JIT and TQM (Gapp et al., 2008). Generally, the success of 5S implementation depends on organizational characteristics (Sousa &Voss, 2008) as this mentioned in many surveys (Bayo Moriones et al., 2008). Survey of one factory in Iran supports pervious findings in this field and indicates that 5S execution provides better condition for implementation of TPM (Moradi et al., 2011). As it is mentioned in several studies, the 5S method is recorded as a way for improving health and safety standard and performance in a holistic operation with high level of efficiency (Khamis, et al., 2009) and also helps improving data management system in factories (Ananthanarayanan, 2006). On the other hand, there is correlation between the 5S and TQM, which further approve the role of 5S as a training tool for TQM and also the need for a sound approach towards TQM (Ho et al., 1995). There is a considerable decreasing in the rate of injuries in the companies where the objective is improving safety through the 5S practice. (Ansari & Modarress, 1997).

The 5S practice is beneficial for every organization, because it helps everyone having a better life (da Silveira, 2006). In fact, many successful organizations in the world have already included some aspects of the 5S in their daily activities without complete awareness of its benefits (Ho, S.K.M; 1999). Indian companies are informed about the quality improvement requirements, although disciplined approach is not yet in place and improvement efforts are not enough to remove weaknesses specially in term of quality (Khanna, 2009). More investigation is needed on implementation of the 5S as an improving tools in a business section and some items like company size and structure could affect application of the 5S and its effectiveness (Eocha, 2000). Actually, there is not much difference between ISO 9001 requirements for implementing quality management system and 5S rules which can be joined by extending the ISO 9000 pattern to combine related 5S rules (Pheng, 2001). This system is beneficial for any workplace to make high quality products and services (Sui PPheng & Khoo, 2001).

5S is applied in most of the factories in manufacturing sections with priority compare to other sections with different ways which can be attributed to the maturity of the 5S program (Warwood & Knowles, 2004). Mixing lean manufacturing initiatives through 5S with safety yield safety results that are well aligned with the rest of the organization (Becker, 2001). Ho in 1998 says the 5S practice is the key to productivity and quality and he also determines the 5S audit methods and reports to adapt and adopt to the business environment via the training sessions and case studies carried out by the industry department. Furthermore, he realized that the 5S practice is very beneficial due to its helps for everybody to have a better lifestyle in the organization (Ho, 1998).

Hamzah and Ho (1994) believe that the 5S is not new and we have had it for long time. We need the 5S at our workplace because many people do their things without thinking about it. In addition, 5S can be a reflection of our behavior. If we have a consideration to 5S, the majority of our routine problems that we face in everyday works could be solved. Hubbard (1999) showed that orderliness which is one of the five pillars of the visual workplace, intends to eliminate three types of waste: searching waste, difficulty-of-use waste, and the waste of returning items to their proper place. Ho (1997) presents Audit Worksheet for 5S, which is a practical tool for 5S implementation. He also believes Japanese 5S fundamentals that must be used for continuous quality improvement.

A useful environmental tool for organization management is 5S, which comes from lean manufacturing process. The 5S practice simplifies the workplace and maintenance system's procedures, decrease waste and non–value added activities. It also improves quality, efficiency and safety. It is the most effective tool of control, which at least reduce or totally avoid different types of pollutions (Nilipour & Jamshidian, 2005).

4. Conclusion

The most important barrier for implementation of 5S effectively is poor communication. Techniques of communication and their efficiency are seldom evaluated and communication faults rarely addressed in an industrial workplace. Poor communication can cause wasting resources, time and money, and lowering moral amongst employees. The results of evolving communication systems in an uncontrolled fashion in industries or business could be confusing and complex. There must be an applicable way for using 5S as an improvement tool for communication system. The surveys indicate that there are difficulties in the effective 5S implementation. Another significant barrier is the space between managerial level and shop floor employees and the poor training and awareness of 5S. Since some critical decisions of 5S activities, including time and budget performance must approve and support by management, therefore more cooperation is recommended during implementation period (Gapp et al., 2008).

It is concluded that 5S key of success is training. 5S implementation is not possible without proper training and employees are not capable to actively standardize the 5S (Ho, S.K.M; 1999). Organization should pay attention to this fact that resistance to change is one issue, which will be occurring during 5S implementation. Therefore, it is believed that continuous training is the key applying to change the organization culture, and assessment should focus on improvement and progress regarding all input from the organization until complete establishment of 5S system (Nilipour & Jamshidian, 2005).

It is obvious that the target of 5S application is vast and diverse and when effectively implemented, the business improvement can be surprising. However, the total benefits of 5S cannot be imagined in industries and business, until the barriers associated, fully understood, addressed and removed.

References

Ahuja, I. P. S., & Khamba, J. S. (2008). Total productive maintenance: literature review and directions. *International Journal of Quality & Reliability Management*,*25*(7), 709-756.

Ahmed, S., & Hassan, M. (2003). Survey and case investigations on application of quality management tools and techniques in SMIs. *International Journal of Quality & Reliability Management*, *20*(7), 795-826.

Ananthanarayanan, K. R. M. (2006). Application of 5S Management System in NDE Laboratory. In *National Seminar on Non-Destructive Evaluation*.

Ansari, A., & Modarress, B. (1997). World-class strategies for safety: a Boeing approach. *International Journal of Operations & Production Management*, *17*(4), 389-398.

Anon, (2007). 5S Management. http://vdb.gib.govtr/edirnevdb/sunumlar/5S Sunum/5Sy. html.

Bayo-Moriones, A., Bello-Pintado, A., & De Cerio, J. M. D. (2010). 5S use in manufacturing plants: contextual factors and impact on operating performance.*International Journal of Quality & Reliability Management*, *27*(2), 217-230.

Bayo-Moriones, A., Bello-Pintado, A., & Merino-Díaz-de-Cerio, J. (2008). The role of organizational context and infrastructure practices in JIT implementation. *International Journal of Operations & Production Management*, *28*(11), 1042-1066.

Becker, J.E. (2001). Implementing 5S to promote safety & housekeeping. *Professional Safety*, 46(8), 29-31.

Celebi, H. T. (1997). *5S and total productive maintenance with total quality perspective* (Doctoral dissertation, M. Sc. Thesis, Istanbul University, Institute of Science, Istanbul, Turkey).

Chin, K. S., & Pun, K. F. (2002). A proposed framework for implementing TQM in Chinese organizations. *International Journal of Quality & Reliability Management*, *19*(3), 272-294.

da Silveira, G. J. (2006). Effects of simplicity and discipline on operational flexibility: an empirical reexamination of the rigid flexibility model. *Journal of Operations Management*, *24*(6), 932-947.

Eckhardt, B. (2001). The 5S housekeeping program aids production. *Concrete products*, 104(11), 56.

Gapp, R., Fisher, R., & Kobayashi, K. (2008). Implementing 5S within a Japanese context: an integrated management system. *Management Decision*,*46*(4), 565-579.

Hamzah, A., & Ho, S. (1994). TQM training for small and medium industries in Malaysia. *Training for Quality*, *2*(2), 27-35.

Ho, S. K., Cicmil, S., & Fung, C. K. (1995). The Japanese 5-S practice and TQM training. *Training for Quality*, *3*(4), 19-24.

Ho, S. K. (1997). Workplace learning: the 5-S way. *Journal of Workplace Learning*, *9*(6), 185-191.

Ho, S.K.M. (1998). 5S practice: a new tool for industrial management. *Industrial Management & Data Systems*, 98(2), 55-62.

Ho, S. K. (1999). Japanese 5-S–where TQM begins. *The TQM Magazine*, *11*(5), 311-321.

Hubbard, R. (1999). Case study on the 5S program: the five pillars of the visual workplace. *Hospital materiel management quarterly*, *20*(4), 24-28.

Karabulut, A. (1999). *Total productive maintenance management"* M.Sc. Thesis, Anadolu University, Institute of Social Sciences, Eskisehir, Turkey.

Khanna, V. K. (2009). 5 "S" and TQM status in Indian organizations. *The TQM Journal*, *21*(5), 486-501.

Khamis, N., Abrahman, M. N., Jamaludin, K. R., Ismail, A. R., Ghani, J. A., & Zulkifli, R. (2009). Development of 5S practice checklist for manufacturing industry. In *Proceedings of the World Congress on Engineering* (Vol. 1, pp. 978-988).

Kocaalan, M.L. (1999). *Improving and increasing machine performance loy using total productive maintenance (TPM) approach.* M.Sc. Thesis, Gazi University, Institute of Science and Technology, Ankara, Turkey.

Kumar, M., Antony, J., Singh, R. K., Tiwari, M. K., & Perry, D. (2006). Implementing the Lean Sigma framework in an Indian SME: a case study. *Production Planning and Control*, *17*(4), 407-423.

Mora, E. (2007). *Essential in The Lean Manufacturing Structure: The "5S" Philosoph.* http://www.tpmonline.com/papakaizen.articls_on_lean_manufacturingstrategies/5s.htm.

Moradi, M., Abdollahzadeh, M. R., & Vakili, A. (2011, September). Effects of implementing 5S on total productive maintenance: a case in Iran. In *Quality and Reliability (ICQR), 2011 IEEE International Conference on* (pp. 41-45). IEEE.

Nilipour, A., & Jamshidian, M. (2005). 5S As an Environmental Organization Management Tool. In *Benefits and Barriers. International Management Conference*.

O'hEocha, M. (2000). A study of the influence of company culture, communications and employee attitudes on the use of 5Ss for environmental management at Cooke Brothers Ltd. *The TQM Magazine*, *12*(5), 321-330.

Osada, T. (1991). *The 5S's: five keys to a total quality environment"* Asian Productivity Organization Tokyo.

Patra, N. K., Tripathy, J. K., & Choudhary, B. K. (2005). Implementing the office total productive maintenance ("Office TPM") program: a library case study. *Library Review*, *54*(7), 415-424.

Pheng, L.S. (2001). Towards TQM - Integrating Japanese 5S principles with ISO 9001: 2000 requirements. *The TQM Magazine*, 13(5), 334-341.

Rahman, M. N., Khamis, N. K., Zain, R. M., Deros, B. M., & Mahmood, W. H. (2010). Implementation of 5S practices in the manufacturing companies: A case study. *American Journal of Applied Sciences*, *7*(8), 1182-1189.

Sarıcoban, E. (2006). The importance of 5S in total productive maintenance activities and an application of 5S. Non-Thesis M.Sc. Project, Dokuz Eylül University, Institute of Social Sciences, Izmir, Turkey.

Sousa, R., & Voss, C. A. (2008). Contingency research in operations management practices. *Journal of Operations Management*, *26*(6), 697-713.

Sui-PPheng, L., & Khoo, S. D. (2001). Team performance management: enhancement through Japanese 5-S principles. *Team Performance Management*, *7*(7/8), 105-111.

Van Patten, J. (2006). A second look at 5S. *Quality progress*, 39(10), 55.

Warwood, S. J., & Knowles, G. (2004). An investigation into Japanese 5-S practice in UK industry. *The TQM Magazine*, *16*(5), 347-353.

Yusof, S. R. M., & Aspinwall, E. (2001). Case studies on the implementation of TQM in the UK automotive SMEs. *International Journal of Quality & Reliability Management*, *18*(7), 722-744.